CHEMICAL REVIEWS

pubs.acs.org/CR

Review

Fluoropolymers in Medical Applications: Recent Progress and Development

Published as part of Chemical Reviews special issue "Fluorine-Specific Interactions".

Chadron M. Friesen* and Jason Pulfer*

Cite This: https://doi.org/10.1021/acs.chemrev.4c00996

Read Online

ACCESS | Metrics & More | Article Recommendations

ABSTRACT: This article aims to present a comprehensive review of the medical applications of fluoropolymers from 2019 to October of 2024. Out of 532 articles, 291 were found to be relevant or imminently relevant to medical applications. The topics of use ranged from drug delivery, implants, sensors, and wound care, with 16 specific application categories noted. All fluorinated polymers were considered, from partially to fully fluorinated. A notable majority were comprised of poly(tetrafluoroethylene) (PTFE) or poly(vinylidene difluoride) (PVDF), leaving much room for additional research in these corresponding fields. The tension between the persistence of fluorinated materials in the environment versus longevity of the material in a medical device requires the need for education and understanding of the applications of fluoropolymers for human health. Fluoropolymers are vital to providing effective medical treatment for patients, especially in the format of long-term interventions.

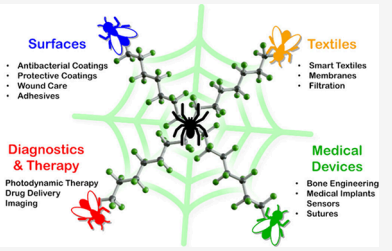

CONTENTS

1. INTRODUCTION

Fluoropolymers are essential in medical applications, although there is growing concern in the public about their connection with perfluoroalkyl substances (PFAS). For a thorough treatment on the difference between PFAS and fluoropolymers please read the following articles by Ameduri in *Molecules*[1] and *Journal of Fluorine Chemistry*.[2] However, it is important to consider their relevance and when they are considered critical for the application. This review looks at the use of all fluoropolymers in medical applications for the last five years (2019−2024) rather than limiting them to strictly polyfluorotetrafluoroethylene (PTFE) or poly(vinylidene difluoride) (PVDF). There are a few reviews that do exist on fluoropolymers in medical applications, but they tend to focus on very specific problems and not necessarily the larger family of fluoropolymers. Due to the nature of these articles, the relevant reviews will be discussed below to allow for historical context of fluoropolymer use.

Medical functionalization of ePTFE was reviewed in a 2021 paper by Roina et al, examining the surface functionalization of ePTFE to improve antibacterial, antistenosis, and tissue integration properties of the material. Methods discussed

Received: December 21, 2024
Revised: July 31, 2025
Accepted: August 4, 2025

involved covalent and noncovalent bonding, chemical impregnation, surface modification, autologous vascularization, and cell seeding.[3] In addition, Roina et al. published a review in 2022 on the surgical efficiency of ePTFE-based biomedical devices, which is useful for putting the use of ePTFE in context for medical applications. The review focuses on the rate of success of ePTFE devices in clinical trials, specifically examining ePTFE-coated stents, hemodialysis and bypass grafts, guidewire coatings, bone and tissue regeneration membranes, and hernia and heart repair applications. Medical devices made of alternative materials are also considered.[4] For a thorough treatment of the polymerization, characterization, processing, application, and reuse of PTFE as a general material, the authors recommend an article published in 2019 by Puts, Crouse, and Ameduri called "Polytetrafluoroethylene: Synthesis and Characterization of the Original Extreme Polymer."[5]

Another review on the roles of intermediate water in the bioinert properties of fluoropolymers was published by Koguchi et al. in 2022, covering the current understanding of bioinert materials and the blood compatibility of fluoropolymers. Intermediate water (IW), or water that has moderately strong interactions with materials, is considered from an analytical perspective for hydration states of polymers, and the tunability of hydration for bioinert fluorine-containing polymers is examined.[6]

Many articles reviewed have focused on triboelectric or piezoelectric nanogenerators (TENGs and PENGs, respectively). Wu et al. published a manuscript in 2021 that covers a broad range topics in piezoelectric materials for wearable electronics, including mechanisms, theoretical research, applications, and sensor fabrication.[7] A review on the fundamentals of TENGs was published in 2023 by Alam et al. and is recommended for a background in triboelectric materials and their use in sensors, biomedical applications, and energy scavengers.[8] Piezoelectric materials are especially interesting to the fluorine community, with poly(vinylidene difluoride) (PVDF) being the archetypical example of a piezoelectric fluoropolymer. Further reading by Sukumaran et al. is recommended for recent advances in flexible PVDF-based energy harvesting materials. This article specifically focuses on the progress in performance enhancement, fillers, and processing methods used to increase piezoelectricity and device output performance in energy harvesting applications.[9] Specific to PVDF, another review by Cui et al. is recommended for background on structural engineering of PVDF for biomedical applications in sensing, disease diagnosis, and treatment.[10] Commonly PVDF is blended with carbon nanomaterials to increase piezoelectric and electric properties of PVDF, as well as give strength to nanomaterials. Kujawa et al. published an article in 2024 which gives excellent context for the current and ongoing applications of these composites toward sensing and energy harvesting, examining the link between structure and physicochemical properties of the materials in sensing, energy harvesting, and material tuning for mechanical properties, bioactivity, and hydrophilicity.[11] Textile based sensors are specifically interesting for noninvasive monitoring, and the article authored by Smith et al. published in 2024 is recommended for specific background in materials typically used in textile sensors, and development of sensors toward integration of sensors into daily use and medical applications.[12]

Therapeutic oxygen delivery based on perfluorocarbon-O_2 nanoemulsions have been demonstrated for hypoxia relief, protection of vital organs in surgery, cancer therapies, and nerve repair. While not significantly represented among the reviewed articles in this manuscript, a review by Krafft and Riess from 2021 covering O_2 delivery, nanoemulsion design, control of bubble/tissue interactions, polymeric micelles, theranostics and perfluorocarbon colloidal nanotherapeutics is recommended as an interesting extension on the topic of medical applications in fluoropolymers.[13]

Fluorinated materials are largely of interest due to the large electronegativity and low polarizability of the fluorine atom (atomic radius of 1.32 Å). The strength of the C−F bond (485 kJ/mol) confers significant stability to fluorinated polymers and is desirable for high performance applications in areas such as coatings, lubricants, wires, cables, and textiles. The first fluoropolymer was discovered in 1938 by Roy Plunkett via the autopolymerization of tetrafluoroethylene (TFE) at autogenous pressure at 25 °C with a Lewis acid catalyst, and now is the most used fluoropolymer in the world. Commonly, poly(tetrafluoroethylene) (PTFE) is made through radical suspension or emulsion polymerization, often using fluorinated surfactants. Despite difficulties in molecular weight characterization, patent literature claims that the mass of polymer is proportional to particle size, with smaller masses in the particle core and larger masses in the particle surface. The polymer is linear, adopting a helical structure and crystallizes in a hexagonal crystal arrangement due to lone pair-lone pair interactions between fluorine atoms on the chain. PTFE is stable to boiling sulfuric, nitric, hydrofluoric, and hydrochloric acids, in addition to base. The polymer does not dissolve or swell even in fluorinated solvents and is only decomposable via alkali and alkali earth metals or aluminum. Finely divided PTFE can be decomposed via steam, and pyrolysis occurs at over 590 °C. PTFE is thermally stable up to 400 °C under pure oxygen and does not exhibit a melt phase. At ∼ 335 °C the material exhibits a first order transition allowing chains to move more freely, and as a result materials are typically sintered rather than molded in typical injection molding or cast molding. Mechanically, PTFE is susceptible to cold flow, or creep, and possesses large elongation-to-break ratios of 300−500%. The polymer is extremely hydrophobic, with contact angles up to 118 °, and the lack of van der Waals interactions prevents adhesion by typical means, making this a polymer with self-lubricating properties and low coefficients of friction. The surface of the material can be modified through plasma, UV, glow discharge, wet chemical, electron beams, or wet chemical techniques to induce chemical handles for grafting. In medical applications, PTFE is utilized in vascular grafts, surgical meshes, stents, catheters, ligaments and tendon repair scaffolds, coating medical devices and tools, and facial augmentation materials due to its chemical inertness and hydrophobicity.[5]

Poly(vinylidene difluoride) (PVDF) is a polymer that exhibits, high intrinsic crystallinity (∼60%), stiffness, toughness, and creep resistance. The material is melt processable through typical compression, transfer, and injection-molding equipment, despite poor solubility in common organic solvents. Vinylidene difluoride (VDF), the monomer, is generally nontoxic, with rats possessing an LC_{50} of 800,000 ppm after 30 min of exposure, is generally considered to be environmentally friendly, and most importantly is nonexplosive, unlike TFE. VDF easily polymerizes under radical

https://doi.org/10.1021/acs.chemrev.4c00996
Chem. Rev. XXXX, XXX, XXX−XXX

Table 1. Fluoropolymers Used in Medical Applications

	Chemical Structure	Medical applications
Polytetrafluoroethylene (PTFE)	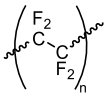	• Artificial blood vessels • Sutures • Stents
Polyvinylidene fluoride (PVDF)	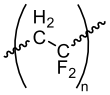	• Water treatment membrane • Piezoelectric biomaterial sensors • Hemodialyzer
Tetrafluoroethylene-hexafluoropropylene copolymer (FEP)	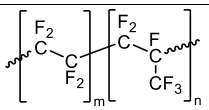	Transcutaneous implants
Polyvinyl fluoride (PVF)	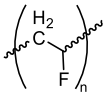	Substrate of protein-repelling
Poly(ethylene-co-tetrafluoroethylene (ETFE)	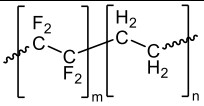	Patch mesh for augmenting myocardial tissue
Fluoroelastomer: Tetrafluoroethylen-propylene (FEPM)	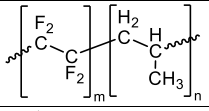	• Soft denture liners • Organs-on-Chips
Amorphous fluoropolymer: Perfluoro(3-butenyl vinyl ether) cyclopolymer	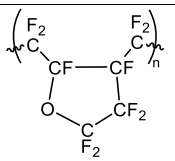	Film for cell observation
Fluoroalkyl homo or copolymer: Fluoroalkyl polymer	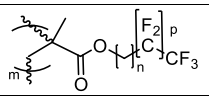	Protein-repelling coating
Ion exchange fluoropolymer: Tetrafluoroethylene-co-perfluoro-3,6-dioxa-4-methyl-7-octensulfonic acid (Nafion®)	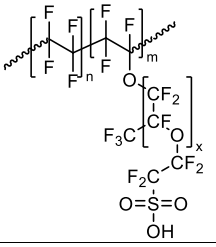	Antimicrobial coating

conditions in suspension or aqueous emulsions and is amendable to a variety of controlled radical polymerization techniques. Five crystalline polymorphs are known, α, β, γ, δ, and ε, with α and β as the most used. The α phase adopts a trans−gauche (TGTG) structure, whereas the β phase adopts an all-trans (TTT) structure attained by straining, stretching, quenching, or application of an electric field during processing (poling). The β-phase exhibits piezo-, pyro-, and ferroelectric properties due to the resulting dipole moment, and has applications in transducers, headphones, sonar arrays, and mechanical actuators. PVDF blends well with other polymers for applications in UV−vis optic transmission (with poly(methyl methacrylate)), paints and coatings (Kynar), and proton exchange membrane fuel cells. Furthermore, PVDF tends to cross-link rather than simply degrade, thus retaining integrity of the material. Copolymers of PVDF with chlorotrifluoroethylene, trifluoroethylene, and hexafluoropropene, are all piezoelectric, and can be used to tune the glass transition temperature (T_g), and VDF is amendable to terpolymerization. Block copolymers of PVDF often have phase separation issues, but can modify material elasticity, solution viscosity, impact resistance, and surface activity. Most block copolymers have applications in thermoplastic elastomers, fuel cell membranes, and surfactants, and these materials can be synthesized through iodine transfer polymerization (ITP), condensation with nucleophiles and Br-PVDF-Br, and macromolecular design by interchange of xanthate (MADIX). Graft copolymers can further be synthesized through copolymerization of macromonomers, grafting of the polymer onto a polymeric backbone, and telomerization of monomers with macrotelogens, and the use of macroinitiators or macroradicals, typically through reversible addition−fragmentation termination (RAFT), nitroxide-mediated living radical polymerization (NMP), or atom transfer radical polymerization (ATRP). These grafts are observed to possess improved mechanical properties, adhesive capabilities, tunable hydrophilicity/hydrophobicity depending on the nature of the block, and have applications in surfactants, rechargeable lithium-ion batteries, coatings, and telechelics. PVDF has applications in chemical and weather resistant paints and coatings, chemical

https://doi.org/10.1021/acs.chemrev.4c00996
Chem. Rev. XXXX, XXX, XXX−XXX

processing equipment, electrical jacketing for cables and high temperature wiring, ink toner, microporous membranes, pizeo- and pyroelectric transducers for motion sensors, ultrasound scanners, pressure switches, actuators, and suture wires.[14]

The current understanding of bioinertness and unusual blood compatibility found in medicinal applications of fluoropolymers is summarized in Table 1 below.[6]

In medical applications, fluoropolymers exhibit phase aggregation and self-assembly due to favorable fluorous interactions. Fluoropolymers largely exhibit lipophobic and hydrophobic properties, inducing self-aggregation of fluorinated blocks. In this way fluoropolymers can be formed into micelles for drug delivery, gene transfection, and peptide delivery. In the specific case of gene transfection, fluoropolymers allow for greater stability of the micelle and overall lower polymer loading, as the material is not destabilized by salts and serum proteins. Self-assembly can also be utilized in ^{19}F MRI as a quantitative probe for cell tracking, nanostructure monitoring, and disease diagnostics due to the lack of background noise and comparable sensitivity to the ^{1}H nucleus (83%). Fluoropolymers further exhibit antifouling and antibiofouling properties. PTFE has been extensively applied in vascular grafts, catheters, cardiovascular valves, ligament and tendon scaffolds, and surgical mesh. PVDF has applications largely due to its piezoelectric nature, with proposed applications as a sinoatrial node cell replacement for pacemaking, scaffolds for cardiac cell cultures, drug-eluting stents and films, and applications in induction of stem cell differentiation. Additional applications of fluoropolymers have been applied toward nanostructured antifouling surfaces, tissue engineering, oxygen delivery, and slippery liquid-infused porous surfaces (SLIPS), where fluoropolymers are allowed to swell with perfluorinated fluids such as Vitreon or Krytox material.[15]

This review will now discuss the 15 different applications of fluoropolymers in the medical industry. The topics discussed will show what is most common in terms of polymers and what room remains for developing new fluoropolymers for various applications, keeping in mind their physical properties and their ability to be reused or recycled. The paper will cover the following topics: adhesives, antibacterial coatings, drug delivery, air filtration, imaging and diagnostics, implants, medical devices, medically relevant textiles, membranes, photodynamic therapy, protective coatings and surfaces, sensors, sutures, tissue and bone engineering, and wound care and dressings. Material will be kept within the period of 2019 to October of 2024 to ensure the reader attains a sense of the current state-of-the-art.

1.1. Adhesives

Moldable temporary adhesives have found many applications in biomedical applications and packaging of consumer products. Researchers have developed a composite solid−liquid adhesive material based on PVDF and poly(dimethyl siloxane) (PDMS), achieving good adhesion without requiring curing of the polymer mixture. Mechanical dispersion of a 1:1 ratio of PVDF in liquid PDMS resulted in a gel-like translucent material, verified by optical microscopy and SEM (Figure 1). The material exhibits excellent chemo- and structural stability up to several months. The adhesive displays a degradation temperature of 461 °C, an increase compared to neat PVDF, due to strong dipole−dipole interactions and was confirmed to be an adhesive from cyclic compressive measurements, with an

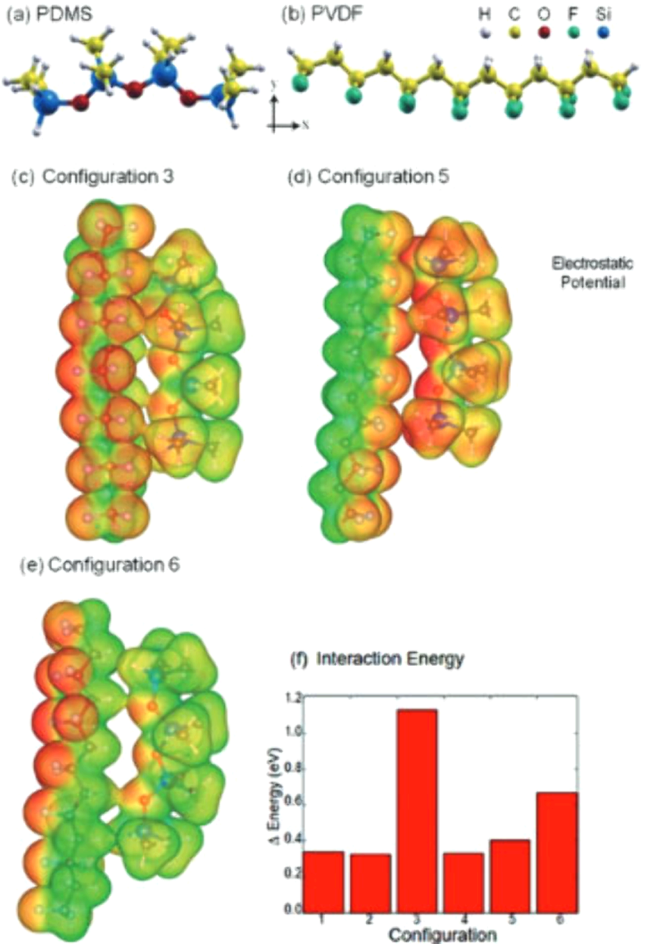

Figure 1. Dipole−dipole interactions for PDMS -PVDF liquid−solid composite calculated by DFT. Reproduced with permission from ref (16). Copyright 2020 Royal Society of Chemistry.

ultimate strength of 1.1 MPa. The adhesive has been shown to be effective on glass/paper, metal/glass, chicken skin, and pig skin, displaying a universal-like adhesion and potential applications for wound dressing adhesives. PDMS and PVDF are hydrophobic materials, indicating the resulting material has functionality as an underwater adhesive.[16]

Typical bandages utilize antibacterial agents and an adhesive to treat wound sites, however these struggle in terms of scalability and application at heavily bleeding sites or joints. Hydrogels present a solution to this problem, having cytocompatibility, scalability, stretchability, and a porous polymer network. Natural hydrogels are limited due to poor mechanical properties, and artificial hydrogels suffer from complex fabrication procedures. Chitosan has found applications as an effective hemostatic agent; however, chitosan-based hydrogels have challenges with self-adhesion in humid conditions, stretchability, and developing effective hemostasis. Researchers have developed a chitosan-based hydrogel (DCS-PEGSH gel), formulated from a 3-(3−4,dihydroxyphenyl) propionic acid modified chitosan cross-linker (DCS) and a sebacic acid-terminated PEG modified with p-hydroxybenzaldehyde (PEGSH) (Scheme 1). This biohydrogel has good cytocompatibility, high stretchability (780%), high blood absorbability (1300% ± 50%), and strong adhesion (~68.5 kPa) on both pig skin and actively bleeding wounds. The dynamic reversibility of the benzaldehyde and the chitosan

https://doi.org/10.1021/acs.chemrev.4c00996
Chem. Rev. XXXX, XXX, XXX−XXX

Scheme 1. Synthesis Process of (A) DCS and (B) PEGS and PEGSH and (C) Representation of the Dynamic Schiff Base Equilibrium between DCS and PEGSH

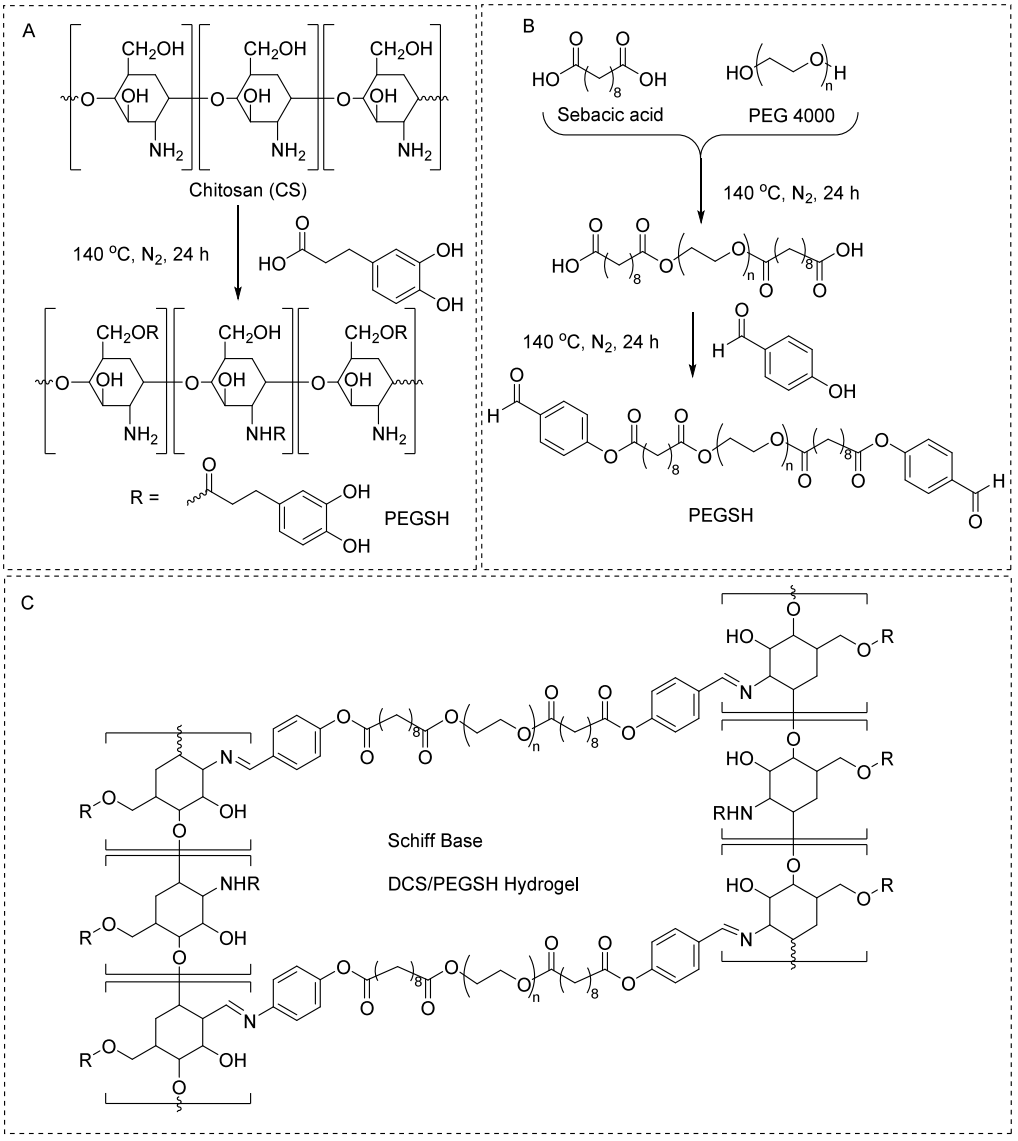

amino groups allows for excellent stretchability and self-healing properties. Chitosan further has natural antibacterial properties, and the hydrogel was demonstrated cytotoxicity toward *E. coli* and *S. aureus*. The material shows good adhesion in humid environments and stimulates blood clotting with a lower blood clotting index (50 s, BCI 41) as compared to performance of a commercial chitosan sponge (288 s, BCI 65). Testing the material in mouse models led to a significantly smaller amount of blood loss (~90%).[17]

1.2. Antibacterial Coatings

The development of sustainable, nontoxic antifouling coatings is increasingly urgent. This study focuses on creating an eco-friendly silicone-based antifouling coating by incorporating isobornyl (borneol) and dodecafluoroheptyl groups into the silicone side chains (Scheme 2) with triethanolamine as a trifunctional cross-linking agent. These additions work synergistically to enhance the ability of the coating to resist fouling. The resulting coatings have excellent properties, including high optical clarity (>92% in the 400−800 nm range), strong adhesion to steel plates (>2 MPa), and effective self-cleaning and fouling release capabilities. One specific coating, poly(dimethyl siloxane) poly(isobutylene oxide) containing fluorine (PDMS-F-PIBO-23), demonstrated outstanding antibacterial and antifouling performance, inhibiting the growth of marine bacteria like *Pseudomonas sp.* by 95.6% and reducing biofilm coverage by 86.9%. It also effectively prevented the attachment of diatoms. These impressive results were due to the unique molecular structure of borneol and the presence of fluoropolymers. Field tests in the Yellow Sea confirmed the strong antifouling ability of the coating, with performance lasting over six months. Compared to traditional coatings that contain harmful toxic substances, this new coating is far less damaging to marine ecosystems. This research opens up new possibilities for designing antifouling coatings that could have applications in medical fields.[18]

Zhao et al. describe the preparation of a submicron spherical polymeric coating, F−SiO_2@PSA, using an emulsifier-free polymerization method to create a styrene-acrylic acid copolymer (PSA) (Figure 2). The surface of the PSA particles was then coated with silica (SiO_2) using a sol−gel method,

https://doi.org/10.1021/acs.chemrev.4c00996
Chem. Rev. XXXX, XXX, XXX−XXX

Scheme 2. Synthesis Process of (A) F-PIBO(OH)$_2$, (B) PIBO(OH)$_2$, and (C) PDMS-F-PIBO-x

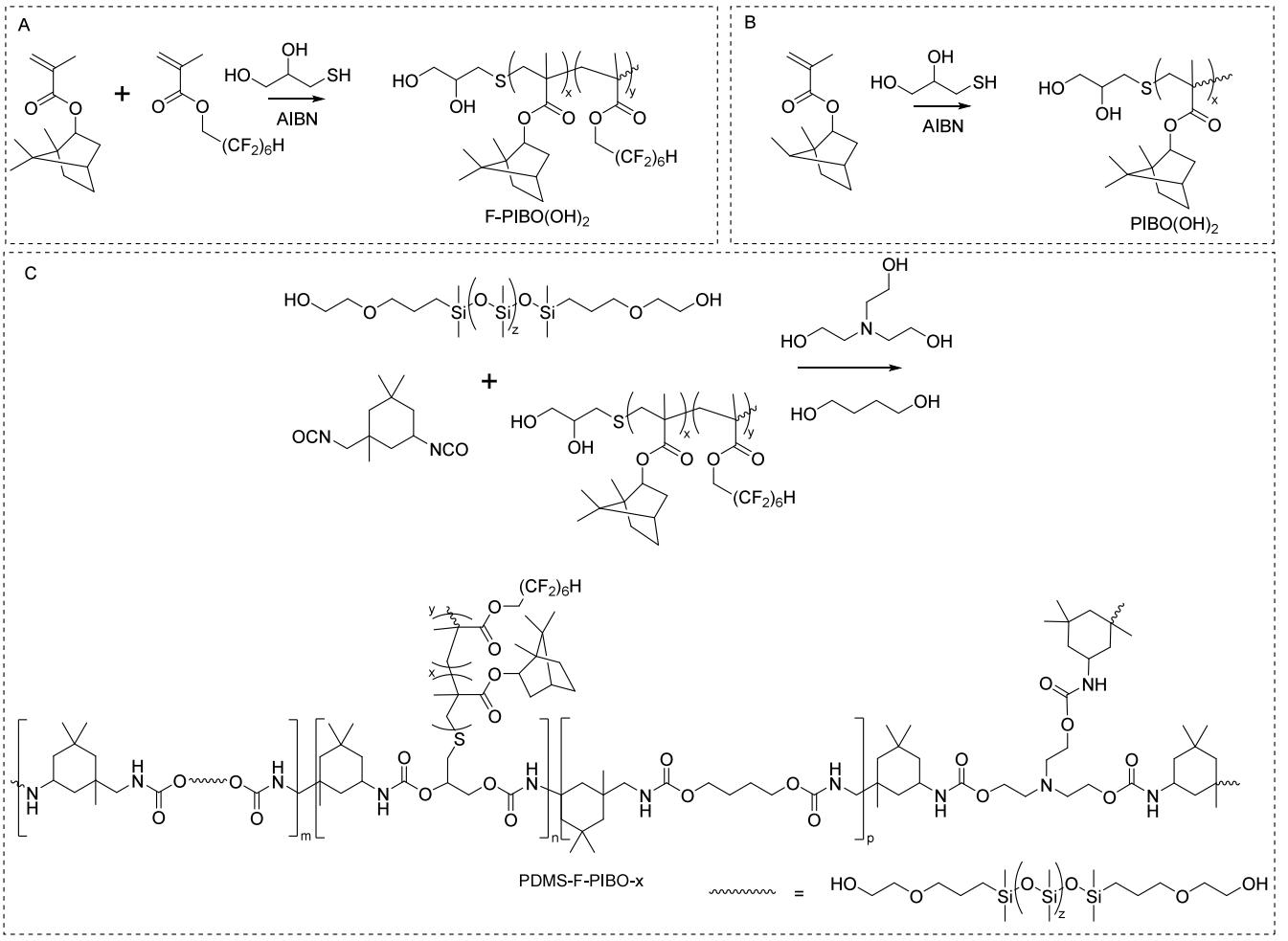

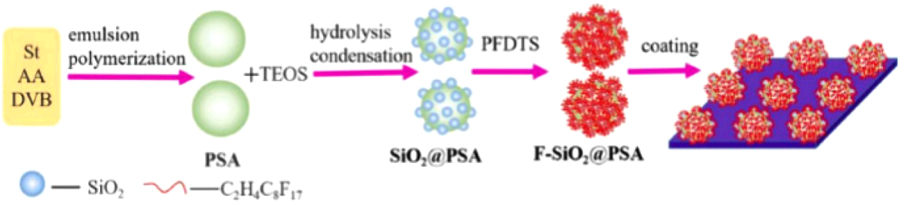

Figure 2. Fabrication of the superamphiphobic F−SiO2@PSA coating. Reproduced with permission from ref (19). Copyright 2023 Elsevier Inc.

resulting in particles with a "raspberry-like" structure when the styrene-to-acrylic acid ratio was 2.5:1.0 and the silica-to-PSA ratio was between 2.17:1.00 and 6.38:1.00. The F−SiO$_2$@PSA-based coatings demonstrated impressive water and oil repellency, with contact angles ranging from 142° to 167° across various liquids, including water, oils, and waste engine oil. The coating induced a 90% reduction in protein adsorption compared to a control surface and prevented the adhesion of bacteria (*E. coli*) and platelets after exposure. These antiadhesion properties suggest strong potential for medical applications, such as implants or devices that minimize bacterial growth and blood clot formation. Further modification with perfluorodecyltrichlorosilane (PFDTS) converted the coating into a superamphiphobic surface. The fluorinated groups reduced surface energy, enhancing the coating's ability to repel both water and oils. The surface fluorine content, which was influenced by both the amount of PFDTS used and the surface topology, contributed to the coating's effectiveness in repelling low-surface-tension liquids. The coating's performance remained stable at temperatures below 200 °C and exhibited excellent resistance to aging in acidic solutions, toluene, and ethanol over 72 h. Overall, the simple synthesis process and excellent antiadhesion and durability properties suggest that these superamphiphobic coatings have strong potential for broad applications, particularly in protective coatings in stent grafts and catheters.[19]

Hydrophilic materials are often considered "bioinert", meaning they are less likely to be recognized as foreign by proteins and cells, which is important for medical and biological applications. However, hydrophilic materials are typically water-soluble, which limits their use. One common solution is to copolymerize hydrophilic monomers with hydrophobic ones to make the resulting material water insoluble. The challenge, however, is that reducing the

https://doi.org/10.1021/acs.chemrev.4c00996
Chem. Rev. XXXX, XXX, XXX−XXX

hydrophilic component can also reduce the bioinert properties of a material. This study presents a way to overcome this challenge by adding small amounts of a fluorinated monomer, 1,1,1,3,3,3-hexafluoropropan-2-yl 2-fluoroacrylate (FAHFiP), to copolymers of hydrophilic mPEGMA (poly(ethylene glycol) methyl ether methacrylate) (Scheme 3). Even in small quantities (7.9 wt %), FAHFiP significantly improved the hydrophobicity of the copolymer, making it water-insoluble while preserving its bioinert properties. Atomic force microscopy (AFM) images showed that the copolymer exhibited phase separation between the hydrophilic mPEGMA domains and the hydrophobic FAHFiP ones. A copolymer with a higher content of FAHFiP (66.2 wt %) displayed a higher concentration of FAHFiP at the polymer−water interface (82%). On the other hand, a copolymer with less FAHFiP and more mPEGMA was enriched with hydrophilic domains at the interface, demonstrating that the material could remain highly hydrophilic at the water interface even when the bulk material was hydrophobic. The enhanced bioinert properties of the poly(FAHFiP-*co*-mPEGMA) copolymers were evident in tests with significantly reduced platelet adhesion and fibrinogen adsorption, outperforming poly(2-methoxyethyl acrylate), a commonly used material in medical devices. This suggests that small amounts of fluorine in copolymers can help in maintaining bioinertness while making the material water insoluble and suitable for biomedical applications.[20]

Scheme 3. Synthesis Route to Poly(FAHFiP-co-mPEGMA) Copolymers, FAHFiP and mPEGMA Standing for 1,1,1,3,3,3-Hexafluoropropan-2-yl 2-Fluoroacrylate and Poly(ethylene glycol) Methyl Ether Methacrylate, Respectively

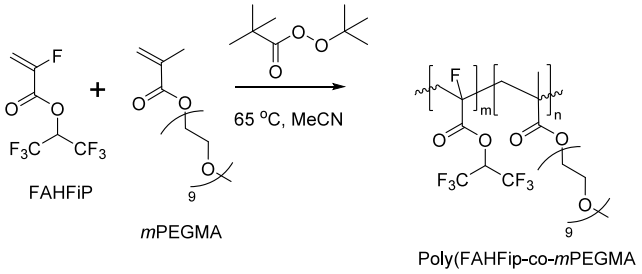

Multidrug-resistant bacteria are a growing global health concern, highlighting the need for new preventive strategies, including antimicrobial surface coatings for hospitals and medical equipment. This study explores a novel approach using a metal−organic framework (MOF)-based composite for controlled iodine release, a nonresistant antimicrobial agent. The composite consists of iodophilic MOF beads (UiO-66, consisting of ZrO_2 and terepthalic acid) that encapsulate gold nanorods (AuNRs) coated with a silica shell. When exposed to near-infrared (NIR) light, the AuNRs generate heat through a photothermal effect, triggering the release of iodine from the MOF. The composite was then incorporated into polyvinylidene fluoride (PVDF) to create antibacterial films. The study evaluates iodine adsorption, as well as both passive and light-triggered iodine release from these films. In vitro tests confirmed that the iodine-loaded composite films exhibited significant antibacterial activity against both Gram-positive and Gram-negative bacteria. This research suggests that the iodine-releasing MOF composite could be an effective material for developing new antimicrobial treatments, offering a promising solution to combat bacterial resistance.[21]

Preventing nonspecific biofouling is essential for the advancement of biomaterials and medical devices. Zwitterionic materials are particularly promising due to their strong fouling-

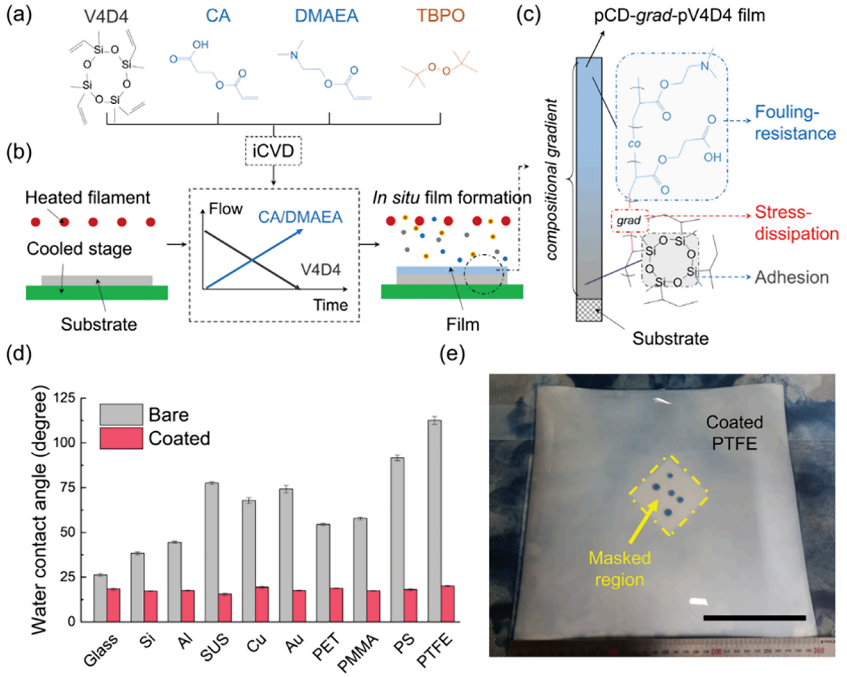

Figure 3. (a) Chemicals used in fabricating the polyampholyte polymer films via iCVD. (b) Schematic illustration of the polymer film deposition process with compositional gradient interface. (c) A schematic representation of the pCD-grad-pV4D4. (d) WCA of a 10 μL water droplet on the pCD-grad-pV4D4 film coated on various substrates. (e) Optical photograph of the pCD-grad-pV4D4 film coated on PTFE. Scale bar = 10 cm. Reproduced with permission from ref (22). Copyright 2022 John Wiley & Sons Inc.

https://doi.org/10.1021/acs.chemrev.4c00996
Chem. Rev. XXXX, XXX, XXX−XXX

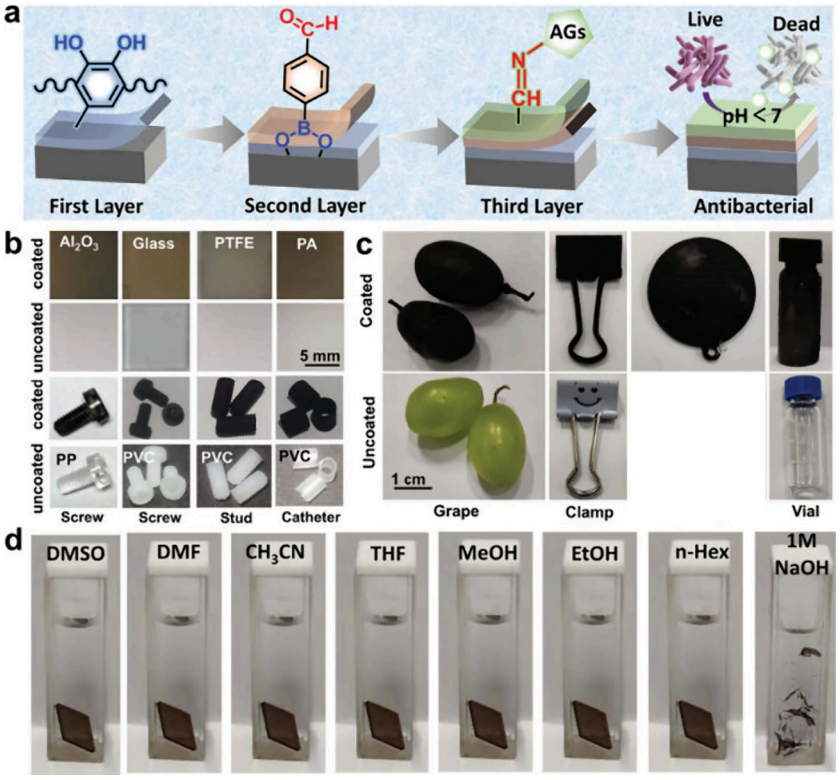

Figure 4. (a) Schematic illustration of the fabrication process toward PDHI/FPBA/AGs antibacterial coating via LBL assembly; (b) flat substrates, screws, studs, and catheters before and after coated with PDHI/4-FPBA/TOB; (c) different shaped devices before and after coated with PDHI/4-FPBA/TOB. (d) Solvent resistance testing of PDHI/4-FPBA/TOB coating on the surface of glass. Cuvette size was 45 mm × 12.5 mm × 12.5 mm. Reproduced with permission from ref (24). Copyright 2022 John Wiley & Sons, Inc.

resistance, biocompatibility, and long-term durability against oxidation. However, creating a substrate-independent zwitterionic surface with excellent fouling resistance has been a challenge. This study presents a solution in the form of a polyampholyte coating created through a vapor-phase method. The coating consists of a bilayer structure: poly(1,3,5,7-tetramethyl-1,3,5,7-tetravinyl cyclotetrasiloxane) (pV4D4) as an adhesion-promoting layer and poly(2-carboxyethyl acrylate-co-2-(dimethylamino)ethyl acrylate) (pCD) as the fouling-resistant top layer (Figure 3). The layers are deposited sequentially using initiated chemical vapor deposition, with a compositional gradient that enhances adhesion and fouling resistance. The pCD surface exhibits excellent fouling resistance, with very low protein adsorption (20.3 ± 1.8 ng cm^{-2} for undiluted human serum) and resistance to microorganisms. The films, made from pCD-grad-pV4D4, are able to stretch up to 50% without losing their fouling resistance. Remarkably, the fouling resistance persists even after stress tests such as sonication, water flushing, and water shearing. Additionally, these films are fully transparent and can be patterned, making them a promising candidate for future biomedical applications in wound care and wound dressing.[22]

The development of thin, stretchable coatings that prevent the unwanted adhesion of biological substances to soft, high-water-content biomaterials is a key area of research. For example, this research introduces a new stretchable antifouling coating called lubricant-infused poly(1,3,5,7-tetramethyl-1,3,5,7-tetravinyl cyclotetrasiloxane) (V4D4), which interfaces with a fluoropolymer to create a bilayer (L-VIP). The bilayer consists of the stretchable adhesive polymer V4D4 and the fluoropolymer 1*H*,1*H*,2*H*,2*H*-perfluorooctyl methacrylate (FOMA). This L-VIP coating has a strong affinity for lubricants, giving it exceptional antifouling and slippery properties. It shows superior resistance to plasma proteins, which contribute to foreign body reactions, as well as to bacteria that form biofilms. The coating can withstand impressive mechanical stress, with an elastic limit of over 200% strain and stability after more than 2000 cycles of stretching at 150% strain, all while retaining its antifouling capabilities. Additionally, the coating demonstrates excellent dielectric performance under accelerated aging conditions (70 °C and 10 V s^{-1} for 50+ days). *In vitro* and *in vivo* tests confirm that the L-VIP coating is nontoxic, making it suitable for biomedical applications. The ability of the coating to prevent bacterial infections, biofilm formation, and nonspecific biological adhesion positions it as a promising candidate to enhance the longevity and performance of medical devices after implantation such as stent grafts, catheters, and other blood contacting medical devices.[23]

Bacterial colonization and biofilm formation on medical implants pose significant risks for patients, leading to infections that are difficult to treat. While antibacterial coatings made using layer-by-layer (LBL) assembly techniques have been widely studied, there remains a need for easy-to-prepare, substrate-independent coatings that can release antibiotics on demand and provide excellent antibacterial performance. This study addresses this need by using LBL assembly to create robust antibacterial coatings for materials such as alumina, PTFE, PVC, polyamide (PA), PP, and glass from naturally derived and commercially available materials, such as aminoglycosides, 5,6-dihydroxyindole, and formylphenylboronic acid. These materials are incorporated using mussel-inspired

https://doi.org/10.1021/acs.chemrev.4c00996
Chem. Rev. XXXX, XXX, XXX−XXX

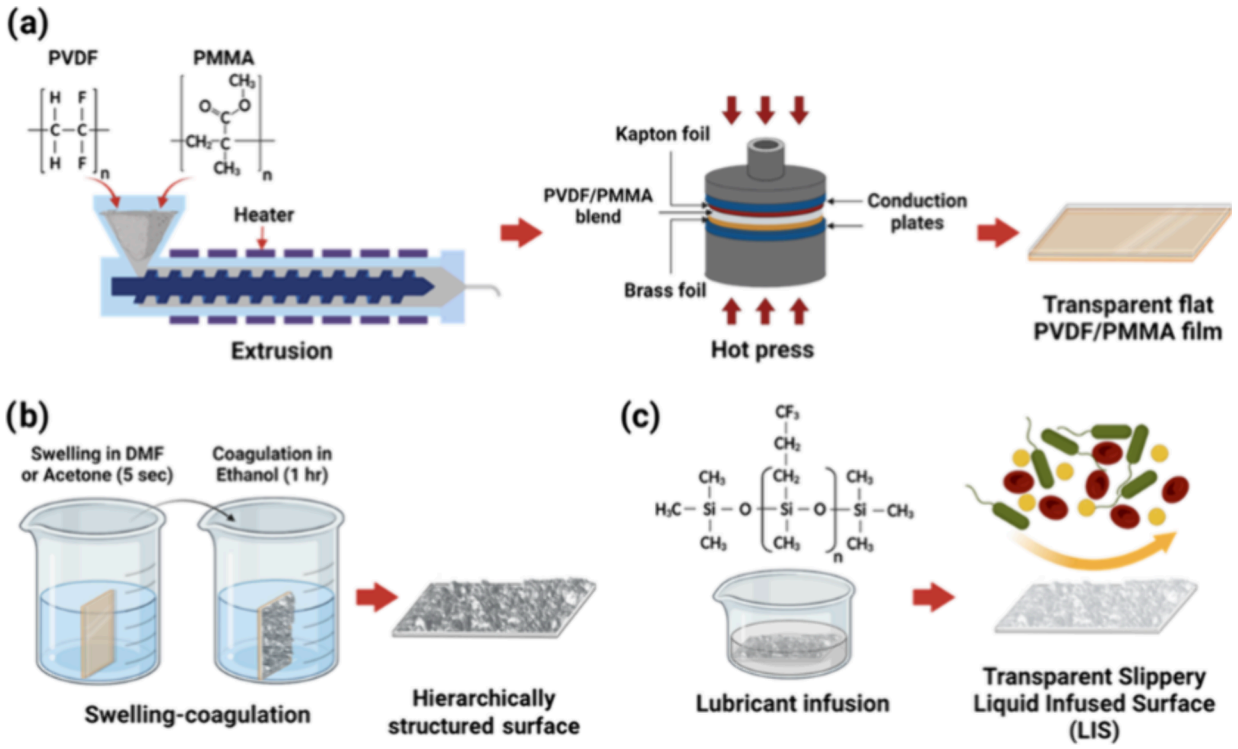

Figure 5. Schematic illustration for the fabrication process. (a) Preparation of the polymer blend by melt compounding using an extruder and hot pressing the material to prepare planar films supported by a brass foil. (b) S−C treatment by immersion of the supported polymer film in DMF or acetone followed by coagulation in ethanol to prepare the hierarchically structured surfaces (D-S and A-S). (c) Infusion of the rough surfaces with lubricant to prepare liquid-infused surfaces (D-LIS and A-LIS). Reproduced with permission from ref (26). Copyright 2022 American Chemical Society.

polymerization and dynamic covalent chemistry. The resulting coatings are pH-responsive, meaning they can release antibiotics in response to changes in the environment, and they show highly effective antibacterial activity both *in vitro* and *in vivo*. The work demonstrates that LBL assembly, combined with natural building blocks and accessible chemistries, can be used to create advanced antibacterial coatings. This approach could expand the potential of LBL techniques to develop the next generation of durable, universal antibacterial coatings for medical devices (Figure 4).[24]

A new type of durable slippery colloidal coating was developed that combines particulate films with a bilayer lubricant, providing exceptional surface protection. The coating offers anticorrosion, antifouling, self-healing, anti-icing, and self-cleaning properties. The process starts with creating micelle dispersions using materials with low surface energy, like PTFE or PDMS. These materials form colloidal dispersions that are then spray-coated onto surfaces. After thermal treatment, the films are tightly packed, creating uniform aggregates with nanopores. A key feature of this approach is that it avoids the complex hole-making process typical of traditional slippery liquid-infused porous surfaces (SLIPS). Instead, a thermally driven surfactant serves as an adhesive primer layer, while the infused lubricant acts as a protective top layer. This bilayer system helps prevent rapid surface degradation under stress and significantly improves durability. The study investigates the anticorrosion and antifouling performance of coatings infused with different functional lubricants, including ionic liquids, silicone oil, and perfluoropolyalkylether oils (e.g., Krytox 103). The PTFE/Krytox 103 coating demonstrated the best stability and performance, particularly in anticorrosion and antifouling. The PDMS/silicone oil coating, being biofriendly, is suitable for biomedical applications, while the ionic-liquid-infused coating is ideal for extreme environments due to its temperature stability and corrosion resistance. The coatings can be applied to various shapes and large surfaces using the simple spray-coating process. An additional advantage is the self-healing property of the slippery films; they can spontaneously recover their structural integrity when damaged, thanks to the mobility of the lubricant. This process also avoids the use of ecologically harmful solvents, making it more sustainable for industrial applications. Overall, this research presents a versatile, durable, and environmentally friendly approach for creating antifouling, corrosion-resistant coatings that have potential in biomedical applications, fuel transport, self-cleaning windows, and optical devices.[25]

Thrombus formation and bacterial infections are major causes of failure in blood-contacting medical devices. A promising strategy to prevent these issues is to design surfaces that repel pathogens but scaling up these surfaces for large-scale production remains challenging. To address this, the study introduces an all-polymeric lubricant-infused system using an industrially viable swelling-coagulation solvent (S−C) method. This method creates micro/nanostructured features on the surface that enhance lubricant infusion. The lubricant used in this study is poly(3,3,3-trifluoropropylmethylsiloxane) (PTFS), an omniphobic oil that is underexplored in the literature. The result is a flexible, transparent, and long-lasting lubricant-infused surface that is effective in repelling blood and bacteria (Figure 5). The repellent properties were tested using human whole blood and methicillin-resistant *S. aureus*

https://doi.org/10.1021/acs.chemrev.4c00996
Chem. Rev. XXXX, XXX, XXX−XXX

(MRSA) bacteria. The lubricated surfaces demonstrated a 93% reduction in blood stains and a 96.7% reduction in bacterial adherence over 72 h. This novel, scalable material has strong potential to reduce blood and bacterial contamination on medical devices, making it a promising solution for improving the performance and safety of devices used in healthcare settings.[26]

This study presents a novel approach for creating durable, eco-friendly coatings with excellent adhesion and unique surface properties, ideal for various industrial applications (Scheme 4). The focus is on the synthesis of poly(glycidyl methacrylate-*co*-fluorinated methacrylate) (P(GMA-*co*-FMA)) random copolymers, which combine glycidyl methacrylate (GMA) and fluorinated methacrylate (FMA) monomers. These copolymers result in coatings with enhanced durability and special surface characteristics, particularly superior water and oil repellency, due to the incorporation of fluorine. The resulting P(GMA-*co*-FMA) coatings exhibit water contact angles ranging from 105° to 125° and decane contact angles from 50° to 85°, with the repellency properties increasing as the fluorine content in the copolymers rises. The coatings also show excellent adhesion and self-cleaning capabilities, which last for up to six months, even under prolonged use. A detailed analysis reveals how the composition of the copolymers affects the surface wettability and contact angle hysteresis, providing insights for optimizing coating properties. The coatings were applied to substrates like Si wafers, aluminum plates, and filter paper, with remarkable durability in terms of both water and oil repellency. Even at low FMA concentrations (2%), the coatings maintained strong repellency, with hydrophobic and oleophobic properties lasting more than six months and remaining intact after multiple peel-off cycles. These durable, self-cleaning coatings have wide-ranging potential applications in industries such as electronics, medical supplies, textiles, and protective clothing. For example, they can be used on medical devices like tubing, endoscopes, and surgical shields, as well as on touchscreens and in protective gear against chemical agents. The long-lasting performance and environmental safety make these coatings highly promising for improving product longevity and functionality across various fields.[27]

Biofouling, the unwanted accumulation of microorganisms on surfaces, poses a significant challenge for various industries, including marine transportation and medical devices (Scheme 5). Traditional solutions, like copper or tin-based paints harm aquatic life, while hydrophilic and zwitterionic materials have limited effectiveness at the solid−liquid−air interface, where

Scheme 4. Synthesis Scheme of the FMA Monomer (a), PGMA Homopolymer (b), and P(GMA-co-FMA) Copolymer (c)[a]

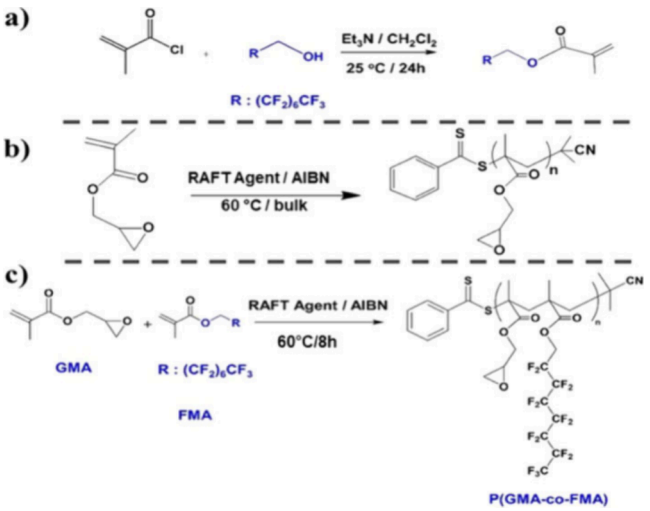

[a]Reproduced with permission from ref (27). Copyright 2024 American Chemical Society.

Scheme 5. Reaction of 1,3-Propane Sultone with P4VP-co-HFBA and P4VP-co-PFOA Copolymers to Produce Zwitterionic Moieties[a]

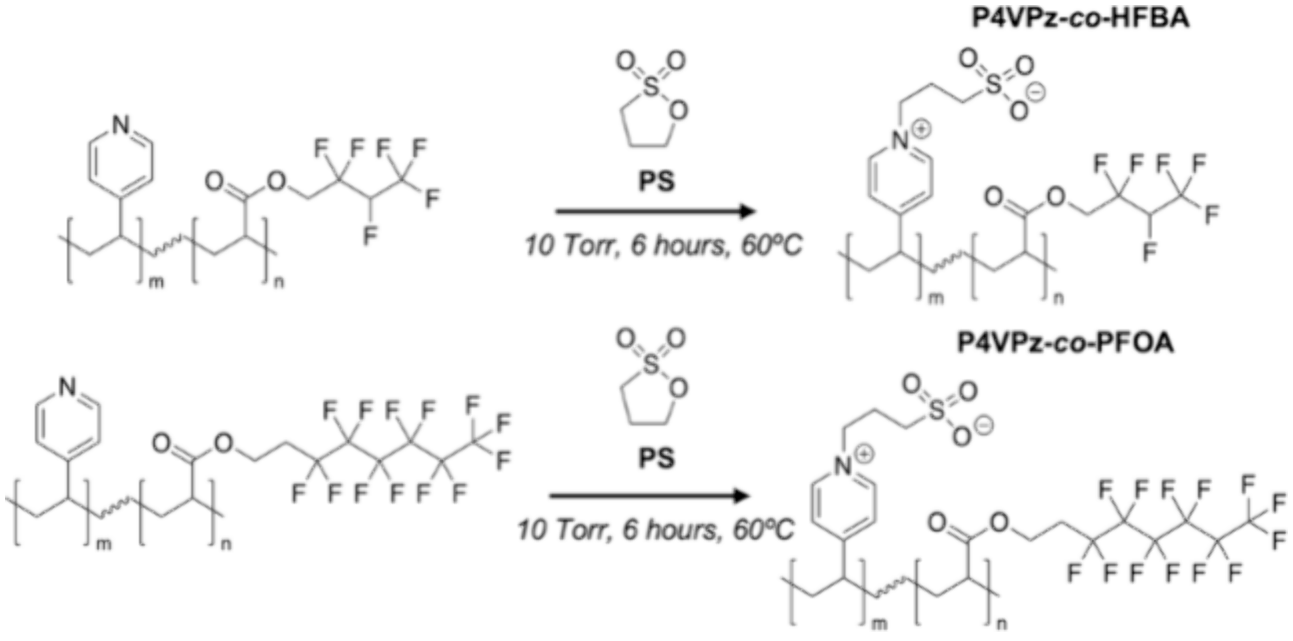

[a]Reproduced with permission from ref (28). Copyright 2022 American Chemical Society.

https://doi.org/10.1021/acs.chemrev.4c00996
Chem. Rev. XXXX, XXX, XXX−XXX

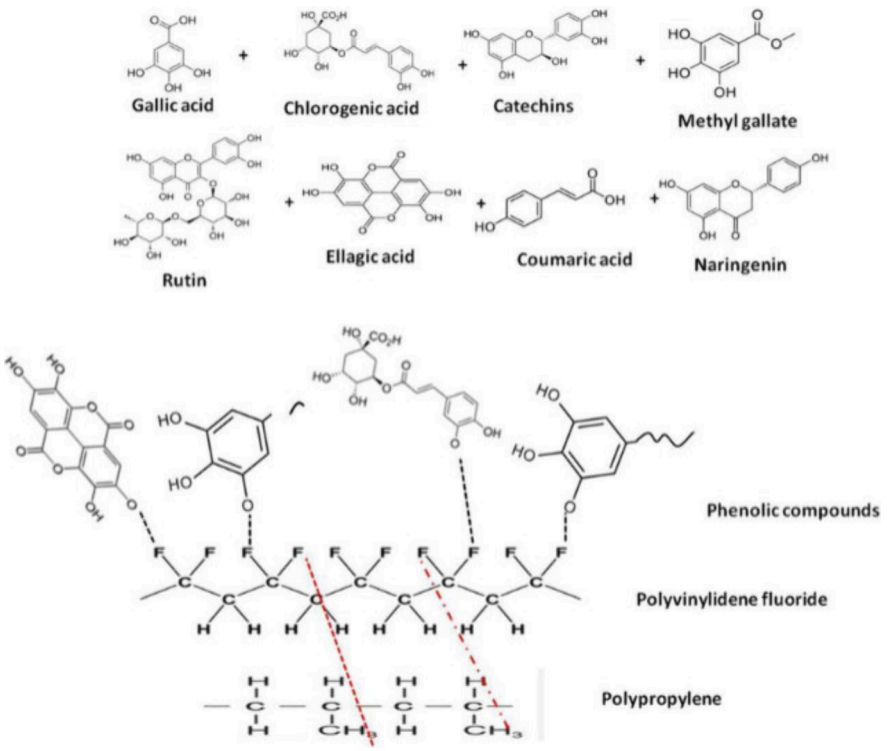

Figure 6. Sinensis extract, with possible formation of covalent bonds between oxygen of polyphenolic compounds and fluorine in PVDF and presence of free OH groups on the surface of the membrane. Reproduced with permission from ref (30). Copyright 2024 Springer.

biofilm formation is most problematic. This study addresses this issue by developing amphiphilic copolymers that combine hydrophilic zwitterionic units with short fluorinated hydrophobic units, which help to prevent biofilm formation without the environmental risks associated with long-chain fluorinated compounds. The copolymers were synthesized using initiated chemical vapor deposition (iCVD) and contained a pyridinium-based zwitterionic monomer (4-vinylpyridine, 4VP) and short fluorinated monomers such as 1*H*,1*H*,3*H*-hexafluorobutyl acrylate (HFBA) or 1*H*,1*H*,2*H*,2*H* perfluorooctyl acrylate (PFOA). These fluorinated chains avoid the harmful environmental effects linked to long-chain perfluoroalkyl substances (PFAS), which are toxic and persistent in the environment. The copolymers were designed to be amphiphilic, allowing for easy reorientation of the surface chains at the solid−liquid−air interface, where the hydrophobic surface at the air−solid interface resists biofilm formation and the hydrophilic surface at the liquid−solid interface prevents bacterial adhesion. Dynamic contact angle (WCA) measurements confirmed that the fluorinated side chains dominated the surface energy, even after the zwitterionic transformation of the pyridine rings. The coatings demonstrated significant antibiofilm performance, with the amphiphilic copolymers outperforming pure zwitterionic coatings in preventing biofilm formation by *P. aeruginosa* at the triple interface (solid−liquid−air). The copolymer made with HFBA (3 fluorinated carbon atoms) displayed a 39.3% better performance than pure zwitterionic coatings, while the one synthesized from PFOA (6 fluorinated carbons) reduced biofilm formation by 43.8%. The research successfully demonstrates the potential of fluorinated amphiphilic copolymers as effective, less toxic antifouling coatings. These coatings can be used in various applications, such as in marine transportation, medical devices, and food manufacturing, where biofouling prevention is critical.[28]

Waterproof and breathable membranes (WBMs) are crucial for applications like outdoor apparel, wearable electronics, and medical hygiene, as they prevent liquid water penetration while allowing water vapor to pass through. However, creating environmentally friendly WBMs that are nontoxic and based on eco-friendly solvents remains a challenge. This study addresses this by developing PTFE-based waterproof and permeable membranes (PWBM), which exhibit impressive performance characteristics. The developed PWBM features a high moisture vapor transfer rate (WVTR) of 11.9 kg m^{-2} day^{-1}, a high hydrostatic pressure resistance of 81.5 kPa, and exceptional tensile strength and flexibility, with a tensile strain of 554%. The membranes also exhibit remarkable chemical resistance and superhydrophobicity, meaning they resist water and oil effectively. The structure of the PWBM, with a sintered bonded network and smaller pore sizes, contributes to these outstanding properties. Additionally, the PWBM maintained its waterproof and mechanical properties even after being submerged in chemical media for 10 days, showing its durability. With its combination of superhydrophobic and oleophobic properties, along with excellent waterproofing, mechanical strength, and flexibility, this new PWBM is poised to offer significant potential for applications in medical hygiene, protective clothing, and wearable electronics. The environmentally friendly and high-performance features make it a promising material for next-generation, sustainable protective fabrics.[29]

Masks are effective in protecting against respiratory pathogens, but pathogens can accumulate on their surfaces, potentially spreading infections (Figure 6). This study addresses this concern by developing a disinfecting coating for masks using a plant extract from *Camellia sinensis* (black tea). The polypropylene base of the mask was coated with a layer of PVDF polymer, infused with 500 μg/mL of *Camellia*

https://doi.org/10.1021/acs.chemrev.4c00996
Chem. Rev. XXXX, XXX, XXX−XXX

sinensis methanolic extract. The plant extract has direct inhibitory effects against *S. aureus* (a respiratory bacterium), influenza A virus (an enveloped virus), and adenovirus 1 (a nonenveloped virus). The effectiveness of the extract against these pathogens was dose- and time-dependent, with inhibition rates of 61% for *S. aureus*, 72% for influenza, and 50% for adenovirus. The addition of the extract to the membrane also helped prevent the infectivity of these pathogens. In addition to its disinfecting properties, the hydrophobic nature and small pore size (154 nm) of the membrane prevented the penetration of dust particles and water droplets that might carry pathogens. The membrane also allowed for 77.2% breathability, ensuring normal airflow. The antibacterial and antiviral effects of *Camellia sinensis* are likely due to its polyphenolic compounds, which can bind to or precipitate proteins on the surface of bacteria and viruses, inactivating them. This study demonstrates that by adding a thin disinfecting layer to masks, they can be made more effective at preventing the spread of respiratory infections, even when handled or worn for extended periods. This approach has the potential to improve mask safety and hygiene in both healthcare and public settings.[30]

Chitosan is a promising material for creating antibacterial coatings due to its broad-spectrum activity against pathogenic microorganisms. However, achieving a stable and effective chitosan coating requires balancing its degree of deacetylation (DD) and molecular weight (MW). In this research, four chitosan samples were characterized by their DD and MW and tested for their antibacterial properties against *E. coli*, *P. aeruginosa*, and *S. aureus*. The sample with the best antibacterial performance was CHI80MW, which had 79.7% DD and a MW of 7.0×10^5 Da. CHI80MW was then used to functionalize PTFE surfaces via plasma grafting, with two different spacer molecules of poly(ethylene glycol) bis (carboxymethyl) ether (PEG) and poly(ethylene-*alt*-maleic anhydride) (PA). The PTFE-Plasma-PA-CHI80MW coating showed superior antibacterial performance compared to PTFE-Plasma-PEG-CHI80MW. After 8 h, PTFE-Plasma-PA-CHI80MW reduced bacterial growth by 77−90% for the three bacterial strains, while PTFE-Plasma-PEG-CHI80MW only achieved a 25−30% reduction. Additionally, cytotoxicity tests revealed that the PTFE-Plasma-PA-CHI80MW coatings were compatible with human fibroblasts, demonstrating the nontoxic nature of the coatings. The study concluded that high DD and MW chitosan (like CHI80MW) provide the best antibacterial properties, and the plasma grafting method successfully created a nontoxic, antibacterial coating on PTFE surfaces. These findings suggest that plasma-assisted chitosan coatings could have broad applications, particularly in antimicrobial surfaces for medical and industrial use.[31]

Li et al. demonstrated that antibacterial fiber mats can be developed by incorporating silver nanoparticles (Ag NPs) into PTFE using electrospinning. PTFE is biologically inert but lacks antibacterial properties, which limits its applications. By adding Ag NPs, the resulting PTFE/Ag NP composite fiber mat had significantly improved antibacterial performance, with optimal antibacterial performance was achieved with 3% Ag NPs concentration. The composite fiber mat demonstrated a 97.1% antibacterial rate against *E. coli* and 97.0% against *S. aureus*, as well as a moisture permeability of 15,500 ± 304 g/m^2·12h, which is a key property for breathability and moisture regulation. The mat also exhibited a high water contact angle of 137.6°, a tensile strength of 1.84 MPa, and an elongation at break of approximately 260.92%, making it both durable and flexible. These properties suggest that the PTFE/Ag NP fiber mats could be highly effective for applications such as medical masks, protective clothing, and other antibacterial fabric uses.[32]

This study focuses on the development of bimetallic, hierarchically macroporous metal−organic frameworks (MOFs), specifically HMUiO-66(Zr/Ce), designed to effectively disrupt bacterial biofilms and inhibit bacterial growth. The researchers designed the HMUiO-66(Zr/Ce) MOFs by adjusting the feed ratios of zirconium (Zr) and cerium (Ce), which allowed for control over the particle size (around 150 nm) and the Zr amount in the structure (ranging from 0% to 69%). These MOFs feature excellent chemical and thermal stabilies, as well as abundant Lewis acid sites that contribute to their DNA-cleaving abilities. The Zr−OH sites effectively capture nucleic acids, while Ce−OH moieties catalyze the hydrolysis of DNA, leading to the breakdown of bacterial biofilms. This DNA-cleaving property allows the MOFs to target and destroy the extracellular DNA within biofilms, making them a promising tool for biofilm eradication. The researchers also incorporated the MOFs into a PVDF film, which exhibited strong antibacterial properties, reducing bacterial adhesion and colonization. This biomimetic MOF/PVDF film holds great potential for applications in antimicrobial therapy and medical devices, offering an innovative approach to combat bacterial infections and biofilm-related complications.[33]

The formation of extracellular polymeric substances (EPS) is a key step in bacterial biofilm development. The composition of EPS is influenced by the substrate the bacteria grow on, and understanding this relationship is important for controlling biofilm growth, particularly on medical device surfaces. This study investigates how biofilms of *E. coli* and *Klebsiella pneumoniae* grow on four common polymer substrates used in medical devices: polyethylene (PE), polypropylene (PP), polycarbonate (PC), and PTFE. These polymers were conditioned with bovine serum albumin (BSA) for 24 h to simulate a biological environment. The researchers used several techniques—contact angle measurements, field emission scanning electron microscopy (FE-SEM), and spectroscopy—to analyze the changes in surface properties and biofilm growth. They found that after BSA conditioning, the surface properties of the polymers shifted from highly hydrophobic to near amphiphilic (having both hydrophilic and hydrophobic characteristics). This transformation was linked to the polymer's interaction with the BSA layer, which influenced the composition of the EPS and the bacteria's ability to colonize the surface. These findings provide important insights into how biofilms form on medical device surfaces, highlighting the impact of the BSA−polymer interaction. This research lays the groundwork for further studies aimed at preventing biofilm formation on medical devices through noninvasive strategies.[34]

Deng et al. developed a piezoelectric dual network dressing (Figure 7). Electrical stimulation therapy is essential for wound healing. However, the use of piezoelectric materials in this therapy has limitations, such as the inability to dynamically match cell activity and a lack of anti-infection properties. These issues restrict its wider clinical application. In this work, they prepared a piezoelectric dual network nanofiber dressing (CuEG/PVDF) using copper/epigallocatechin 3-gallate (Cu^{2+}/EGCG) and PVDF. *In vivo* experiments demonstrated that this dual-network piezoelectric dressing reduces the

https://doi.org/10.1021/acs.chemrev.4c00996
Chem. Rev. XXXX, XXX, XXX−XXX

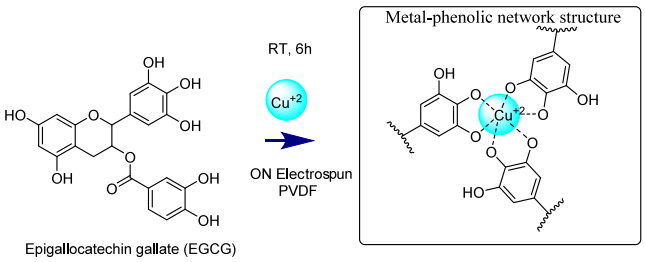

Figure 7. Piezoelectric dual network dressing using copper/epigallocatechin 3-gallate (Cu^{2+}/EGCG) and PVDF electrospinning technology.

inflammatory response, eliminates Methicillin-resistant *S. aureus* (MRSA), and accelerates wound repair.[35]

In 2024, Hu et al. developed an innovative wound dressing. Effective wound healing requires a contamination-free, sterile, and breathable environment. However, creating an ideal wound dressing that incorporates all these functionalities simultaneously presents significant challenges. In their work, they designed a wound dressing that mimics the structure of skin, offering both breathability and protective features. The dressing consists of a hydrophilic membrane made from Poly(3-hydroxybutyrate-*co*-4-hydroxybutyrate) (P34HB), which is coated with zinc oxide nanoparticles, and a hydrophobic PVDF membrane (Figure 8). To enhance the bonding between these two layers, plasma treatment was applied, resulting in a 60% improvement in mechanical properties. The cross-linked fibrous membranes demonstrated uniform stress distribution during stretching. Thanks to its unique structure, the wound dressing effectively manages wound exudate, possesses antibacterial properties, and promotes hemostasis. The hydrophobic layer directs wound exudate toward the hydrophilic layer, while the zinc oxide nanoparticles serve as a barrier against external bacteria and release zinc ions to inhibit bacterial growth in the exudate. Additionally, the water vapor transmission rate (WVTR) was measured at over 86.55 kg/m^2/day, the hemolysis rate was 2.38%, and an impressive healing rate of 81.98% was recorded during in vitro wound healing tests. This skin-mimicking wound dressing has great promise as a potential solution for the treatment of chronic wounds and infections.[36]

A hybrid air filter was developed incorporating three key layers: filtration, heating, and thermal insulation. The filtration layer is made from an 8 wt % polyacrylonitrile (PAN) material, which is produced through electrospinning. This layer is effective at capturing airborne particles that are less than 1.0 μm in diameter. The heating layer consists of a copper-plated microfiber mat, created by electroplating electrospun PAN nanofibers with a solution of copper sulfate, sulfuric acid (H_2SO_4), hydrochloric acid (HCl), and formaldehyde. This layer allows the air filter to reach temperatures exceeding 100 °C when voltage is applied, effectively incapacitating *E. coli* bacteria. Finally, the thermal insulation layer is made from PTFE and features a mesh size of 0.75Φ, measuring 300 mm^2 by 500 mm^2. This layer serves to prevent heat from being transferred directly to human skin.[37]

Li and colleagues developed a triblock copolymer consisting of poly(2-(dimethylamino)ethyl methacrylate), poly(poly-(oligo ethylene glycol) methyl ether methacrylate), and poly(dodecafluoroheptyl methacrylate) (PDMAEMA-*b*-PEGMA-*b*-PDFHMA) through reversible addition−fragmentation chain transfer (RAFT) polymerization followed by quaternization (Scheme 6). Their research demonstrated that the combination of fluoropolymer and PEG resulted in remarkable antiadhesion and antibacterial properties against *S. aureus* and *E. coli*, as well as effective antifouling capabilities on platelets and red blood cells. Additionally, the SPCA hydrogel exhibited strong adhesion to various surfaces, including plastic, wood, glass, PTFE, nitrile gloves, and aluminum, thereby improving the antifouling characteristics of the coating.[38]

Xue Li and colleagues developed a fluoro-copolymer aggregate coating that exhibits hydrophobic characteristics and facilitates rapid coagulation. This coating is associated with reduced blood loss, minimal secondary bleeding, and limited bacterial infiltration. The multifunctional, temperature-responsive fluoropolymer aggregate coating demonstrates antifouling, antibacterial, and hemostatic properties, indicating significant potential for biomedical applications. The block copolymer used in this research is quaternized poly(N,N-dimethylami-

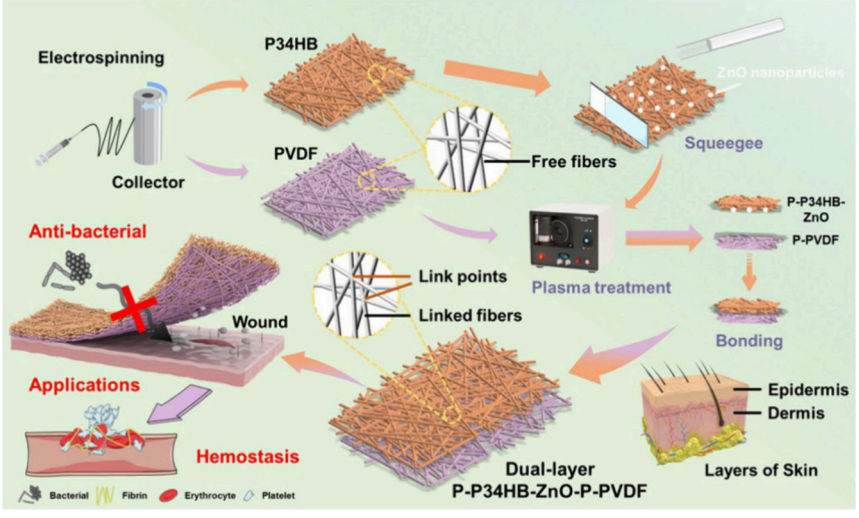

Figure 8. Processes of fabrication of skin-inspired dual-layer P−P34HB-ZnO-P-PVDF and applications.. Reproduced with permission from ref (36). Copyright 2024 Elsevier Inc.

https://doi.org/10.1021/acs.chemrev.4c00996
Chem. Rev. XXXX, XXX, XXX−XXX

Scheme 6. Route for the Synthesis of PDMAEMA-b-PEGMA-b-PDFHMA Triblock Copolymers Using RAFT Polymerization and Quaternization of PDMAEMA Block to Form QPDMAEMA-b-PEGMA-b-PDFHMA

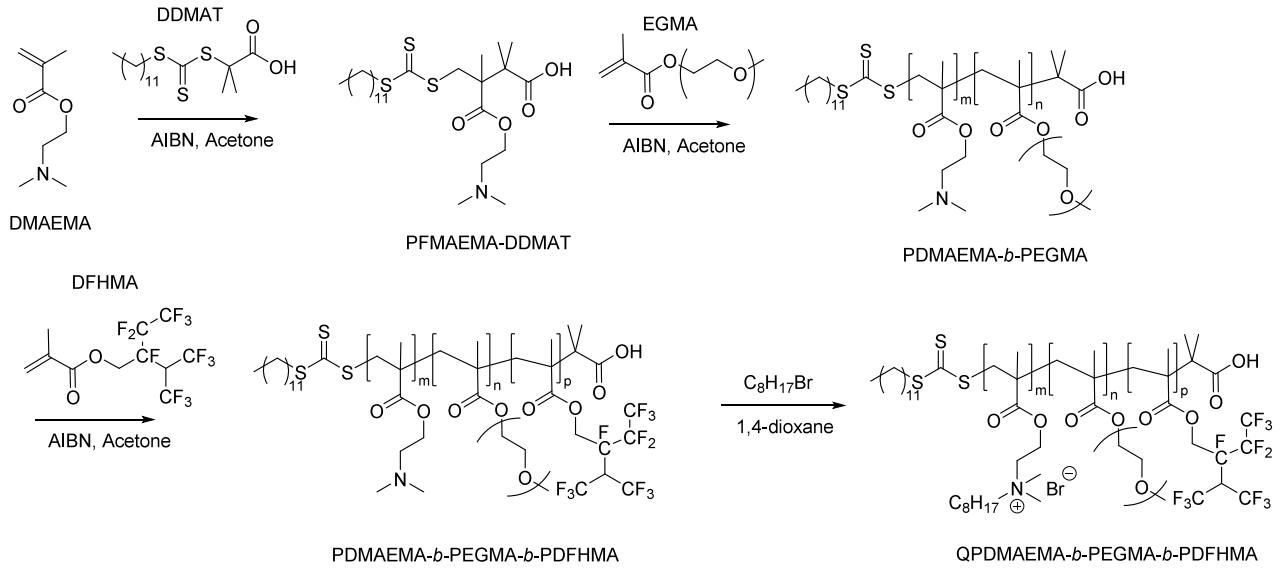

Scheme 7. Synthesis Route of $PDMA_7$-*b*-$PFOEMA_{20}$ via RAFT Polymerization

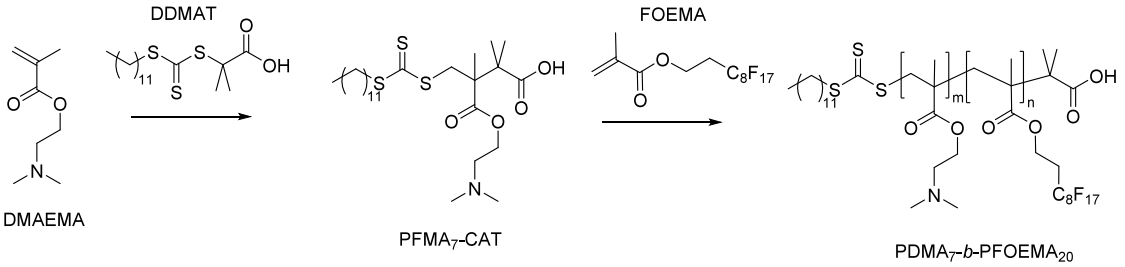

noethylmethacrylate)-b-poly(1H,1H,2H,2H-heptadecafluorodecyl acrylate) (PDMA-b-PFOEMA) (Scheme 7).[39]

Sung et al. developed a TENG featuring a two-layer structure (Figure 9). One layer consists of PTFE, which serves as the contact material connected to a gold electrode. The other layer is made of a conductive and triboelectric combination of chitosan and glycerol. This innovative electroactive dressing not only has the potential to enhance wound healing but also allows for noninvasive, real-time monitoring of the healing process. As such, it represents a promising advancement in device-based dressings for wound management in telemedicine.[40]

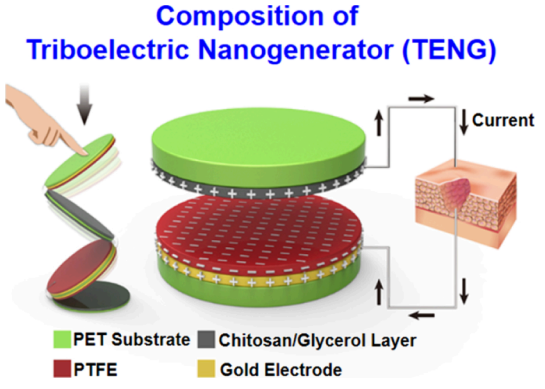

Figure 9. TENG composition with a PET substrate, gold electrode, and PTFE and chitosan/glycerol as triboelectric layers. Reproduced with permission from ref (40). Copyright 2022 Elsevier Inc.

The treatment of diabetic foot ulcers (DFUs) presents significant challenges. Researchers led by Ghosh have developed an innovative solution: a composite dressing that incorporates a conducting hydrogel made from carbonized polydopamine, polydopamine, and polyacrylamide, along with an electroactive electrospun PVDF membrane. This dressing can generate electrical impulses in response to biomechanical activities. The result is a self-powered, wearable, multifunctional, adhesive, and antibacterial dressing designed to enhance wound healing in cases of impaired repair. The biocompatible PTENG dressing was shown to promote the proliferation of fibroblasts and the formation of endothelial networks. Evidence indicates that it accelerates wound healing by facilitating faster closure, re-epithelialization, and the regeneration of blood vessels and hair follicles. This dressing effectively combines the benefits of moist wound care with electrical stimulation to promote healing.[41]

Wang et al. conducted tests on various adherends to assess the versatility of the stitching polymer polyurethane-Lysine-Dopamine (PU-LDA). The materials evaluated included glass, mica, stainless steel, Al_2O_3, CuO, PP, expanded polystyrene (EPS), PET, polyvinyl chloride (PVC), PMMA, PTFE, as well as biological tissues such as bovine bone, porcine skin, and liver. The catechol-containing PU-LDA polymer demonstrated the ability to adhere to these diverse surfaces through various mechanisms, including hydrogen bonding with inorganic

https://doi.org/10.1021/acs.chemrev.4c00996
Chem. Rev. XXXX, XXX, XXX−XXX

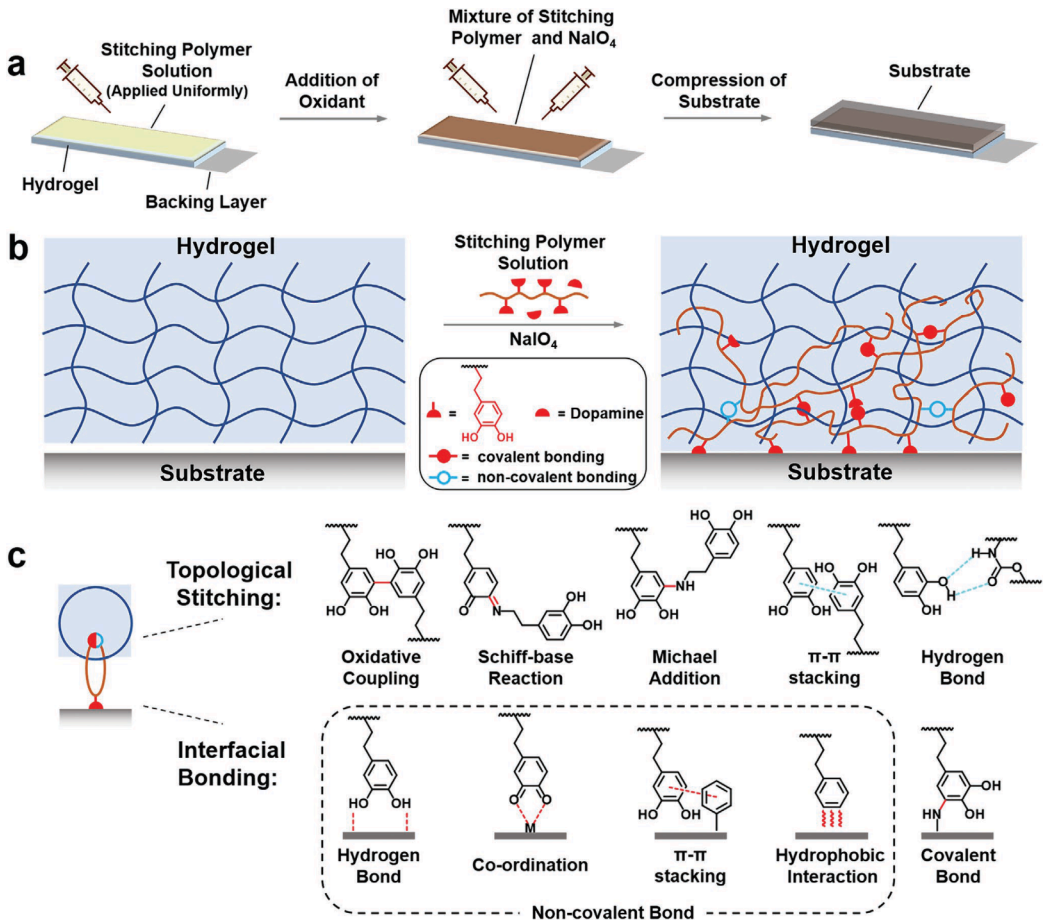

Figure 10. Principle of the topological stitching strategy. (a) Schematic of experimental procedure of the stitching strategy. (b) Mechanism of the topological stitching strategy. (c) Representative interactions in topological stitching and interfacial bonding. Reproduced with permission from ref (42). Copyright 2021 John Wiley & Sons Inc.

silicates, coordination with metal ions, $\pi-\pi$ stacking or hydrophobic interactions with polymers that have benzene rings or long alkane chains, and covalent bonding with amino groups in living tissues (Figure 10).[42]

An electrogenerative dressing (EGD), which combines triboelectric nanogenerators with negative-pressure wound therapy (NPWT), was found by researchers to enhance wound healing. The TENG consists of multiple layers, including two friction layers made of aluminum (Al) and PTFE, two support substrates of PET, two electrode layers of Cu and Al, a spacer layer, and an encapsulation layer made of Kapton (a type of polyimide tape). The use of EGD significantly accelerates wound closure and improves the quality of the healing process, resulting in skin tissue that is more mature, better able to withstand external forces, less prone to secondary damage, and with reduced scarring. This innovation holds promise for applications in diabetic dermatology.[43]

Zhang et al. developed a plant-inspired hydrogel composed of polyacrylamide, soybean protein isolate, and pyrogallol/borax (PAM-SPI-P/B) using an environmentally friendly method. This method relies on dynamic coordination cross-linking between pyrogallol and borax. The adhesion strengths of the PAM-SPI-P/B (1:2) hydrogel were tested on various substrates, yielding the following average values: wood (68.0 ± 3.0 kPa), steel (42.7 ± 2.52 kPa), glass (29.0 ± 2.0 kPa), poly(vinyl alcohol) (PVA) (22.0 ± 2.65 kPa), PTFE (15.2 ± 3.51 kPa), and porcine skin (34.3 ± 2.51 kPa). The obtained hydrogels also exhibited good antibacterial activities against *E. coli* and *S. aureus*. They envision that the PAM-SPI-P/B hydrogels have great potential for use in biomimetic tissues and biosensors.[44]

Hu and colleagues have developed an electroactive hydrogel composed of polyacrylonitrile-acrylamide-styrene sulfate-poly (vinylidene fluoride) (PAAN−PVDF). This hydrogel exhibits impressive stretchability of approximately 380% and ductility similar to human skin, with a Young's modulus of 0.48 ± 0.03 MPa, comparable to the range of human skin (0.5−1.95 MPa). The strength of the composite hydrogel is enhanced by dipole−dipole interactions between acrylonitrile and PVDF, which also improves its piezoelectric properties. Notably, the PAAN−PVDF hydrogel (15%) demonstrated stable and sensitive mechanical-electric responses. The study found that this hydrogel could promote in vitro angiogenesis when subjected to piezoelectric stimulation and possesses good biocompatibility, indicating its potential for facilitating the formation of fine blood vessels in areas affected by pressure injuries or ulcers (PIs/PUs). Additionally, finite element analysis and pressure dispersion experiments confirmed that the hydrogel effectively prevents PIs/PUs by redistributing forces, minimizing tissue distortion, and preserving the skin's microenvironment.[45]

Nanofibrous membranes composed of PVDF and poly(2-methacryloyloxyethyl phosphorylcholine-co-methacryloylox-

https://doi.org/10.1021/acs.chemrev.4c00996
Chem. Rev. XXXX, XXX, XXX−XXX

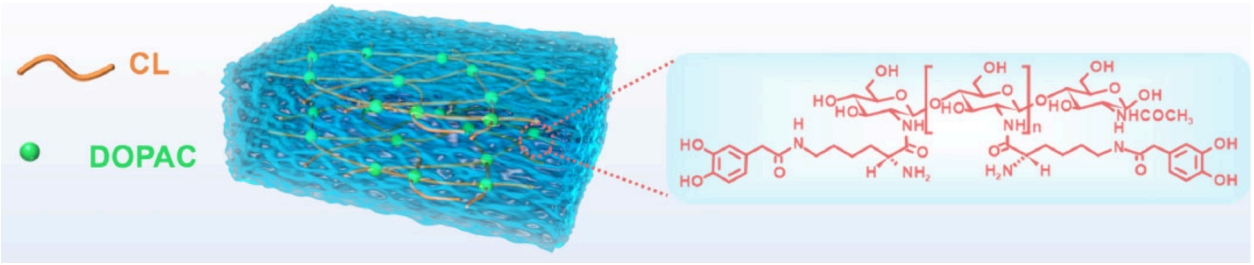

Figure 11. Preparation of CLD hydrogel wound dressing. Reproduced with permission from ref (51). Copyright 2023 Elsevier Inc.

yethyl butylurethane) (PMBU) have been developed to enhance the healing of both acute and chronic wounds. The polymer solutions for electrospinning were created by combining the PMBU copolymer with PVDF in a solvent mixture of dimethylformamide (DMF) and acetone in a 6:4 volume ratio. The PVDF concentration was maintained at 20 wt %, while the PMBU content varied at 0, 1, 3, or 5 wt %. The inclusion of the zwitterionic copolymer in the membranes was found to facilitate the wound healing process by reducing inflammation, promoting cell proliferation, and aiding in the formation of a smooth and thin outermost layer of skin, known as the stratum corneum.[46]

Hillig and colleagues investigated the strong adhesion of *Listeria monocytogenes* to food contact surfaces, which heightens the risk of cross-contamination. They focused on effective cleaning and disinfection methods, as well as sampling strategies for early detection to prevent food contamination. Their research assessed the effectiveness of three swab materials—cotton, viscose, and nylon-flocked—for detecting *L. monocytogenes* on food contact surfaces (100 cm^2). The findings indicated that cotton swabs were optimal for sampling stainless steel and PVC surfaces, while viscose or nylon-flocked swabs were best for PTFE and HDPE surfaces.[47]

Wang and colleagues developed bilayered drug-loaded fiber membranes made of PVDF for the bottom layer and disulfiram (DSF)/polylactic acid (PLA) for the top layer. They enhanced the wettability of the top surface through oxygen plasma modification. These membranes exhibited significant antibacterial activity against both *E. coli* and *S. aureus*. The hydrophilic PLA surface promotes cell adhesion and proliferation, while the hydrophobic PVDF layer protects against waterborne microorganisms, thereby preventing infection.[48]

Liu, Ge, and their team created a self-powered nanocomposite wound repairer that integrates a film made from 2-hydroxypropyltrimethylammonium chloride chitosan (HTCC), alginate (ALG), and poly dopamine/Fe^{3+} nanoparticles (PFNs) with a motion-driven self-powered nanogenerator (SN). The friction layers of the power supply module are made from Al and PTFE, which have distinct triboelectric properties. PTFE gains electrons easily, while Al loses them.[49]

Chen and colleagues from Jiangsu University produced a PVDF/tea polyphenol (TPs) composite thin film using an electrically assisted 3D printing method. The addition of 0.1 g of TPs resulted in the highest crystallinity (44.32%) and β-phase content (33.29%). The TPs created holes that facilitated the deposition of silver nanoparticles on the surface. With 0.9 g of TPs, the composite thin film achieved a 97.22% inhibition rate against *E. coli*, while the PVDF/TPs/Ag composite thin film reached 99.58%.[50]

He, Cui, and their team developed a method to modify surfaces including fluoropolymers. Their chitosan dihydroxyphenylacetic acid (DOPAC) polymer enables rapid self-healing and strong adhesion for tissue and wound dressings (Figure 11). Their tensile adhesion tests revealed the highest bonding strengths of the hydrogel to various materials, including ceramics, PTFE, wood, and pig tissues, with values ranging from 0.88 to 88.64 kPa.[51]

Chenand colleagues developed a soluble hemostatic spacer dressing designed for wound healing. This dressing consists of three layers: a skin contact layer made from a braided yarn of PTFE (core) and carboxymethylated viscose (shell), a spacer layer of nylon monofilament (core) wrapped in Coolmax (shell), and a waterproof layer made from UHMWPE yarn. The carboxymethylated viscose effectively stops bleeding, while PTFE provides low adhesion and maintains the structural integrity of the dressing. The nylon monofilament enhances comfort, resilience, and fatigue resistance, while Coolmax aids in blood absorption. Additionally, the sodium carboxymethyl cellulose in the dressing releases negative ions that activate the coagulation system, and the spacer filaments help concentrate coagulation factors at the wound site.[52]

Li and colleagues developed a fluorinated, biocompatible, superhydrophobic coating for medical wound dressings to enhance their antibacterial and hemostatic properties. This coating is made from multifunctional antibacterial composite nanoparticles derived from acrylic acid (AA), 1*H*,1*H*,2*H*,2*H*-perfluorododecyl acrylate (PFDA), and poly(hexamethylene biguanide) hydrochloride (PHMB) (Scheme 8). The resulting PAA-*co*-PFDA/PHMB composite nanoparticles can be applied to various substrates, forming transparent coatings that exhibit strong antibacterial activity against *E. coli* and *S. aureus*. When the fluorine content reaches 5.0 wt %, these composite nanocoatings become superhydrophobic and demonstrate rapid coagulation capabilities, effectively preventing blood loss and secondary bleeding.[53]

Vinault et al. have developed an ideal wound dressing characterized by high porosity, which facilitates gas exchange and drainage of exudates. This dressing promotes a moist healing environment, prevents bacterial adhesion to reduce infection risk, and resists the attachment of human cells, making it nonsticky. The dressing is composed of nanofibers made from PVDF and a zwitterionic copolymer, zP(S-*r*-4VP), synthesized from 3-iodopropionic acid and a polystyrene/poly(4-vinylpyridine) polymer. Compared to standard PVDF, the PVDF/zP(S-r-4VP) nanofibers exhibit enhanced hydration capacity, resulting in significant reductions in fibrinogen (75%), *P. aeruginosa* (over 90%), *S. aureus* (over 80%), *E. coli* (over 95%), whole blood cells (over 95%), as well as L929 cells (85%).[54]

https://doi.org/10.1021/acs.chemrev.4c00996
Chem. Rev. XXXX, XXX, XXX−XXX

Scheme 8. Multifunctional Antibacterial Composite Nanoparticles Derived from Acrylic Acid (AA), 1*H*,1*H*,2*H*,2*H*-Perfluorododecyl Acrylate (PFDA), and Poly(hexamethylene biguanide) Hydrochloride (PHMB)[a]

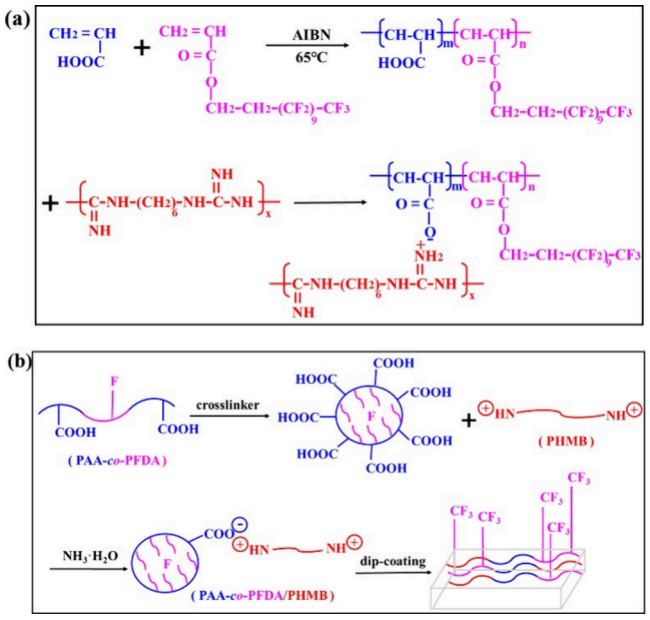

[a]Reproduced with permission from ref (53). Copyright 2022 Elsevier Inc.

Hu et al. have designed a skin-like wound dressing featuring a hydrophilic healing interlayer and a hydrophobic protective surface, also based on PVDF. The dressing incorporates polyvinyl butyral (PVB), dimethylformamide (DMF), lithium chloride (LiCl), and polysorbate (Tween-20). It demonstrates impressive mechanical properties, including a tensile strength of 25.9 MPa, toughness of 12.2 MJ/m^3, and a water vapor transmission rate (WVTR) exceeding 17.4 kg/(m^2·d). The dressing also has a high absorption capacity of 4.2 mL/s, a pore filtration efficiency of 99.9%, excellent biocompatibility, and a faster scratch healing rate compared to the commercial product Nexcare. Its mechanical properties are comparable to human skin, with a tensile strength of 21.6 ± 8.4 MPa and a failure strain of 54 ± 17%.[55]

Freire et al. developed dual-function API-ILs by transforming analgesic and anti-inflammatory drugs, resulting in a remarkable increase in water solubility—up to 470 times—without compromising their cytotoxicity (Table 2). These API-ILs were integrated into a bilayer wound dressing, which consists of a hydrophobic PVDF membrane that serves as a drug reservoir and a biocompatible hyaluronic acid (HA) layer. The PVDF membrane provides essential mechanical stability, while the HA layer promotes fibroblast cell proliferation, migration, and adhesion. Importantly, the PVDF/HA membranes do not activate macrophages, indicating their immunological safety and biocompatibility. The study demonstrated that the membranes loaded with API-ILs exhibit an anti-inflammatory effect on LPS-activated macrophages like that of the original APIs. Additionally, both unloaded and loaded membranes do not adversely affect fibroblast proliferation and migration in vitro, suggesting a favorable safety profile for their use as effective transdermal drug delivery systems.[56]

Table 2. PVDG and PVDF/HA Membrane Uptake of API-ILs, Noncharged APIs, and API Sodium Salts

		PVDF (Uptake ± σ)%	PVDF/HA (Uptake ± σ)%
API-ILs	[Lido][Ibu]	15.8±0.5	13.9±0.3
	[Lido][Nap]	16.1±0.3	14.2±0.1
	[Lido][Diclo]	16.3±0.3	14.4±0.2
API sodium salts	Lidocaine.HCl	3.7±0.1	3.2±0.4
	Ibuprofen.Na	19.1±0.2	17.2±0.3
	Naproxen.Na	19.7±0.3	17.7±0.4
	Diclofenac.Na	20.3±0.2	18.5±0.5
Noncharged APIs	Lidocaine	5.7±0.5	5.1±0.6
	Ibuprofen	20.6±0.4	18.7±0.5
	Naproxen	21.2±0.5	19.1±0.4
	Diclofenac	21.7±0.6	19.5±0.3

Amini et al. developed a membrane composed of PVDF nanofibers, which provide tensile strength, and polyhydroxybutyrate/chitosan (PHB/CTS) nanofibers loaded with gentamicin for controlled drug delivery. This membrane is particularly suitable for treating postsurgical ulcers. The drug release profile indicated that increasing the CTS ratio enhances drug delivery, with gentamicin being released in a sustained manner over approximately 1 week.[57]

Abadi and colleagues investigated electrospun dressings made from a 2:1 (w:w) blend of PVDF and starch, which exhibited mechanical properties ideal for wound dressing applications. Electrospinning is an efficient method for creating wound dressings from various natural and synthetic materials. In their study, they prepared PVDF and starch composite mats containing ciprofloxacin (CIP) loaded onto titanium dioxide nanoparticles (TiO_2) (Figure 12). The release rate of CIP indicated that around 40% of the drug was released within the first 2 days. Additionally, the antibacterial effectiveness of the dressings was tested against *E. coli* and *S. aureus*, revealing clear zones of inhibition around the samples on agar plates.[58]

Researchers developed a novel piezoelectric hydrogel scaffold (ZPFSA) by modifying PVDF with zinc oxide (ZnO) nanoparticles and combining it with sodium alginate (SA) using 3D printing technology. This ZPFSA scaffold features two piezoelectric response mechanisms: vertical swelling and horizontal friction. These mechanisms can simulate and enhance endogenous bioelectricity, thereby promoting wound healing and reducing scar formation (Figure 13). The PVDF component continuously responds to stress, generating electrical stimulation, while the SA serves as the structural support, allowing the PVDF to swell and stretch as it absorbs wound exudate. The uniformly distributed ZnO nanoparticles enhance the hydrophilic properties of the PVDF and provide effective antimicrobial activity.[59]

Zheng et al. developed a composite material by grafting ePTFE with a polyvinylpyrrolidone (PVP) brush, resulting in a hydrogel with an adhesion energy of approximately 80 kJ m^{-2}. This composite benefits from the ePTFE backing, which offers excellent breathability, water resistance, and a bacterial barrier, helping to maintain a moist wound environment and alleviate pain through water evaporation while preventing bacterial invasion due to its smaller pore size compared to most bacteria.[60]

Hu and colleagues created a wettable composite wound dressing featuring a hydrophobic PVDF outer layer and a

https://doi.org/10.1021/acs.chemrev.4c00996
Chem. Rev. XXXX, XXX, XXX−XXX

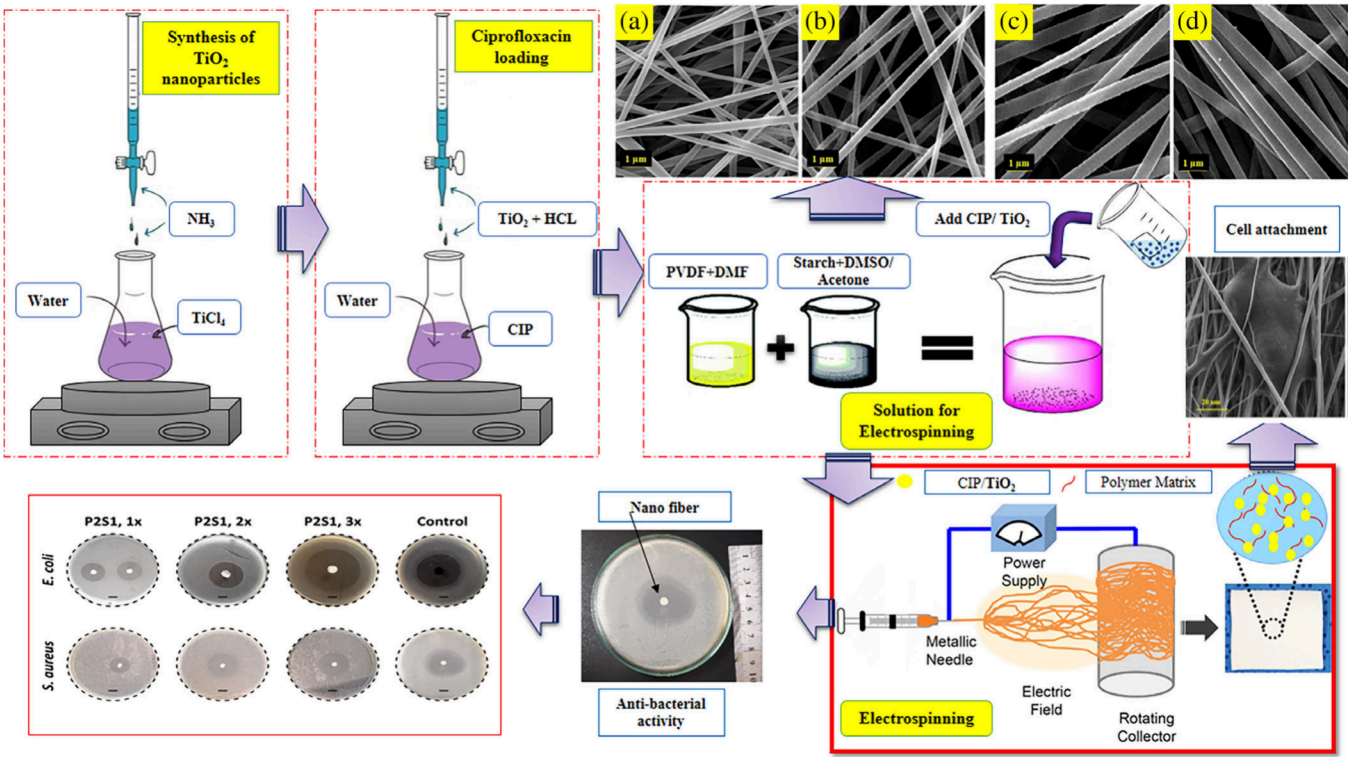

Figure 12. Electrospun dressings made from a 2:1 (w:w) blend of PVDF and starch. Reproduced with permission from ref (58). Copyright 2020 John Wiley & Sons Inc.

hydrophilic layer of polydopamine (PDA) coated silver nanoparticles (Ag NPs)/PVDF (PVDF-Ag-PDA) using electrospinning and PDA coating. The hydrophilic PVDF-Ag-PDA layer effectively reduces bacterial growth, while the hydrophobic PVDF layer prevents bacterial adherence due to its small pore size. Cytotoxicity tests indicated that the PVDF/PVDF-Ag-PDA combination maintains high cell viability (over 80%), attributed to the thin PDA layer mitigating the cytotoxic effects of Ag NPs.[61]

Dzhimak and colleagues introduced Fluorex, a polyester thread with a fluoropolymer coating. The interaction mechanism with Ag nanoparticles involves the participation of carbonyl and ester group oxygens. This Ag gel, containing silver nanoparticles, has promise for treating sutures immediately after wound closure, potentially preventing proinflammatory complications, especially with polymer suture materials used in emergency surgeries. It is particularly suitable for natural suture materials or those with chemically inert coatings.[62]

Gómez-Gil and researchers noted that titanium coatings or PVDF interwoven with PP in hybrid meshes did not prevent adhesions. Hybrid meshes combining polypropylene with PVDF, a highly inert polymer with superior long-term stability and low inflammatory response, are of particular interest. Titanium-coated polypropylene meshes are also considered hybrid due to titanium's excellent biocompatibility and minimal inflammatory reaction, making it suitable for implantation in various locations. However, when in contact with the visceral peritoneum, these implants may still lead to complications such as adhesion formation or intestinal fistulas.[63]

Heise and colleagues emphasized the importance of material geometry for biocompatibility. Modifying the geometry of foreign materials can influence foreign body granuloma formation and inflammatory responses. They found that profiled (snowflake) sutures resulted in significantly smaller foreign body granulomas compared to standard sutures. PVDF, being a newer polymer for textile implants, demonstrated superior biocompatibility. Their study indicated that geometry-modified multifilament PVDF sutures have improved foreign body and inflammatory reactions compared to commercially available sutures like Mersilene and Prolene.[64]

Taniguchi et al. described a "multiple-knot" technique for chordal replacement using ePTFE to correct anterior mitral leaflet prolapse. This technique involves tying multiple knots until the suture reaches the free edge of the normal leaflet, addressing challenges such as achieving the correct chord length and preventing ePTFE slippage. Their findings indicated that this technique yields intermediate-term outcomes comparable to previous reports, although a 26 mm annuloplasty was associated with a higher mitral valve gradient at rest. More than half of the patients who underwent this repair experienced a mean pressure gradient greater than 5 mmHg during late follow-up, potentially linked to postoperative functional mitral stenosis (Figure 14). Two patients experienced recurrent mitral regurgitation due to degenerative changes unrelated to the procedure. The 5-year freedom rate from recurrent mitral regurgitation was 94 ± 4%. Stepwise logistic regression analysis identified the use of a full ring (odds ratio 8.9; 95% confidence interval 1.2−64; p = 0.031) and a 26 mm annuloplasty (odds ratio 7.5; 95% confidence interval 1.1−50; p = 0.037) as significant independent risk factors for a mean pressure gradient exceeding 5 mmHg. The conclusion was that the intermediate-term outcomes of the original chordal replacement technique are comparable to previously reported results.[65]

https://doi.org/10.1021/acs.chemrev.4c00996
Chem. Rev. XXXX, XXX, XXX−XXX

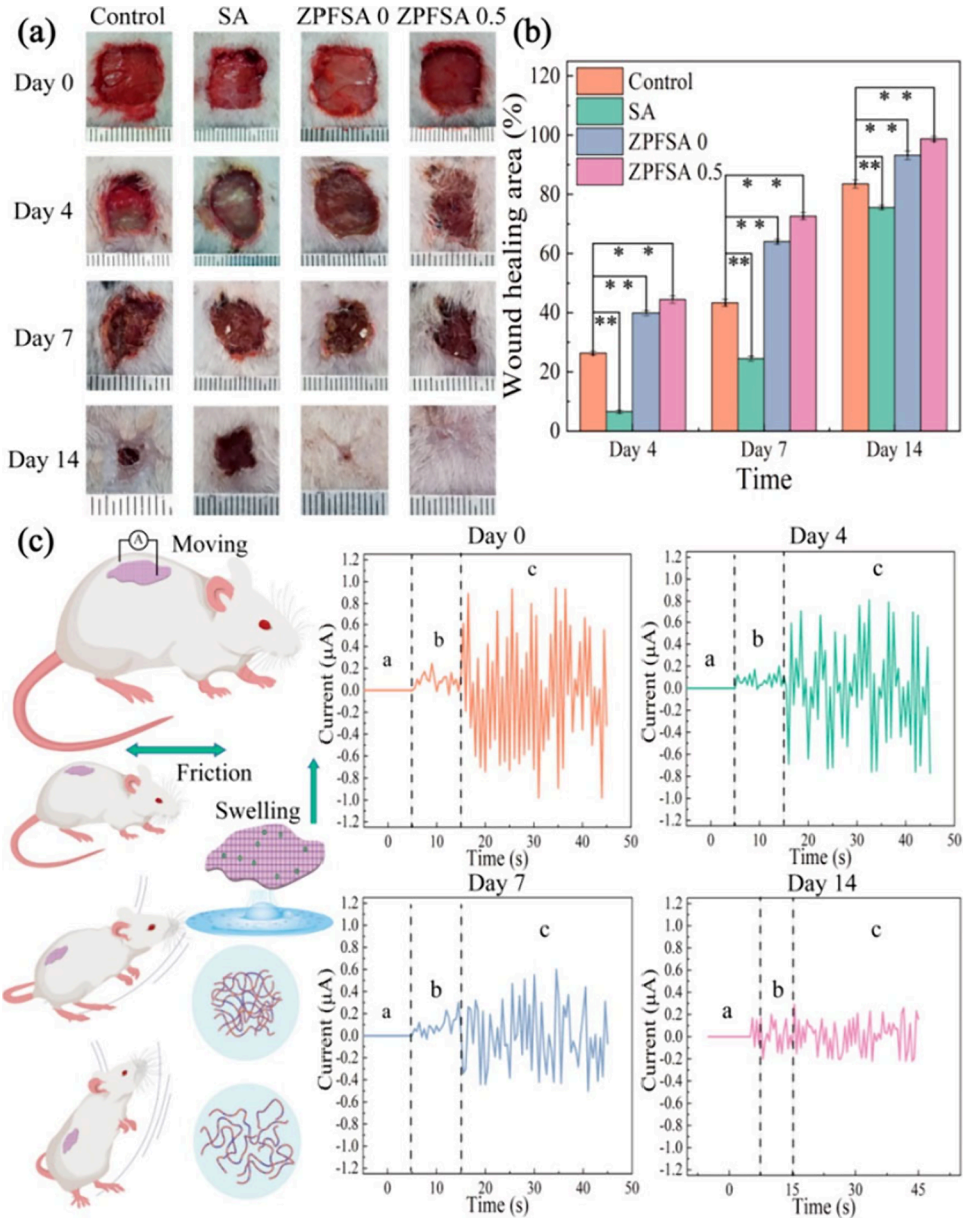

Figure 13. Novel piezoelectric hydrogel scaffold (ZPFSA) by modifying PVDF with zinc oxide (ZnO) nanoparticles and combining it with sodium alginate (SA) using 3D printing technology. Reproduced with permission from ref (59). Copyright 2022 American Chemical Society.

The fabrication process for superamphiphobic paper is illustrated in Figure 15. Initially, TiO_2 nanoparticles, water, and fluorocarbon surfactant were mixed in ethanol and sprayed coated onto PTFE−PVDF paper using an airbrush. During the spraying process, the solution was atomized and evenly adhered to the substrate. The high temperature of the substrate allowed the liquid to solidify rapidly, creating a uniform superamphiphobic coating that maintained the Cassie state for both water and hexadecane. Researchers also discovered that PTFE−PVDF papers with varying pore sizes, as well as nylon paper, fiberglass, metal mesh, and fabric, could serve as suitable substrates for flexible superamphiphobic surfaces. Researchers believe that this method, which combines spraying and solidification on paper substrates, represents a significant advancement in the accessible and efficient fabrication of flexible superamphiphobic surfaces. This technique has broad applications, including petroleum extraction, chemical transport, anticorrosion measures, breathable self-cleaning medal gauze, and droplet-based analyzers and sensors.[66]

1.3. Drug Delivery

Drugs can be delivered and made highly bioavailable through a polymer matrix, allowing for simple administration, slow release, and reduced side effects but typically require toxic solvents or high temperatures which potentially can lead to drug degradation. Rao et al. sought to utilize a one-pot polymerization methodology with supercritical CO_2 as a solvent to control particle formation of biodegradable polymers. Fluorolink D10H was used as the central link between -Caprolactone (CL) and P-Dioxanone (PDO) to create a stabilizer for polymerization (Scheme 9). PPDO was synthesized in the presence of paclitaxel (PTX) and sCO_2 to form drug-loaded microspheres which are used with the surfactant still present. The fluorinated surfactant was chosen due to its low melting point and CO_2-philicity, in addition to

https://doi.org/10.1021/acs.chemrev.4c00996
Chem. Rev. XXXX, XXX, XXX−XXX

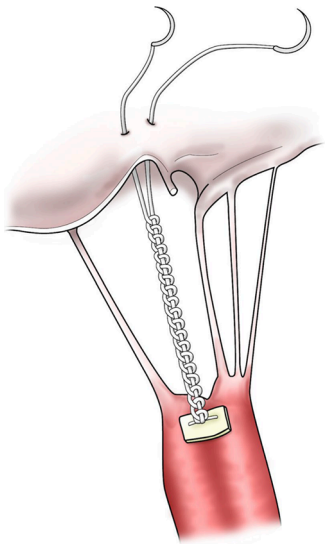

Figure 14. A simple chordal replacement technique for anterior mitral leaflet prolapse. A double-armed 4−0 polytetrafluoroethylene (CV4 [Gore-Tex]) suture is passed twice through the most fibrous part of the papillary muscle and multiple knots are tied. The two arms of the suture are then The two arms of the suture are then passed through the thickened free edge of the prolapsed cusp from the ventricular side to the atrial side, allowing the ends to be tied together without slippage. Reproduced with permission from ref (65). Copyright 2019 Springer.

the relative nontoxicity of PFPAEs. Polymerizations were conducted at body temperature (37 °) and 9 MPa pressure, which provides the smallest particle size (5 μm) and highest yield of product (87%). These optimized conditions were used for the encapsulation of up to 5 wt % of PTX, with larger loadings of PTX displaying larger particle size (5 wt % provides 20 μm, 3 wt % provides 7 μm). Particles between 5 and 100 μm can fill pathological sites when injected, allowing for precise treatment of tumors and long-term sustained drug release, minimizing injections and patient discomfort. Encapsulation efficiencies are 80.1% for 3% PTX by weight and 85.0% for 5 wt % PTX. 25% of the drug is released after 7 days, and 50% after 30 days, allowing this to be a potential slow-release drug candidate.[67]

An LBL strategy for rapid drug release was developed by Zhang et al. utilizing a dual-stimulus methodology. Poly(*N*-isopyopyl) acrylamide (PNIPAM) becomes hydrophobic and collapses into clusters rather than chains if the temperature is higher than the Lower Critical Solution Temperature (LCST). Flexoelectric stimulation is introduced through a PVDF-HFP film, converting mechanical movement into electricity. Multilayered films incorporating positively charged poly(allylamine hydrochloride) in the forms of $(PAH/SiO_2)_5$-$(PAH\text{-}rGO/PNIPAM)_n$ were produced and assembled on a porous PVDF-HFP film (Figure 16). This porous film produces a voltage of 4.8 V and a current of 115 nA when exposed to rough finger tapping, while a smooth film produces a voltage of 1.5 V and a current of 32 nA. Mesoporous SiO_2 was used to hold the drug molecules, allowing the films to act as a drug reservoir. $(PAH/SiO_2)_5$ films are assembled with electrostatic interactions, which can then hydrogen bond to the $(PAH\text{-}rGO/PNIPAM)_n$ section on top of a PVDF-HFP base layer. Release of encapsulated methylene blue (MB) molecules shows an increase in release over 1 h by 539.5% with n = 20 films compared to no stimulation. Thermal stimulation only results in a 42% increase in release, and flexoelectric stimulation results in a 16.8% increase, indicating the dual-release system is a good candidate for selective drug delivery applications.[68]

Direct introduction of drugs into specific cells is highly desirable for precision therapeutics. Typical electroporation uses high-voltage pulses of electricity to open channels in the plasma membrane for introduction of molecules to cells directly. While effective, electroporation often causes irreparable damage to cells through heat and high voltage, making its clinical use quite limited. A hand-powered device consists of a TENG, a rectifier bridge, a silicon nanoneedle array electrode as the anode, and a stainless-steel electrode under the dorsal skin as the cathode (Figure 17). The disk TENG itself is a friction layer of copper strips layered radially, a layer of PTFE as another frictional layer, and a layer of copper strips as electrodes. One rotation of the device produces approximately 20 V and 4 μA. Fluorescein isothiocyanate-labeled dextran was successfully delivered, giving an efficiency of 86% for 10 kDa and 49% for 70 kDa, and a cell viability of 94%. Further, siRNA was able to be delivered with 82% delivery efficiency into MCF-7 cells. The TENG was connected to a volunteer's forearm skin and delivery drug release was achieved on-demand to the dorsal skin of a mouse attached to the needle array. Tissue cryosections reveal the labeled dextran penetrated much further into the skin (23 μm) compared to the flat electrode (11 μm) and the needle array without electrical stimulation (6 μm). The TENG-needle composite system was capable of delivery drugs over 3 times further than the needle height (7 μm), giving excellent penetration of the drug into tissue and indicating good potential for wearable drug-delivery devices.[69]

PTFE displays excellent properties for drug delivery devices, such as antiwetting by water or aqueous solutions, minimizing adsorption of the drug to the surface of the device. Researchers utilized a hollow needle array made of PTFE fabricated through a digital light processing (DLP)-based 3D printing process. The 3 × 1 hollow needle arrays were fabricated from a vat polymerization technique of a solution of PTFE (Figure 18) in the presence of a proprietary binder. The PTFE in this case does not undergo polymerization but rather is embedded in a photopolymerizable binder which is removed after printing by thermal annealing. The average needle height was 4.59 mm ± 0.03 mm from the planar orientation and 4.66 mm ± 0.01 mm from the top-down orientation. The needle possesses a reduced elastic modulus of 1.94 ± 0.22 GPa, and a hardness of 77.87 ± 6.53 MPa, which is appropriate for skin penetration and is similar to bulk PTFE. Methyl blue (MB) was successfully delivered as a model drug to surgically discarded human abdomen skin as determined by light microscopy. This suggests that DLP-based 3D printing is a good candidate for needle array production for vaccines and other drug delivery mechanisms.[70]

Paclitaxel coated balloon catheters (PCB) are a method of drug delivery as an alternative to drug-eluting stents which do not require implantation. Paclitaxel is useful in femoropopliteal peripheral artery disease when released from stents, delivering superior lipophilicity, good tissue retention, and antirestenotic properties, typically delivering a drug payload in minutes. Researchers examined coating micromorphology of PCB catheters and the effects on drug transfer in porcine femoral arteries, analyzing amorphous/flaky coatings on nylon, microcrystalline coating on nylon, and microcrystalline coating on

https://doi.org/10.1021/acs.chemrev.4c00996
Chem. Rev. XXXX, XXX, XXX−XXX

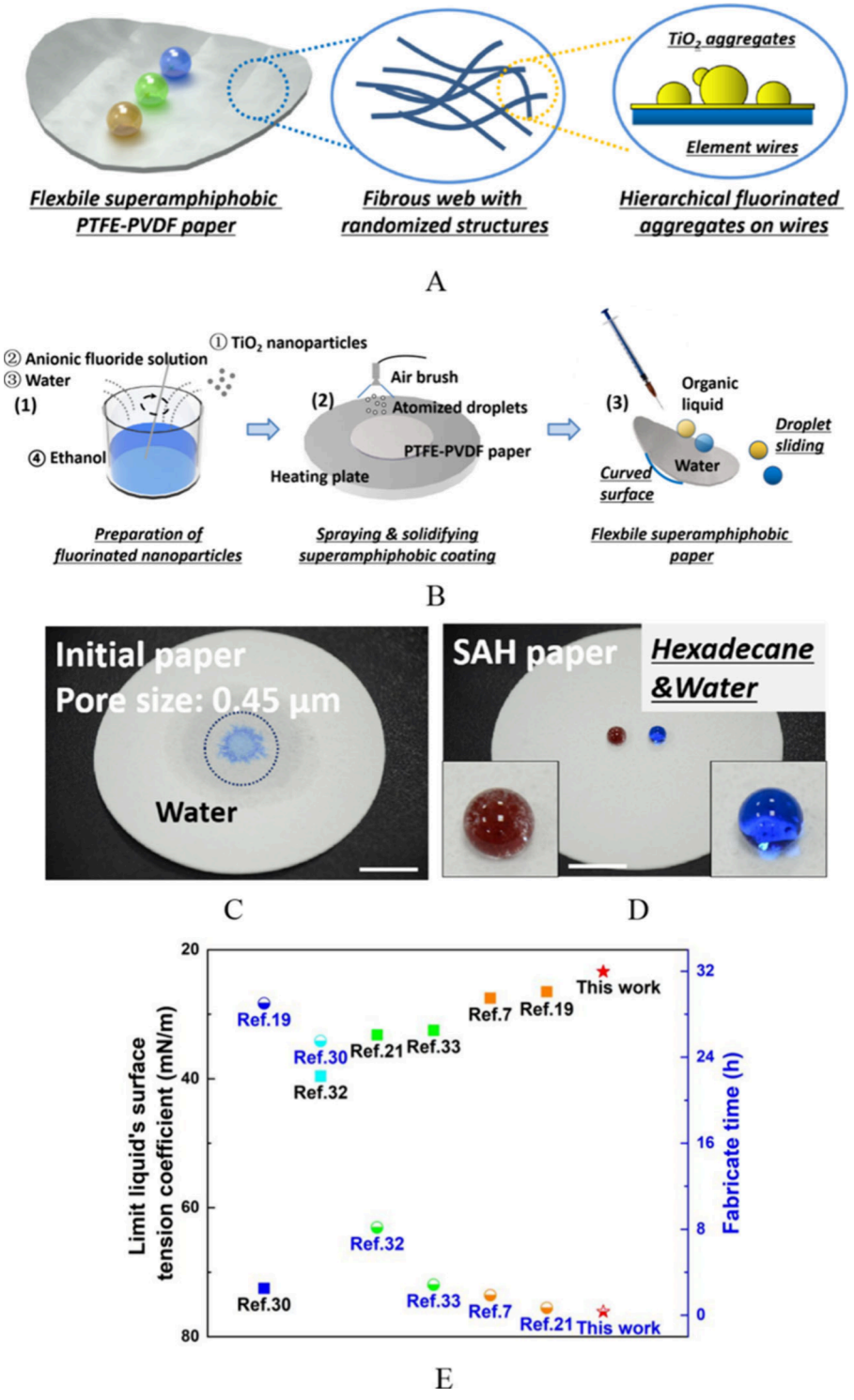

Figure 15. (A) The schematic of flexible superamphiphobic paper and (B) its fabrication method. Images of (C) a water droplet on the initial paper and (D) water and hexadecane droplets on the superamphiphobic paper. (E) Comparison of the surface's fabrication time and the limit liquid's surface tension coefficient between this work and some pioneering works. The scale bars in (C) and (D) are 1 cm, and the amplification factor of insets in (D) is 3.8. Reproduced with permission from ref (66). Copyright 2023 Springer.

ePTFE. The ePTFE surface displayed clear needle-shaped microcrystals, and the amorphous/flaky nylon surface presents as a cracked surface with microcrystals in the cracks. Microneedle coating was found to cover 1.5 times the area compared to amorphous/flaky coatings (16.1% vs 10.7%), and 1.5 times higher tissue concentration by MS (1933 vs 1298 μg/g) over 0.5 h. Better performance was shown by the micromorphologies that amplify angioplasty pressure such as microneedles. Development of safe and predictable PCB-like devices is expected to develop an understanding of endoluminal coating distributions and predict how the drug will be distributed in the body.[71]

Rabies is a deadly viral disease that approaches a 100% fatality rate once the virus reaches the central nervous system.

https://doi.org/10.1021/acs.chemrev.4c00996
Chem. Rev. XXXX, XXX, XXX−XXX

Scheme 9. Synthesis Procedure for P(CL-GA)-PFPE-p(CL-GA)[a]

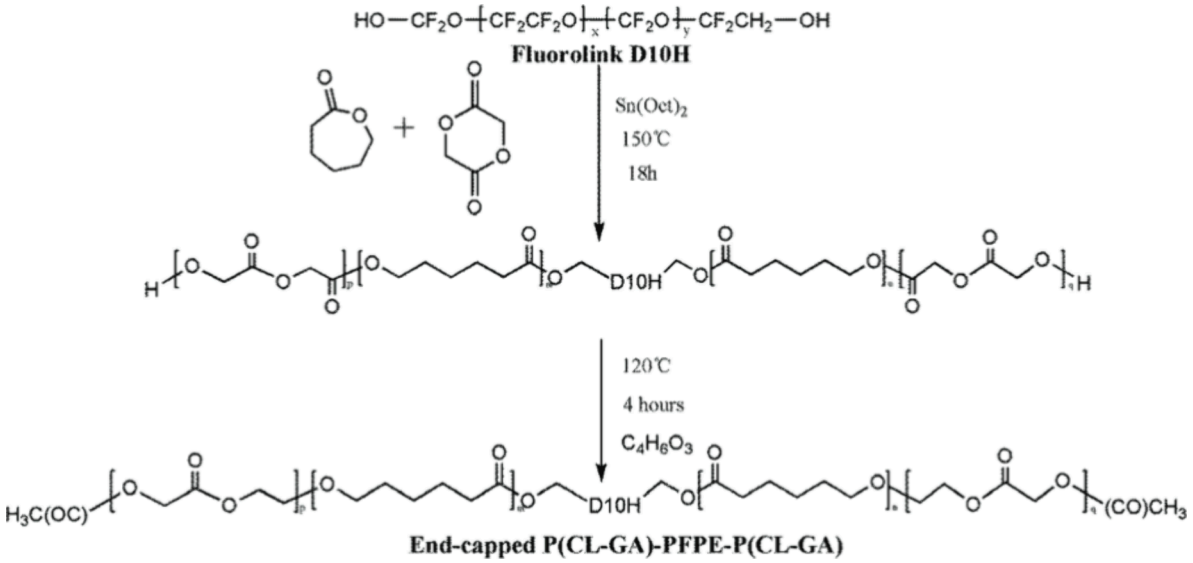

[a]Reproduced with permission from ref (67). Copyright 2020 Royal Society of Chemistry.

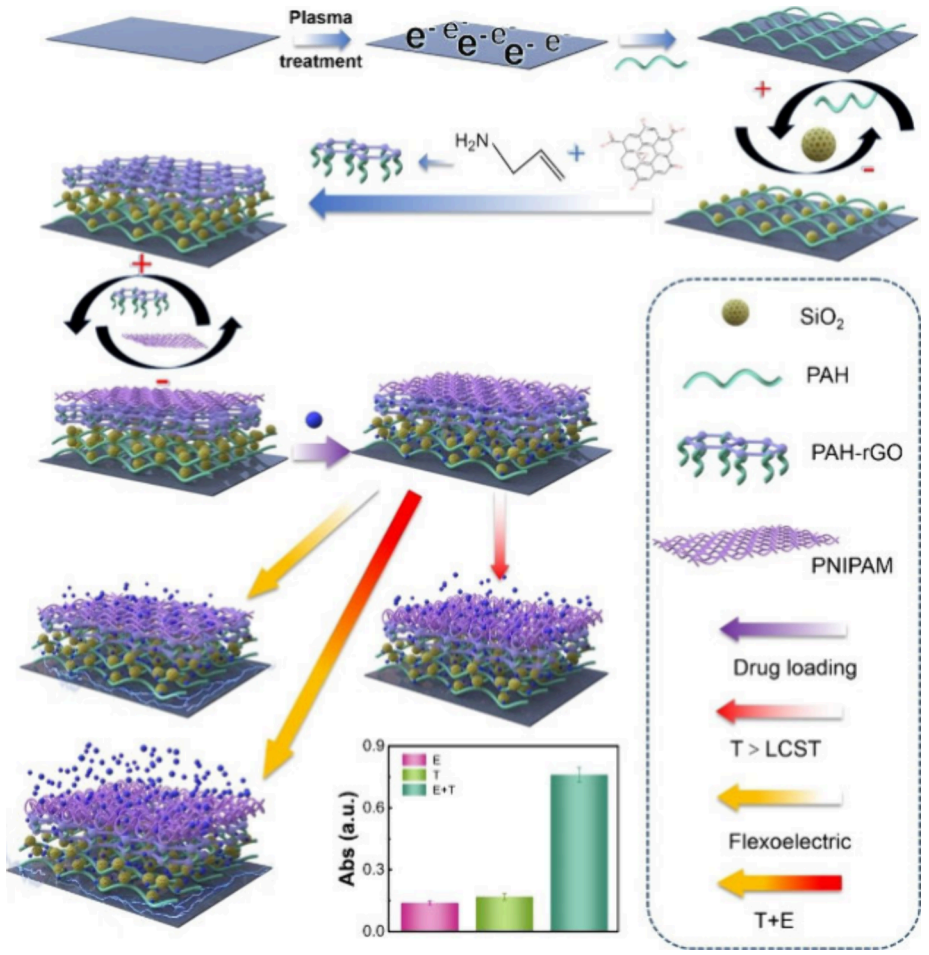

Figure 16. Fabrication process for $(PAH/SiO_2)_5$-$(PAH\text{-}rGO/PNIPAM)_n$ film on a piezoelectric PVDF-HFP film, and drug release behavior under flexoelectric and thermal stimuli. Reproduced with permission from ref (68). Copyright 2020 John Wiley & Sons Inc.

Researchers have developed a fluoropolymer-modified rabies nanovaccine (FiR NV) for improved vaccine delivery. Polyethylenimine (PEI), enhances the delivery of genes and proteins by increasing transmembrane activity, while the fluorinated variant (F13-PEI) reduces polymer toxicity and prevents protein denaturation, improving overall vaccine stability. FiR NVs are fabricated by combining fluorinated PEI (F13-PEI) with the inactivated rabies virus (iRABV)

https://doi.org/10.1021/acs.chemrev.4c00996
Chem. Rev. XXXX, XXX, XXX−XXX

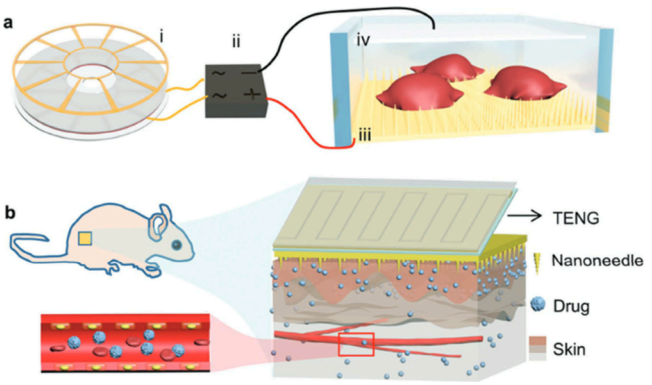

Figure 17. Schematic of TENG electroporation system (a) in vitro and (b) in vivo. Reproduced with permission from ref (69). Copyright 2022 John Wiley & Sons Inc.

antigens through electrostatic interactions, forming F13-PEI@iRABV nanovaccines. The NVs are then incorporated into dissolvable hyaluronic acid (HA)-based microneedles. FiR NVs have had success in *in vivo* mouse studies, including a 22% increase in dendritic cell (DC) maturation and a 42% increase in antigen cross-presentation in IgG, IgG2a, and IgG2b antibodies. This method of vaccine introduction induces higher virus-neutralizing antibody (VNA) titers, persisting for at least 5 weeks *in vivo*. The platform is self-administered, portable, and eliminates biohazardous waste, providing promise in increasing capabilities for rabies vaccination.[72]

The rise of antimicrobial resistance is recognized as a public health concern, primarily due to the overuse and misuse of antibiotics, which are becoming less effective against an increasing number of microorganisms. There is an urgent need for advanced antimicrobial strategies that involve the development of alternative drugs and materials capable of controlling microbial infections, particularly in clinical environments. In this study, researchers developed nanocomposite films using PVDF infused with nickel nanowires (NiNws) to enhance antimicrobial activity through the application of a magnetic stimulus. The nanocomposite was created by crystallizing PVDF into the electroactive β-phase upon incorporating anisotropic and negatively charged NiNws at a concentration of 1.5 wt %. These nanocomposites exhibited antimicrobial properties that could be significantly enhanced when subjected to a magnetic field. Researchers observed over 55% inhibition of bacterial growth under controlled dynamic magnetic conditions for representative Gram-positive and Gram-negative bacteria, compared to only 25% inhibition under static conditions without magnetic stimulation. Additionally, the antibiofilm activity was notably improved under dynamic conditions. This work serves as a proof-of-concept for materials that can enhance their antimicrobial activity on demand, paving the way for applications in innovative medical devices aimed at better controlling healthcare-associated infections.[73]

The synthesis of functional polymers from pentafluorophenyl acrylate (PPFPA) using "amine-active ester" chemistry is an effective method for creating polymers with precise and complex functional groups (Scheme 10). A novel nanofibrous

Scheme 10. Synthetic Route of P(DEEA-co-BA-co-DMNOBA-co-ABP)[a]

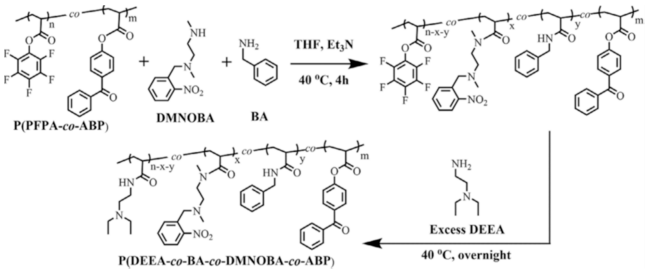

[a]Reproduced with permission from ref (74). Copyright 2019 John Wiley & Sons Inc.

mat exhibiting UV-induced CO_2-responsive behavior was created through electrospinning, intended for controlled drug release applications. Initially, a random copolymer for electrospinning, poly(N,N-diethylaminoethyl acrylamide-*co*-N-benzylacrylamide-*co*-N,N-dimethyl-N-(2-nitrobenzyl)-ethaneamine acrylamide-*co*-4-acryloyloxy benzophenone) [P(DEEA-*co*-BA-*co*-DMNOBA-*co*-ABP)], was synthesized from pentafluorophenyl esters via active ester-amine chemistry. In this context, DMNOBA serves as the UV-responsive component, while the tertiary amine group in DEEA provides CO2-responsiveness. Following this, doxorubicin hydrochloride (DOX)-loaded P(DEEA-*co*-BA-*co*-DMNOBA-*co*-ABP) nanofibers were produced, resulting in a new drug-loaded nanofibrous mat suitable for use as a wound dressing. These DOX-loaded nanofibers are responsive to tandem UV irradiation and CO_2 stimulation. CO_2-responsive behavior is activated upon irradiation, causing the nanofibers to swell slightly and release approximately 42% of the DOX. Further

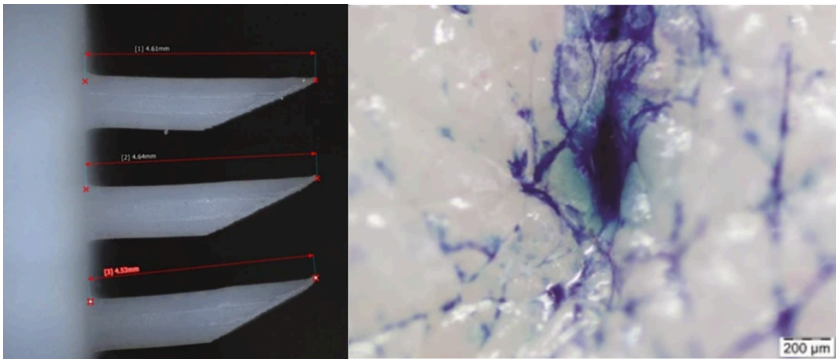

Figure 18. PTFE hollow needle array (left) and human cadaver skin impregnated with MB by the needle array (right). Reproduced with permission from ref (70). Copyright 2021 Springer.

https://doi.org/10.1021/acs.chemrev.4c00996
Chem. Rev. XXXX, XXX, XXX−XXX

CO_2 purging can increase the release to about 85%, accompanied by a morphological transition from a nanofibrous mat to a porous hydrogel film.[74]

Particle replication in nonwetting templates (PRINT) is an innovative, roll-to-roll, high-resolution soft lithography technique that enables the design and fabrication of defined microparticles and nanoparticles. This method utilizes low surface energy materials, such as fluoropolymers and photocurable perfluoropolyalkylethers. PRINT offers a flexible approach to mold particles with tailored physicochemical properties. For instance, Garcia et al. successfully engineered zanamivir microparticles using PRINT technology, achieving a 3.19-fold enhancement in fine particle fraction (FPF) compared to traditional dry powder inhalers (DPI). Additionally, an in vivo lung deposition study revealed that PRINT aerosols (composed of lactose, albumin, and leucine in a 64:32:4 ratio) labeled with technetium-99 exhibited uniform lung deposition and precise control over the mass median aerodynamic diameter (1.5 μm). The distinctive capabilities of PRINT may lead to significant advancements in particle morphology for enhanced pulmonary drug delivery.[75]

Wearable piezoelectric micropumps have the potential to enhance drug delivery in medical applications. P(VDF/TrFE)), an organic ferroelectric polymer, is an ideal material for the piezoelectric layer in medical micropumps due to its biocompatibility and flexibility. However, a high voltage is typically required to operate these micropumps, as the piezoelectric response of P(VDF/TrFE) is lower than that of inorganic materials like lead zirconate titanate. This study focuses on thin films of P(VDF/TrFE) that can reduce the required voltage while improving the overall flexibility of the actuators. Additionally, actuators sealed with poly(monochloroparaxylene) (Parylene C) are considered, as this material offers excellent chemical resistance, flexibility, and biocompatibility. The fabricated P(VDF/TrFE) thin films exhibited a piezoelectric constant of 42 mC m^{-2}, which is higher than that of bulk P(VDF/TrFE) films (38 mC m^{-2}). A significant deformation of 1 mm was observed in cantilever-type actuators sealed with Parylene C when a voltage of 160 V was applied. Furthermore, the actuators demonstrated vibration on the water surface due to the reverse piezoelectric effect, with clear resonance at frequencies of 280 and 510 Hz, resulting in displacements of 0.6 and 1.3 μm, respectively. These findings indicate that P(VDF/TrFE) thin-film piezoelectric actuators sealed with Parylene C can be effectively driven at low voltages in medical micropump applications.[76]

An effective active wound dressing that is biomechanically and biochemically suitable is crucial for wound care and skin tissue regeneration. This study introduces a straightforward method using a PVDF substrate embedded with zeolitic imidazolate framework (ZIF-8) seeds of varying sizes to facilitate the development of a highly flexible metal−organic framework membrane with a consistent honeycomb structure, ideal for drug loading and release. The embedded seeds act as a control center, resulting in a honeycomb membrane with pore openings ranging from 0.7 to 3 μm. These adjustable microscale pores, along with the inherent nanopores in ZIF-8, enable efficient loading of the anti-inflammatory drug curcumin (CCM) and allow for its rapid and controlled release, promoting antibacterial activity and cell growth. Notably, the 0.7-μm honeycomb membrane produced on the 40 nm seed exhibited a 2-fold increase in cell proliferation compared to the 2-μm honeycomb membrane (equivalent to the bare PVDF substrate). Additionally, it demonstrated 5 and 2.4 times greater antibacterial efficacy against *S. aureus* and *E. coli*, respectively, compared to the substrate. These results are attributed to the synergistic effects of CCM and Zn^{2+} release properties facilitated by the optimal pore geometries. The controllable and hierarchical pore-arrayed membrane presents unique features that make it a promising candidate for wound healing applications and offers valuable insights for future biomedical designs.[77]

1.4. Filtration (Air)

In laboratories, various methods are used to sample and extract atmospheric particulate matter (PM), but the lack of standard protocols makes it hard to compare toxicity results across studies. This research introduces a new approach for PM sampling and cell exposure using agar membranes, which are prepared through a simple freeze-drying process. The agar membranes have a flat surface and a porous structure, making them an effective alternative material for PM sampling. The study compares two methods of extracting PM: one using agar membranes with a culture medium via vortexing, and the other using the traditional ultrasonic method with water on PTFE filters. The extraction efficiency was evaluated, and cytotoxicity tests were performed on macrophage cells to assess the toxic effects of the extracted PM. The findings showed that PM extracted from the agar membranes caused higher cytotoxicity and more changes in protein expression compared to PM extracted by the traditional method. Overall, the agar membrane-based strategy offers a simple, biocompatible, and low-disturbance method for sampling and extracting PM, making it a promising alternative for PM toxicity assessments.[78]

Wearable electronics that combine high-efficiency particulate matter (PM) filtration with real-time respiratory monitoring have the potential to serve as personal healthcare systems. However, challenges related to power supply, breathability, and filtration performance remain. In this study, a self-powered air filter integrated with a facemask was developed, using a respiration-driven triboelectric nanogenerator (R-TENG) for efficient PM filtration and breathing monitoring. The key innovation is the use of a conductive cellulose aerogel/MOF (metal−organic framework) composite, which was synthesized through an environmentally friendly *in situ* method. This composite served as both the filtration material and the triboelectric component of the R-TENG. The air filter was created by combining this composite with a PVDF film as the negative triboelectric material. The self-powered air filter demonstrated excellent filtration capabilities, removing PM particles as small as 1.0, 0.5, and 0.3 μm with removal efficiencies of 98.4%, 97.3%, and 95.0%, respectively, and maintained a relatively low pressure drop of 86 Pa, ensuring breathability. Furthermore, the R-TENG system enabled real-time monitoring of the wearer's breathing patterns without the need for an external power source and holds great promise for applications in air purification and personal healthcare.[79]

Improving indoor air quality with air purifiers has become a key focus, particularly in developing filters that are efficient, have high particle-holding capacity, and maintain a low-pressure drop to improve the clean air delivery rate (CADR). While much research has gone into filter media development and performance evaluation, few studies have examined pleated filters. This study aimed to address this gap by

https://doi.org/10.1021/acs.chemrev.4c00996
Chem. Rev. XXXX, XXX, XXX−XXX

synthesizing flat and pleated filters using a combination of PTFE membranes (PT) and melt blown (MB) materials (PM). These new filters were compared to traditional air purifier filters such as MB, glass fiber (GF), and PTFE filters. The researchers evaluated the initial performance of the PM filters and how their efficiency changed as particles were loaded onto them. The results indicate that the PM filter initially had a higher quality factor (QF) than the other filters, meaning it was more efficient at capturing particles. However, the CADR and submicron-sized CADR (sCADR) were highest for the MB filter, likely due to its lower initial pressure drop. This suggests that while the PM filter shows promise, further improvements are needed to enhance its CADR for broader application in air purifiers. The study concludes that the PM filter could be a viable alternative for air purifiers in medical centers or facilities serving vulnerable populations, where high-efficiency particulate air (HEPA) filters are necessary.[80]

Medical protective masks with high antibacterial activity and filtration efficiency are essential for preventing respiratory diseases. In this study, researchers developed silver nanoparticle-decorated polyvinylidene fluoride (AgNPs/PVDF) membranes that exhibit both high antibacterial activity and excellent filtration efficiency. The AgNPs/PVDF membranes demonstrated an antibacterial efficiency of 99.98% against *E. coli* and 99.86% against *S. aureus*, with a bacterial filtration efficiency of over 95% and PM0.26 filtration efficiency maintained above 95% after 144 min of continuous filtration. The addition of silver nanoparticles (AgNPs) promoted the formation of a distinct hierarchical structure in the membrane improving its filtration efficiency. Overall, the nanofiber/net membranes produced in this study have smaller pore sizes but high porosity, enabling them to capture particles effectively. The uniform embedding of AgNPs into the PVDF fibers increases the interaction sites between the nanoparticles and microorganisms, enhancing antibacterial performance. The membranes achieved continuous filtration with high efficiency for extended periods and demonstrated high bacterial filtration efficiency (BFE) and antibacterial properties. These AgNPs-doped nanofiber/net membranes have promising potential for use in medical PPE and other applications requiring efficient air filtration and antibacterial protection.[81]

The outbreak of COVID-19 highlighted the importance of medical protective masks, which are commonly made using electret polypropylene melt blown cloth. However, these masks rely on electrostatic filtration, which can lose effectiveness over time as the static charge decays, especially when exposed to moisture from breathing. In this study, researchers developed a more durable and efficient mask filter by combining PTFE/PVA fibers and PVDF fibers using a conjugate electrospinning method. The result was a hybrid electrospinning nanofiber membrane (HENM) that blends these materials, offering enhanced filtration properties. This new filter works through both air slip effects and triboelectric secondary electret mechanisms, enabling it to maintain high filtration efficiency, low resistance, and a longer service life. The HENM demonstrated an initial filtration efficiency above 95%, which increased to nearly 100% after 24 cycles of filtration. It had a low filtration resistance of about 110 Pa, with high air permeability (262.88−370.70 mm/s) and moisture permeability (7721−8471 g/(m^2·24 h)). Unlike traditional electret masks, this hybrid membrane can replenish its electrostatic charges in a self-charging manner, providing more reliable long-term protection against harmful airborne particles. Overall, the work presents a more efficient and durable air filter that could significantly improve the performance and lifespan of medical masks, especially in long-term use scenarios.[82]

With ongoing concerns about air pollution and COVID-19 prevention, personal protective masks have become essential. However, many high-performance masks that filter fine particles like PM0.3 often suffer from poor air permeability and are disposable, contributing to environmental waste. In this study, a reusable membrane was developed using piezoelectric P(VDF-TrFE) nanofibers embedded with barium titanate ($BaTiO_3$) nanoparticles (BTO NPs). The composite nanofibers offer enhanced piezoelectric properties and surface polarity, along with smaller fiber diameters, which improve the mask's ability to capture PM0.3 particles through electrostatic attraction, polar interactions, and mechanical sieving. Additionally, the BTO NPs boost the charge storage capacity, enhancing filtration efficiency after corona treatment. The piezoelectric mask made from P(VDF-TrFE)/BTO composite nanofibers demonstrated high filtration efficiencies—96% for PM0.3 and 98% for bacteria—while maintaining a low pressure drop of only 182 Pa, which is well below the commercial N95 standard of 343.2 Pa. The mask also had stable performance after five cycles of alcohol disinfection, indicating that this P(VDF-TrFE)/BTO composite membrane could be a promising material for reusable and comfortable personal protective masks.[83]

Self-powered wearable electronic products, especially for health monitoring, face challenges in using triboelectric materials with sufficient surface polarity and structural integrity. This study explored using bagasse fibers as a raw material, functionalized with polydopamine (PDA) and embedded with silver nanoparticles to enhance the triboelectric performance, antibacterial properties, and filtration capacity of lignocellulosic materials. The resulting Ag/PDA/cellulose nanofibril (CNF)-based TENG achieved an open-circuit voltage of 211 V and a short-circuit current of 18.1 μA. When freeze-dried into an aerogel and combined with electrospun PVDF nanofibers, this material was used to create a self-powered respiratory detection mask. The mask demonstrated excellent filtration, with 94.23% efficiency for 0.3 μm particles, and antibacterial effectiveness over 99%. Additionally, it accurately detected respiratory patterns such as slow, normal, and shortness of breath, with the electrical output corresponding to the breathing frequency. This study significantly advances the use of wood fiber-based triboelectric materials, offering a sustainable, petroleum-free alternative for self-powered wearable electronic devices, particularly in medical applications.[84]

In this body of research, Wang et al. introduced a novel approach to fabricating filters for personal protective equipment (PPE) using the triaxial electrospinning technique. The resulting filtration membranes featured a unique fiber-in-tube structure and β-phase PVDF shell layer, which enabled the integration of PENG and TENG technologies. These technologies help maintain high electrostatic charge levels in the filters, unlike traditional electret filters where charge decay occurs quickly, reducing their efficiency over time. The new filters, charge-laden triaxial electrospinning membrane (CTEM), could generate charge from mechanical and acoustic energy, maintaining their electrostatic adsorption capabilities during use. When exposed to 102.8 dB of acoustic vibration at 150 Hz, the optimal output voltage and current were 166 V

https://doi.org/10.1021/acs.chemrev.4c00996
Chem. Rev. XXXX, XXX, XXX−XXX

and 17.1 μA, respectively. The CTEM masks also demonstrated a broad response to acoustic waves across various frequencies. When compared to conventional melt blown polypropylene filters, the CTEM masks showed better long-term performance, maintaining higher particulate filtration efficiency even after 72 h of hydrothermal aging, and a filtration efficiency of 98% for particles as small as PM0.3 with low breathing resistance (24.4 Pa cm^{-2}). Furthermore, the filters' ability to generate renewable static electricity and their reusability make them a promising option for high-performance masks that can reduce environmental waste. The fiber-in-tube design ensures sustained filtration performance, even after exposure to harsh conditions like humidity, heat, and acoustic vibrations, making it a promising material for future medical and emergency protective equipment.[85]

This research focuses on the development of electrospun films, created by blending PVDF and polystyrene (PS). The PVDF/PS (70/30) electrospun film demonstrated excellent air filtration capabilities, outperforming traditional polypropylene (PP) melt-blown nonwoven materials across various particle sizes. Additionally, this film can generate charges through friction, enhancing its filtration efficiency. Consequently, it has promise as a next-generation mask filter layer.[86]

Researchers from China introduced a cost-effective method to produce fluffy, electret PVDF nanowool felts (NWFs) using moisture-assisted self-crimping technology and incorporating hydroxylapatite (HAP) nanoparticles to enhance charge retention. This technique resulted in curly nanofibers with a diameter of approximately 0.6 μm and an impressive porosity of 98.7%. Compared to traditional electrospun nanofiber aerogels, PVDF NWFs offer advantages in terms of simplified one-step fabrication.[87]

In Israel, a novel approach was developed for recyclable facemasks, addressing the environmental and health issues associated with disposable masks. The researchers synthesized nanoporous membranes made from carbon dots (C-dots) and PVDF, which can be used for self-sterilizing facemasks. These composite films feature a hydrophobic surface that prevents moisture buildup and a compact nanopore network that ensures breathability while effectively filtering particles larger than 100 nm. Notably, the membranes exhibit self-sterilization when exposed to sunlight, as the embedded C-dots absorb visible light and generate heat.[88]

Researchers from Estonia and Sweden created nanowire PVDF membranes activated with silver (Ag) and zinc (Zn) nanoclusters through electrospinning. The membrane structure was modified by adjusting polymer concentrations, electric field strength, and the concentrations of $AgNO_3$ and $ZnCl_2$ in the electrospinning solution. The virucidal efficacy of these filtration materials was tested against the human influenza A virus (IAV) strain A/WSN/1933 (H1N1). Results indicated that the virucidal activity increased with higher concentrations of Ag nanoclusters, while the Zn nanocluster-activated nanofibers exhibited significantly higher virucidal activity, independent of concentration, being 2 orders of magnitude more effective than those activated with Ag.[89]

A bilayer composite filter medium with inherent antimicrobial properties was developed by integrating cotton fabric modified with magnetron-sputtered Ag/Zn coatings and electrospun PVDF/PS nanofibers. The presence of external moisture generated electrical stimulation within the composite fabric, imparting antimicrobial functionality. This resulting composite fabric demonstrated significant effectiveness in controlling air pollution, achieving a high filtration efficiency of 99.1% for PM0.3 (with a pressure drop of 79.2 Pa) and exceptional interception rates of 99.64% against *E. coli* and 98.75% against *S. aureus* within 20 min of contact. The efficient contact sterilization capability of the fabric could enhance the disinfection and reuse of filter media, offering a novel approach to designing high-performance face mask materials for public health protection.[90]

The Membrane Technology Group (MTG) from Belgium found that using low concentrations of PVDF combined with LiCl and either DMF or Tamisolve NxG as solvents yielded optimal results. SEM and porometry analyses indicated that PVDF filters could be tailored to exhibit properties comparable to those of commercial masks.[91]

Challenges associated with the performance of typical commercial face mask membranes and nanofiber membranes, such as low air filtration efficiency and high pressure drop at the most penetrating particle size (MPPS), were partially mitigated by controlling the density of the nanofiber membranes. Utilizing nanofibers instead of microfibers for face mask applications effectively doubled the air filtration efficiency for 300 nm aerosol particles. By optimizing the electrospinning process parameters, the density of the nanofiber membranes could be controlled through adjustments in interfiber spacing and tortuosity. The electrospun PVDF nanofiber membranes not only outperformed commercial surgical mask membranes and respiratory standards in air filtration but also exhibited superior mechanical strength and water contact angles.[92]

In a study by Feng et al, a novel multilayer composite membrane was created by thermally laminating a PP melt blown filter layer (serving as the dust-holding layer) with a PTFE nanofiber layer (acting as the filtration layer) to enhance filtration stability and capacity. The performance of this composite membrane was assessed concerning key laminating parameters (temperature, pressure, and speed) on dust-holding capacity, filtration efficiency, and resistance. Using NaCl aerosol as a model dust source, the composite membrane achieved a dust-holding capacity of 12.21 g m^{-2}, six times greater than that of the PTFE nanofiber membrane alone. After ten cycles of NaCl aerosol filtration, water washing, and alcohol disinfection, the composite membrane maintained a steady filtration efficiency exceeding 99.9%, with a dust-holding capacity above 8 g m^{-2} and a resistance below 70 Pa.[93]

Tan et al. from Xavier University and the Nano and Advanced Materials Institute evaluated three types of nanofiber materials, cellulose diacetate (CDA), poly(acrylonitrile) (PAN), and PVDF produced via solution blow spinning for their filtration performance against particulate matter of at least 2.5 μm (PM2.5). The capture efficiency and pressure drop of the nanofiber filters were tested using simulated burnt cigarette smoke as a PM2.5 source. Among the materials tested, PAN nanofiber exhibited the highest filtration performance with a quality factor (QF) of 0.05 Pa^{-1} and acceptable air permeability, while PVDF had the lowest QF at 0.02 Pa^{-1}. The study discusses how the molecular functionalities of the polymeric nanofibers significantly influence their filtration performance, concluding that all tested nanofibers outperformed commercial surgical masks.[94]

Wang et al. highlighted the growing interest in developing antivirus air filter materials in response to the COVID-19 pandemic. The filtration efficiency (FE) of these materials against viruses is crucial for their effectiveness in disease

https://doi.org/10.1021/acs.chemrev.4c00996
Chem. Rev. XXXX, XXX, XXX−XXX

prevention. Due to the high costs and biosafety concerns associated with using actual virus samples, virus surrogates are often employed in filtration tests. This study explored the use of polymersomes—hollow shell nanoparticles with amphiphilic bilayer membranes—as a new type of surrogate. The performance of commercial KN95 and surgical masks, along with electrospun PVDF and PAN nanofibers, was evaluated against fluorescent-labeled virus-surrogate particles (VSPs). The results underscored the importance of hydrophobicity in designing nanofibrous filter materials, with electrospun PVDF nanofibers achieving a FE of 99%, comparable to KN95 masks, while surgical masks showed a slightly lower FE of 97%. The study confirmed the potential of PVDF nanofibers as a scaffold for developing antiviral filter materials.[95]

Ray et al. noted that the COVID-19 pandemic has underscored the need for efficient and reusable face masks. Significant efforts have been made to design masks that effectively filter dust and droplets. This study developed a three-layered sandwich structure consisting of a hydrophilic spongy layer, a hydrophobic support layer, and an antidroplet layer using electrospun nanofibers. The structure included PVDF coated with silica nanoparticles and modified with perfluorooctyl trichlorosilane, providing antifouling, antidroplet, and splash resistance capabilities. The resulting electrospun nanofibrous nonwoven three-layered structure exhibited high performance and competitive antidroplet abilities, suggesting its potential for fabricating face masks that ensure personal safety.[96]

Lee et al. demonstrated that adding silica nanoparticles to an electrospun PVDF nanofibrous membrane, followed by low-surface-energy treatment, enabled the membrane to repel various liquids effectively. This modification facilitated the easy removal of fine dust particles and reduced bacterial adhesion. The modified membrane also proved compatible with ethanol sterilization, maintaining its structure and surface properties. By applying these modified PVDF nanofibrous membranes as a skin layer over unmodified counterparts, high-performance, mechanically robust, and reusable air filters were developed.[97]

In this study, a series of two-layer photosensitized membranes using the electrospinning technique were fabricated. The goal was to (i) develop highly efficient and robust photosensitized electrospun nanofibrous membranes that can both physically capture and chemically disinfect coronavirus aerosols, and (ii) elucidate the mechanism of photooxidation and inactivation of coronaviruses at a molecular level. The process involved creating a uniform electrospinning solution that contained varying concentrations (8−20 wt %) of PVDF along with a dye photosensitizer, dissolved in a mixture of DMF and acetone (in a 7:3 volume ratio). This solution was then electrospun onto a layer of PP fabric, With various dyes incorporated into the membranes, such as rhodamine B (RB), methylene blue hydrate (MB), crystal violet (CV), (RF), and toluidine blue O (TBO). It was found that photosensitized disinfection was less chemical and energy intensive and did not compromise the aerosol filtration efficiency after disinfection.[98]

In this study, an electrostatic air filter membrane was presented designed for use in face masks, which exhibits the ability to generate and retain electrostatic charges in humid breathing environments. The filter membrane consists of sequentially stacked layers of nylon mesh and PVDF nanofibers (PVDF NF). This layer-by-layer configuration enhances self-charging properties due to triboelectric effects at the polymer interfaces and piezoelectric effects in the polar crystals of PVDF NF. Increasing the number of nanofiber layers improves filtration efficiency for particulate matter (PM) of size 0.3 μm, achieving a filtration efficiency of 99.5% at an air velocity of 18.6 cm/s and a pressure drop of 200 Pa. Performance analysis of the face mask filter indicates that the generation and retention of electrostatic charges are maintained during the bending of the filter, which occurs throughout the human breathing cycle in humid conditions. Compared to a single-layer nanofiber filter, a triple-layer configuration demonstrates optimal filtration performance, achieving a quality factor (QF) of 0.019 Pa^{-1} for electrostatic charge generation. Even under conditions of electrical discharge due to humid and dry air, the triple-layer filter maintains superior filtration efficiency. These findings suggest that the multilayer structure of PVDF NF and nylon mesh serves as an effective self-charging electrostatic filter, particularly for fine particulate matter in face mask applications.[99]

Kilic et al. built upon the positive results from their well-dispersed nanofibers and developed a bimodal melt blown (MB) layer using a solution-blowing (SB) method on the same collector. The combination of 1024 and 250 nm fibers was further optimized with a Bimodal Masterbatch Layer (BML) created from a 90:10 PP and PVDF masterbatch. Following corona discharge treatment, the resulting 4BML structure exhibited exceptional performance, achieving a filtration efficiency of 99.99% with a pressure drop of 155 Pa, marking it as the most effective filter in their study.[100]

Nanofibrous sponges, characterized by their ultralow density and high specific surface area, and have significant potential for filtration and separation applications. For high-temperature smoke filtration, PTFE was selected due to its corrosion and heat resistance. PTFE nanofibers produced via electrospinning feature irregular concave-convex pores that enhance the specific surface area and filtration performance. However, PTFE nanofiber sponges experienced considerable shrinkage, which hindered product development. To address this, polyimide (PI) nanofibers, derived from polyamic acids (PAAs), were incorporated into the PTFE sponges to improve dimensional stability. Researchers investigated various parameters affecting the morphology, porosity, shrinkage ratio, and thermodynamic properties of the composite sponges, as well as their filtration performance. The results indicated that PTFE/PI composite nanofiber sponges achieved high porosity (94.34−98.12%), excellent thermal stability (above 550 °C), and impressive filtration efficiency (up to 99.97% for PM 2.0), demonstrating their potential for high-temperature filtration applications.[101]

Traditional medical masks typically use polypropylene melt blown cloth as the core filter material, which relies heavily on electrostatic filtration and exhibits high filtration resistance. The static charge in these masks diminishes rapidly due to moisture from breathing, reducing their effective lifespan. In this study, researchers fabricated PTFE/PVA and PVDF fibers using a conjugate electrospinning method, resulting in a blended fluffy fiber membrane. This membrane benefits from the air slip effect and triboelectric secondary electret properties, leading to higher filtration efficiency, lower resistance, and extended service life. The initial filtration efficiency exceeds 95%, approaching 100% after 24 cycles of filtration, with a filtration resistance of approximately 110 Pa and air permeability ranging from 262.88 to 370.70 mm/s,

https://doi.org/10.1021/acs.chemrev.4c00996
Chem. Rev. XXXX, XXX, XXX−XXX

alongside high moisture permeability (7721−8471 g/(m^2·24 h)).[102]

Recently, there has been an urgent need for wearable and breathable healthcare devices capable of air filtration and real-time vital sign monitoring due to health risks posed by viruses and particulate matter. This research group introduce a trap-induced dense monocharged hybrid perfluorinated electret nanofibrous membrane (HPFM) that efficiently removes ultrafine PM 0.3 with an efficiency of 99.712% at a low pressure drop of 38.1 Pa and a high quality factor of 0.154 Pa^{-1}. Initially, HPFM-PEO (poly(ethylene oxide)) was created using electrospinning of a PTFE and fluoroethylene propylene (FEP) suspension mixed with a PEO aqueous solution, followed by sintering the HPFM-PEO at 330 °C for 5 min to remove PEO and yield the final HPFM. Additionally, researchers developed a recyclable multifunctional healthcare mask that integrates the HPFM-based nanogenerator, enabling simultaneous efficient PM 0.3 filtration and wireless real-time monitoring of human respiration. Notably, the mask's performance remains stable even under conditions of 100% relative humidity and temperatures of 92 °C for 48 h, indicating its potential for reuse after disinfection.[103]

To further enhance filtration efficiency, polymeric multiscale stencils made from perfluoropolyalkylether (PFPAE) resin were developed. The PFPAE prepolymer resin is created by mixing MD 700 with 2-hydroxy-2-methylpropiophenone as a photoinitiator. It has been reported that viscoelastic PFPAE residue remains after the UV curing process, which can improve filter efficiency by increasing adhesion between particles and the stencil surface, thereby reducing particle bounce-off. Experimental results confirm that a greater number of particles are captured on the PFPAE stencil surface compared to polyurethane acrylate (PUA) stencils under identical conditions. Consequently, the three-stacked layer filter with multiscale PUA stencils achieved filtration efficiencies of 57% (PM 1.0), 75% (PM 2.5), and 93% (PM 5.0) with a low-pressure drop of 42 Pa. In contrast, the three-stacked layer filter with multiscale PFPE stencils demonstrated even greater performance, achieving 68% (PM 1.0), 85% (PM 2.5), and 94% (PM 5.0) efficiencies with a low-pressure drop of 64 Pa, thanks to the enhanced adhesion properties provided by the viscoelastic PFPAE residue. The QF for the three-stacked layer filter with multiscale stencils ranged from 0.02 to 0.06, surpassing that of commercial filters.[104]

This study evaluates the filtration efficiency of electrospun air filters and commercial face masks against aerosols produced from the coronavirus strain MHV-A59 and NaCl. The average filtration efficiency for MHV-A59 aerosols is represented by red and blue diamonds for the electrospun air filters and commercial face masks, respectively, while gray pentagons indicate the average efficiency for NaCl aerosols. The red, blue, and gray bars illustrate the maximum and minimum filtration efficiency values observed in the replicates (Figure 19). The study utilized a customized electrospinning system to create air filters using solution of PVDF dissolved in a mixture of DMF and acetone (7:3, v/v). This solution was electrospun onto a layer of polypropylene fabric and designated as PVDF20 and PVDF30, corresponding to their respective fabrication times in minutes. To enhance the virus removal efficiency through electrostatic attraction, researchers coated the PVDF20 filters with a positively or negatively charged polyelectrolyte, specifically PEI or poly(vinylphosphonic acid) (PVPA). This coating was applied through a soaking and drying process,

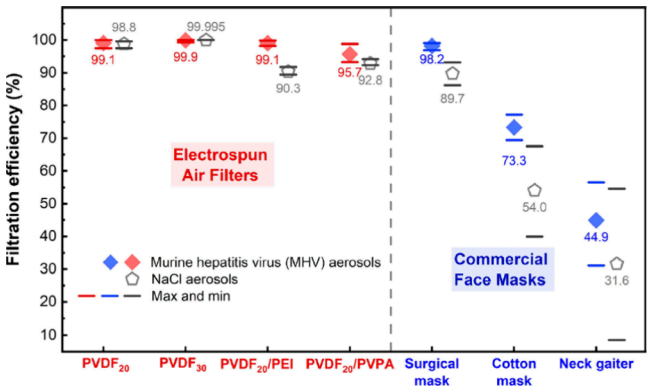

Figure 19. Study evaluates how effectively electrospun air filters and commercial face masks filter aerosols generated from the MHV-A59 coronavirus strain and sodium chloride (NaCl). Reproduced with permission from ref 105. Copyright 2021 American Chemical Society.

resulting in the filters being labeled as PVDF20/PEI and PVDF20/PVPA, respectively.[105]

In this study, researchers present nanostructured membranes with adjustable thickness and porosity designed to filter aerosols of coronavirus size. Poly(methacrylic acid) (PMAA) was integrated into commercial PVDF400 membranes by A polymerization using methacrylic acid (MAA), N,N′-Methylenebis(acrylamide) (MBA), and potassium persulfate (KPS; 1 mol % relative to MAA) in water. These membranes are further enhanced with antiviral enzyme functionalization capable of denaturing the spike glycoproteins of the SARS-CoV-2 virus in low-hydration conditions, incorporating subtilisin enzyme and exhibiting over 98.90% filtration efficiency for 100 nm unfunctionalized and protein-functionalized polystyrene latex aerosol particles. Unfunctionalized membranes achieved a protection factor of 540 ± 380 for coronavirus-sized particles, surpassing the Occupational Safety and Health Administration's standard of 10 for N95 masks. The subtilisin enzyme-functionalized membranes were able to denature the SARS-CoV-2 spike glycoprotein on the surface of coronavirus-sized particles within 30 s, even at a water content of 0.02−0.2% on the membrane surface,[106]

A drop-shape analytical method using image brightness successfully measured sliding angles with an error margin of less than 0.2 degrees. This technique was applied to assess the fluid resistance of various commercial face masks, including disposable surgical masks and reusable fabric masks. The findings revealed that the outer layer of single-use surgical masks could moderately repel a water droplet, achieving a sliding angle of 49.4°. In contrast, precoated fabric masks maintained high protection efficiency with a sliding angle of less than 45° after approximately 20 wash cycles. Additionally, raw muslin fabric treated with a commercial water-repellent spray emerged as a promising and cost-effective alternative to surgical masks during the pandemic, exhibiting high water repellency even after several washes. The results indicate that, in addition to the hydrophobicity indicated by typical contact angles, the precise sliding angle measured by this alternative method could provide critical insights into the fluid repellency of textured materials such as PTFE-based surfaces.[107]

ZnO-NPs were incorporated into PVDF composite nanofibers through electrospinning. Molecular docking calculations assessed the binding affinity of PVDF and ZnO@PVDF against the hexon protein of adenovirus (PDB ID: 6CGV). The

https://doi.org/10.1021/acs.chemrev.4c00996
Chem. Rev. XXXX, XXX, XXX−XXX

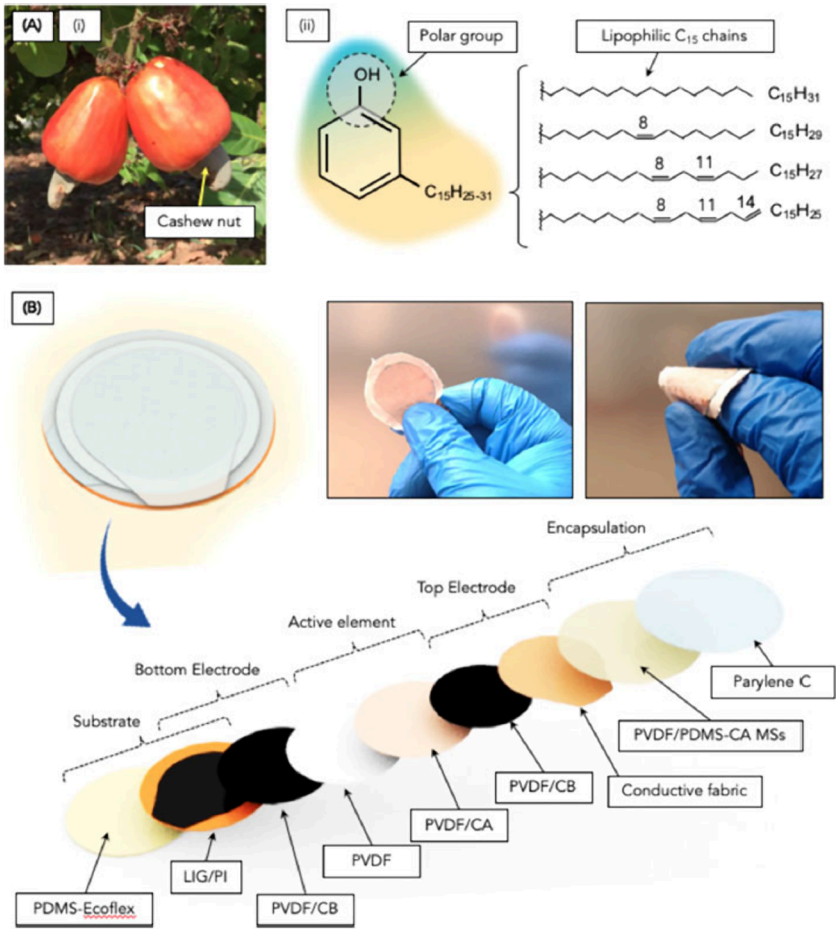

Figure 20. (a) (i) Cashew nut as a source for the production of cardanol oil. (ii) Chemical structure of cardanol with the indication of the polar group and lipophilic chains. (B) Illustration and exploded view of the fabricated hybrid PENG with an indication of all of the deposited layers. The real photos of the final device highlight its flexibility. Reproduced with permission from ref (110). Copyright 2021 American Chemical Society.

cytotoxicity of the materials was evaluated using the MTT assay, and nontoxic doses were subjected to antiviral testing against human adenovirus type-5 as a model for respiratory viruses, analyzed via quantitative polymerase chain reaction assay. IC_{50} values were determined for 0, 2, and 5% ZnO-loaded PVDF, with no cytotoxic effects observed in the nanofibers. The 5% ZnO-loaded PVDF nanofibers effectively inhibited both viral entry and replication through adsorption and virucidal mechanisms, establishing them as potent antiviral filters or masks. Consequently, ZnO-loaded PVDF nanofibers represent a promising prototype for filters embedded in commercial face masks, demonstrating significant potential to reduce the transmission of infectious respiratory diseases, including COVID-19 and similar viruses.[108]

Melt blown polypropylene is commonly used as a filter material in face masks; however, PVDF, whether electrospun or melt-blown, is less frequently utilized for this purpose. PVDF was selected as a nanofibrous filter for face masks due to its smoother morphology, uniform pore structure, and strong bonding capability with spunbond PET. A polypropylene-based melt-blown filter (found in N95 masks) was purchased commercially and compared to an electrospun PVDF-based nanofibrous filter supported by spunbondPET. The composition of the nanofibrous filter was 98:2 (PET/PVDF). Both melt blown and nanofibrous filters underwent cleaning using two methods: spraying with 75% ethanol for 1−10 cycles (where one cycle consists of three presses) and soaking in 75% ethanol for durations ranging from 5 min to 24 h. The melt blown filter is effective for single use only, displaying a significant efficiency drop to approximately 64% after ethanol cleaning, while the nanofibrous filter demonstrated consistent efficiency (around 97−99%) and can be reused multiple times following simple ethanol cleaning. Thus, it can be concluded that while both melt blown and nanofibrous filters exhibit similar filtration performance for single-use applications, the melt blown filter cannot be reused due to its drastic efficiency decline, whereas the nanofibrous filter can be successfully reused multiple times after straightforward cleaning with ethanol.[109]

Surgical masks fit closely to the face and are subjected to constant movements such as facial expressions, breathing, and speaking, which can generate mechanical energy which can be harnessed using electromechanical transducers to power sensors integrated into the masks. While piezoelectric and triboelectric nanogenerators are commonly used for this purpose, many existing devices are too thick or rigid, making them unsuitable for embedding in masks, especially since they can be affected by humidity. The hybrid piezoelectric nanogenerator (hPENG) utilizes PVDF membranes, both in their pure form and with a biobased plasticizer derived from cardanol oil, which is extracted from cashew nuts (Figure 20). These membranes are electrospun onto a flexible polyimide substrate that has been laser-ablated and is attached to a skin-conformable elastomeric blend of PDMS and Ecoflex. The

https://doi.org/10.1021/acs.chemrev.4c00996
Chem. Rev. XXXX, XXX, XXX−XXX

multilayer structure of the device captures the piezoelectric properties of the PVDF nanofibers and the triboelectric effects from friction. Additionally, encapsulation using PVDF, PDMS, cardanol, and parylene C ensures that the hPENG maintains optimal reliability and resistance to the humid and warm environment around the face mask. This proposed device has promising applications for the future development of smart masks that not only provide protection against infections but also power sensors or active antibacterial and antiviral devices.[110]

A six-layer charged PVDF nanofiber filter was developed, which offers effective personal protection against airborne COVID-19 viruses and nanoaerosols. To create this filter, PVDF pellets dissolved in dimethylformamide and acetone, to fabricate a uniform electrospun nanofibrous mat After electrospinning, the nanofiber mat was dried in an oven overnight at 40 °C to allow any residual solvent to evaporate. The device was found to meet the N98 standard for virus and aerosols, while being at least ten times more breathable than a conventional N95 respirator.[111]

Certain facemasks are treated with per-and polyfluoroalkyl substances (PFAS) which are known to be harmful to human health and well-being. PFAS is an excellent fluid and particle repellent, but no exposure assessment for PFAS in facemasks has been conducted, The ultimate end location for facemasks is in landfills or incineration facilities, reaching the environment through landfill leachate. Exposure from daily use of 9 types of facemasks was modeled by ConsExpo, a tool developed by the Danish National Institute for Public Health and the Environment. The dominant exposure route was determined to be inhalation, accounting for about 40−50%, followed by ingestion at 15−40%, and then dermal at 11−20%. Children were also determined to be at a higher risk for PFAS exposure from PFAS-containing masks due to their high physical activity increasing the risk of inhalation exposure, representing a potential health risk through mask use. Children were determined to likely exceed the reference dose of 5 $\mu g\ kg^{-1}\ day^{-1}$, resulting in a potential health risk. The models used assumed 100% leaching of PFAS from masks and an annual disposal of 29−91 billion masks based on consumer use. With these parameters, mask disposal only contributes approximately 6% of the global PFAS mass loads and represents 11 kg of PFAS discharged into US wastewater, a relatively insignificant value compared to the 600 kg of PFAS discharged per year in landfill leachate. The authors determined that the likely estimate of PFAS from masks is approximately 90% from SUD masks and 10% from N95 masks, indicating that certain types of masks should be avoided due to their high PFAS content.[112]

Microplastics (MPs) are pervasive across aerial, terrestrial, and aquatic environments and pose an inevitable exposure risk via oral, dermal, and inhalation routes. PTFE, primarily used in nonstick cookware, semiconductors, and medical devices, has been less studied for its toxicity with regards to MPs. MPs range in size from <5 mm to over 100 μm and can be produced intentionally (primary MPs) or degrade from larger plastics (secondary MPs). Researchers examined PTFE MPs with average diameters of 6.0 and 31.7 μm and tested them on the following cell lines: HaCat (skin), CaCo-2 (intestinal epithelial barrier), A549 (alveolar epithelial cells), THP-1 (dendritic cells), U937 (macrophages), and Jurkat (T lymphocytes), as models representing various tissues exposed to PTFE. Although no cytotoxicity was observed in any conditions, both particle sizes induced significant oxidative stress, including the production of nitric oxide (NO) and reactive oxygen species (ROS), with the 6.0 μm particles showing the most pronounced effects. Both particle sizes also triggered the secretion of proinflammatory cytokines, including tumor necrosis factor alpha (TNF-α) in the U937 cell line and interleukin-6 (IL-6) in the A549 lung epithelial cell line. MPs further induced mitogen-activated protein kinase (MAPK) signaling, especially the extracellular signal-regulated kinase (ERK) pathway, in A549, U937, and THP-1 dendritic cell lines. The expression of the NLRP3 inflammasome was downregulated in U937 and THP-1 cells, while the apoptosis regulator BCL2 was markedly upregulated in A549 and U937 cells. The findings indicate that MPs induce oxidative stress, potentially leading to inflammation, apoptosis, and autophagy, primarily through ROS and NO release, with the ERK pathway being a key mediator in inflammatory responses, especially in lung tissue where inhalation exposure is a concern.[113]

Filtration efficiencies are a common way to evaluate filter performance. Table 3 below summarizes the filtration performance of some of the novel materials found in this section for various particle sizes and bacteria.

Table 3. Novel Filtration Membranes and Filtration Efficiencies for Various Particles Sizes

Filtration membrane	Filtration Efficiency (%)	Particle Size (μm)
Conductive cellulose aerogel/MOF composite[79]	98.4	1.0
	97.3	0.5
	95.0	0.3
AgNPs/PVDF[81]	>95	<0.26
HENM[82]	>95 (PM0.26)	0.26 ± 0.04
	>95 (bacteria)	
P(VDF-TrFE)/BTO composite nanofibers[83]	96 (PM0.3)	<0.3
	98 (bacteria)	
Ag/PDA/cellulose nanofibril TENG[84]	94.23 (PM0.3)	<0.3
	>99 (bacteria)	
CTEM[85]	98 (PM0.3)	<0.3
Ag/Zn coated PVDF/PS nanofibers[90]	99.1	<0.3
	99.64 (*E. coli*)	
	98.75 (*S. aureus*)	
PP/PTFE nanofiber[93]	>99.9	0.3−10
PVDF nanofiber[95]	99 (aerosol)	0.114
	99 (VSP)	4
PVDF NF and Nylon mesh[99]	99.5	0.3
4BML[100]	99.99	0.26 ± 0.3
PTFE/PI composite nanofiber sponge[101]	99.97	2.0
PTFE/PVA/PVDF fiber[102]	95−>99	0.26 ± 0.4
HPFM[103]	99.712	0.3
PFPAE resin[104]	68	1.0
	85	2.5
	94	5.0

1.5. Imaging and Diagnostics

$Cs_3Cu_2I_5$ nanocrystals (NCs) are promising materials for X-ray imaging due to their high photoluminescence efficiency, lead-free composition, and X-ray responsiveness. However, during the crystallization process, these NCs tend to agglomerate and have uneven size distribution, leading to light scattering that reduces imaging resolution. To address this, a high-resolution

https://doi.org/10.1021/acs.chemrev.4c00996
Chem. Rev. XXXX, XXX, XXX−XXX

Scheme 11. Schematic for the Alteration of a Functionalized PVDF Membrane by AGET ATRP and Subsequent Ring-Opening of the Epoxide by a Diamine to Produce the Amine-Functionalized Membrane[a]

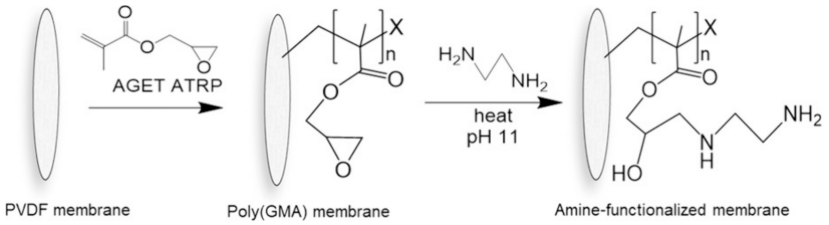

[a]Reproduced with permission from ref (116). Copyright 2022 American Chemical Society.

scintillator film was developed by embedding $Cs_3Cu_2I_5$ NCs in a hybrid polymer matrix of PVDF and PMMA. This combination helps control the size and uniformity of the NCs, preventing agglomeration and ensuring consistent distribution. The resulting film achieves a high spatial resolution of 14.3 lp mm^{-1} and a low detection limit of 105 nGy s^{-1}, along with excellent flexibility and stability. The inclusion of PMMA in PVDF prevents the PVDF chains from aligning, which reduces the interaction between PVDF and $Cs_3Cu_2I_5$, promoting more uniform crystallization. This results in a stable, high-performance scintillator film suitable for high-resolution X-ray imaging, even in complex environments. The film's flexibility and waterproof properties also make it ideal for imaging irregular objects, demonstrating its potential for low-cost, flexible medical imaging applications.[114]

Ultrasound computed tomography (UCT) has great potential for imaging soft tissues like the breast, particularly for analyzing biomarkers such as the speed of sound (SoS) and ultrasonic attenuation, which is relevant for disease classification. However, accurately reconstructing images of ultrasonic attenuation has been challenging due to the aberrating nature of breast tissue and the limitations of conventional piezoelectric detectors used in UCT systems. This study introduces a large-area (LA) phase-insensitive detector that utilizes the pyroelectric effect in PVDF membranes. These detectors are particularly suited for quantitative imaging of soft tissue ultrasonic attenuation. The key advantages of this detector include a broad directional response (±1 dB) up to an angle of ± 60° at 3.2 MHz, and the thermal nature of the signal allows it to be sensitive to acoustic radiation in a wide range of anglesThe high sensitivity of this detector allows it to measure time-averaged acoustic powers of several milliwatts, with temperature increases near the PVDF membrane of just a few millikelvins. This combination of high sensitivity and broad directional response make the sensor a promising tool for improving the reliability and accuracy of UCT imaging in soft tissues.[115]

Targeted radiopharmaceuticals are an emerging treatment modality for cancer patients, where radiopharmaceuticals are conjugated to carrier molecules and used for localized tumor irradiation via $\alpha$and βparticles, minimizing damage to healthy tissues. Copper-67 (Cu-67) is a promising theranostic isotope with a half-life of 2.58 days and emits both γrays for imaging and β particles for cancer treatment. High isotopic purity is crucial for theranostics, but current separation processes using resin-packed columns face limitations in scalability. Researchers have designed amine-functionalized membrane adsorbers for the selective adsorption of Cu^{2+} from acidic solutions (pH 2), utilizing poly(glycidyl methacrylate) (PGMA) films coated on PVDF membranes (Scheme 11) The amine-functionalized membrane adsorbers are synthesized via AGET ATRP (activator generated by electron transfer atom-transfer radical polymerization), followed by the addition of amine functionality. The permeabilities of these membranes range from 300 to 2650 LMH·bar^{-1}, depending on the polymerization reaction time (0.5 to 6 h, resulting in filtration times of less than 2 min for 50 mL of water at 100 kPa pressure. At 70 kPa, these membranes are 25 times faster than current state-of-the-art technologies, which operate at 1 mL/min.[116]

This work presents a process for fabricating long, flexible polymer fibers that can be doped with a variety of organic–inorganic hybrid luminescent materials, such as $Cs_3Cu_2I_5$ nanoparticles, Cu_2I_2 nanoclusters, and Mn-doped $Cs_4CdBi_2Cl_{12}$ phosphors (Figure 21). These fibers can emit

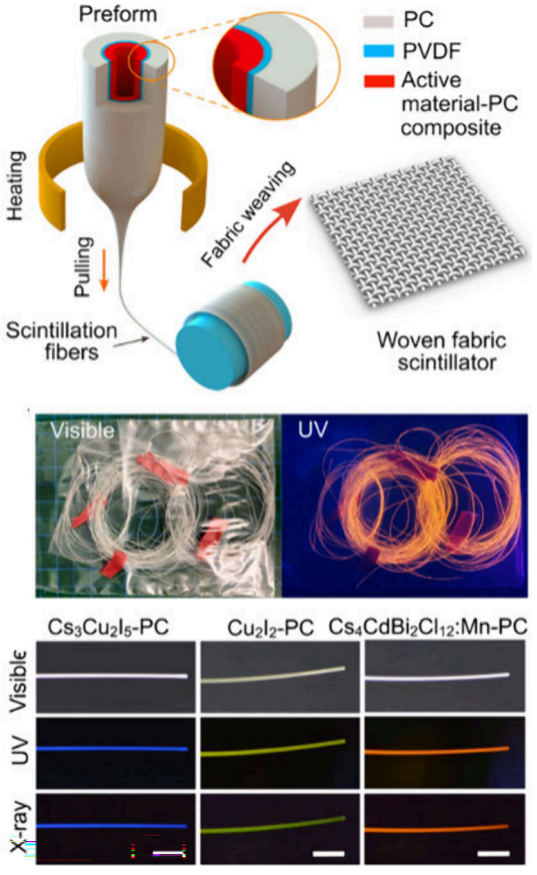

Figure 21. (Top) Woven scintillation fabric production. (Middle) Cs4CdBi2Cl12:Mn-PC fibers under visible light and UV illumination and (bottom) fabric production under visible light, UV and X-ray irradiation. Reproduced with permission from ref (117). Copyright 2024 American Chemical Society.

https://doi.org/10.1021/acs.chemrev.4c00996
Chem. Rev. XXXX, XXX, XXX−XXX

light in different colors, making them versatile for applications in photonic systems, such as single-photon sources, radiation sensors, and wireless optical communication networks. The fibers are designed with a hollow core surrounded by an active material, and a layer of PVDF separates the active material from a thicker polycarbonate (PC) outer layer. This PVDF layer has multiple advantages: it protects the active material during selective etching of the PC, maintains fiber flexibility, and enhances light extraction due to its lower refractive index compared to PC. The result is a fiber that is flexible, durable, and efficient for light emission and can be used to create high-performance scintillator screens for X-ray imaging, especially for nonplanar, complex shapes, without the image distortion and resolution loss seen in rigid planar screens. The fibers can also be used in advanced applications such as personalized medical imaging, including breast cancer screening, and in large-area high-energy radiation and particle detection. In addition to scintillation screens, the fibers are also suitable for UV detection and down-conversion LED devices, broadening their potential uses.[117]

This document presents a concise overview of key applications of ionizing radiation across various doses and energy levels. It emphasizes the importance of monitoring radiation doses in irradiated materials and assessing radiation fields. The text highlights that, globally, these challenges are addressed through dosimetric Electron Paramagnetic Resonance (EPR) systems and detectors based on L-α-alanine. An example is provided regarding the sterilization of medical devices using radiation from an electron accelerator. Experimental results demonstrate the feasibility of employing PTFE as a detector within dosimetric EPR systems for monitoring radiation processes. Calibration exposures of PTFE and alanine detectors were conducted within the dose range recommended for sterilizing disposable medical devices and food products, with corresponding EPR spectra measured Table 4 and Figure 22). The irradiation was performed using

Table 4. Dose and Parameters of EPR Signals of PTFE Detector[a]

No.	D_n, kGy	H, a.u.	$S_1 + S_2$, a.u.	B_0, Gs
1	12.2	21.9	286.2	3494.0
2	23.5	40.5	530.9	3494.5
3	34.0	58.2	770.6	3493.7
4	45.6	71.3	962.1	3493.0
5	54.9	83.0	1104.1	3492.6
6	66.6	102.1	1364.5	3492.5

[a]Copyright 2019, reproduced with permission from Springer.

an industrial electron accelerator alongside standard film dosimeters. The calibration results obtained confirm that PTFE detectors can effectively serve as operational detectors in EPR dosimeters for routine monitoring and evaluation of radiation processes involving electron accelerators.[118]

Researchers have developed a real-time motion monitoring sensor (RMS) to address motion artifacts during magnetic resonance imaging, which can interfere with diagnostic accuracy. Body movement during the scan can cause blurring, deformation, or double shadows in the resulting images, affecting both pre- and postsurgery evaluations. Traditional motion sensors contain magnetically conductive materials that could be disrupted by MRI machines, however this system uses a TENG to power the sensor without external electricity,

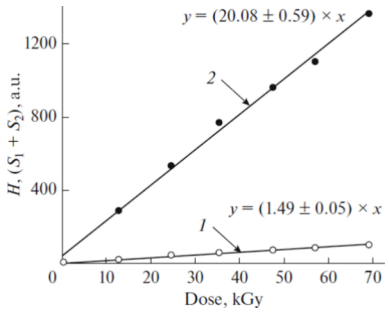

Figure 22. Magnitude of EPR signal constructed based on peak (1) and area (2) versus PTFE-detector radiation dose. Reproduced with permission from ref (118). Copyright 2019 Springer.

solving the issue of interference with scans. The TENG consists of two layers of FEP film sandwiching a silicone layer, with electrodes printed using conductive ink through a mask printing method. When the movement surpasses a set threshold, the scan is paused. Thes output is visualized using cloud-based images and a 3D surface map, with a pop-up window alerting the physician of the detected motion. In testing, the system successfully detected motion from a 25-year-old male test subject during an active scan, generating an output voltage that triggered the pop-up alert to the physician. The system was able to distinguish signal noise caused by vibrations in the machine and the magnetic field from actual patient movement, allowing for a more efficient and accurate scanning process.[119]

^{19}F MRI is a promising noninvasive diagnostic tool that expands the capabilities of conventional proton MRI. However, a suitable tracer for routine medical use is still under development. In this study, the authors explore a series of polymeric systems based on poly[N-(2,2-difluoroethyl)-acrylamide] (PDFEA), designed as BAB triblock copolymers, where the B blocks are thermoresponsive PDFEA, and the A block is hydrophilic PEG. These triblock copolymers can self-assemble into nanoparticles in dilute aqueous solutions, which then transition into physically cross-linked hydrogels at higher concentrations. The thermoresponsive properties of these systems make them suitable for various biomedical applications, including theranostic uses. The study examines how the ratio of the BAB blocks affects the self-assembly, thermoresponsiveness, mechanical properties, and MRI suitability of the hydrogels. The biocompatibility of these systems was also evaluated using a relevant cell line, making them a promising candidate for future medical applications in MRI (Figure 23).[120]

Drug delivery systems (DDSs) have the potential to improve the distribution and pharmacokinetics of various medications. In this study, researchers introduce diblock polymers made from poly(2-methyloxazoline) and N-(2,2′-difluoroethyl)-acrylamide, along with N-[2-(ferrocenylcarboxamido)ethyl]-acrylamide, which function as novel DDSs. These thermoresponsive diblock copolymers self-assemble at body temperature and disassemble in the presence of oxidative agents, such as ROS, facilitating the release of their therapeutic payload. Notably, these polymers do not undergo spontaneous oxidation when exposed to air or hydrogen peroxide under physiological conditions; however, they are highly sensitive to ROS in acidic environments. This property enables the tracking of the biodistribution of their DDS using ^{19}F MRI. As a result, these polymers are well-suited for both localized

https://doi.org/10.1021/acs.chemrev.4c00996
Chem. Rev. XXXX, XXX, XXX−XXX

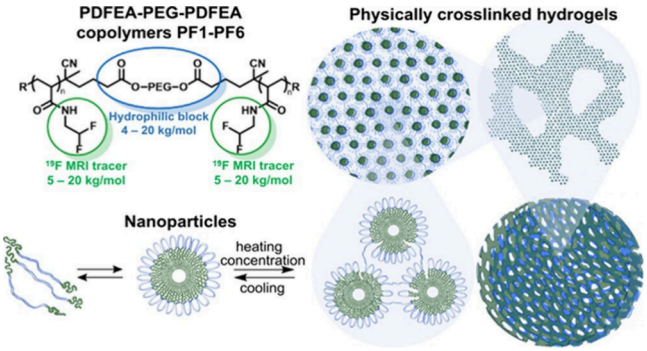

Figure 23. General concept of the thermoresponsive system. BAB block copolymers based on PDFEA-fluorinated thermoresponsive block B combined with the hydrophilic PEG block A. The amphiphilic and thermoresponsive polymers form particles in dilute aqueous solutions and can physically cross-link into hydrogels upon heating and for increasing the polymer concentration. Reproduced with permission from ref (120). Copyright 2022 American Chemical Society.

and systemic drug delivery in ROS-rich environments, such as tumors or inflamed tissues. Additionally, the characteristics of the polymers can be extensively tailored to meet various clinical requirements. In summary, researchers demonstrate that the copolymers (i) preferentially release their cargo in ROS-rich environments, (ii) are biocompatible, and (iii) can be easily visualized *in vivo*.[121]

Biocompatible polymers were developed using the hydrophilic monomer N-(2-hydroxypropyl) methacrylamide (HPMA) and the thermoresponsive monomer N-(2,2-difluoroethyl)acrylamide (DFEA). These polymers contain a high number of magnetically equivalent fluorine atoms, which enhances their effectiveness as MRI tracers (Scheme 12). In this pilot study, researchers further modified these polymers by adding a redox-responsive monomer. This modification allows the polymers to alter their physicochemical properties when exposed to an oxidative environment. Researchers created ROS-responsive polymers by incorporating small amounts of the N-[2-(ferrocenylcarboxamido)ethyl] acrylamide (FcCEA) monomer. In its reduced state (Fe(II), ferrocene), this monomer is hydrophobic and diamagnetic, while in its oxidized state (Fe(III), ferrocenium cation), it becomes hydrophilic and paramagnetic. This unique property is particularly beneficial for theranostic applications especially in ROS-responsive drug delivery systems, releasing the drug upon oxidation in ROS-rich tumors or inflamed tissues.[122]

1.6. Implants

Endovascular devices are usually ultrathin metallic structures with a polymer membrane. These devices require the ability to be collapsed into a small diameter on the order of a few millimeters and later expand in the target area up to 3 cm in diameter. Patient specific instrumentation is important in the case of custom implants such as total knee arthroplasties but also applies to stents due to tapered vasculature in the torso, as well as other vascular devices. Templates can be created from CT scans, MRI, and X-ray images to generate a digital print file for a 3D printer. ePTFE is the choice material in this study, possessing high tensile strength, controlled porosity, low surface energy, and good hemocompatibility. An ePTFE tube is used as a customizable graft material, coating a laser-welded nitinol backbone (Figure 24). Radial stress testing shows a strain at break of 550%, and 0.7 mPa stress. Longitudinal expansion is much more limited, with 8% strain at break and stress of 23 mPa. Fluid testing at 120 mmHg demonstrates a radial expansion of 167%, and a longitudinal decrease of 8% with no leakage. The material displays good hemocompatibility when stretched, with some moderate thrombosis developing in some locations. Porcine studies demonstrate facile deployment of the stent graft and rapid control of venous bleeding to a traumatic vena cava injury, indicating good applications for applications in endovascular trauma.[123]

Long-term studies of ePTFE coatings in the body indicate whether ePTFE stent grafts are suitable for long-term interventions. The typical approach to stents in the heart is the introduction of a spacer to block spacer or heart lesions, making a surface for leaflet coaptation. Self-expanding nitinol mesh does not require a secondary expansion, making it an attractive option for heart stents. ePTFE also displays good biocompatibility, making it an idea candidate to avoid foreign body reactions. Stents were implanted in swine and location was verified through X-ray fluoroscopy and echocardiography. In this case, blood itself acts as the filler for the material, allowing self-expansion of the mesh into an organized material. The heart was then dissected after 6−8 weeks to examine interactions of the material with the surrounding tissue. Acute survival was 100%, with no apparent side effects presented. The ePTFE coating had a smooth epithelial layer adhering it to the surrounding tissue (Figure 25), with no signs of damage to the tissue or thrombosis. No leaflet damage was observed; however, a slight thickening of the anterior leaflet was found,

Scheme 12. Synthesis of Multiresponsive Fluorinated PHPMA-block-P(DFEA-stat-FcCEA) Copolymers HF1, HF2, and HF3[a]

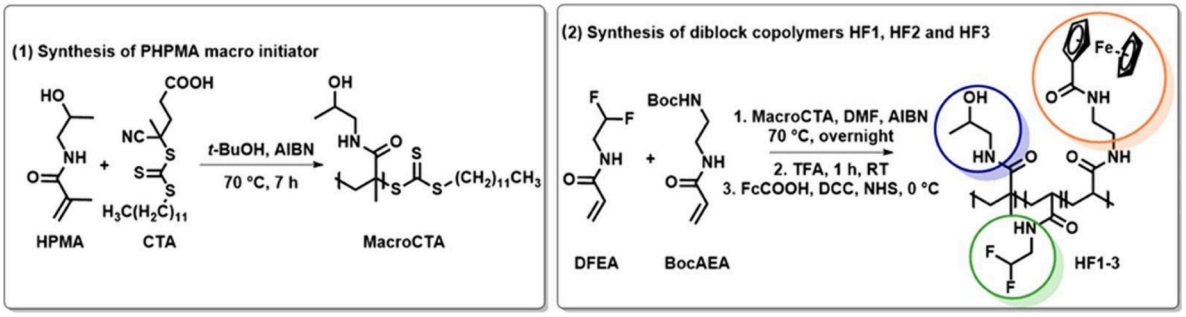

[a]The polymer chain end moieties were omitted for clarity. Reproduced with permission from ref (122). Copyright 2023 American Chemical Society.

https://doi.org/10.1021/acs.chemrev.4c00996
Chem. Rev. XXXX, XXX, XXX−XXX

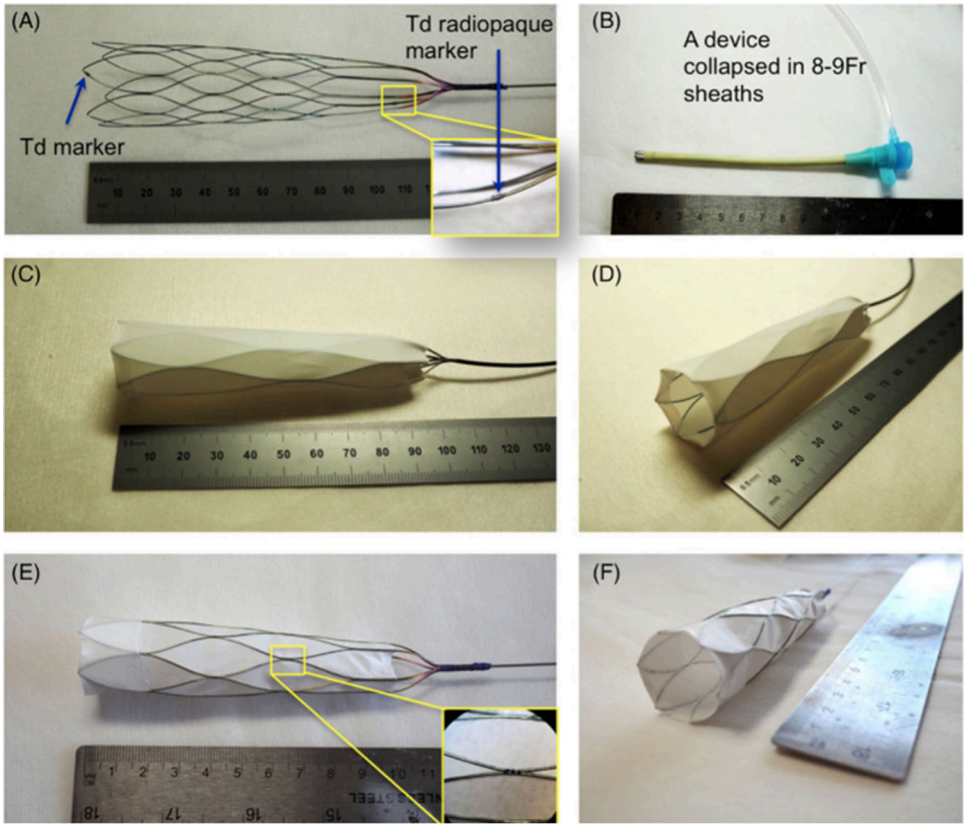

Figure 24. (A) Expanded nitinol stent graft material expanded without ePTFE sheath, (B) the collapsed catheter device for expanding stent grafts, (C–F) the ePTFE coated stent graft expanded with a ruler for scale. Reproduced with permission from ref (123). Copyright 2019 John Wiley & Sons Inc.

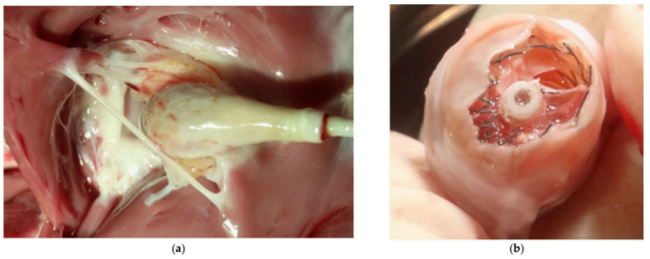

Figure 25. (a) The ePTFE coating surrounded with a smooth cell layer with slightly enlarged anterior leaflet, and (b) the device with seroma-like material found inside the nitinol mesh. Reproduced with permission from ref (124). Copyright 2021 MDPI.

presumably due to contact with the stent and resulting mechanical stress.[124]

Polyether urethanes have been successful long-term biomedical implants due to their biocompatibility and good mechanical performance. Polydimethylsiloxane (PDMS) as a soft ether component helps resist oxidative damage and is clinically biostable for 10 years in the case of PDMS/PEU copolymers PurSil and Elast-Eon, poly(tetramethylene oxide) and poly(hexamethylene oxide) respectively. Introduction of fluorine to the system can increase both biostability and oxidative stability, creating a more attractive alternative for long-term implantation. Samples of polyurethane (PEU), silicon-containing PEU (SPEU), and fluorinated silicon-containing PEU (FSPEU) were aged in PBS at 70 °C for up to 32 weeks, and analyzed by SEM, GPC, ^{1}H NMR, and LC-MS (Figure 26). Samples were denoted as FSPEU-X, where x

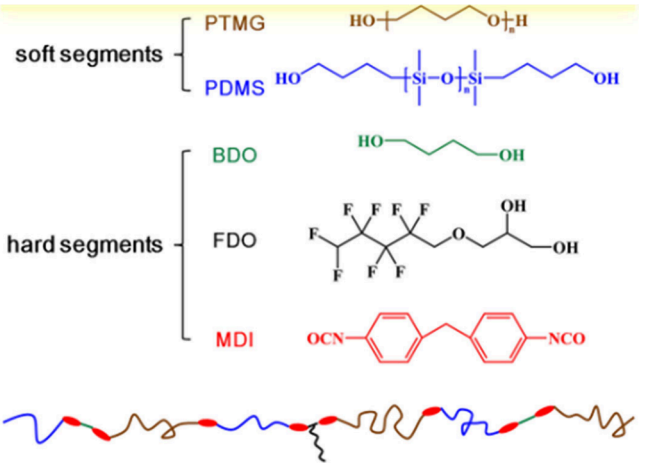

Figure 26. Rational design of fluorinated, silicon-containing polyurethanes for enhanced hydrolytic resistance through incorporation of fluorinated diols and silicon blocks. Reproduced with permission from ref (125). Copyright 2020 American Chemical Society.

is the mole fraction of the ether extending the chain on the end. Hydrolysis occurs in the bulk material, with visible surface defects forming by SEM, with pits of 10 μm occurring with cracks and scaly defects in the case of PEU. PEU has a retention of molecular mass of 66%, while SPEU-10 and FSPEU-10 retain 72% of molecular mass. Segmented PEU is prone to phase separation into hard and soft segments, changing material properties. PDMS encourages this phase separation, but the fluorinated chains were found to inhibit

https://doi.org/10.1021/acs.chemrev.4c00996
Chem. Rev. XXXX, XXX, XXX−XXX

chain movement due to their electronegativity, thus inhibiting the phase transition process and inhibiting cracking. Ultimately, enhanced hydrolytic resistance and improved surface performance was demonstrated, with the motion of silicon-containing segments to the material surface aided by fluorinated materials, thus decreasing hydrolysis.[125]

Implantable medical devices such as cardiac pacemakers and implantable cardioverter defibrillators (ICDs) typically run on battery power and require surgical replacement after 5−8 years. One strategy to avoid such an issue is to utilize implanted triboelectric nanogenerators (iTENG) to harvest the body's energy to recharge cardiac devices. A piezoelectric bioinspired helical device was created as a pacemaker lead, using mechanical energy from the heart's cyclical expansion and aortic recoil to produce a self-charging pacemaker. The device is a sandwich structure of PDMS/PVDF-TrFE/PDMS, with 20 μm layers of PDMS and 45 μm layers of PVDF-TrFE with a gold electrode. 36 s of stimulus produces 0.28 V, with a practical power of 0.036 μW. Connecting the units in series results in a potential of 1.25 V, indicating a mixture of series and parallel devices could increase electrical output. The samples were found to be biocompatible after culturing with mouse fibroblast cells and demonstrated a voltage output of 0.5 and 0.65 V in pigs in an *in vivo* model. If a pacemaker had a battery capacity of 1 Ah and a longevity of 10 years, energy consumption is projected to be around 28.75 μW. Ten EH deviecs in series give 2.8 V of energy, with a 10 × 10 array of the leads potentially extending the battery life of a pacemaker by 1.5 years.[126]

Radiological findings are rarely reported in cosmetic rhinoplasty but can be extremely helpful for physicians. Implant visualization is important for evaluation of inflammation, dislocation, and extrusion. In this study, 80 patients with analyzed with facial bone CT or ostiomeatal unit CT for dorsal implants to visualize complications. The fibrous capsule of silicone implants has a peri-implant radiolucent halo, while the Gore-Tex implants display tissue ingrowth expressed as intraimplant low attenuation. Both these features are diagnostic, allowing the surgeon to develop a strategy regarding implant removal without identification through surgery.[127]

Trifluoromethyl-functionalized poly lactic acid (PLA) represents a new class of polyesters displaying hydrophobicity relative to their hydrocarbon analogues, demonstrating no *in vitro* toxicity when tested with mouse fibroblast cells. The polymers were synthesized by the synthesis of monomers from 3,3,3-trifluorolactic acid (Scheme 13). The acid is allowed to react with 2-brompropionyl bromide to form the anhydride, followed by intramolecular transfer to a carboxylic acid intermediate, and finally nucleophilic substitution to make a cyclic monomer. Ring-opening polymerization produces a high molecular weight polymer with $Sn(Oct)_2$ as a catalyst and benzyl alcohol as an initiator. The resulting material displays a water contact angle of 88.21 ± 1.5°, compared to the starting material PLA contact angle of 70 ± 1.3° due to reduced surface energy from the CF_3 group. The materials adsorb a higher alumin/fibronogin ratio compared to PLA, suggesting superior hemocompatibility due to the control of adsorbed proteins on the surface. This protein adsorption is comparable with PVDF-HFP, a polymer with known low thrombogenicity, with an adsorption of 83 ng cm^{-2} compared to 85 ng cm^{-2} for PVDF and 3 ng cm^{-2} for PLA, indicating good hemocompatibility. The material adsorbs less fibrinogen than PVDF-HFP,

Scheme 13. (A,B) Cyclization to form novel trifluoromethyl-PLA derivatives, (C) polymerization of trifluoromethyl-PLA derivatives with $Sn(Oct)_2$ as a Lewis acid catalyst, (D) general scheme for the synthesis of substituted PLA-derivatives and subsequent polymerization. Reproduced with permission from ref (128). Copyright 2019 Royal Society of Chemistry

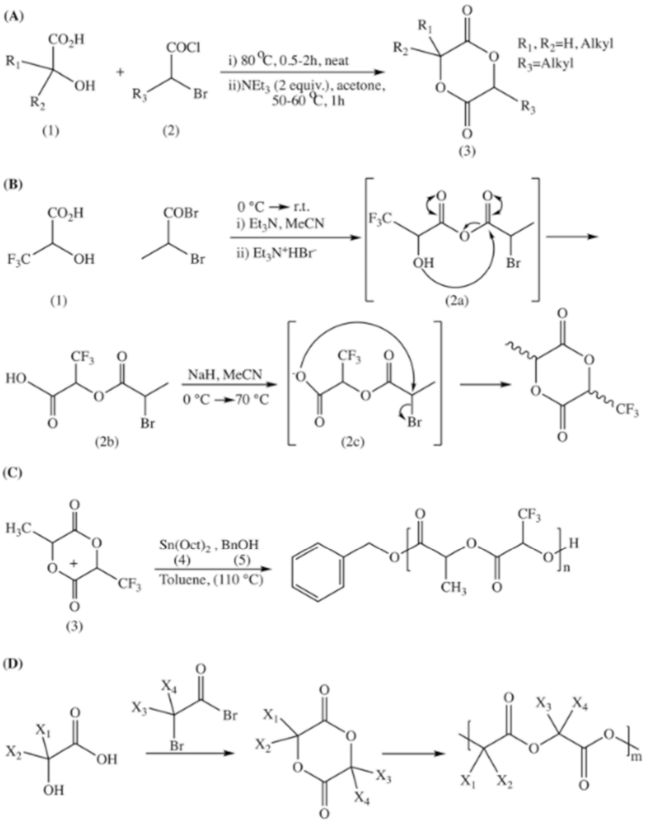

adsorbing 20 ng cm^{-2} compared to 22 ng cm^{-2}. This material extends the medical utility of polylactides and indicates a polylactide with low thrombogenicity has been successfully synthesized by incorporating fluorinated groups.[128]

Bioinertness of a material can be indexed by the presence of intermediate water (IW) and the water molecules loosely bound to a polymeric material. PHEMA is a hydrophilic polymer with high equilibrium water content (40 wt %) used in many medical applications due to its bioinertness and hydrophilicity. A research group analyzed copolymers of PHEMA with 2-(dimethylamino) ethyl methacrylate (DMAEMA) and 2,2,2,-trifluoroethyl methacrylate (TFEMA) (Figure 27). Homopolymers of DMAEMA and TFEMA do not display bioinert behavior, but copolymers with even a small amount of these materials with HEMA display higher bioinert properties than PHEMA, tuning the hydration state of the material, TFEMA, a hydrophobic polymer, migrates to the air−polymer interface away from the water, and switches to the water−polymer interface when hydrated, causing free water (FW) to convert to IW and nonfreezing water (NFW). DMAEMA, a hydrophilic polymer ionized in physiological pH, causes migration of the amino group to the water−polymer interface, causing more interaction with circulating proteins, thus allowing control over the morphology of PHEMA to afford greater bioinert properties.[129]

https://doi.org/10.1021/acs.chemrev.4c00996
Chem. Rev. XXXX, XXX, XXX−XXX

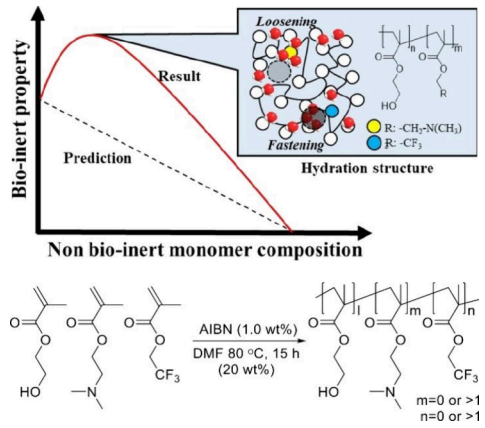

Figure 27. Schematic predicting the bioinert properties of a material versus nonbioinert monomer composition (top), and polymerization of a copolymer of pHEMA with hydrophobic components (bottom). Reproduced with permission from ref (129). Copyright 2020 American Chemical Society.

Endocardial pressure (EP) is an important cardiac parameter for analysis of function, but typically requires invasive cardiac catheterization, as well as a large recorder which is impractical for long-term monitoring and patient compliance. Researchers developed a miniaturized, flexible, TENG-based self-powered endocardial pressure sensor (SEPS) and integrated it in a porcine model with a minimally invasive surgical catheter, minimizing heart tissue damage for long-term implantation (Figure 28). The device is fabricated from a nano-PTFE film

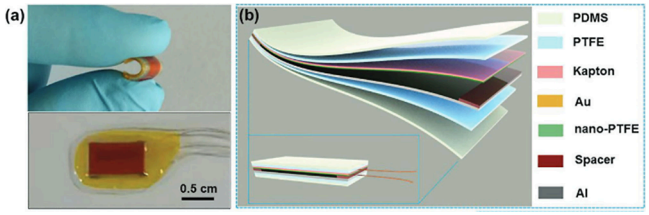

Figure 28. (a) Demonstration of the flexibility and the relaxed state of the SEPS and (b) schematic depiction of the composition of the SEPS device. Reproduced with permission from ref (130). Copyright 2019 John Wiley & Sons Inc.

(25 μm) treated by the inductively coupled plasma (ICP) method, followed by corona discharge. The material has excellent blood compatibility and is reliable long-term, making this an excellent choice for an implantable medical sensor. Implantation of the device gives ultrasensitivity (1.195 mV $mmHg^{-1}$) from 0 to ~ 350 mm Hz of pressure, and high mechanical stability. The SEPS shows a V_{oc} of 0.45 V, I_{sc} of 0.2 μA, and transferred charge (Q_{tc}) of 0.16 nC under 350 mmHg of pressure. The SEPS is capable of sensing ventricular fibrillation and ventricular premature contraction, is self-powered, eliminating the need for a battery and reducing device size, with excellent stability of over 100 million cycles in vitro. The device additionally displays good biocompatibility with low risks of thrombosis, with no blood cascade reaction observed.[130]

Aortic dissection (AD) is caused by lesions of the intima of the aorta, with typical risk factors such as hypertension and atherosclerosis. Tearing of the intima from blood flow causes separation of the intima from the arterial wall, leading to formation of true and false lumen. An aortic dissection indicates a defect of the ascending aorta, but Type B indicates AD of the descending aorta. Type A is usually treated with a thoracotomy, whereas Type B is usually reparable with a stent graft. A stent graft provides a much milder solution, with the graft keeping the blood away from the false lumen, eliminating risk of blood perforation, with stability up to 10 years without performance compromise. Researchers developed a trilayer stent graft made of nitinol stents in a z-wave design and 2 layers of ePTFE for use in a trans-catheter endovascular aortic repair (EVAR) procedure, providing a minimally invasive method to repair Type B AD (Figure 29). The asymmetric z-wave design allows for excellent aortic curve compatibility, and the stent demonstrates 96% cell viability and 2.2% hemolysis. No thrombus or stenosis were observed in a canine model after 6 months, and 1-year follow-ups indicated general safety of the device, and a 66-year-old human patient was successfully treated by loading the stent graft through the femoral artery to repair a thoracic intimal tear 2 cm from the LSA branch.[131]

Reduction of flow drag forces and blood damage in cardiovascular medical devices can be achieved with the use of superhydrophobic (SHP) surfaces due to their ability to enable fluid slip and prevent coagulation cascade reactions. Plastrons (micro/nanoscale surface asperities) reduce liquid–solid contact and thereby reduce friction, as well as exhibit antibiofouling and antithrombogenic properties, however the air plastron is easily destroyed by mechanical agitation or dissolution into the fluid. Researchers designed a modified porous PTFE foam that is abrasive-resistant and porous, with suitable surface structures for enhanced slip flow and antibiofouling properties. Sanding the foam with 400 grit aluminum oxide roughened the surface to create narrow, uniform grooves. Surface wettability demonstrated a contact angle increase of 156.43 ± 3.59° compared to 150.96 ± 3.74° for the unsanded surface. Hemolysis was low at 3.75 ± 3.12%, and the foam yielded 2.18 ± 0.09 ng mL^{-1} of fibrinopeptide A (FPA), indicating low agglomeration of fibrinogen on the surface. The air plastron was found to be capable of replenishment with the porosity allowing pressurized air to resist fluid impalement. The treatment of the foam with high velocity water (3.5 m/s) showed little variation in contact angle, through after 5 h the foam increased from a release angle of 6.46° to 11.88° due to protein fouling. Even protein fouled material was found to reduce drag up to 50% from closed loop pressure drop tests and high-speed water jetting, indicating good applications in blood-contacting medical devices when the inherent hemocompatibility of PTFE is accounted.[132]

Medical devices such as guidewires and catheters are extensively used for intravascular procedures and patients who have undergone such procedures have been found to have polymer fragments in the body from autopsy reports. Embolisms from 100 μm to 1.9 mm cross sectional diameter and 8 mm to 2.3 cm length have been found in the lungs, brain, heart, kidney, liver, colon, arteriovenous graft, skin/extremities, pancreas, spleen, muscle, and adrenal glands. Bench tests provide a simple, efficient evaluation of coating separation and performance. Hydrogel or PTFE coatings were applied on 304 V stainless steel guidewire models, and the coating integrity was examined after soaking with rotary bend fatigue testing and abrasive testing. In the case of the hydrogel coating, deionized water was found to cause more microscopic changes compared to 0.9% saline at room temperature and 37 °C but did not alter the integrity of the coating after 11 h. PTFE was not affected. Abrasive testing was found to provide

https://doi.org/10.1021/acs.chemrev.4c00996
Chem. Rev. XXXX, XXX, XXX−XXX

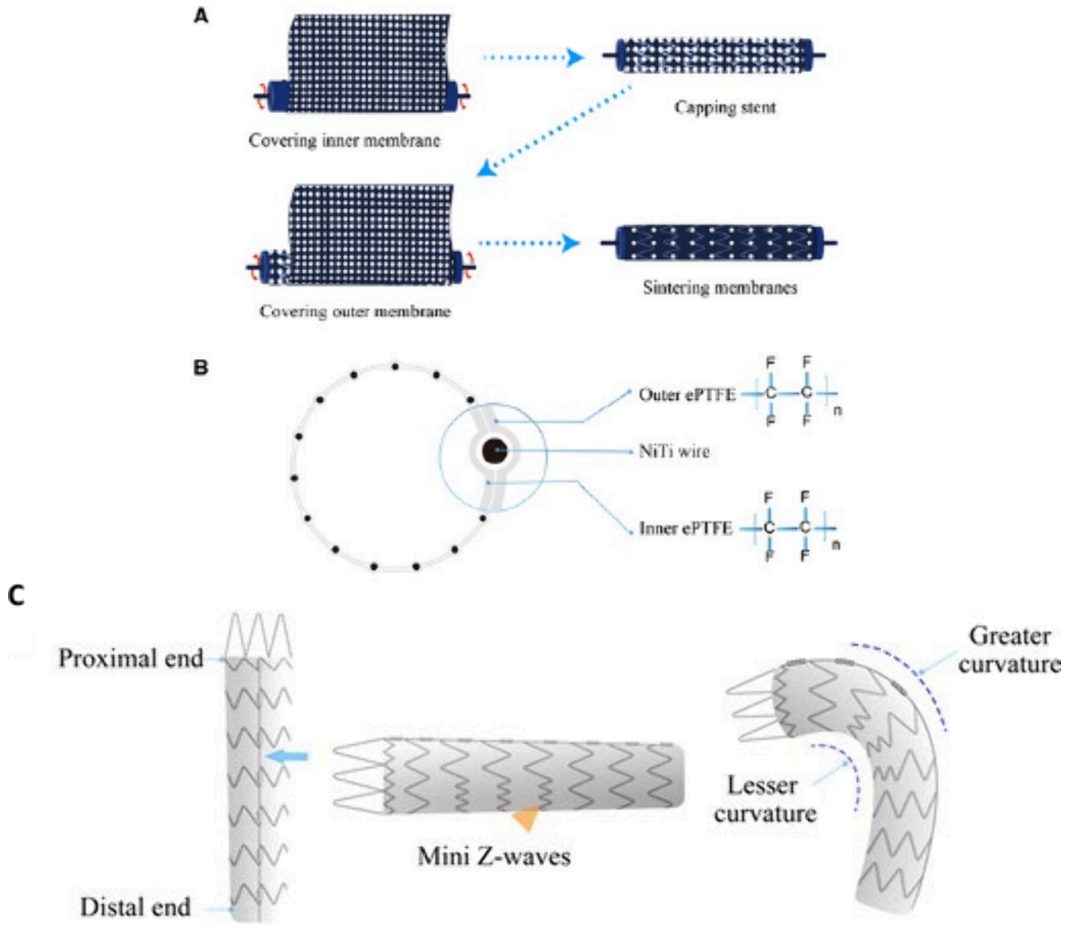

Figure 29. (A) Fabrication process for a trilayer stent-graft comprised of ePTFE, (B) top-down schematic of the trilayer stent-graft, (C) schematic displaying the stent-graft's compatibility with the aortic arch and the practicality of the z-wave design. Adapted with permission from ref (131). Copyright 2022 Oxford Academic.

useful information for evaluating coating performance, PTFE surfaces have higher friction forces on PTFE pads versus Delrin Acetal pads. Delrin pads also displayed more abrasion on both hydrophobic and hydrophilic surfaces. Because more distortion, but not delamination, is seen in DI water versus 0.9% saline (reminiscent of physiological conditions), it appears saline is a better choice for preconditioning medium. Future testing must be done at physiological conditions with abrasion to determine material degradation with pad materials similar to commercial medical devices.[133]

Chronic implanted electrodes are effective for monitoring neurotransmitters, but issues such as electrode passivation by proteins and damage to brain tissue pose challenges. To improve stability, Nafion coatings have been used, however an approach toward increasing biocompatibility is less emphasized in the literature. Researchers have developed cell membrane-based electrodes to mitigate rejection issues, using a red cell membrane (RCM) reference electrode by extracting RCM from rat blood and applying it to chemically modified Ag/AgCl electrodes. The ionic liquid 1-butyl-2,3-dimethylimidazolium hexafluorophosphate (BDMI) outperformed Nafion in protecting AgCl and supporting the cell membrane. Electrochemical impedance spectroscopy (EIS) demonstrated that charge-transfer resistance remained stable for 28 days postimplantation in rat brains. The glial scarring around the Ag/AgCl/BDMI/RCM electrodes was smaller than that around Nafion-coated electrodes, indicating enhanced biocompatibility. After implantation, the BDMI-coated electrodes possess a cathodic peak current of −1.6 mA, compared to −0.78 mA for Nafion-coated ones, suggesting potential for use in a two-electrode system for glucose microsensors. Current−voltage curves indicated that these electrodes could serve as polarized electrodes, highlighting significant advancements in biocompatibility and stability in brain implantation applications.[134]

Reticular polypropylene is commonly used as an abdominal mesh but has adverse effects such as adhesion formation with intestinal obstruction, migration, or intestinal fistula when contacting the visceral peritoneus. The researchers sought to use Surgipro (PP), DynaMesh (PP−PVDF), Preclude (ePTFE), and TiMESH (PP+Ti) to determine *in vitro* and *in vivo* performances to determine mesothelialization of the mesh and collagen deposition in rabbits. Meshes seeded with mesothelial cells displayed covering of the films in MC colonies, with laminar ePTFE (Preclude) having the greatest cell coverage. Preclude possesses a higher content of collagen III fibers but limited collagen presence at the mesh-subcutaneous tissue interface, indicating a lack of mesh integration into tissue. Reticular polypropylene meshes display unsatisfactory behavior when in contact with the peritoneal cavity, however this is due to structure and not chemical identity. Laminar polypropylene displays optimal behavior at the peritoneal interface, and the consensus is that reticular PP meshes should not be implanted on the intraperitoneal side, due to adhesion to the bowels. Pores in the structure present a

https://doi.org/10.1021/acs.chemrev.4c00996
Chem. Rev. XXXX, XXX, XXX−XXX

hazard to the intestines due to the exposure of the bowels to the mesh, and all reticular meshes display adhesion. Reticular meshes display blood remains and tissue arrangement following filament outlines, giving a rough surface as opposed to the laminar mesh smooth surface. The findings of this study show that PP-hybrids like TiMESH and DynaMesh do not improve adhesion compared to Surgipro (PP), and the reticular structure is the determining factor of adhesion due to the lack of MC continuous layer formation, preventing injury of other surfaces.[135]

TENG based devices possess ultrahigh sensitivity and excellent signal-to-noise ratios, having promise for improved cardiac monitoring. Researchers have developed a zero-power consumption, implantable, bias-free cardiac monitoring capsule (BCMC) that uses the triboelectric effect to monitor cardiac contractility. The BCMC is compact, making it suitable for minimally invasive implantation in animals, the shell is fabricated from a plant-based photosensitive resin via 3D printing, and nickel hooks are used to secure it between muscle bundles in the right ventricle. Inside the BCMC, aluminum films are pasted onto the walls, glass pellets filled with PTFE powder occupy the cavity, and the outer layer of Parylene C provides biocompatibility (Figure 30). At 10 Hz and a displacement of 0.25 mm the device generates an open circuit voltage of approximately 20 mV, making it sensitive enough to monitor extreme cardiac conditions. The BCMC has no significant signal attenuation after 105 cycles of fatigue and can achieve an optimal output voltage of 5.69 V. It also demonstrates good biocompatibility and low hemolysis, making it an ideal candidate for implantable cardiac monitoring.[136]

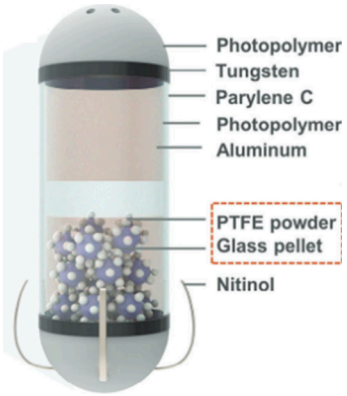

Figure 30. Schematic for the design of the implantable BCMC device consisting of a PTFE powder with glass pellets inside a aluminum coated chamber and a biocompatible exterior coating of Parylene C for cardiac monitoring. Adapted with permission from ref (136). Copyright 2024 John Wiley & Sons Inc.

Bacterial nanocellulose (BNC) is a naturally derived hydrogel with excellent tissue-like properties, making it suitable for biomedical applications. However, BNC lacks innate anticoagulant and antimicrobial properties, which requires postmodification to improve its performance in biointerfaces. In this study, a new class of flexible, lubricant-infused BNC membranes was developed with enhanced antithrombotic and antibacterial properties. The BNC membranes were functionalized with fluorosilane molecules Trichloro(1*H*,1*H*,2*H*,2*H*-perfluorooctyl)silane (TPFS), through chemical vapor deposition, followed by impregnation with a fluorocarbon-based lubricant (perfluoroperhydrophenanthrene (PFPP)) (Figure 31). The modified membranes outperformed unmodified BNC and commercially available PTFE felts in several key areas. They significantly reduced plasma and blood clot formation, prevented bacterial adhesion and biofilm formation, and possess superior resistance to fats and enzymes. Mechanical testing revealed that the lubricant-infused BNC membranes had higher tensile strength and better fatigue resistance compared to both unmodified BNC and PTFE felts. These enhanced properties make the modified BNC membranes promising for use in biofluid-contacting medical implants and tissue engineering applications, where both mechanical durability and biological performance are critical.[137]

This study presents a highly efficient, biocompatible ultrasonic energy harvester (H-UEH) that serves two functions: providing power to implantable bioelectronics and acting as a neuroprosthetic for peripheral nerve stimulation. The H-UEH is constructed from a polyvinyl butyral (PVB)-based cylindrical polyhydroxyalkanoate (PHA) dielectric layer, sandwiched between two FEP electrets (Figure 32). This design enhances strain and output when exposed to external pressure, resulting in a high piezoelectric coefficient (d_{33}) of up to 4680 pC N^{-1}. The harvester demonstrates excellent performance, generating peak powers of 15.61 mW underwater, 13.92 mW under fat, and 12.86 mW under muscle, with effective acoustic impedance matching. It is also compatible with biological tissues and maintains output stability during peripheral nerve stimulation. The H-UEH meets the power requirements for nerve stimulation and bioelectronic devices, making it a promising technology for advancing wireless power supplies, neuroprosthetics, and drug delivery in the next generation of medical implants.[138]

Ferroelectric materials are commonly used in medical implantable devices, but their nondegradable nature often requires removal through secondary surgeries. In this study, a new biodegradable ferroelectric molecular crystal, 1*H*,1*H*,9*H*,9*H*-perfluoro-1,9-nonanediol (PFND), was discovered (Figure 33). This material undergoes a phase transition from cubic to monoclinic at 339 K, facilitated by a 2D hydrogen bond network formed through O−H···O interactions. PFND demonstrates a strong ferroelectric performance, including reversible phase transitions at 339 K/290 K with significant thermal hysteresis. It also exhibits plastic deformation under stress, with a rare ferroelectric plastic phase transition and a large entropy change of 52.12 J mol^{-1} K^{-1}. Moreover, PFND displays exceptional *in vitro* biocompatibility and *in vivo* biodegradability, making it a promising material for medical implants, such as biosensors and neurorepair devices. This work opens up new possibilities for developing biodegradable ferroelectric materials for biomedical applications.[139]

Medical devices inserted into blood vessels can trigger thrombosis, making the surface properties of these devices critical. This study aimed to characterize the thrombogenic properties of various cardiovascular biomaterials by examining how the adsorption of fibrinogen, polymerization into fibrin, and analyzing the resulting structures. Fibrin formed fiber-like structures on metallic surfaces and branched, fractal-like patterns on polymeric surfaces. When using vascular guidewires as clotting substrates, the study observed that fibrin adsorption depended on the exposed parts of the guidewire, with the morphology of fibrin on uncoated guidewires resembling that on raw stainless steel. In terms of polymer-

https://doi.org/10.1021/acs.chemrev.4c00996
Chem. Rev. XXXX, XXX, XXX−XXX

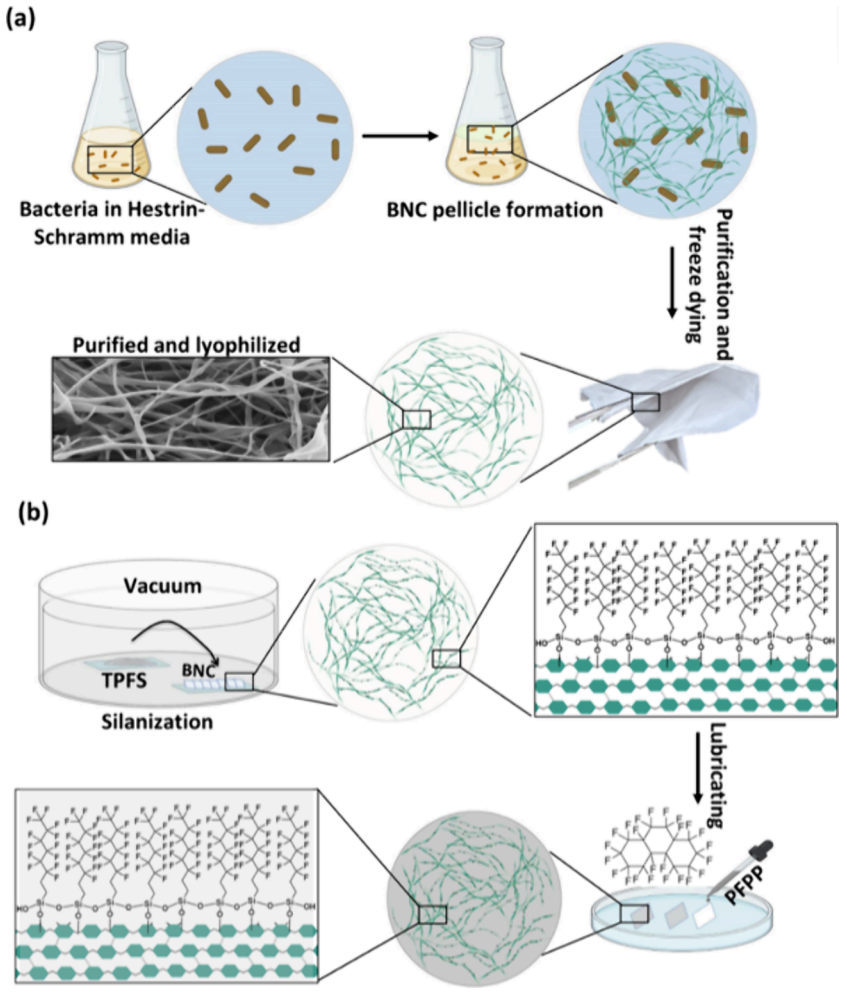

Figure 31. (a) Bacterial nanocellulose (BNC) culture in Hestrin−Schramm medium following the purification and lyophilization steps. Samples were flash-frozen using liquid nitrogen and lyophilized in order to obtain membranes with optimal mechanical strength and porosity. (b) After purifying and drying the BNC samples, they were functionalized with trichloro(1H,1H,2H,2H-perfluorooctyl)silane (TPFS) through chemical vapor deposition (CVD) and lubricated with perfluoroperhydrophenanthrene (PFPP) lubricant. Reproduced with permission from ref (137). Copyright 2023 American Chemical Society.

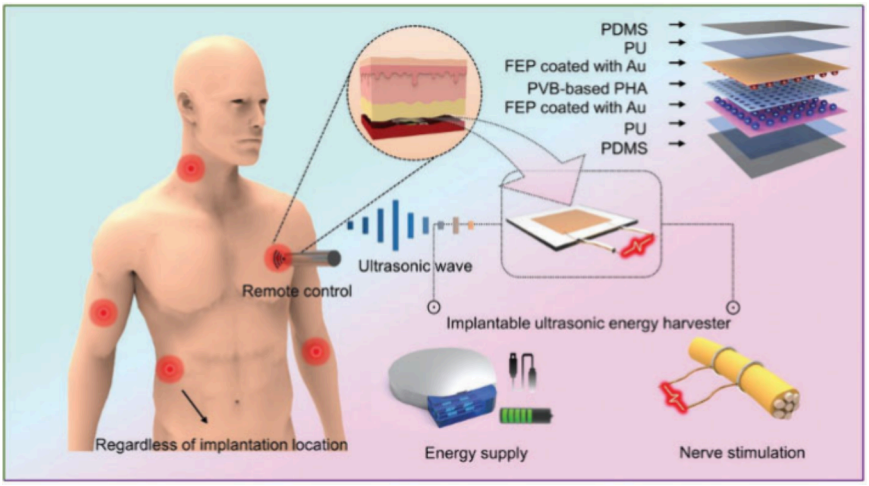

Figure 32. Illustration of H-EUH as implantable bioelectronics for energy supply and neuroprosthetics, and structure diagram of H-EUH. The device can be driven by the ultrasound remotely to produce tunable electrical outputs. Reproduced with permission from ref (138). Copyright 2022 John Wiley & Sons Inc.

https://doi.org/10.1021/acs.chemrev.4c00996
Chem. Rev. XXXX, XXX, XXX−XXX

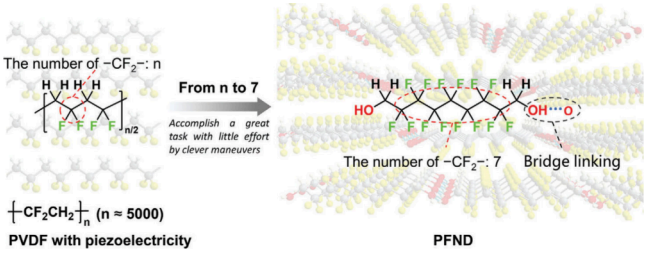

Figure 33. Design concept of biodegradable ferroelectric molecular crystal PFND structurally inspired by PVDF. Reproduced with permission from ref (139). Copyright 2024 John Wiley & Sons, Inc.

coated surfaces, fibrinogen and fibrin adsorption increased in the order: AF < PBMA < PS, with corresponding differences in thrombogenicity (Figure 34).[140]

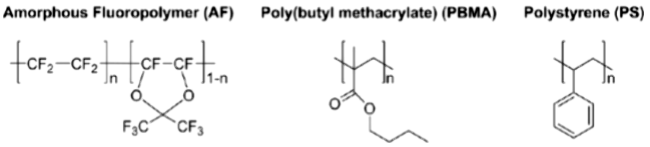

Figure 34. Polymeric biomaterials include fluoropolymers, polymethacrylates, and polystyrene. Reproduced with permission from ref (140). Copyright 2023 American Chemical Society.

There is a growing demand for high-performance flexible batteries, especially for applications in flexible electronics, wearable sensors, and implantable medical devices. To address this, gel electrolytes with superior ionic conductivity and safety are being explored as a solution for flexible batteries. This study focuses on creating two types of high-quality ionic liquid-based gel polymer electrolyte membranes (Polyvinylidene Fluoride-Ionic Liquids, PVDF-ILs) using a solution-casting method (Figure 35). These membranes were incorporated into flexible aluminum-air batteries, and their performance was analyzed under different bending conditions. The results demonstrate that the PVDF-ILs have a porous structure and an interwoven skeleton, providing high ionic conductivity (up to 2.97 × 10^{-3} S cm^{-1}), with excellent electrochemical performance and stable energy transfer capabilities, including an output voltage of 0.86 V and a specific capacity of 532.7 mA h g^{-1}. These batteries can operate while bent at angles of 30° or 90°, making PVDF-ILs promising for applications in flexible electronics, energy storage, and sensors.[141]

Bacterial infections and corrosion are among the leading causes of failure in biomedical metallic implants. In this work, the research group developed a straightforward two-step method to create a TiO_2−PTFE nanocomposite coating on a stainless-steel substrate, which exhibits both antibacterial and anticorrosion properties. This was achieved using a sol−gel dip coating technique. Initially, a bioinspired PDA sublayer was applied to stainless steel to enhance adhesion and reactivity. Subsequently, the TiO_2−PTFE coating was uniformly deposited onto the PDA sublayer. The proportions of PTFE and TiO_2 significantly affected the surface energy of the coating. The coating, with a total surface energy of 26 mJ m^{-2}, demonstrated minimal bacterial adhesion against both Gram-negative *E. coli* WT F1693 and Gram-positive *S. aureus* F1557, a phenomenon explained by the extended DLVO theory. The TiO_2−PTFE coating benefited from the synergistic effects of its components, indicating improved corrosion resistance in artificial body fluids compared to coatings made solely of TiO_2 or PTFE. Additionally, the TiO_2−PTFE coating exhibited excellent biocompatibility with fibroblast cells in culture, presenting a promising solution to current challenges associated with metallic implants.[142]

Thermoplastics are particularly sensitive to temperature and loading rates, distinguishing them from other material classes, making it essential to characterize how these factors influence their mechanical properties. To this end, dynamic mechanical analyses were conducted to assess the application temperature range, alongside tensile tests at various crosshead speeds (10^3,

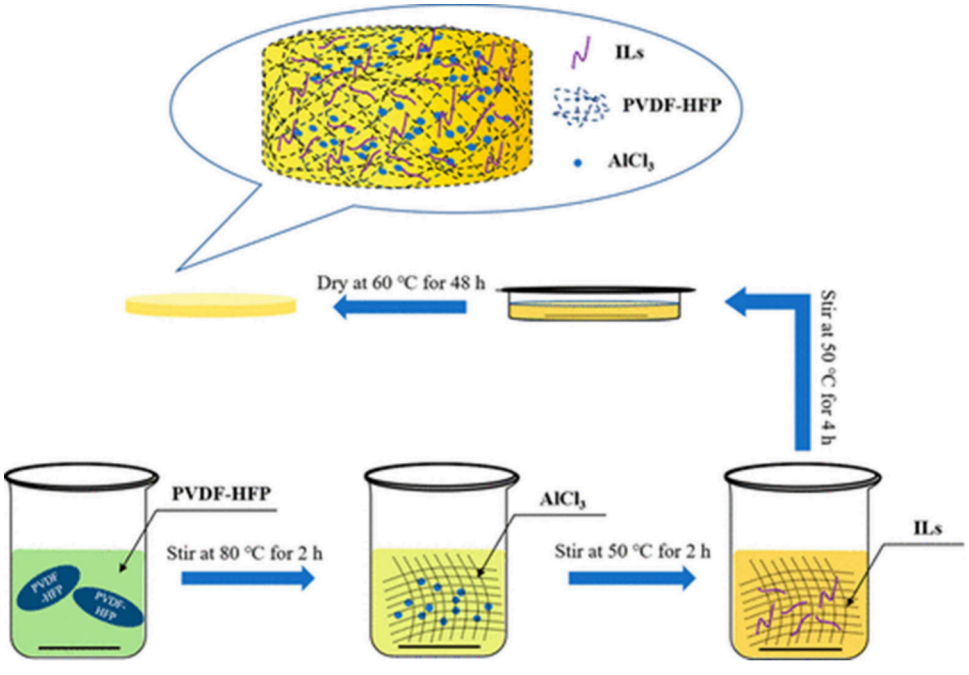

Figure 35. Synthesis route of PVDF-ILs. Reproduced with permission from ref (141). Copyright 2022 American Chemical Society.

https://doi.org/10.1021/acs.chemrev.4c00996
Chem. Rev. XXXX, XXX, XXX−XXX

Scheme 14. Synthesis Reaction Diagram of P(AAm-co-NaAMPS)-xanthan Hydrogel

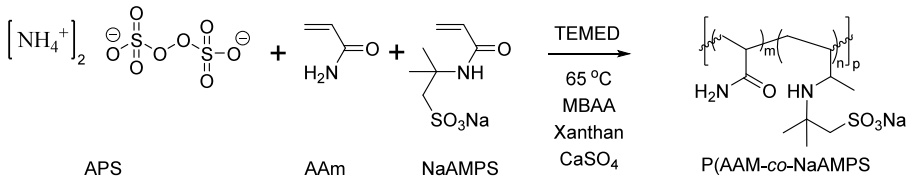

10^{1}, 10^{-1}, and 10^{-3} mm/s) on several 3D-printable polymers, including PEEK, PLA, PMMA, glycol-modified poly(ethylene terephthalate) (PETG), PVDF, and PP. The results indicated that the mechanical properties of PEEK, PLA, PMMA, and PETG were largely unaffected by temperature variations typical of the human body. In contrast, PVDF and PP exhibited a significant reduction in stiffness as body temperature increased. Furthermore, the stiffness of these materials has an increasing dependency on strain rate across PLA, PP, PEEK, PETG, PMMA, and PVDF. In addition to assessing mechanical integrity (strength, stiffness, and their dependencies on strain rate and temperature), the materials were ranked based on their filling density as an indicator of processability. This analysis provides valuable insights for selecting materials for medical applications and designing 3D-printed implants. The high flexibility of PP and PVDF makes them suitable for use as suture materials or meshes. However, their potential for cranial bone reconstruction, particularly for smaller defects where high stiffness is less critical, should not be overlooked. Moreover, the ductility of PP and PVDF helps prevent brittle failure of implants in the event of an accident. PETG appears to offer a balanced compromise between the two material groups, making it suitable for applications that do not require high load capacity or elasticity, such as bite guards.[143]

Mesh implants are commonly used in hernia repair and urogynecological reconstruction, with polypropylene being the most widely utilized material for nonresorbable mesh implants. A degradation phenomenon in PP mesh, characterized by cracking, flaking, and peeling on the surface, was identified in the 1990s and has raised concerns due to associated litigations. PVDF has emerged as an alternative material for nonresorbable mesh implants since 2003, owing to its high biocompatibility. To date, no degradation of PVDF mesh has been reported, although research on this material remains limited. The surface conditions of PVDF mesh after 3, 6, 12, and 24 months of implantation were compared with two types of PP meshes. XPS results confirmed the successful removal of tissue residues, as indicated by the absence of nitrogen. SEM analysis revealed no significant morphological changes in the PVDF mesh, while both types of PP mesh exhibited progressive surface cracking over time. FTIR spectra of the implanted PVDF meshes displayed no significant differences from those of pristine meshes, whereas the FTIR spectra of both types of PP meshes displayed additional chemical functional groups (carbonyl (C = O) and hydroxyl (−OH) groups) that increased with implantation time, indicating ongoing degradation. This study underscores the morphological and chemical stability of PVDF mesh, demonstrating its superior resistance to degradation compared to the two types of PP meshes.[144]

Parastomal herniation is a common complication following colorectal surgery, with a prevalence ranging from 30% to 80%. This study aimed to develop a new intraperitoneal colostoma mesh prosthesis (IPST) with improved elastic properties, constructed from thermoplastic polyurethane (TPU) monofilaments. Researchers conducted open terminal sigmoid colostomies in a total of 10 minipigs, using either a 10 cm by 10 cm PVDF mesh or the newly developed TPU/PVDF composite mesh. The colostomas were positioned paramedian in the left lower abdomen, and the IPST meshes were secured intraperitoneally. The implantation of the new IPST mesh with enhanced elastic properties was successfully achieved in the minipig model over the 8-week period. Immunohistochemical analysis revealed that the Collagen I/III ratio, an indicator of tissue integration, was significantly higher in the TPU group compared to the PVDF group (9.4 ± 0.5 vs 8.1 ± 0.5, p = 0.002). Additionally, the TPU group exhibited a significantly lower inflammatory response, as evidenced by a smaller inner granuloma at the mesh-colon interface (17.6 ± 3.3 μm vs 23 ± 5 μm, $p < 0.001$). The improved tissue integration, indicated by the Collagen I/III ratio, suggests advantages over standard elastic PVDF-IPST meshes.[145]

The Hydrogel 40:60 formulation demonstrated excellent hemocompatibility, an extended activated partial thromboplastin time (aPTT), and favorable mechanical properties. Bilayered poly(AAm-*co*-NaAMPS)-xanthan hydrogel-ePTFE vascular grafts utilizing the Hydrogel 40:60 composition may effectively address the significant issue of thrombus formation in vascular graft transplantation (Scheme 14).[146]

Treatment of PTFE with argon plasma or piranha solution generates reactive functional groups, such as O═, OH−, and OOH−, on the PTFE surface. These groups are then activated through cross-linking with 1-ethyl-3-(3-(dimethylamino)-propyl) carbodiimide hydrochloride (EDC) and *N*-hydroxysulfosuccinimide (NHS) to covalently bond with the thrombin-inhibiting peptide UV037. The UV037 sequence is specifically designed to contain a single primary amine from a lysine side chain at its C-terminus, ensuring unidirectional cross-linking. Although researchers have demonstrated that their peptide-grafted PTFE material is drag-reducing, antithrombotic, and resilient to mechanical wear in bench tests, further evaluation is necessary to confirm its clinical applicability. Additional testing of its functional durability over extended periods is recommended to determine its suitability for long-term applications, such as ECMO or vascular prostheses.[147]

1.7. Medical Devices

In this study, the effects of polymer concentration and feed rate on the morphology and piezoelectric output voltage of electrospun PVDF-TrFE nanofibers were examined. The findings revealed that increasing the polymer solution concentration and feed rate resulted in larger nanofiber diameters. Additionally, both experimental results and finite element method (FEM) simulations showed that as the nanofiber diameter increased, the output voltage generated by the nanofibers decreased. This is attributed to the reduced strain in the thicker nanofibers during deformation, which affects their piezoelectric performance.[148]

https://doi.org/10.1021/acs.chemrev.4c00996
Chem. Rev. XXXX, XXX, XXX−XXX

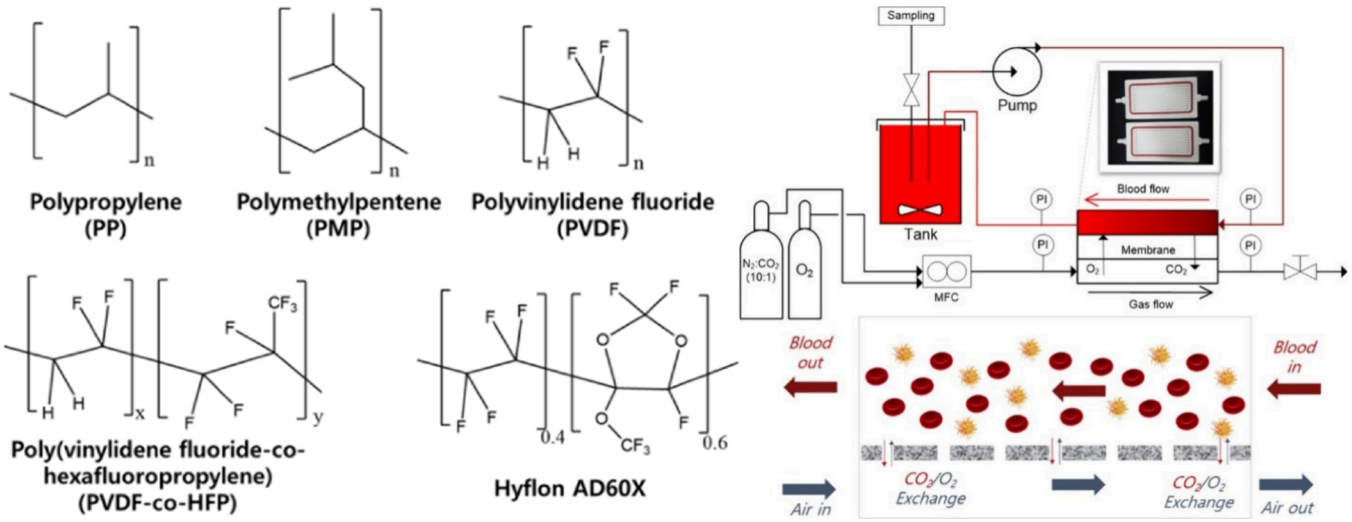

Figure 36. Polymers mentioned and employed in this study (left) and schematic representation of a blood oxygenation apparatus (right). Reproduced with permission from ref (150). Copyright 2020 American Chemical Society.

Nai et al. evaluated the effectiveness of surface treatment of silicone and ePTFE vascular prostheses in reducing bacterial contamination. *S. aureus*, *S. epidermidis*, *P. mirabilis*, and *E. faecalis* were all selected as bacterial targets, with the goal of determining the efficacy of pre- or postcontamination washing of these prostheses to decrease bacterial presence and potentially prevent infections. The results indicated that prewashing with chlorhexidine was particularly effective in inhibiting the growth of *S. epidermidis*, while also resulting in a significant 53% reduction in *S. aureus* colonization density in the prewashed group. Postcontamination washing yielded effective inhibition of all bacteria, including a 60% decrease in *S. aureus* colonization density. Chlorhexidine treatment led to a complete absence of *E. faecalis* colonization, highlighting its efficacy as an antiseptic. Additionally, lidocaine demonstrated its ability to reduce *S. aureus* growth in both silicone and ePTFE prostheses, suggesting its potential as an adjuvant treatment in this context. Further testing revealed no growth of *P. mirabilis* following any treatment. The findings also indicated that prewashing did not significantly affect *S. aureus* or *E. faecalis* in silicone, though there were marked differences observed in the presence of *S. epidermidis* and *E. faecalis* when antibiotics were applied.[149]

Artificial lung membranes are utilized for blood oxygenation through artificial lungs as well as hemodialysis. Initial first generation membranes were made of polypropylene but are only useable on the order of a few hours to 2 weeks due to risk of wetting. second generation polymethylpentene (PMP) membranes possess a higher gas permeability and have a thin silicon coating to eliminate risk of wetting. PMP membranes require a larger surface area to be effective, so therefore require a high prime volume (extracorporeal blood supply). These membranes can last from 2 to 4 weeks before blood begins to coagulate, and fatal hemolysis occurs. The mortality rate is around 60% for patients with extracorporeal membrane oxygenators (ECMO), and the models tend to be quite large. Additionally, the material requires both low biofouling (typically hydrophilic materials) and low wetting capabilities (hydrophobic materials). Researchers designed an ECMO from PVDF-*co*-HFP in a 95/5 PVDF/HFP ratio due to its ease of processing, low surface energy to eliminate protein adsorption, and high hemocompatibility (Figure 36). The material was coated with Hyflon AD60X to minimize wetting. Hyflon AD60X-coated PVDF-*co*-HFP produced a contact angle of 115° and liquid entry pressure (LEP) of 5 bar. A material was desired with a contact angle above 90°, as above 90° positive (LEP) is required to push liquid through the membrane. LEP is an inverse function of pore size, resulting in a desire for the highest LEP for long-term stability but also large pores for maximum transport flux, resulting in an optimum pore size of 30−50 nm. Compared to commercially available membranes, PVDF and uncoated PVDF-*co*-HFP display similar performance. Commercially available PP and PMP membranes give sufficient performance of 150 mL m^{-2} min^{-1} in a proper clinical setting, indicating that fluoropolymers are at least competitive with commercial membranes.[150]

Typically, PTFE, PU, and PET are used in blood-contact applications, but all display issues with fibrinogen absorption. Fibrinogen is at 4% of plasma concentration, but plays a crucial role in clotting, mediates platelets, and triggers a coagulation cascade. Adsorption of proteins on hydrophobic surfaces suggests that favorable hydrophobic−hydrophobic interactions occur, hence why polymers such PTFE develop thrombosis over time. PVDF has good blood compatibility, but problematic hydrophobicity can induce coagulation. A blood-inert surface was proposed to be helpful, wherein albumin was adhered to the surface of a PVDF graft copolymer. Researchers utilized perfluoromethymethacrylates (PFMMA) as a graft material onto a P(VDF-CTFE) substrate by ATRP, with PFMMA lowering the surface energy of the material (Figure 37). The resulting material is a bendable, free-standing film due to the PVDF-CTFE backbone. Material surface energy is in the range of 11.1−18.7 mN m^{-1}, correlating to the n-value of fluorocarbons. P(VDF-CTFE)-*g*-HFBMA (number of fluorinated carbons = 3) is the most effective in inhibiting adsorption. Albumin pretreatment of the substrate reduces fibrinogen adsorption from 2069 ng cm^{-1} to 5.6 ng cm^{-1}. A similar effect is seen with other copolymers, where albumin pretreatment blocks fibrinogen adsorption, thus reducing incidents of thrombosis and coagulation in a blood-contact scenario.[151]

Long-segment peripheral nerve injuries (PNI) tend to have incomplete nerve tissue recovery and often do not result in functional reconstruction. 2−5% of traumas result in PNIs,

https://doi.org/10.1021/acs.chemrev.4c00996
Chem. Rev. XXXX, XXX, XXX−XXX

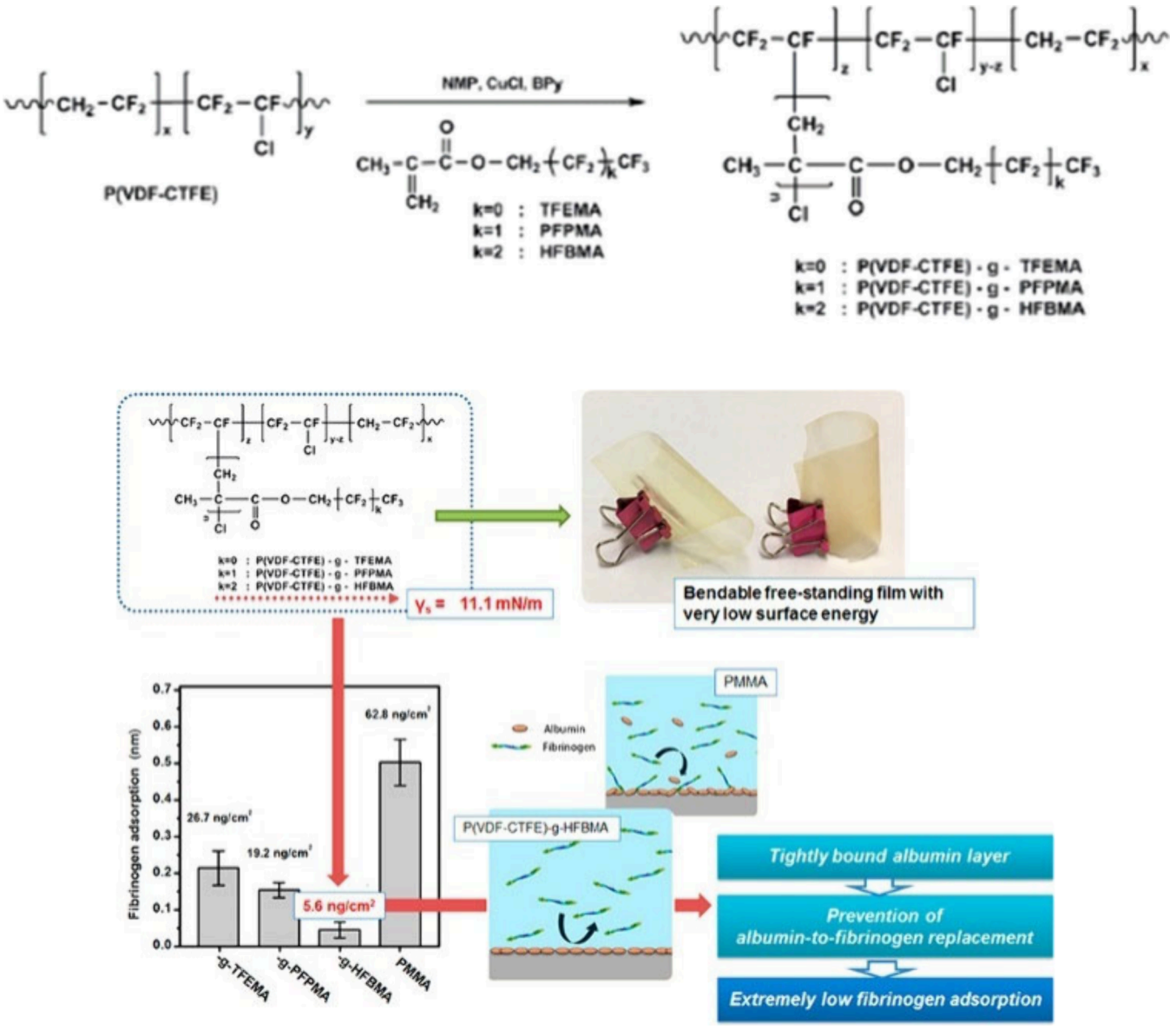

Figure 37. Synthesis of P(VDF-CTFE) acrylate graft copolymers by ATRP (top), and development of a bendable, low surface energy film from copolymerization of fluorinated acrylates with P(VDF-CTFE) (bottom). Adapted with permission from ref (151). Copyright 2019 American Chemical Society.

with low-frequency electrical stimulation apparatuses assisting in recovery. However, ES systems do not adapt to the changing physical states of the autonomous nervous system (ANS) and tend to fail in nerve repair, causing excessive inflammation, pain, or immune responses due to charge overflow and mechanical mismatch. A novel tribo/piezoelectric hybrid nanogenerator (Tp-hNG) with a nanoporous nerve guide conduit (NP-NGC) was designed to fabricate an implantable neural electrical stimulation (FI-NES) system which self-regulates according to nervous system stimulation. The TP-hNG was created from electrospun PVDF nanofiber mats doped with ZnO NPs as a negative layer (Figure 38). Silicon rubber is used as the positive layer, and the device can produce a voltage of 16.8 ± 0.2 V cm^{-2} with a maximum power density of 72 mW m^{-2}. The material was found to be able to power 15 LEDS and charge a 1 μF capacitor to saturation in 400 s. Biostimulation from a human volunteer displays broad peaks of 1−5 s, compared to <0.1 s of other NGs. The NP-NGC was fabricated of chitosan nanofibers coated with PEDOT:PSS (poly 3,4 ethylene dioxythiophene:poly styrenesulfonate), PSS was etched away and the material spray coated with poly l-lactic acid (PLLA). With the two devices implanted and connected with Pt wires to make the FI-NES system, the device was tested in rats with a 15 mm section of sciatic nerve removed. Twelve weeks of use results in no cracks or abrasions, and the device was found to have excellent biocompatibility after 2 months, giving stable electric stimulation. Compared to a nerve autograft, the clinical gold standard, similar levels of reconstruction were observed, with the rats regaining perfect neuromotor function.[152]

Endoprostheses are designed to strengthen damaged tissue after surgery and must have appropriate strength and deformation properties to counter pressure in the abdomen. As deformation of the mesh is linked to deformation of the thread and base mechanical properties of the fabric, creep is an important characteristic to analyze to determine the role of

https://doi.org/10.1021/acs.chemrev.4c00996
Chem. Rev. XXXX, XXX, XXX−XXX

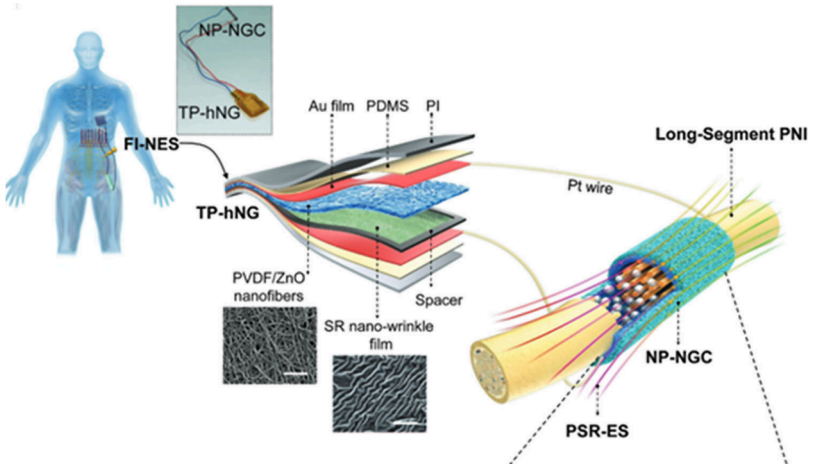

Figure 38. Fabrication of the FI-NES device for the regrowth of long-segment PNI injuries through piezoelectric stimulation by PVDF/ZnO nanofibers. Adapted with permission from ref (152). Copyright 2021 John Wiley & Sons, Inc.

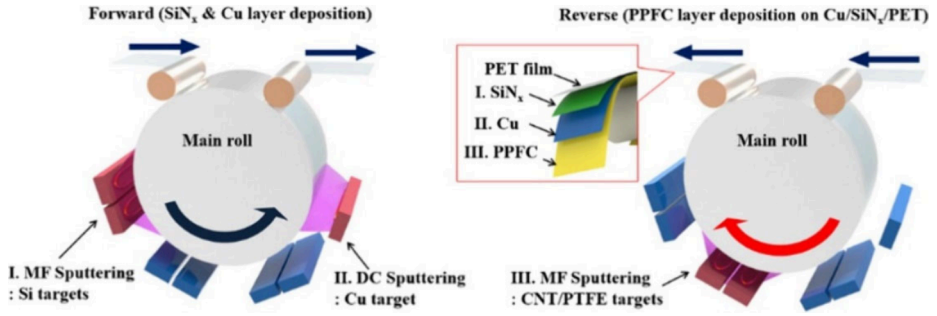

Figure 39. Roll-to-roll process for sputter coating a PET substrate to fabricate the PCS film heater. Adapted with permission from ref (154). Copyright 2020 John Wiley & Sons Inc.

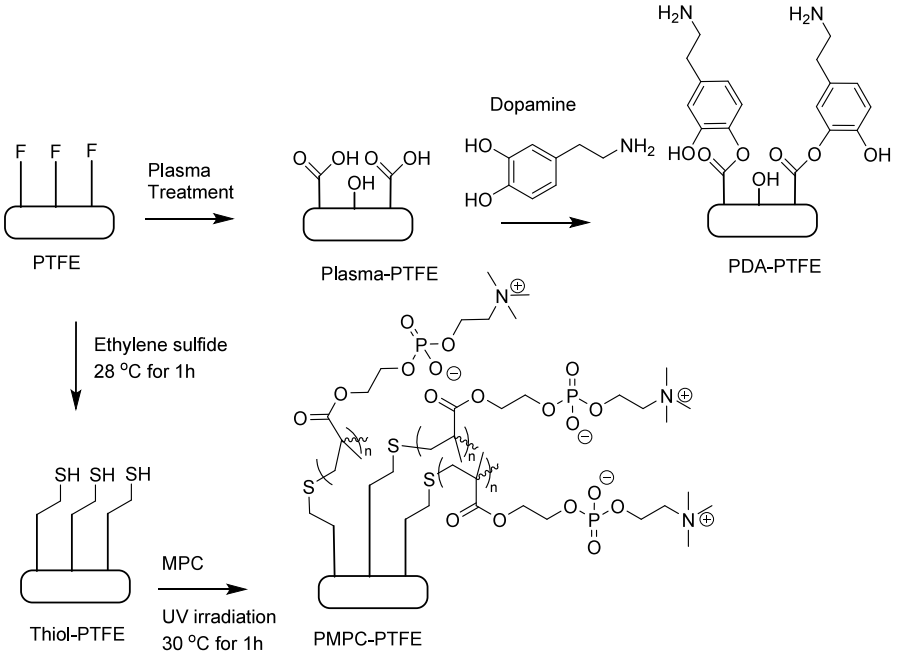

Figure 40. Chemical modification of PTFE surfaces for antibiofouling applications.

thread properties in creep of mesh endoprostheses. Researchers determined a mathematical model of viscoelasticity and data from long-term deformation of constant load to allow for the prediction of creep once the basic steps are determined. Polypropylene and PVDF threads were tested on a deformation relaxometer from 65 to 320 mPa and gaining linear deformation curves by using short-term creep data at different tensile stresses. PP and PVDF were found to have

https://doi.org/10.1021/acs.chemrev.4c00996
Chem. Rev. XXXX, XXX, XXX−XXX

almost identical barriers of activation for creep at about 1 eV. Added tensile stress causes twisted (gauche) conformers to switch to trans (straightened) conformers and transitions were found to occur once the energy barrier for internal rotation and intermolecular interaction was overcome, from $0.8 \leq U_0 \leq 1.0$ eV. Tensile stresses were found to be equal to the mean cross-sectional stress, itself a ratio of tensile stress to cross-sectional area. Hence, basic steps of creep kinetics can be compared to mesh creep and deformation behavior appropriately evaluated.[153]

Transparent, flexible film heaters have applications in many industries, including vehicle windows, camera lenses, and solar cells. Typical transparent film heaters are created by depositing highly electrically conducting materials on transparent films such as PET. Tin-doped indium oxide (ITO) thin films are used commonly for touch screens, LEDs, and solar cells, but crack easily when bent and require synthesis at high temperatures (~300 °C). Polymer/metal/inorganic (PMI) or polymer/metal/polymer transparent film heaters can be developed using SiN_x and ITO with plasma-polymer-fluorocarbon (PPFC). A film heater was fabricated from a plasma-polymer-fluorocarbon/Cu/SiN_x (PCS), demonstrating excellent mechanical flexibility, transparency, and self-cleaning characteristics (Figure 39). The material was found to be hydrophobic with a WCA of 105°, displays a maximum transmittance of 78.25% in the visible region, and had a sheet resistance of 4.6 Ω sq^{-1}. While Ag-based heaters display superior optical properties, the visible light region transmittance of the PCS film is comparable to Ag, with a smaller maximum inner bending radium of 4 mm. Cyclic fatigue testing shows mechanical bending reliability outperforms Ag films, indicating potential applications in foldable and rolling devices. The material has good potential to be applied in thermotherapy, maintaining uniform heating distribution, and the film can be easily attached to the human body with a low surface temperature of 44 °C at 15 V.[154]

PTFE medical devices often induce extensive inflammation and infection at the device-tissue interface, limiting long-term medical applications of implanted devices. PDA coatings provide an excellent material-independent modification but generally fail to form stable layers on PTFE due to the hydrophobic and chemically inert surface. Researchers utilized Plasma-treated PTFE as a method of functionalization of PTFE surfaces with mussel-inspired PDA (Figure 40). Sonication of the plasma-treated PTFE−PDA demonstrates good stability of the PDA layer on PTFE treated with 40 and 100 W of plasma energy for 5 and 60 s respectively, with lower energy plasma providing less stability of the PDA layer. The higher strength plasma was thought to introduce more hydrophilic functionalities on the PTFE, thus stabilizing the dopamine layer. The PDA layer is then treated with ethylene sulfide to introduce a thiol group, and graft polymerization of MPC is photoinitiated, causing tandem thiol activation and MPC polymerization. Protein adsorption on the resulting surface was 0.40 μg cm^{-2} compared to 25 μg cm^{-2} for virgin PTFE. PTFE−PMPC shows small amounts of albumin and fibrinogen adsorbed, with protein adsorption suppressed with no time dependence. The material also suppresses the adsorption of plasma proteins compared to virgin PTFE, indicating the devices will have an increased lifespan in the body.[155]

Regulatory approval requires testing of blood-contacting medical devices, with the ISO standard 10993−4 (2017) acting as a useful source for potential tests. Few standardized thrombogenicity tests are available, and most laboratories utilize *in vivo* animal studies to attain results, such as the nonanticoagulated venous implant (NAVI) assay. Key parameters in thrombosis responses need to be well understood to understand how materials interact with blood, and a reliable cost-effective *in vitro* methodology would allow for facile screening of antithrombogenic materials. No standardized dynamic flow experiments exist, causing a need for study on the specific contributions of various variables to blood coagulation. Researchers investigated the effect of temperature on thrombosis in a closed-loop PVC system using whole sheep or cow blood (heparinized to animal-specific levels). Blood was circulated at 22−24 °C as a room temperature model for 1 h, or 37 °C as a body temperature model for 1−2 h, utilizing different materials. Latex was used as a positive control thrombogenic material, PTFE as a negative control thrombogenic material, and both were compared to silicone and high-density polyethylene (HDPE). PTFE and HDPE both displayed low thrombus formation, indicating that they are functional as antithrombogenic materials. Thrombogenicity was measured by percent thrombus coverage, thrombus weight, and percent platelet count. Bovine blood at 37 °C did not yield sufficient thrombus on test materials to differentiate thrombogenicity, this suggests a room temperature closed loop system is a promising model for determining relative thrombogenic potentials in a dynamic *in vitro* testing model.[156]

ePTFE is an excellent material in biomedical applications due to its good mechanical properties and excellent biocompatibility. ePTFE production processes utilizing typical biaxial stretching create a bowed material with thinner sides and a thicker edge. The researchers in this group utilized an olive-shaped winding roller to fabricate ePTFE tape with a uniform thickness and a node-fibril microstructure. The roller provides a greater longitudinal stretching amplitude to avoid the tendency of the material to retract longitudinally in response to transverse stretching. When compared to a common roller, the membrane displayed a thicker middle compared to the edges, with a range of 15.5 ± 9.5 μm and variation up to 19 μm, whereas the olive roller improved thickness uniformity with the fluctuations within 10 μm. The material was then examined to determine the effect of internal microstructures on material performance, examining hemolysis, coagulation, bacterial reverse mutation, *in vivo* thrombosis, intracutaneous reactivity tests, pyrogen tests, and subchronic systemic toxicity tests. The material met international standards and was successfully implanted into rabbit muscle, producing acceptable degrees of inflammation. The material was synthesized in a clean room on an industrial scale and offers an excellent way to fabricate raw material for stent grafts.[157]

Intrinsically conducting polymers (ICP) have higher flexibility and can form conducting networks with PVDF, presenting an attractive ceramic alternative. ICPs can conduct ionic charges, are known to have antibacterial properties, and can be fabricated via electrospinning. Polyaniline-PVDF (PVDF/PANI) blends possess an increase in ionic conductivity, lowering of impedance, increase in dielectric properties, and electroactive responses. Polycarbazole offers a good target due to possibilities of conjugation on the ring (N, C3−C3′, etc.) for increased biocompatibility, detection of biological targets, and derivatization, as well as favorable

https://doi.org/10.1021/acs.chemrev.4c00996
Chem. Rev. XXXX, XXX, XXX−XXX

electrical properties. PVDF/PANI and PVDF/PCZ nanofibers were found to reduce viable *E. coli* to 16 CFU/mL and 12 CFU/mL respectively, compared to 21 CFU/mL for pure PVDF. In the case of *S. aureus*, PVDF/PANI and PVDF/PCZ reduced the colony count to 18 CFU/mL and 10 CFU/mL respectively, compared to 25 CFU/mL for pure PVDF. The device has higher resistance to biofilm adhesion and can further be electrostimulated to reduce biofouling. Compared to PVDF/PANI composites, a higher open circuit potential was observed and the PVDF/PCZ composite only reduced flexibility by 20% compared to pure PVDF nanofibers. A 2.7 cm × 2.3 cm nanogenerator based on PVDF/PCZ was found to instantly light a 15 LED array and charge a 2.2 μF capacitor through periodic vertical compressive force. Gentle toe and heel movements generated a voltage of 0.5 and 0.2 V, wrist motion generated a voltage of 0.12 V, and finger motion generated about 0.1 V. Increasing PCZ to PVDF from 1%, 2%, and 6% results in an open-circuit voltage increase from 0.5 to 1.6 V to 2.3 V, respectively, indicating the device can be modulated by PCZ content.[158]

Management of environmental humidity is important for health and comfort of humans, as well as masks worn for medical purposes such as surgery, or protective masks for skiing or cycling. Smart breathing valves based on moisture-responsive actuators work for humidity management and require a fast response. Researchers have designed actuators based on a bilayer of methacrylated hyaluronic acid (HAMA), a polysaccharide, as a moisture-sensitive layer and porous PVDF as a moisture-inert layer are capable of rapid, reversible, and repeatable bending based on moisture-actuation by environmental relative humidity (Figure 41). The films are fabricated by spin-casting HAMA solutions on ethanol-treated porous PVDF films, then UV curing to cross-link the material, producing a HAMA-based hydrogel. The material exhibits excellent interfacial bonding due to the penetration of the HAMA solution into the porous PVDF film prior to cross-linking. Pretreatment of PVDF with plasma and ethanol shows a decrease in contact angle from 123.4° to 91.7° and 54.7° and soaking in 75% ethanol for 1 s indicating the material possesses great surface hydrophilicity and complete penetration of ethanol into PVDF. Ethanol slowly evaporates over time, making the surface of PVDF reversibly hydrophilic. Larger molecular weights were found to induce a larger deformation because of its higher absorption capacity. Smaller molecular weights absorb less water but do so faster, so HAMA150k was selected for speed of actuation, being capable of a minimum response time of 0.5 s to achieve 70% of the deformation. When patterned into fence-like structures the materials can be attached to outdoor masks to manage humidity inside the mask. Humidity levels of a mask without the smart device reached 97.6%, inducing condensation, whereas the smart mask maintains around 82.3%, improving wearer comfort.[159]

Serum creatinine is a key indicator of kidney function, with elevated levels resulting from intense exercise, high protein intake, dehydration, medications, infections, serious diseases like cancer, or kidney disorders. Chronic kidney disease (CKD) affects 11−13% of the global population, with advanced CKD necessitating dialysis and posing infection risks such as Hepatitis B to healthcare workers. A novel sensor utilizing the Internet of Things (IoT) technology is proposed for salivary creatinine detection, enabling point-of-care diagnosis for advanced kidney disorders and providing real-time data for preventive and clinical evaluations of CKD. A

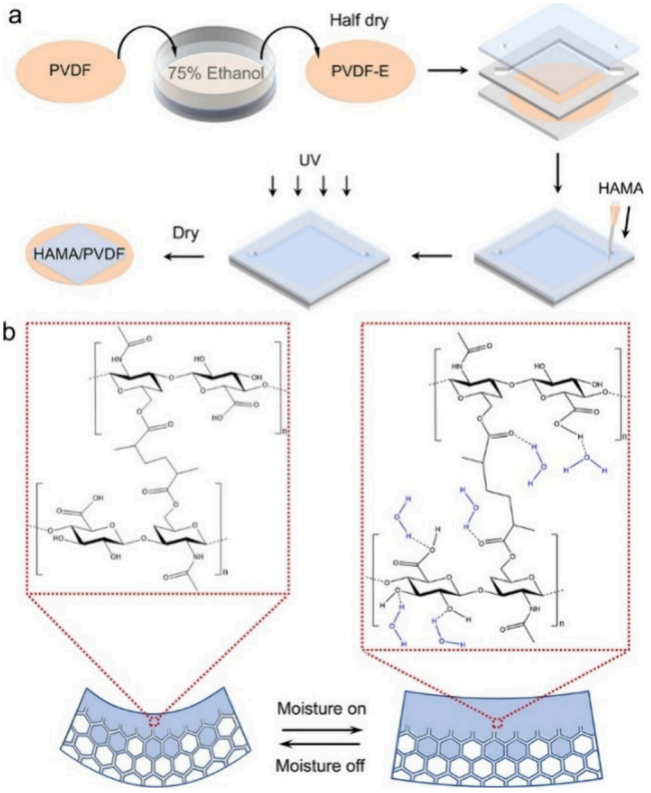

Figure 41. (a) Schematic for the fabrication process of moisture-actuated PVDF-HAMA bilayer actuators and (b) moisture-based activation behavior of the PVDF-HAMA bilayer. Reproduced with permission from ref (159). Copyright 2022 American Chemical Society.

polyacrylic gel-Cu^{2+} is created by mixing poly(acrylic acid) with $CuSO_4$ and cross-linking via cyclic voltammetry (Figure 42). A modified electrode is formed by drop-casting a Nafion/polyacrylic gel-Cu^{2+}/cuprous oxide solution onto the SPCE, followed by heating and further Nafion coating to enhance cross-linking. The sensor's performance is based on a catalytic

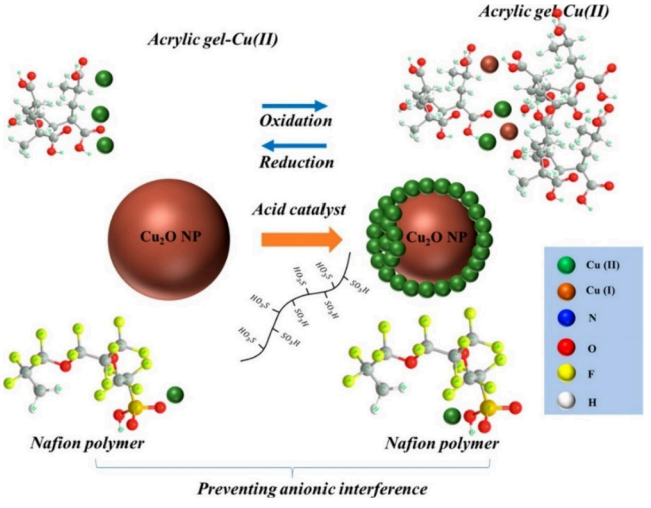

Figure 42. Schematic for the phase separation of Cu^{2+}/Cu^{+} of the sol−gel cross-linking of the polyacrylic gel with Nafion as an acid catalyst. Reproduced with permission from ref (59). Copyright 2020 American Chemical Society.

https://doi.org/10.1021/acs.chemrev.4c00996
Chem. Rev. XXXX, XXX, XXX−XXX

mechanism where Cu^{2+} ions bind irreversibly to the C = N functional groups in creatinine. The material displayed a linear response between anodic currents and creatinine concentrations from 1 to 2000 μM, with a selectivity efficiency of 97.2% and a detection limit of 0.3 μM. The sensor retained 96.4% efficiency after one month. In trials with a healthy individual, a creatinine level of 4.2 μM was accurately detected, supporting its application across all CKD stages (3−400 μM). The sensor interfaces with a wireless smartphone system for real-time monitoring, enabling user freedom while tracking health data.[160]

SERS is an ultrasensitive technique that identifies molecules through their vibrational fingerprints in scattering spectra, although the low probability of inelastic Raman scattering is significantly enhanced when analytes are attached to nanostructures that support electromagnetic (EM) near-field "hot spots." Control of wetting behavior is crucial to enhance analyte concentration on SERS-active sites. Researchers developed an analyte-enrichment system coupled with a SERS-active sensor site, produced through direct femtosecond (fs)-laser printing. A micropillar-patterned water-repellent PTFE surface supports water droplets in a Cassie−Baxter superhydrophobic state, facilitating the delivery of analytes to the hydrophilic SERS-active site. The fabrication process involves smooth PTFE subjected to laser treatment, followed by the deposition of 600 nm thick silver (Ag) and 25 nm thick gold (Au) films via e-beam evaporation. Spallative surface textures are produced on the Ag/Au-coated central site, creating dense hexagonal arrangements. The micropillars, 15 μm wide, achieve a WCA of 170°, allowing for 98% analyte deposition on the central site from the droplet. As water evaporates, the contact angle remains constant, following the Cassie−Baxter model, and the analytes concentrate on the central hydrophilic site, even if initially misaligned. Successful tests with Rhodamine 6G (R6G) at concentrations of 10^{-10} M and DAPI (a DNA marker) at 10^{-11} and 10^{-9} M demonstrate superior sensitivity compared to previous methods, having a detection limit at concentrations of 10^{-4} to 10^{-6} M. Further tests with solutions of various pharmaceuticals at 10^{-8} M yielded good SERS signals, achieving a low limit of detection (LOD) of 1 ppb and allowing for the detection of organic dyes and medical drugs down to 10^{-12} M.[161]

Changes in potassium ion (K^+) concentration can influence dopamine release, making it essential to monitor K^+-evoked dopamine release from neural cells to understand dopaminergic dysfunction. Antipsychotic medications, such as pimozide, act by regulating dopaminergic functions, inhibiting dopamine receptor activity, and reducing K^+-induced dopamine release. Researchers developed a floating electrode-based CNT biosensors for monitoring the effects of antipsychotic drugs on dopamine release from PC12 cells under potassium stimulation. The modified CNT-FET devices are fabricated by the adsorption of CNTs on SiO_2, with source and drain electrodes (Pd/Au) fabricated via thermal deposition. A photoresist-based passivation layer insulates the device, followed by direct application and drying of the Nafion solution with 2,2′-azino-bis(3-ethylbenzothiazoline-6-sulfonic acid) (ABTS*) radicals. The material achieves a detection limit of 10 nM and high selectivity against interference from glutamate and acetylcholine. The negative charge of Nafion attracts positively charged molecules and serves as a catalytic layer for dopamine, facilitating redox reactions that generate protons (H^+) and increasing positive charge density near the transducer, leading to changes in electrical current. Notably, the addition of dopamine results in a drop in source-drain current, while no current change is observed with glutamate or acetylcholine, indicating high selectivity. The device effectively monitors the depression of dopamine release in response to K^+ stimulation, providing a valuable tool for assessing the effects of antipsychotic drugs.[162]

Advancements in AI and IoT technology have made micro and nano pressure sensors increasingly significant, particularly for monitoring human movement. Traditional piezoelectric sensors often use lead zirconate titanate (PZT), which poses challenges for health applications. Researchers developed a novel hierarchical composite piezoelectric sensor using PVDF-HFP and ZnO nanofibers, fabricated from ZnO nanosheets grown *in situ* through a hydrothermal method on electrospun PVDF-HFP fibers, resulting in sheets that wrap around the fibers. When an external force is applied, it induces extrusion deformation in the fibers, altering the dipole positions, reducing polarization intensity, and generating an electric signal. At applied forces of 0.02 and 0.5 N at a frequency of 1 Hz the sensor produced open circuit voltages of 0.58 and 2.8 V, respectively, with a pressure sensitivity of 1.92 V kPa^{-1} and a response time of 20 ms. The device demonstrated durability, with stable performance over 5000 cycles at 10 N and 0.75 Hz. When compared to a pure PVDF-HFP membrane, the PVDF-HFP/ZnO composite exhibited about double the output and higher sensitivity, with the PVDF-HFP/ZnO sensor achieving 1.92 V kPa^{-1} compared to 1.27 V kPa^{-1} for the PVDF-HFP sensor. The device can be integrated with a Bluetooth signal transmission system, facilitating high-precision detection and safety monitoring in medical and rehabilitation contexts. The sensor can detect minute changes in motion, such as water droplets and falling coins, and can monitor an athlete's physical condition in real time via Bluetooth connectivity, indicating potential for real time monitoring applications.[163]

Three-dimensional (3D) force sensors are vital in industrial and medical applications, providing critical data about force components at specific points or over larger contact areas. Researchers developed a new flexible 3D force sensor using polymer nanocomposite (PNC) sensing elements to enhance sensitivity and adaptability. The sensor utilizes multiwalled carbon nanotube (MWCNT) and PVDF nanocomposite films that leverage piezoelectric and piezoresistive properties to capture both dynamic and static strain. The MWCNTs significantly enhance the strain sensitivity of the sensor, which is deposited on flexible substrates. The 3D sensor features four sensing elements arranged in a cross-beam configuration, sandwiched between two layers of silicone rubber for flexibility. Testing revealed high force sensitivity during static loading at engagement angles of 0°, 45°, and 90°. The sensor achieved an average sensitivity of 4.2×10^{-4} V/N and 4.5×10^{-4} V/N under normal and shear loading conditions, respectively. Under dynamic loading conditions, the sensor can effectively track load cycles and distinguish load directions. This flexible 3D force sensor demonstrates significant potential across various fields, including robotics, medical applications, human-machine interfaces, impact testing, vibration monitoring, physical therapy tracking, and sports performance evaluation.[164]

Researchers have developed a novel, lotus-leaf inspired method for creating a lubricant-infused skin (L-skin) coating, consisting of thin layers of a bioadhesive and lubricant-swellable perfluoropolymer (Figure 43). The L-skin material is

https://doi.org/10.1021/acs.chemrev.4c00996
Chem. Rev. XXXX, XXX, XXX−XXX

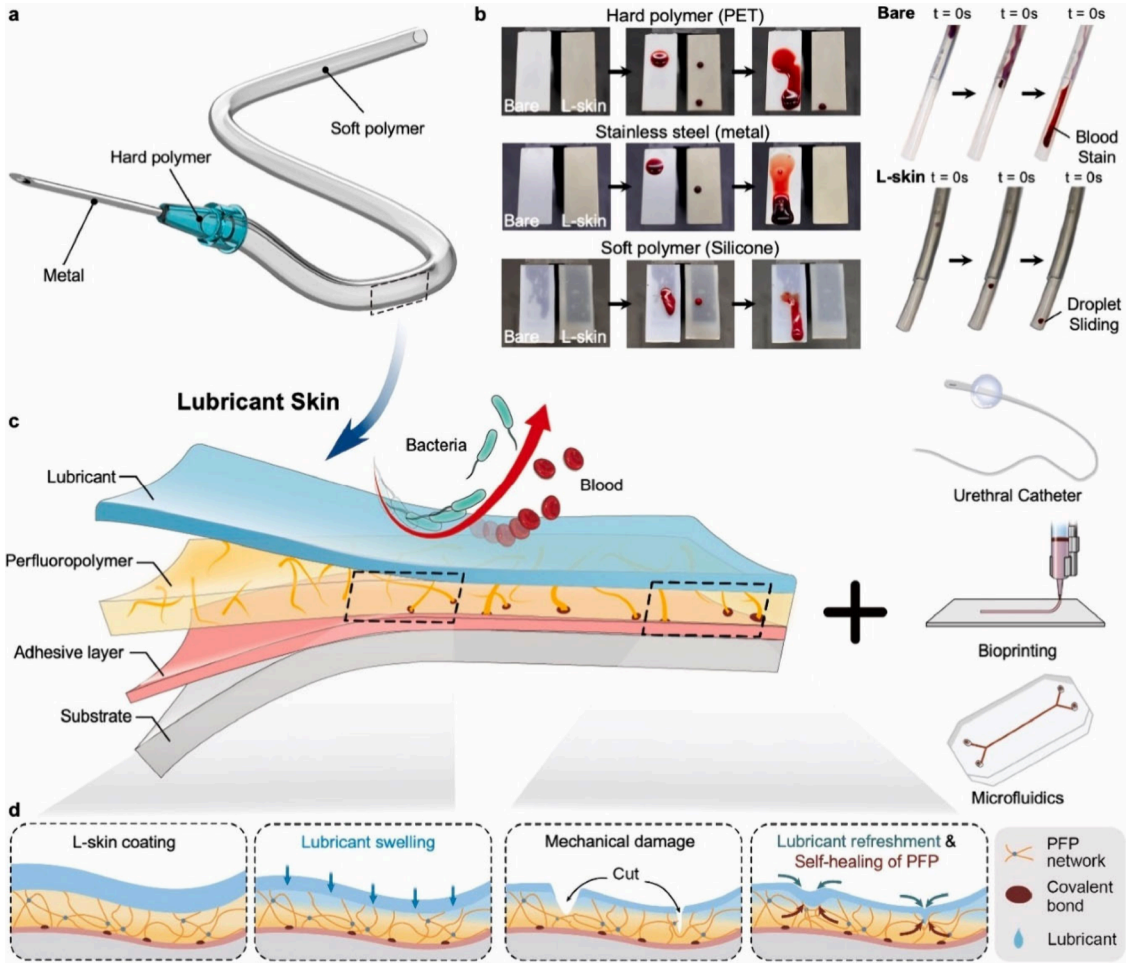

Figure 43. (a) Representative example of a complex material comprised of soft polymer, hard polymer, and metal with complex geometries which can be coated with the L-skin, (b) blood contact angle tests on surfaces treated with L-skin and bare surfaces, (c) schematic demonstrating the L-skin composition, repellent properties, and broad application to various complex geometries, and (d) schematic illustration of the various characteristics of L-skin, its swelling behavior, and self-healing abilities. Reproduced with permission from ref (165). Copyright 2023 KeAi Publishing.

biocompatible, sterilization-safe, and has been demonstrated to function effectively in medical applications such as bioprinting, microfluidics, catheters, and narrow medical tubing. L-skin surfaces are fabricated by coating the substrate with PDA, the dip-coating with carboxylic acid-terminated perfluoroalkylpolymer (CTX-109A, MW ∼ 300,000) and curing to promote amide and hydrogen bond formation. The fluorine-rich surface is then immersed in a fluoropolyether-based lubricant (Krytox GPL 101) which induces swelling and lubricant impregnation. The resulting L-skin repels various substances, including viscoelastic fluids (such as food, saliva, and bacterial suspensions) and solids (like feces and biological tissues). The coating was successfully applied to several medical devices, including bioprinting needles (53 μm internal diameter), microfluidic channels (150 μm height), narrow silicone tubing (2 m long), micropipettes, and urethral catheters, demonstrating its frictionless, antibiofouling, and absorption-barrier properties. This method was successfully applied to a variety of materials, including glass, silicone, PTFE, PP, PVC, stainless steel, PE, PET, and titanium, all of which exhibited strong antibiofouling properties.[165]

Tuberculosis (TB) remains a critical global health issue, with an estimated 10 million cases annually, though cases dropped during the COVID-19 pandemic to 5.8 million in 2020. Researchers have developed a novel method for concentrated specimen smear microscopy, termed sandwich filtration vessel-concentrated sputum/specimen smear microscopy (SFV-CSSM), wherein samples are vacuum filtered through a nanometer silicon PVDF polymer membrane. This method concentrates acid-fast bacilli (AFB) from sputum samples and was compared to direct sputum smear microscopy (DSSM) for performance evaluation. In a study of 4114 clinical samples from 2328 patients in Sabah, Malaysia, the SFV-CSSM method showed higher sensitivity (79.4%) than DSSM (60.5%) and produced less background interference, making it more effective for detecting low levels of AFB, especially in paucibacillary cases. Although SFV-CSSM is more expensive than DSSM in terms of reagents and manpower, it provides a much faster turnaround time of 24 h versus 1−2 months for solid agar cultures, making it suitable for early TB diagnosis and treatment initiation. Overall, SFV-CSSM demonstrates an 18.9% higher sensitivity than conventional DSSM for AFB detection in both sputum and extra-pulmonary samples, offering a more cost-effective and efficient solution for early TB detection.[166]

Optofluidics, which combines photonics and fluidics, is attractive for its simplicity and potential for integration with techniques like electric chromatography and capillary electro-

https://doi.org/10.1021/acs.chemrev.4c00996
Chem. Rev. XXXX, XXX, XXX−XXX

phoresis. Researchers have developed a high-performance, self-powered all-optical liquid flow sensor (ALFS) for microfluidic applications, based on triboelectrification-induced electroluminescence (TIEL). The TIEL mechanism combines triboelectrification and electroluminescence, where tribocharges on a material surface create a strong local electric field, exciting electroluminescent (EL) materials without the need for chemical reactions or pollutants. The TIEL signal is generated through contact electrification between a polymer-fluid-air interface and the moving fluid, where the amplitude and time span of the electric field can be modulated by adjusting the geometric design of the bottom grid electrode. This design allows for a high sensitivity of 0.089 s mm^{-1} and a low flow velocity limit of 1 mm s^{-1}, making it suitable for applications such as infusion monitoring and integration into microfluidic chips for biomedical uses. The ALFS device developed by this research group includes an electrification layer made of FEP, a luminescent layer of PDMS with ZnS phosphor fillers, an electrode layer, and a flexible substrate. As the device is flooded with water, the positive charges in the water neutralize the negative charges on the FEP surface, generating an alternating electric field with varying amplitude. The ALFS was successfully applied for infusion monitoring and used in a microfluidic chip to detect and image biological samples, such as onion cells, pine needle cells, and a fly leg, without requiring an external light source.[167]

Researchers have developed a wearable, self-powered electronic device that simultaneously utilizes piezoelectric and triboelectric conversion in a monolayer-structure membrane, addressing challenges in enhancing both electric output and structural performance. The device is fabricated from single-layer binary fiber nanocomposite membranes (SBFNMs), made from a combination of PVDF, CNTX (multiwalled carbon nanotubes), and PAN through coelectrospinning (Figure 44). Incorporation of CNTs into both

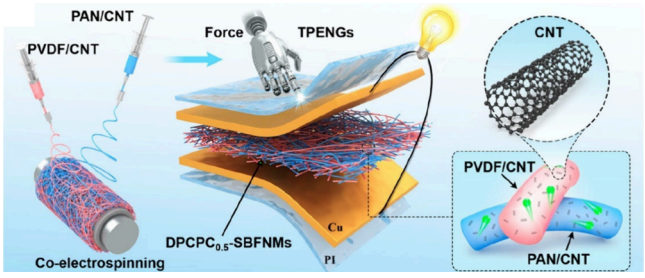

Figure 44. Schematic for the preparation of the TPENG by coelectrospinning of PAN/CNT with PVDF/CNT to form a simultaneously piezoelectric and triboelectric layer for wearable energy harvesting and self-powered sensors. Reproduced with permission from ref (168). Copyright 2024 American Chemical Society.

PVDF and PAN develops an interpenetrating structure of PVDF@CNT and PAN@CNT nanofibers that enhances electron transfer efficiency, reduces charge loss, and promotes the formation of the β-phase in the material. The device can also illuminate 50 commercial LEDs, with the output voltage being 5.1 and 4.6 times higher than those from virgin PAN or PVDF single-fiber membranes, respectively. When attached to a human arm it deforms with movement, generating a signal corresponding to bending angles which can power LEDs for self-illumination on clothing or on shoes to enhance visibility at night. When connected to a single-chip microcomputer, the device can trigger an LED and buzzer as an alarm when a preset voltage is reached, giving applications in medical alarm systems.[168]

Researchers developed a self-powered mask designed for real-time monitoring and uploading of exhaled oxygen concentration, with potential applications in lung disease diagnosis. The mask integrates tetrapod ZnO (T-ZnO) nanostructures with PVDF on a flexible fabric substrate (Figure 45). The ZnO nanostructures have high gas-sensing properties, with the adsorption and desorption of gas molecules affecting carrier density and mobility which correlates to the oxygen concentration in the exhaled air. T-ZnO nanostructures are suspended in a PVDF solution and coated on 3 M KN95 polypropylene fabric and polarized in an electric field. The combination of the piezoelectric properties of T-ZnO/PVDF and the gas-sensing capabilities of T-ZnO enables the mask to convert breath into a piezoelectric signal without requiring an external power supply. As the concentration of oxygen in exhaled breath increases, the voltage output from the device was found to increase proportionally. The mask is equipped with data processing and Bluetooth modules, allowing the signal to be transmitted wirelessly to a mobile device for real-time monitoring of lung oxygenation capacity. The system is particularly useful for patients with lung diseases like COVID-19 pneumonia, which causes hypoxia due to impaired oxygen exchange in the alveoli.[169]

1.8. Medically Relevant Textiles

Smart outdoor clothing designed for health monitoring and multifunctional interactions incorporates essential features such as thermal insulation, moisture permeability, quick-drying capabilities, antibacterial properties, and energy supply interfaces for communication systems. To enhance triboelectric efficiency, a key approach involves selecting triboelectric (TE) materials with distinct polarity differences based on the triboelectric series, modulating surface permittivity, and increasing effective contact area through micropatterning and physical or chemical methods. A thermal-insulating textile-based TENG (TI-TENG) was developed that has multifunctional layers, including triboelectrification components, silver-coated nylon electrodes, a windproof outer textile, and an inner lining. The core of the TI-TENG comprises FEP and a TI-textile, providing flexibility and allowing for multidirectional stretching to accommodate joint movement. Under frequencies of 1−5 Hz, the short-circuit current (I_{sc}) ranges from 1.15 to 9.31 μA, with an open-circuit voltage (V_{oc}) of 87.98 V and a charge storage capacity (QSC) of 51.32 nC This technology enables intelligent human motion monitoring and outdoor wireless signal transmission, functioning as self-powered wearable sensors and human-machine interactive interfaces, including an emergency call feature. It exhibits antibacterial properties against *E. coli* and *S. aureus* and maintains constant output after 10 h of washing, indicating suitability for applications in smart clothing. The material retained stability after 8,000 cycles at 3 Hz and displayed improved thermal insulation compared to standard polyester and cotton-poly blends.[170]

The development of finger skin electronics aims to enhance capabilities of humanoid soft robots and medical applications by mimicking the mechanoreceptors found in human skin. Researchers developed a sensor consisting of a 20 × 20 pixel

https://doi.org/10.1021/acs.chemrev.4c00996
Chem. Rev. XXXX, XXX, XXX−XXX

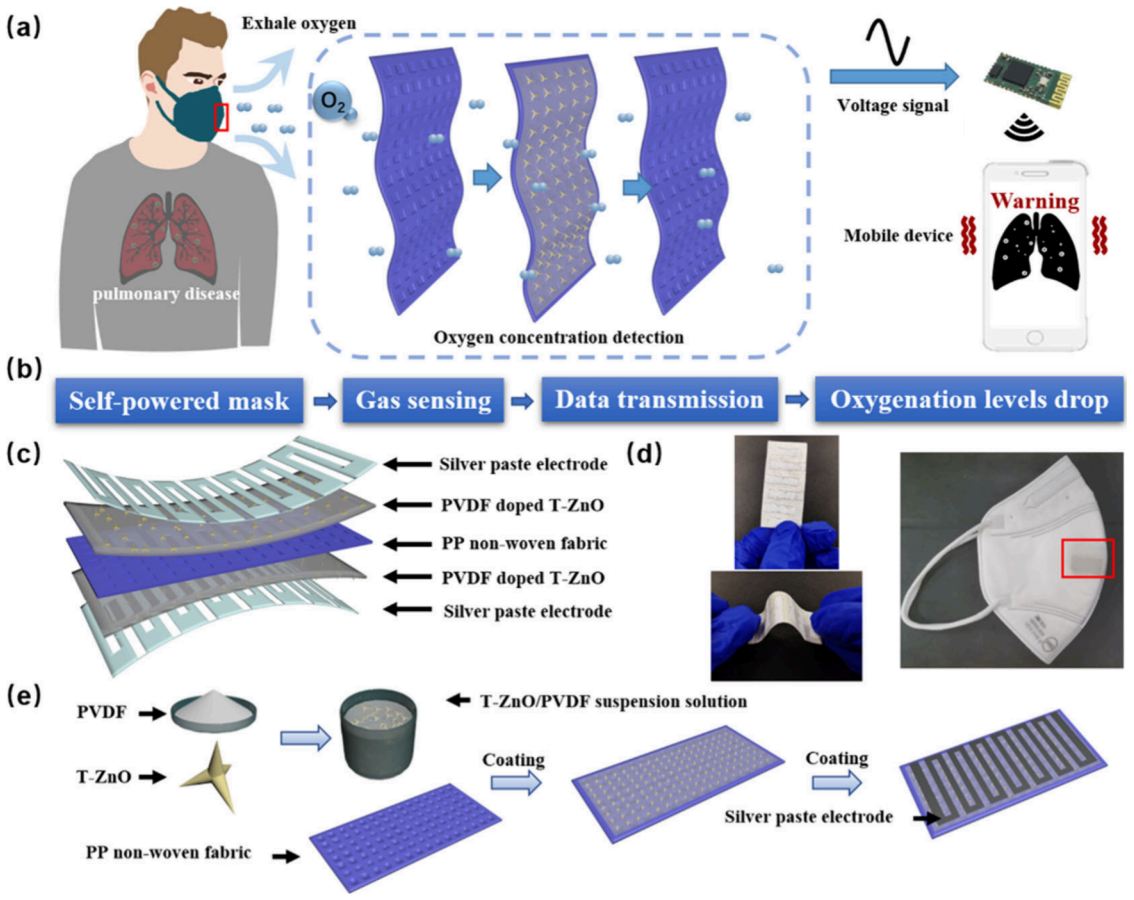

Figure 45. (a) Diagram for real time oxygen detection through a smart mask by piezoelectric voltage generation and transmission through a Bluetooth module, (b) flow-chart for the transmission of gas-sensing data for the monitoring of lowered oxygenation in a sick individual, (c) schematic for the fabricated layers of the smart mask, (d) pictures of the modified smart 3 M KN95 mask, and (e) fabrication process utilizing PVDF and tetrapod ZnO to form the smart mask by coating PP nonwoven fabric. Reproduced with permission from ref (169). Copyright 2022 IOP Publishing.

array covering 4 cm^2, designed to emulate slow adaptive (SA) mechanoreceptors, which responded to sustained stimuli like pressure and skin stretching (Figure 46). A TENG is laminated onto the array to detect high-frequency vibrations similar to fast adaptive (FA) mechanoreceptors and to generate electric power from dynamic pressure and vibrations. The TENG consists of a graphene suspension of nanoplatelets (GNPs) spray-coated onto flexible polyethylene naphthalate (PEN) substrates, creating an interlocked architecture through patterned platinum electrodes. Fabrication of the sensor is straightforward and compatible with conventional photolithography, producing a flexible matrix with 100 sensors/cm^2 on a 2 × 2 cm^2 area, mirroring the spatial density of human skin. The sensor utilizes PEN and PTFE surfaces, topped with a 1 mm high acryl bumper. The sensor has a response time of 3 ms, allowing it to detect vibrational pressures up to 330 Hz, within the human sensitivity range of less than 400 Hz, and it remains functional over 10,000 cycles under pressures of 10 and 100 kPa. It accurately distinguishes pressure distribution, with an average voltage output of 240 V and a current of 37 μA. A pressure of 51 kPa at 4 Hz effectively illuminated 100 LEDs, and the material demonstrated the capability to recognize 12 complex fabric types with 99.1% accuracy, suggesting its potential in skin electronics.[171]

A next-generation hybrid mesh, Synecor—a combination of PTFE and PGA/TMC (polyglycolic acid/trimethylene carbonate)—was tested on 35 patients with ventral hernias to improve mechanical strength and promote tissue growth and vascularization. Over a two-year follow-up period, there were no hernia recurrences, and the infection rate aligned with previous studies. Patients reported significant improvements in self-esteem and pain relief, with only one requiring reoperation. In a separate trial involving 157 patients, Synecor was demonstrated to be safe and effective for inguinal hernia repairs, with low recurrence and complication rates and reduced patient-reported pain.[172]

Creating superhydrophobic membranes for use in energy, environmental, and medical applications require a balance of durability, waterproofness, and breathability, which has been challenging. This study presents a new method for producing superhydrophobic membranes by combining humidity-induced electrospinning with coat-cross-linking technology. The electrospinning process forms a micro/nano rough surface, while waterborne acrylic resins (WAR) are used to coat and cross-link the surface, enhancing its low surface energy and stability (Figure 47). The result is a membrane with excellent superhydrophobicity (water contact angle of 154°), good self-cleaning and anti-icing properties, strong waterproofness (83.4 kPa), and high breathability (3.71 kg m^{-2} d^{-1}). The membrane structure is made from PVDF/blocked isocyanate (PVDF/BIC) nanofibers. The humidity-controlled electrospinning process induces phase separation, forming irregular nano-

https://doi.org/10.1021/acs.chemrev.4c00996
Chem. Rev. XXXX, XXX, XXX−XXX

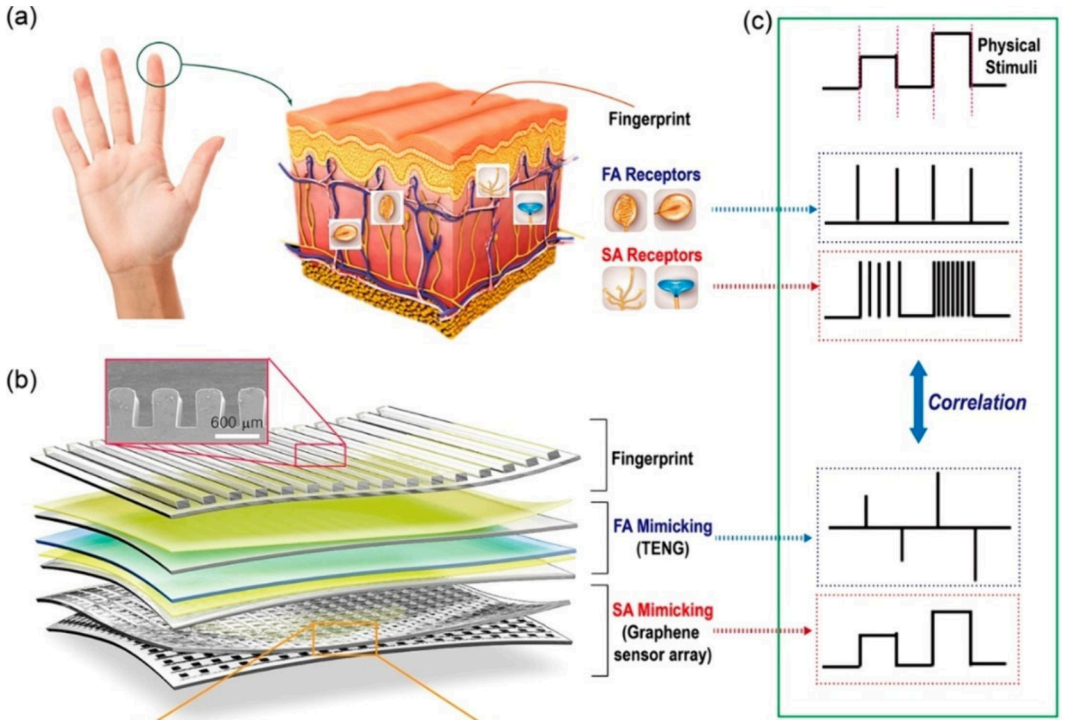

Figure 46. (a) Structure of human skin and FA/SA receptors (b) schematic of the TENG device mimicking the SA and FA sensors with fingerprint-like microlines, (c) correlation between human skin electrical outputs and the outputs of the artificial fingerprint structure of the device. Reproduced with permission from ref (171). Copyright 2019 American Chemical Society.

spheres on the fiber surface. The BIC component helps bond the waterborne acrylic resin to the nanofibers, creating a durable, hydrophobic layer. These PVDF@WAR nanofibrous membranes are not only highly durable but also offer comfort due to their breathability, making them suitable for use in protective clothing, medical hygiene, and electronics.[173]

In this study, a piezoelectric polymer yarn with an internal electrode structure (IEPY) was developed for use in wearable healthcare sensors (Figure 48). The yarn, with an average diameter of approximately 900 μm, was fabricated using a simple and efficient method. The IEPY exhibits piezoelectric properties, generating a maximum power output of 292 mV and 16.2 μW under a 60 kg load. This yarn is strong, flexible, and capable of harvesting electrical energy from human motion, making it suitable for integration into socks and insoles to capture biomechanical energy from walking. Additionally, it can accumulate gait data for healthcare monitoring and be woven into multifunctional electronic fabrics for mass production. For the foot-pressure sensor application, the yarn was coated with (P(VDF-TrFE-CTFE)), a material known for its high piezoelectric constant, flexibility, and strength. The coating was applied using reverse dip coating with plasma etching, ensuring the entire surface of the conductive fiber was coated. The inner electrode structure minimized noise, enhancing the durability and flexibility of the sensor. The resulting fibers are durable, scalable, and customizable, making them suitable for use in applications like foot-pressure sensors in wearable healthcare devices.[174]

This study introduces a composite yarn made of AgNY/ polyvinylidene fluoride (PVDF)@TiO2/ /PVDF (APTAP), designed for wearable electronic skin applications (Figure 49). The yarn, fabricated using conjugate electrospinning and wet chemical deposition, has a 3D hierarchical structure and exhibits excellent piezoelectric performance. With a silver-plated concentration of 2%, the yarn produces a voltage output of 1650 mV and a current output of 70 nA. The composite also demonstrates strong mechanical properties, including a tensile strength of 284.37 MPa and an elongation at break of 61.80% with a 3% silver-plated concentration. A fabric woven from this yarn is highly sensitive, able to detect subtle signals, making it suitable for applications like human health monitoring and clinical diagnosis.[175]

In this research, an all-textile piezoelectric sensor (ATPS) was developed using a piezoelectric PVDF nanofiber membrane (NFM), 3D knitted flexible electrodes, and an elastic self-adhesive bandage for easy skin attachment and comfort (Figure 50). The sensor is cost-effective, scalable, and highly flexible due to the use of knitting technology. It offers impressive performance, with a high-pressure sensitivity of 0.68 V/kPa and excellent air permeability (130 mm/s). Performance is influenced by the structure of the fabric electrodes, with simulations and experiments revealing that 4 × 1 rib knitted electrodes provide the best sensitivity. The ATPS maintains stable voltage output after 3350 cycles and can detect a wide range of forces (0.098 to 724 N) in a self-powered mode, making it suitable for applications like human motion detection (e.g., throat swallowing, wrist bending, walking, and running). Additionally, a 3 × 3 pixel-array piezoelectric sensor was developed using a custom knitted conductive digit pattern electrode, which simplifies the detection circuit and enhances the versatility of the system. The flexible, knitted conductive fabric electrodes demonstrate significant potential for integration into wearable, self-powered electronic devices, offering new opportunities for stable and long-term textile-based wearables.[176]

Carbon fiber (CF) reinforced PTFE composites have undergone modifications through proton irradiation, with subsequent investigations into their surface energy, hardness,

https://doi.org/10.1021/acs.chemrev.4c00996
Chem. Rev. XXXX, XXX, XXX−XXX

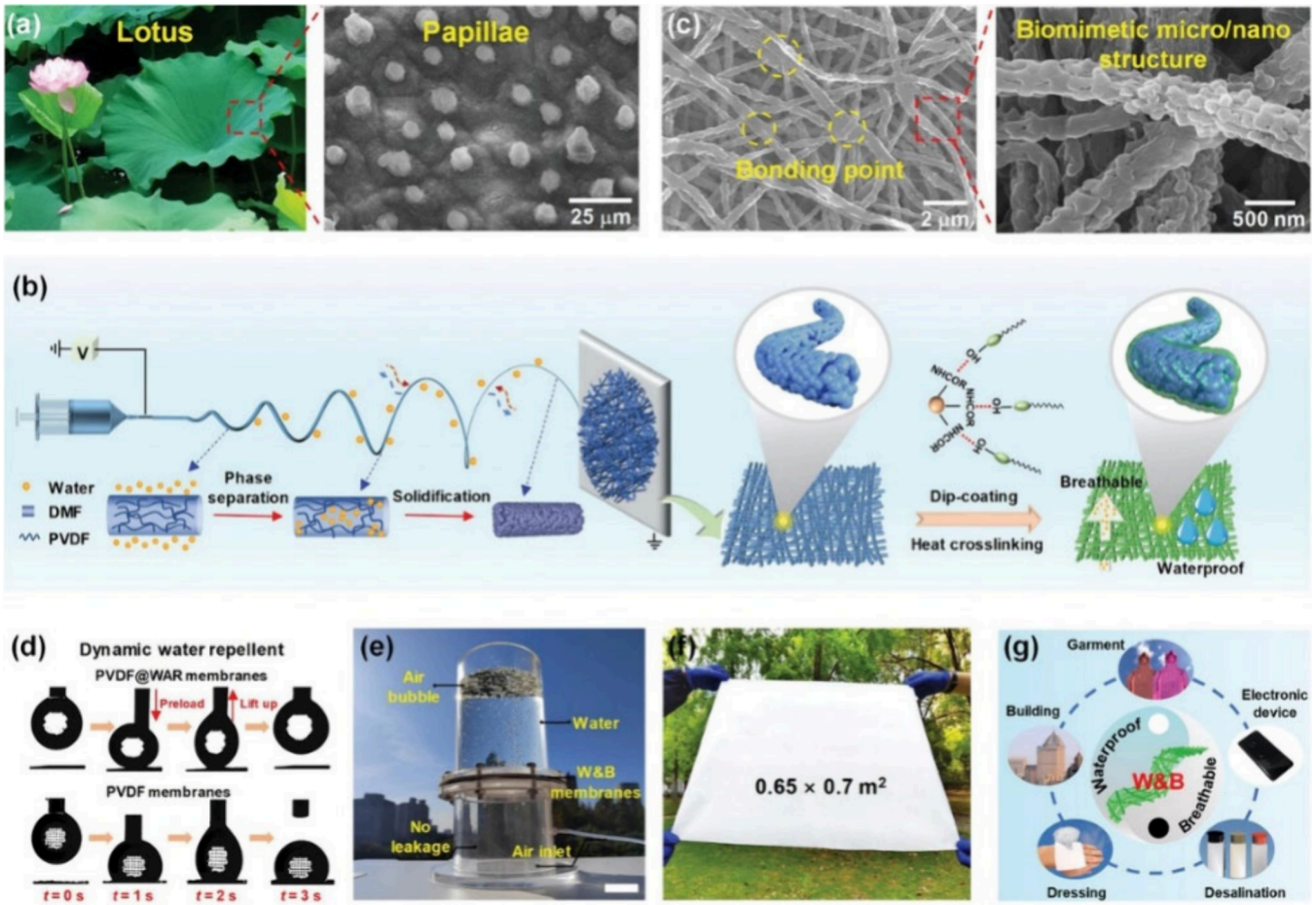

Figure 47. (a) Optical image and microstructure of the lotus leaf. (b) Schematic illustration of fabricating superhydrophobic PVDF@WAR membranes based on humidity-induced electrospinning and coat-cross-linking technology. (c) SEM images showing the microstructures of the PVDF@WAR nanofibrous membranes. (d) Demonstration of dynamic water repellent of PVDF@WAR and common electrospun PVDF membranes, respectively. (e) Photographs illustrating waterproof and breathable properties of PVDF@WAR membranes. Scale bar is 5 cm. (f) Optical image of the large-sized membranes. (g) Various potential applications of the superhydrophobic PVDF@WAR nanofibrous membranes. Reproduced with permission from ref (173). Copyright 2024 John Wiley & Sons Inc.

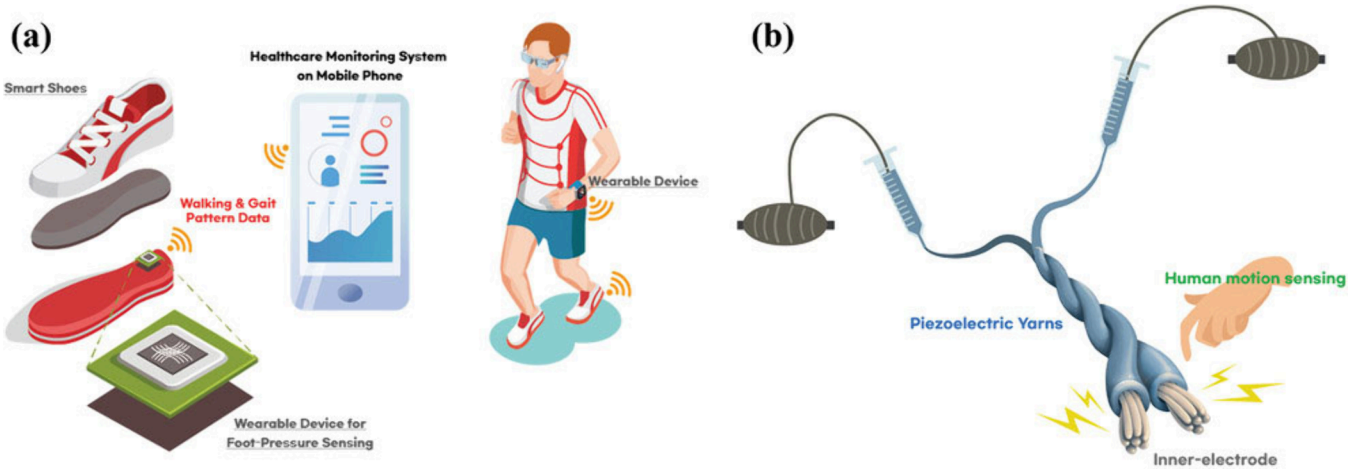

Figure 48. (a) Schematic illustration of wearable devices for healthcare and (b) electronic fibers for energy harvest and signal sensing. Reproduced with permission from ref (174). Copyright 2021 John Wiley & Sons Inc.

and tribological properties both before and after the irradiation process. The incorporation of CFs enhanced the hardness and wear resistance of the composites. Proton irradiation resulted in defluorination and carbonization of the CF/PTFE composite surface, leading to a reduction in surface wettability and surface energy. The depth of irradiation was measured at 820 nm from the material surface, as calculated using the SRIM software package. Additionally, the wear resistance of the

https://doi.org/10.1021/acs.chemrev.4c00996
Chem. Rev. XXXX, XXX, XXX−XXX

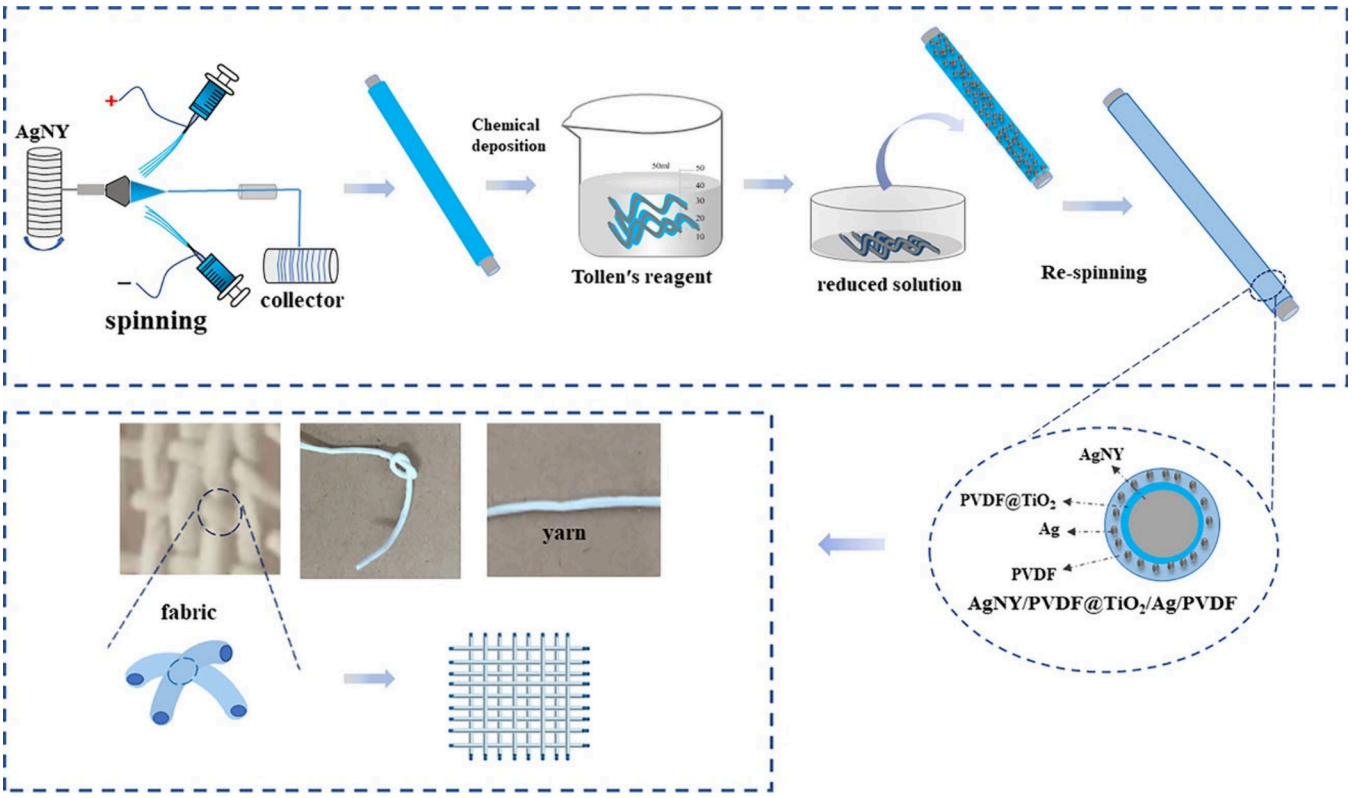

Figure 49. Schematic diagram of preparation of AgNY/PVDF@TiO_2/Ag/PVDF nanofiber composite piezoelectric yarn. Reproduced with permission from ref (175). Copyright 2022 John Wiley & Sons Inc.

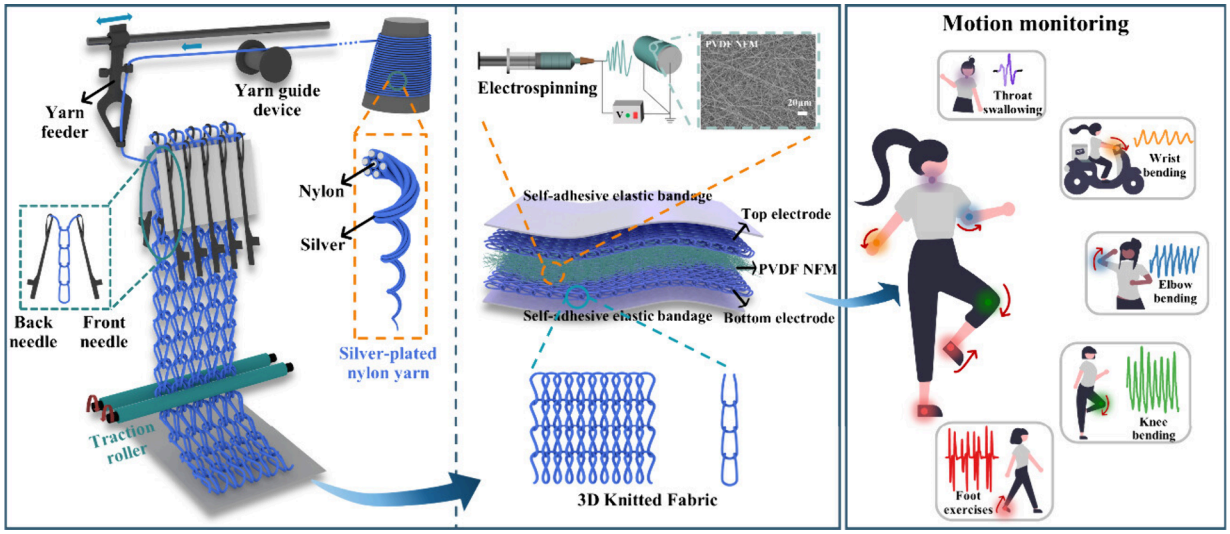

Figure 50. Fabrication, working mechanism, and application of ATPS. Reproduced with permission from ref (176). Copyright 2022 American Chemical Society 2024.

composite improved following proton irradiation, which facilitated material transfer from the copper alloy surface to the CF/PTFE composite. These notable enhancements suggest potential applications in aeronautics and advanced medical materials.[177]

Fiber supercapacitors (FSCs) have garnered significant interest as promising energy storage solutions for wearable electronics. Notably, silk composite membranes, characterized by their ultrathin, soft texture and adequate mechanical strength, have been utilized for the first time as encapsulating materials, providing FSCs with enhanced flexibility. A tight spiral-winding encapsulation strategy has led to improved electrochemical performance, achieving a 28% increase in performance for FSCs encapsulated with silk composite membranes compared to those using traditional plastic tubes. Specifically, the asymmetric FSCs encapsulated with silk membranes demonstrated excellent performance metrics, including a high energy density of 12.9 mW cm^{-3} at 80 mW cm^{-3} and remarkable bending stability, retaining approximately 97.1% capacitance after 1000 bending cycles, outperforming many state-of-the-art supercapacitors. Additionally, an energy

https://doi.org/10.1021/acs.chemrev.4c00996
Chem. Rev. XXXX, XXX, XXX−XXX

storage device composed of 12 FSCs can effectively power a watch and 65 light-emitting diodes.[178]

This review highlights the increasing demand for self-powered devices and microsensors in intelligent electronics and flexible wearables, particularly for applications in medical healthcare and human-computer interaction robotics. High-sensitivity sensors that are flexible, stretchable, wearable, and breathable can monitor subtle environmental changes, offering solutions for personalized medical care. A comparison of ten types of polymers and composites with human skin in terms of elastic modulus revealed that PLLA/PDMS, electrospun PVDF, and ZnO/PVDF exhibit higher elastic moduli (50,500, and 27,900 MPa, respectively) compared to human skin (18.8 MPa), making them more suitable for wearable device applications.[179]

Functional fillers can enhance the triboelectric properties of PVDF, which is commonly used as a negative dielectric layer in TENGs. MXene fillers can significantly improve the triboelectric performance of PVDF-based negative dielectric layers through dielectric modulation. However, the impact of MXene as a highly electronegative filler on the electron-withdrawing (EW) capability of PVDF/MXene composite films is often overlooked. In this study, this research group prepared PVDF-TrFE)/MXene (Ti_3C_2Tx) composite nanofiber films (PMNFs) using electrospinning. At a MXene content of 0.8 wt %, the TENG based on PMNFs achieved a maximum output power density of 250 mW m^{-2} with a matching external load resistance of 4 MΩ, and a maximum open-circuit voltage (VOC) of 85 V, which is 2.66 times greater than that of the PVDF-TrFE-based TENG. The enhancement of the EW capability and dielectric properties due to the addition of MXene was confirmed by analyzing the work function (WF) and dielectric constant (and loss). Additionally, researchers designed a tremor-based TENG using PMNFs and developed an innovative respiratory monitor for real-time respiratory tracking, offering new insights into the creation of respiratory monitoring devices.[180]

There is an increasing global demand for smart nanofibrous membranes that are both waterproof and breathable, due to their extensive applications in medical hygiene, wearable electronics, and outdoor apparel. Designing such high-performance materials using environmentally friendly solvents is essential yet challenging. In this study, researchers present a straightforward and effective method to produce environmentally friendly waterborne polyurethane nanofibrous membranes that exhibit high levels of waterproofness and breathability. This is achieved through a water-based emulsion electrospinning technique combined with a heating treatment. The hydrophobic channels within the waterborne polyurethane nanofibrous membranes, characterized by small pore sizes and high porosity, are created using in situ doping of a water-based fluoropolymer and an aziridine cross-linker, followed by heating. The resulting environmentally friendly nanofibrous membranes demonstrate a hydrostatic pressure of 74.3 kPa, impressive air permeability of 9.3 mm/s, a remarkable water vapor transmission rate of 12.8 kg m^{-2} day^{-1}, and high elasticity of 67.4%. These properties provide excellent personal protection and a comfortable microclimate in challenging environments. The successful development of these innovative nanofibrous membranes may inspire the green synthesis of other fibrous materials for various applications.[181]

In this investigation of the effects of sterilization on textiles, it was found that the method of sterilization—specifically steam, ethanol, and ethylene oxide—significantly influenced the number of viable cells present on composite and ePTFE swatches after 15 days of culture (Table 5). Notably, swatches

Table 5. ePTFE, Polybutester, and Silk Swatches

Part 2	ePTFE	Polybutester	Silk	Cell
	0.02 cm,	0.015 cm, USP	0.02 cm, USP	Control
	ASM 5.0 filament	4−0 filament	3−0 filament	No swath
Warp/weft combinations	ePTFE/ePTFE	Polybutester/ Polybutester	Silk/Silk	
	ePTFE-Polybutester/ Silk			

sterilized with ethylene oxide exhibited nearly no viable cells. Conversely, the sterilization method did not result in significant differences in the number of viable cells on polybutester or silk sutures. Regardless of the sterilization technique used, silk suture swatches showed almost no viable cells after 15 days. In contrast, polybutylester suture weaves displayed between 20,000 and 30,000 cells on swatches cultured for the same duration, which was more than double the cell count observed on ePTFE and composite fiber swatches. Additionally, silk swatches exhibited signs of bacterial infection, characterized by rod- and cocci-shaped bacteria. Polybutester and composite swatches contained cells and multilayered cell sheets that were attached to the swatches, found in the spaces between fibers, and bridging between the swatches and the culture dish.[182]

The use of fluorinated solid-state polymer electrolytes (SPEs) has emerged as a promising approach to create a stable solid-electrolyte interphase (SEI) on lithium metal, which can effectively regulate lithium deposition during cycling. However, the *in situ* polymerization of highly fluorinated monomers often faces challenges such as weak polymerization kinetics and a low degree of polymerization. These researchers proposed and synthesized a partially fluorinated SPE reinforced with melt blown cloth through UV-curing. The resulting partially fluorinated melt blown cloth reinforced SPE (PFMC-SPE) demonstrated significantly enhanced performance due to the improved mechanical properties from the melt blown cloth and optimized electrochemical characteristics from the partial fluorination. The PFMC-SPE exhibited superior room temperature ionic conductivity (1.0 mS cm^{-1}) and a wide electrochemical stability window (up to 5 V). Furthermore, the Li//$LiFePO_4$ cell maintained stable operation for over 750 cycles at a 1.0 C rate, with a capacity retention of 84.7%, decreasing from 141.2 mAh g^{-1} to 119.6 mAh g^{-1} at 30 °C. The use of reliable and cost-effective melt blown cloth-based separators for solid-state electrolytes, combined with the partial fluorination strategy, indicates great promise for the development of next-generation ultrastable solid-state lithium batteries.[183]

In this research, the researchers have focused on developing a human health monitoring system suitable for both home and hospital use. Initially, researchers fabricated PVDF/multiwalled carbon nanotubes (MWCNT) composite electrospun nanofibers, which were then utilized to create a piezoelectric pressure sensor that functions as self-powered electronic skin (E-skin). The surface morphology was analyzed using FE-SEM, while vibrational modes were characterized through FT-IR. The incorporation of conducting MWCNTs into the

https://doi.org/10.1021/acs.chemrev.4c00996
Chem. Rev. XXXX, XXX, XXX−XXX

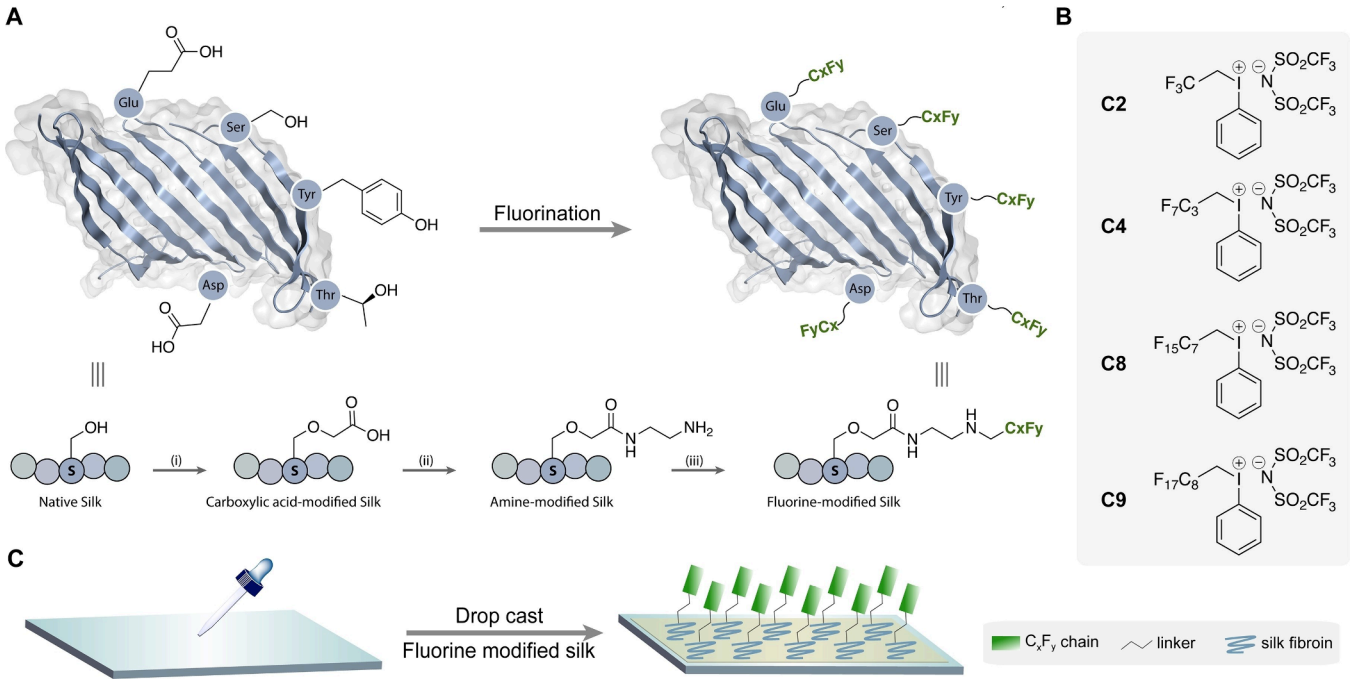

Figure 51. (A) Schematic overview of the synthesis of fluorinated silk films. (i) a. NaOH, H_2O (pH 13) b. $ClCH_2COOH$ (ii) a. NaOH, H_2O (pH 5.5) b. EDC, MES buffer, c. $H_2N(CH_2)_2NH_2$, MES Buffer, d. pH > 10.5 (iii) Iodonium Salt, CH_2Cl_2, b. Lutidine, CH_2Cl_2. (B) Series of iodonium salts used to modify silk with C2, C4, C8, and C9 carbon chains. (C) Drop casting of fluorine modified silk on surfaces to examine mechanical stability and hydrophobicity. Reproduced with permission from ref (186). Copyright 2022 Chemistry Europe.

PVDF matrix resulted in a flexible, self-powered E-skin that exhibits remarkable sensitivity to human movements, enabling noninvasive monitoring of physiological signals and reducing the potential for human error.[184]

A triboelectric nanocomposite was developed using a blend of PVDF and PMMA, to which nanoparticle fillers were added, resulting in a sprayable dispersion capable of producing a superhydrophobic coating. Dielectric nanoparticle fillers, specifically ZnO, were incorporated to increase surface roughness, which is crucial for enhancing contact area and promoting triboelectrification. The nanocomposite formation process was adapted from their previous work, which utilized a cyanoacrylate-based acrylic. A solution of PVDF and PMMA was spray coated onto electrodes, followed by annealing in air. This multifunctional triboelectric coating is nontoxic, ultrathin, and can be directly integrated onto the fingertips of surgical gloves, providing antifouling properties, antibacterial properties, is superhydrophobic (self-cleaning), and is noncytotoxic. The sensor-coated gloves enable mechanical energy harvesting, force sensing, and detection of material stiffness changes directly from the fingertips, potentially enhancing proprioceptive feedback for clinicians. Importantly, the sensors remain effective even with a second glove worn over them, ensuring sterility during interventional procedures. As a practical application, the sensors successfully detected *ex vivo* injuries to the pig anal sphincter, which could improve the accuracy of diagnosing obstetric anal sphincter injuries, leading to timely repairs, fewer complications, and enhanced quality of life.[185]

Silk fibroin protein is a biomaterial known for its excellent biocompatibility and low immunogenicity, making it a leading choice for applications in stents, catheters, and wound dressings. However, modifying the hydrophobicity of silk fibroin to broaden its applications has proven challenging. This research group reports that adding perfluorocarbon chains to the surface of silk fibroin converts this water-soluble protein into a highly hydrophobic polymer suitable for solvent casting (Figure 51). A clear correlation was observed between the fluorine content of the modified silk and the hydrophobicity of the resulting film, with water contact angles for the most fluorinated silk fibroin exceeding those of PTFE. Additionally, researchers found that water absorption in prefabricated silk bars was significantly reduced, enhancing their longevity and mechanical integrity. These findings underscore the effectiveness of moderate chemical conditions in introducing non-natural groups onto the silk fibroin surface, paving the way for further exploration of this versatile biomaterial's applications. Modification of prefabricated silk scaffolds enhances mechanical stability *in vitro*, suggesting significant potential for biomedical device applications.[186]

Medical protective clothing is crucial for safeguarding healthcare personnel from viruses and other infectious agents. The balance between comfort and reliable protection in such clothing has garnered increasing attention. Medical staff often experience significant discomfort when wearing traditional protective clothing for extended periods due to poor breathability and humidity. In this context, this research group presents (PVDF)/ (PU)/ TiO_2 composite nanofibrous membranes that offer multiple protective functions while ensuring adequate moisture permeability. The inclusion of PU in the PVDF-3/PU-7 composite membranes significantly enhanced tensile strength, achieving 9.9 MPa—three times that of the original PVDF membranes. The resulting multifunctional PVDF/PU/TiO_2 membranes exhibited unique properties, including an ultraviolet protection factor of 867 and a hydrostatic pressure of 24.3 kPa, while maintaining comfort with a water vapor transmittance of 7023 g m^{-2} day^{-1}. Furthermore, with a TiO_2 concentration of 2 wt %, the antisynthetic blood penetration was measured at 7 kPa,

https://doi.org/10.1021/acs.chemrev.4c00996
Chem. Rev. XXXX, XXX, XXX−XXX

achieving a Level 4 rating. Overall, the PVDF/PU/TiO_2 composite nanofibrous membranes show great promise for applications in medical protective clothing, outdoor sportswear, and military apparel.[187]

Medical textiles require repellency to bodily fluids such as blood, urine, or sweat, which may carry infectious agents that can contaminate surfaces and spread to others. These researchers present a simple, durable, and scalable coating for nonwoven polypropylene textiles that is both superhemophobic and antibiofouling. The treatment involves applying PTFE nanoparticles in a solvent, thermally sintered onto polypropylene microfibers, resulting in a robust, low-surface-energy, multilayered rough surface. The treated textiles exhibited a static contact angle of 158.3 ± 2.6° and a hysteresis of 4.7 ± 1.7° for fetal bovine serum, reducing serum protein adhesion by 89.7 ± 7.3% (0.99 log). The coated textiles also demonstrated a reduction in the attachment of adenovirus type 4 and 7a virions by 99.2 ± 0.2% and 97.6 ± 0.1% (2.10 and 1.62 log), respectively, compared to untreated controls. These repellency properties are maintained by achieving a Cassie−Baxter state of wetting, which reduces the surface area in contact with liquids by an estimated 350 times (2.54 log) compared to control textiles. Moreover, the treated textiles exhibited exceptional mechanical durability, retaining their liquid, protein, and viral repellency even after extensive abrasion and washing. The multilayered, multiscale roughness contributes to mechanical durability through self-similarity, and the samples demonstrated high-pressure stability with a breakthrough pressure of approximately 255 kPa. These characteristics highlight the potential for durable, repellent coatings in medical gowns, scrubs, and other hygiene textile applications.[188]

A suspension of colloidal graphite in propanol with PTFE powder was utilized to spray coat knitwear (composed of 65% cotton, 25% polyester, and 10% polyurethane) to develop a new electrically conductive fiber composite. Laboratory samples measuring 10 × 70 mm^2 were cut from the knitted fabric, and the graphite-PTFE dispersion was sprayed onto one side. The potential for using this layered composite as a cyclic strain sensor has been demonstrated, achieving a minimum hysteresis of less than 4% in the electrical signal during cyclic deformation due to the Patrikeev−Mullins effect.[189]

Soft and stretchable electrodes are critical components for skin-tight wearable devices, providing comfortable, unobtrusive, and accurate physiological monitoring and physical sensing for applications in healthcare, medical treatment, and human-machine interfaces. Metal−elastomer nanocomposites represent a promising approach, combining high conductivity and stretchability derived from metallic conduction and percolation networks of metal nano/micro fillers. However, their practical application is often limited by inferior cyclic stability and long-term durability. In this study, researchers report a highly durable nanofiber-reinforced metal−elastomer composite comprising (i) metal fillers, (ii) an elastomeric binder matrix, and (iii) electrospun PVDF nanofibers to enhance both cyclic stability and conductivity. The embedded PVDF nanofibers improve toughness and inhibit crack growth by providing a reinforcing effect. Furthermore, the conductivity of the nanofiber-reinforced elastic conductor is four times greater than that of the pristine material due to the self-assembly of a silver-rich layer on the top surface through a filtering effect. Consequently, the stretchable electrode made from this nanofiber-reinforced elastic conductor exhibits excellent cyclic durability, high conductivity, and stretchability of up to 800%. The cyclic degradation (ΔR/R0) remains at 0.56 after 5000 stretching cycles (50% strain), with initial conductivity and sheet resistance recorded at 9903 S cm^{-1} and 0.047 Ω sq^{-1}, respectively. By utilizing this highly conductive and durable elastic conductor as sensor electrodes and wiring, researchers successfully demonstrated a skin-tight multimodal physiological sensing suit capable of continuous long-term monitoring of electrocardiograms, electromyograms, and movements during weightlifting exercises without significant degradation in signal quality.[190]

PTFE, octenidine dihydrochloride (OCT), and ZnO were utilized to modify polypropylene nonwoven materials through "wet chemistry" and low-energy electron beam deposition (EBD) techniques. The effect of modificationon the morphology, chemical composition, filtration efficiency, and antibacterial properties of the nonwoven material were assessed. The modified materials exhibited antibacterial activity against the Gram-positive bacterium *S. aureus* and Gram-negative bacteria *E. coli* and *Klebsiella pneumoniae*, with OCT achieving a 100% suppression of bacterial growth and ZnO achieving 70%. The application of PTFE to Aquaspun significantly increased the contact angle from 141.3° to 152.7° and improved air filtration efficiency from 78.3% to 83.4%, enhancing the barrier properties of the material. Additionally, the material produced via low-energy EBD demonstrated superior antimicrobial efficacy against the tested strains of *S. aureus*.[191]

While electrospun nanofibers are gaining traction for various commercial applications, the aspect of energy efficiency—crucial for cost reduction and technological viability—has not been extensively explored. This study introduced a concentric spinneret featuring a solid Teflon-core rod to facilitate an energy-efficient electrospinning process. Ketoprofen, a poorly water-soluble drug, and polyvinylpyrrolidone (PVP), a filament-forming matrix, were employed to create nanofibrous films using both traditional tube-based electrospinning and the new solid rod-based method. Comparative *in vitro* drug dissolution and *ex vivo* sublingual permeation tests revealed that both film types performed similarly in medical applications. However, the new method consumed only 53.9% of the energy required by the traditional approach. This reduction was achieved through several engineering enhancements, including a less energy-dispersive air-epoxy resin surface on the spinneret, free liquid guidance without backward capillary forces from the Teflon-core rod, and reduced fluid-Teflon adhesive forces. Future research could explore other nonconductive materials to develop new spinnerets that offer improved engineering control and energy efficiency for producing low-cost electrospun polymeric nanofibers.[192]

This research highlighted the impact of β-chain alignment on the performance of PENG. A simple, safe, and cost-effective fast-centrifugal spinning technique was employed to produce self-poled PVDF nanofibers. PENGs made from acetone-prepared PVDF fibers, which exhibited high β-chain alignment, generated open-circuit voltages and short-circuit currents five times greater than those from film counterparts. The degree of β-chain alignment increased with higher ratios of (DMF solvent. The optimal nanofiber achieved a β-chain alignment degree, β-fraction, and piezoelectric charge coefficient of 0.93, 91.8%, and −120 pC N^{-1}, respectively. The PENG based on this optimal fiber displayed the highest V_{oc}, I_{sc}, and power

https://doi.org/10.1021/acs.chemrev.4c00996
Chem. Rev. XXXX, XXX, XXX−XXX

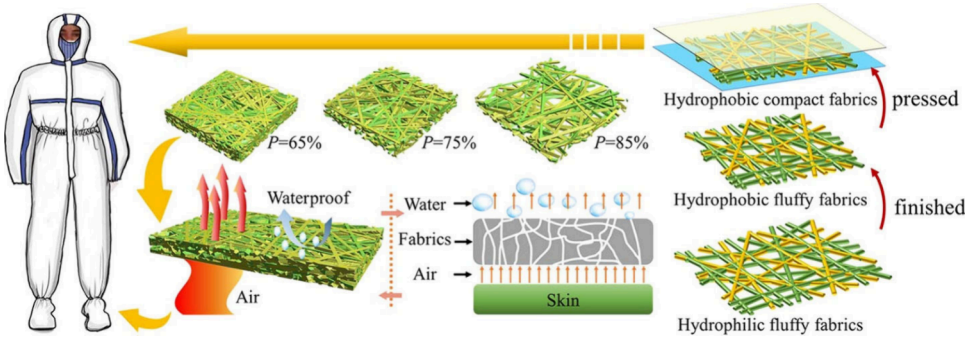

Figure 52. Illustrations showing the preparation process to make bicomponent microfilament fabrics with tunable porosity via the thermal-belt bonding process. Reproduced with permission from ref (197). Copyright 2022 American Chemical Society.

density of 14 V, 1.4 μA, and 6.7 μW cm^{-2}, respectively, surpassing any PENG made from electrospun PVDF fibers. The exceptional performance of the fabricated PENGs was closely linked to the high alignment of β-chains along the fiber axis. Additionally, due to the low Young's modulus (1.63 MPa) of the optimal fibers, the lead-free PENG is sensitive to minor movements, making it suitable for wearable and implanted medical devices.[193]

The development of intelligent wearable protection systems is crucial for human health engineering. An ideal intelligent air filtration system should ensure reliable filtration efficiency, low pressure drop, healthcare monitoring capabilities, and man-machine interaction. In this study, this research group created an intelligent wearable filtration system (IWFS) using advanced nanotechnology and machine learning. Leveraging the triboelectric mechanism, the IWFS demonstrated high particle filtration efficiency and bacterial protection rates of 99% and 100%, respectively, with a low-pressure drop of 5.8 mmH_2O. The charge accumulation in the optimized IWFS (87 nC) was 3.5 times greater than that of the unmodified nanomesh, significantly enhancing particle filtration efficiency. Furthermore, researchers integrated healthcare monitoring and man-machine interaction capabilities into the IWFS through machine learning and wireless transmission technology. The system successfully detected and classified crucial physiological signals, such as breathing, coughing, and speaking, with a recognition rate of 92%. The IWFS can collect healthcare data and transmit voice commands in real-time without interference from portable electronic devices. This innovative IWFS not only holds practical significance for human health management but also offers substantial theoretical value for advanced wearable systems. Researchers concluded that the IWFS can achieve stable high-performance protection, human health management, and effective man-machine interaction.[194]

TENGs are increasingly utilized in wearable and implantable electronics, smart medical devices, and soft robotics. However, producing stretchable TENGs that combine exceptional elasticity with high output performance remains a challenge, limiting their application range. This study developed high-performance stretchable TENGs using a thermo-compression (TC) fabrication process. A PVDF film was tightly bonded to an elastic TPU substrate, which maintained excellent stretchability with a strain capacity of up to 815%. The TC composite film-based TENGs exhibited output performance 2−4 times greater than that of unlaminated film-based TENGs, attributed to the large surface area, tight contact, and effective vertical transport of tribo-induced charges between the fibrous tribo-layer and soft substrate. The versatility of this method was demonstrated with various triboelectric and substrate materials. This innovative technology offers a promising approach to simultaneously enhance the output and stretchability of TENGs, indicating strong potential for applications in self-powered wearable and flexible electronics.[195]

Liao et al. demonstrated that Nylon and PTFE emerged as the top choices for adhesion performance in membrane materials for the further development of novel and emerging technologies such as membrane carbonated microalgal biofilm reactors (MCMBR) and extractive membrane microalgal biofilm reactors (EMMBR) for wastewater treatment. The main reason being that membrane surface roughness played a dominant role in determining microalgal cell adhesion and biofilm formation. A rougher membrane surface was positively correlated to higher microalgal cell adhesion and biofilm formation rate under tested hydrodynamic conditions.[196]

Medical protective materials have garnered significant attention for their role in preventing the spread of infectious diseases and ensuring the safety of healthcare professionals. However, developing materials that effectively combine superior liquid barrier properties, exceptional mechanical strength, and high breathability remains a complex challenge. In this study, researchers present a polyester/polyamide 6 (PET/PA6) bicomponent microfilament fabric designed for comfortable medical protective clothing (Figure 52). This fabric was produced using dip-coating technology and a straightforward thermal-belt bonding process that allows for tunable porosity. The dip-coating with a C6-based fluorocarbon polymer provided the fabric with remarkable hydrophobic properties, achieving alcohol contact angles between 130° and 128°. Additionally, by varying the temperature and pressure during the thermal-belt bonding process, researchers were able to adjust the porosity of the fabric within a range of 64.19% to 88.64%. The resulting materials exhibited excellent softness scores (ranging from 24.3 to 34.5), satisfactory air permeability (between 46.3 and 27.8 mm/s), and high hydrostatic pressure resistance (from 1176 to 4130 Pa). Importantly, these textiles effectively filter aerosols from the air and demonstrate high tensile strength. Collectively, these outstanding properties suggest that the developed PET/PA6 bicomponent microfilament fabrics are a promising option for medical protective apparel.[197]

Waterproof and breathable membranes (WBMs) are in high demand globally due to their valuable applications in outdoor protective clothing, medical hygiene, and electronic devices. However, creating materials that are both environmentally friendly and highly functional has been a persistent challenge (Figure 53). In this study, researchers present polyamide

https://doi.org/10.1021/acs.chemrev.4c00996
Chem. Rev. XXXX, XXX, XXX−XXX

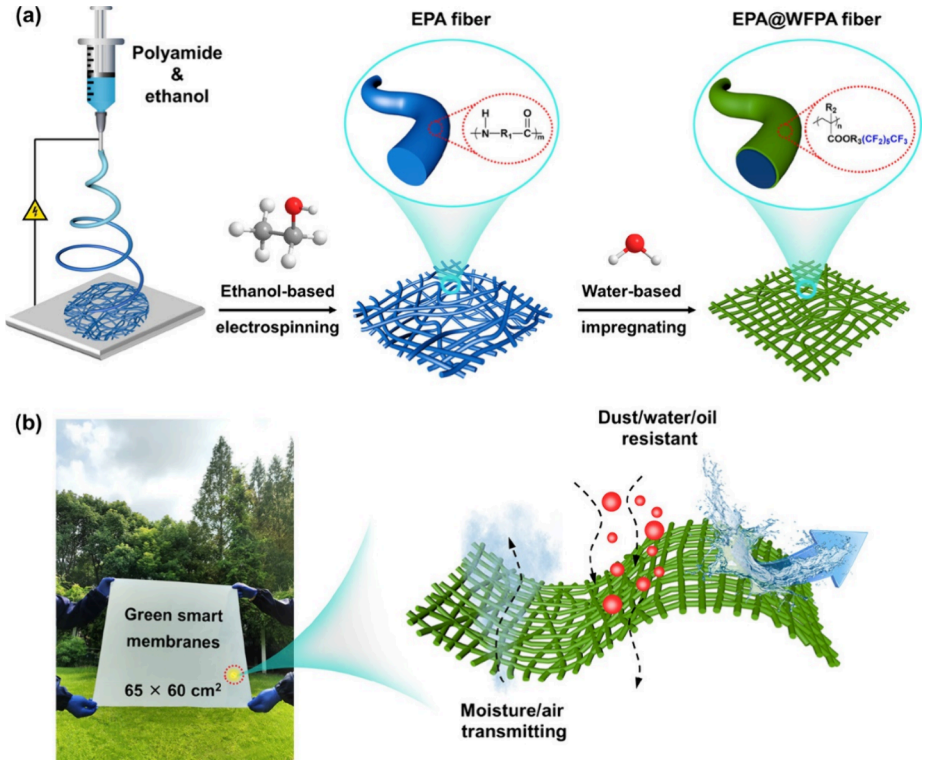

Figure 53. (a) Schematic illustration of the fabrication procedures of green smart PA fibrous membranes. (b) Digital photograph of the fabricated large-scale green smart membranes and schematic diagram of moisture/air transmitting and dust/water/oil-resistant properties of the fibrous membranes. Reproduced with permission from ref (198). Copyright 2020 American Chemical Society.

fibrous membranes processed with green solvents, which exhibit amphiphobic properties and a unique bonding structure. This was achieved through ethanol-based electrospinning and water-based impregnation techniques, resulting in membranes that are highly resistant to water, oil, and dust while maintaining good breathability. The developed green smart fibrous membranes demonstrate impressive characteristics, including water and oil intrusion pressures of 101.2 and 32.4 kPa, respectively, a dust removal efficiency exceeding 99.9%, a water vapor transmission rate of 11.2 kg m^{-2} d^{-1}, air permeability of 2.6 mm s^{-1}, tensile strength of 15.6 MPa, and exceptional toughness of 22.8 MJ m^{-3}. These properties enable the membranes to effectively protect both individuals and electronic devices. This research may provide valuable insights for the development of the next generation of environmentally friendly smart fibrous WBMs for protective textiles.[198]

A helpful study to determine fluorine content in textiles was conducted by Benskin et al. Due to their extensive production volumes and potential to form persistent perfluoroalkyl acids (PFAAs), there are growing concerns regarding the ongoing use of side-chain fluorinated polymers (SFPs) in consumer products. Accurate quantification of SFPs typically relies on matrix-assisted laser desorption ionization time-of-flight mass spectrometry, which can suffer from poor accuracy and high detection limits. Alternatively, total fluorine (TF)-based methods may be employed; however, these approaches report concentrations on a "fluorine equivalent" basis (e.g., fluorine per square meter for textiles) and do not provide insights into structure or chain length. Here, this group presents a new method for comprehensive characterization of SFPs, utilizing the total oxidizable precursor assay for fingerprint-based structural elucidation and combustion ion chromatography for TF quantification. When applied in tandem, this method allows for the quantitative determination of SFPs (expressed in mass of C_nF_{2n+1} per square meter of textile). Reporting SFP concentrations in terms of the mass of the side chain (rather than fluorine equivalents) facilitates estimation of both the structure and quantity of PFAA degradation products. As a proof of principle, this method was applied to six unknown SFP-coated medical textiles from Sweden, revealing that four products contained C6-fluorotelomer-based SFPs (concentration range of 36−188 mg of C_6F_{13}/m^2), one contained a C4-sulfonamide-based SFP (718 mg of C_4F_9/m^2), and one contained a C8-fluorotelomer-based SFP (249 mg of C_8F_{17}/m^2).[199]

Soft pneumatic actuators (SPA) are known for their low cost, lightweight, possess large deflection, fast response times, and high output force, making them ideal for delicate operations like human rehabilitation. Researchers developed a soft pneumatic actuator (SPA) with a piezoelectric membrane (SPA-P) for applications in robotics, medical rehabilitation, and wearable devices. The SPA-P consists of a flexible conducting polymer nanocomposite (CPNC) membrane embedded inside a silicone rubber body, with PVDF as the dielectric, carbon nanofibers (CNFs) for charge transport, and an ionic liquid (1-butyl-3-methyl imidazolium hydrosulfate, BMIM) to enhance flexibility and ion availability. This composite material enables the actuator to generate a significant voltage change when actuated by pneumatic pressure, providing real-time feedback corresponding to bending deformation. The SPA-P device was tested on human finger rehabilitation, where the bending angle of the actuator was found to be proportional to the applied pneumatic pressure. At rest the device produced a voltage of

https://doi.org/10.1021/acs.chemrev.4c00996
Chem. Rev. XXXX, XXX, XXX−XXX

81.4 mV due to natural vibrations, and at 20 kPa the maximum voltage observed was 257 mV. This voltage feedback can be used to monitor finger movement, creating potential for automated rehabilitation devices. The SPA-P actuator demonstrated bending angles up to 134° at 29 kPa and 5° at 18 kPa, proving its effectiveness as a soft actuator for robotics and rehabilitation. The integration of the flexible CPNC membrane into the SPA body significantly enhanced its performance, offering both actuation and sensing capabilities in soft robotics applications.[200]

Researchers developed an autonomous triboelectric smart textile sensor (AUTS) to address power consumption issues in wearable biosignal sensors for health monitoring, particularly in cardiovascular disease diagnosis. The system is based on TENGs, which are effective in healthcare monitoring as they can generate energy from weak signals (e.g., respiration) within a frequency bandwidth below 10 Hz. The device is fabricatedfrom reduced graphene oxide/manganese dioxide/PDMS (RGO-M-PDMS) and a PTFE-knitted silver electrode, is flexible, self-powered, and capable of measuring vital signs such as respiration and pulse. The sensor exhibits a sensitivity of 7.8 nA kPa^{-1}, a response time of approximately 40 ms, has a stretchability of up to 40%, can withstand over 15,000 cycles of use and more than 20 machine washes. The AUTS sensor is integrated into two wearable devices: the TriBreath respiratory belt, which monitors respiration, and the TriPulse pulse strap, which measures pulse signals at different points on the body. Both devices wirelessly transmit data to a smartphone for real-time health monitoring. This setup allows the device to generate 24 V, 0.3 μA, and 20 nC at 50 Hz oscillation frequency, providing reliable, self-powered functionality without external energy sources. The TriBreath device can detect different breathing patterns during various activities, such as lying down, walking, or jogging, offering potential applications in diagnosing conditions like sleep apnea. The TriPulse platform effectively captures pulse wave signals from the radial artery, providing detailed characteristics of pulse waves, including systolic (P_s) and dicrotic (P_d) peaks, as well as the point of inflection (P_i), making it useful for cardiovascular health monitoring.[201]

Table 6 below summarizes the voltage performance of some of the novel materials found in this section for various particle sizes and bacteria.

1.9. Membranes

Some strategies have been implemented to increase hemocompatibility in membranes, typically grafting hydrophobic membranes with hydrophilic components to increase hemocompatibility and decrease hemolysis. Carbon nanotubes offer a solution, acting as channels for the water to pass through the membranes, however, CNTs can potentially damage cell membranes. This is solved through CNT functionalization with PEG to reduce cell damage by making the CNTs more hydrophilic. Membranes of PVDF and PEG-multiwalled carbon nanotubes (PMWCNTs) were prepared using the phase inversion method to give hybrid ultrafiltration membranes that display a high water flux of 384 L m^{-2} h^{-1}. MWCNTs were produced through chemical grafting and then modified with PEG to produce PMWCNTs, which blended to fabricate hybrid membranes with PVP, and spin coated on glass plates (Figure 54). These membranes display significantly higher flux than PVDF membranes, better antifouling properties, and a more stable rejection rate of albumin (>90.0%). Hydrophilicity of the material was improved compared to standard PVDF, and the surface morphology was smooth with finger-like pore structures. As hydrophilic PMWCNT content increases, WCA decreases with a minimum of 66.6° at a 1 wt % loading of PMWCNT. Antifouling properties can be increased with a weak electric current of 2 V cm^{-1}, and this membrane displays a hemolysis ratio of 0.4%, showing excellent hemocompatibility and blood stability. Red blood cell adhesion is minimized in the presence of the weak electric field, indicating that the material may have potential applications in electric field enhanced hemodialysis.[202]

PVDF is a material well-suited for membrane separation due to its high resistance to chemical and physical degradation, and has been successfully applied to Microfiltration (MF)/Ultrafiltration (UF) for liquid separation. Alternating current (AC) applied to the membrane causes turbulence on the surface, removing cake/gel layers and cleaning the membrane pores, restoring membrane permeability. The researchers fabricated electroactive membranes from P(VDF-TrFE) in a P(VDF-TrFE)/PVP/DMAc/water system for structural design. A DMAc solution of P(VDF-TrFE) was spin coated on a glass slide and coagulated in a water bath, after which the membranes were annealed in glycerin from 120 to 140 °C. Annealing in glycerin was found to increase β-phase content as the annealing temperature increased. A grain-like surface is formed from stacks of edge-on lamellae, with the crystalline polymer displaying excellent filtration properties and good antifouling performance (95% FRR after 2 h). The annealed membranes possess excellent flux in a 13.5 mg/L humic acid (HA) solution, thought to be from the weak hydrophobic interaction between the HA and β-phase crystals. The excellent antifouling properties indicate the formation of a membrane which exhibits electroactivity withpromise in energy harvesting and other related fields.[203]

Biomedical gas exchange membranes are crucial for blood oxygenation and artificial lung technologies. Membrane products primarily include dialysis membranes for blood purification and gas-exchange membranes for blood oxygenation used in cardiopulmonary bypass (CPB) and ECMO systems. To minimize immune responses initiated by protein adsorption, low protein-binding membrane surfaces are essential to avoid platelet adhesion, activation, and aggregation. Hemodialysis typically employs hydrophilic membranes such as polysulfone and polyacrylonitrile, while gas exchange membranes require hydrophobic characteristics to prevent wetting and blood plasma leakage. To address issues of hemocompatibility, researchers have developed antithrombogenic and antifouling coatings that enhance hemocompatibility

Table 6. Medically Relevant Textiles with Corresponding Voltage and Current Values for Materials in This Section[a]

Filtration membrane	Voltage output (V)	Current (μA)
TI-TENG[170]	87.98	1.15−9.31
GNP/PEN/PTFE[171]	240	37
IEPY[174]	0.292	-
APTAP[175]	1.650	0.0070
PVDF nanofiber PENG[193]	14	1.4
SPA-P[200]	0.0814−0.257	-
AUTS[201]	24	0.3

[a]Note: All values in the table are relative to the size of the device, pressure or force applied, and do not represent a direct comparison between material classes.

https://doi.org/10.1021/acs.chemrev.4c00996
Chem. Rev. XXXX, XXX, XXX−XXX

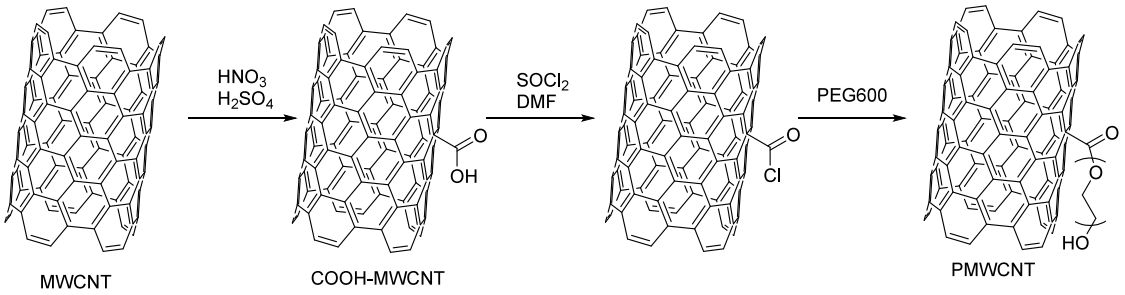

Figure 54. Schematic for the functionalization of MWCNT by oxidation, transformation to the acid chloride, and PEGylation to form PMWCNTs.

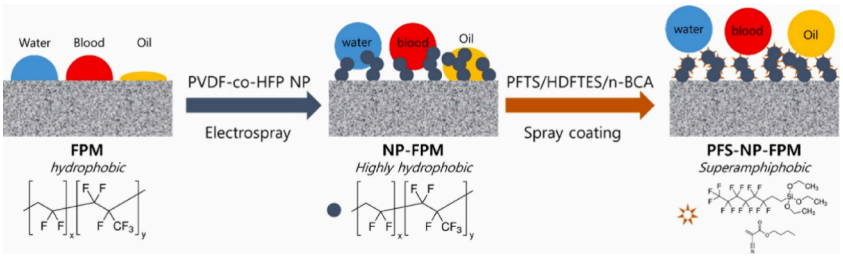

Figure 55. Schematic for the production of amphiphobic FPM membranes through electrospraying with PVDF-co-HFP NPs and spray coating with PFTS, HDFTES, and n-BCA to afford the PFS-NP-FPM membranes. Reproduced with permission from ref (204). Copyright 2022 Elsevier Inc.

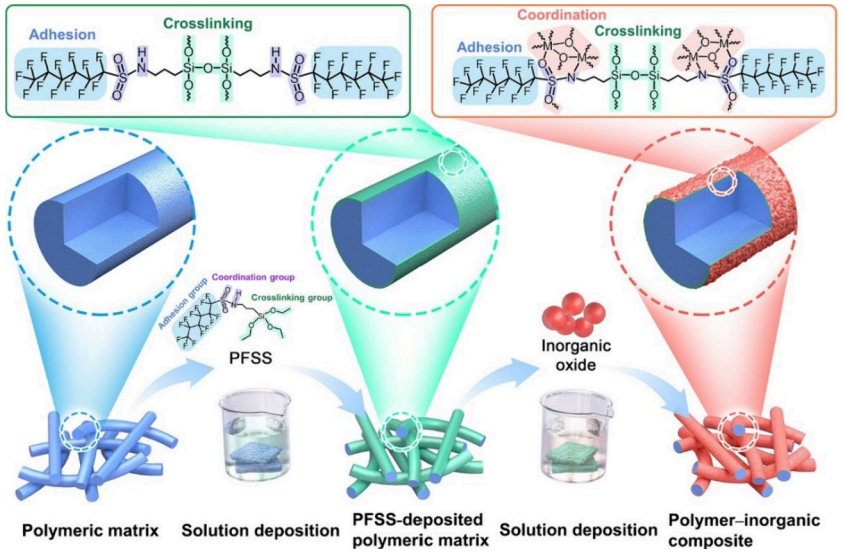

Figure 56. Schematic for the synthesis of a biomimetic polymer-inorganic composite through silane-cross-linked fluorocarbons with a sulfonamide coordinating group for surface metal-oxide mineralization. Reproduced with permission from ref (205). Copyright 2023 American Chemical Society.

and extend the lifespan of membranes used in long-term membrane oxygenation (MO) and implanted artificial lungs. Researchers designed a superamphiphobic, blood-repellent structure based on porous PVDF-HFP membranes by electrospraying PVDF-HFP nanoparticles onto a porous membrane surface followed by thermal fusion (Figure 55). The surface is then coated with perfluoro-silane using a biocompatible adhesive, resulting in a soot-like re-entrant structure that exhibits high contact angles over 150° for water, blood, and hexadecane. The device displayed significantly increased liquid entry pressure, achieving up to 8 bar after PFS coating, a low surface energy of 1.3 mN m^{-1} and minimal protein adhesion (<1 μg cm^{-2}), indicating potential for long-term MO and artificial lung applications. Membrane fouling and clotting were not observed during 12 h of continuous blood oxygenation and 2 weeks of stationary blood contact. Although the PFS coating decreased air permeance, the membrane retained higher gas permeance compared to commercial PMP and PP membranes, measuring 20,000 GPU compared to 430 GPU and 15,600 GPU, respectively.[204]

Biomineralization is a process where living organisms naturally form functional structures from their surroundings. While biomimetic mineralization holds great potential in applications such as hydrophilic membranes for oil removal from wastewater, antibacterial fabrics, and high-performance mechanical plates, practical applications have been limited. Researches have designed a simple, universal method for mineralizing polymer surfaces using a triple-functional bridge,

https://doi.org/10.1021/acs.chemrev.4c00996
Chem. Rev. XXXX, XXX, XXX−XXX

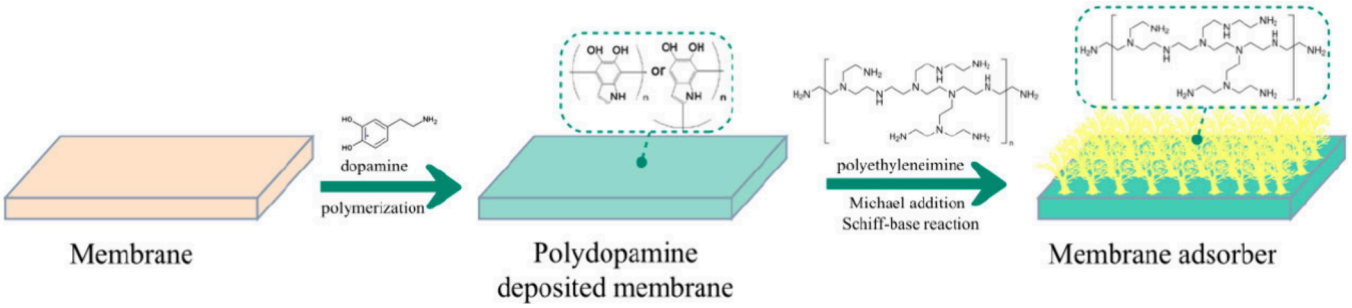

Figure 57. Schematic diagram of membrane adsorber prepared by depositing PDA layer on membrane to couple PEI. Reproduced with permission from ref (209). Copyright 2023 MDPI.

3-[(perfluorohexyl sulfonyl) amino] propyltriethoxy silane (PFSS) (Figure 56). This two-step solution deposition process enables the adhesion and immobilization of PFSS onto polymer surfaces through hydrophobic interactions, followed by chemical cross-linking and the growth of inorganic nanoclusters via PFSS sulfonamide coordination. The method successfully mineralizes oxides such as TiO_2, SiO_2, and Fe_2O_3 onto polymers, resulting in robust, multifunctional materials suitable for harsh environments. This technique is demonstrated on PTFE, PVDF, PP, and PET to create ultrathin inorganic films, With PTFE@PFSS@TiO_2 membranes exhibit excellent oil/water separation efficiency (99.1%) and hydrophilicity, outperforming existing membranes. A hollow-fiber PTFE composite membrane (PTFE-HF@PFSS@TiO2) was applied in a local sewage treatment plant, and was easily restored to working condition with dilute oxalic acid washing after fouling, further indicating the applicability of these materials in real-world environments.[205]

Traditional Mixed Matrix Membranes (MMMs) face several challenges, including poor interfacial compatibility between the substrate and polymer, agglomeration of functional additives, and instability over time, making it difficult to create high-performance membranes. In this work, a new approach inspired by mussel biomimetic chemistry was developed to overcome these limitations. The researchers introduced a 3D nanohybrid seeding strategy, which involved in situ assembling nanosized zeolitic imidazolate frameworks (ZIFs) onto polydopamine (PDA)-coated nanofibers. This was followed by the creation of specific imprinting sites in the nanofiber membranes using a boron-affinity sol−gel strategy. The result was a highly efficient membrane for selectively separating shikimic acid (SA), a valuable compound in medicinal chemistry. The ZIF-8 functionalized membranes, such as PVDF, maintained superior stability and performance over long-term cyclic tests. Additionally, the membranes exhibited excellent antifouling and antibacterial properties, thanks to the ZIF-8-functionalized PDA-connected nanofibers. The ZIF-8-based membrane achieved impressive performance, with a flux of 13732.0075 LMH bar^{-1} and a perm-selectivity value of 9.03. The combination of ZIF-8's hydrophilic nanocrystalline structure, the strong cross-linking effect of PDA, and the boron-affinity sol−gel imprinting strategy allowed for both effective SA selection and enhanced hydrophilicity, contributing to the membrane's antifouling and antibacterial properties. The approach offers great promise for the development of functional materials that can meet the growing demands of selective molecular separations, especially in fields like medicinal chemistry, while also addressing challenges in energy efficiency and sustainability.[206]

This research focused on evaluating the adsorption behavior of polysorbate-20 (PS-20), a commonly used surfactant in therapeutic protein formulations, when filtered through different sterilizing-grade microfiltration (MF) membranes. The goal was to better understand how membrane properties—such as material, modification, and layer configuration—affect PS-20 retention, which can impact the final product's consistency and quality. The study found that PS-20 adsorption was highly influenced by the membrane material and the concentration of PS-20 in the feed solution. Hydrophilic membranes, such as PES (polyethersulfone) and PVDF, exhibited the lowest PS-20 adsorption, requiring less solution to reach saturation. One key finding was that modified hydrophilic PES membranes (e.g., Express PLUS) showed lower PS-20 adsorption than previously expected, even when compared to hydrophilic PVDF membranes. This contrasts with earlier research, which suggested that PES membranes bind more PS-20 due to their intrinsic hydrophobicity. However, advancements in membrane modification techniques have overcome this issue, making PES a viable option for PS-20 retention in the final filtration process. This study also suggests that other nonionic surfactants, like polysorbate 80, may have similar adsorption behavior, but with potentially higher adsorption due to the longer aliphatic tail of PS-80, which could promote greater hydrophobic interactions. Overall, the study highlights the importance of choosing the right filter material and developing appropriate preflush strategies to ensure consistent PS-20 levels in therapeutic protein products. This is especially critical as regulations around per- and polyfluoroalkyl substances (PFAS) may limit the use of PVDF filters in the future, making modified PES filters a promising alternative.[207]

This study investigates the use of mixed-matrix membranes (MMMs) for removing pharmaceutical contaminants from water, addressing the limitations of conventional wastewater treatment plants. The focus was on four model pharmaceuticals—diclofenac (DCF), sulfamethoxazole (SMX), carbamazepine (CBZ), and metoprolol (MTP)—which have medical significance and varied chemical properties. To enhance the adsorption properties, three types of strong anion-exchange particles were used, including nonporous and porous polymer adsorbents. The adsorption efficiency of the anion-exchange particles was evaluated for individual pharmaceuticals and multicomponent mixtures using Freundlich and Langmuir isotherm models. The results indicate that all particles exhibited excellent adsorption of DCF, with Freundlich constants (KF) reaching up to 278 $(mg\ g^{-1}/mg\ L^{-1})^n$. The nonporous and porous adsorbent particles effectively removed DCF while also adsorbing SMX or CBZ. Mixed-matrix

https://doi.org/10.1021/acs.chemrev.4c00996
Chem. Rev. XXXX, XXX, XXX−XXX

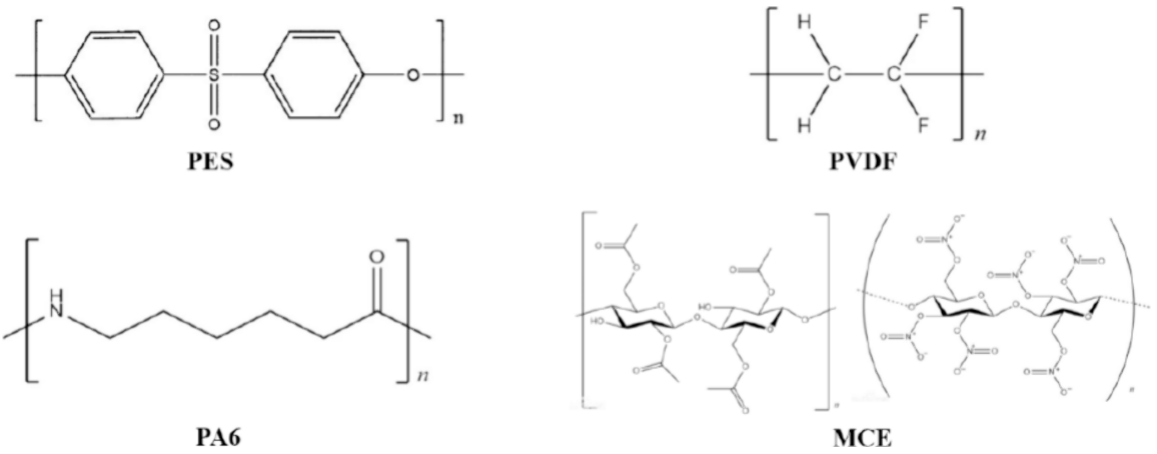

Figure 58. Molecular structures of PES, PVDF, PA6 and MCE. Reproduced with permission from ref (209). Copyright 2023 MDPI.

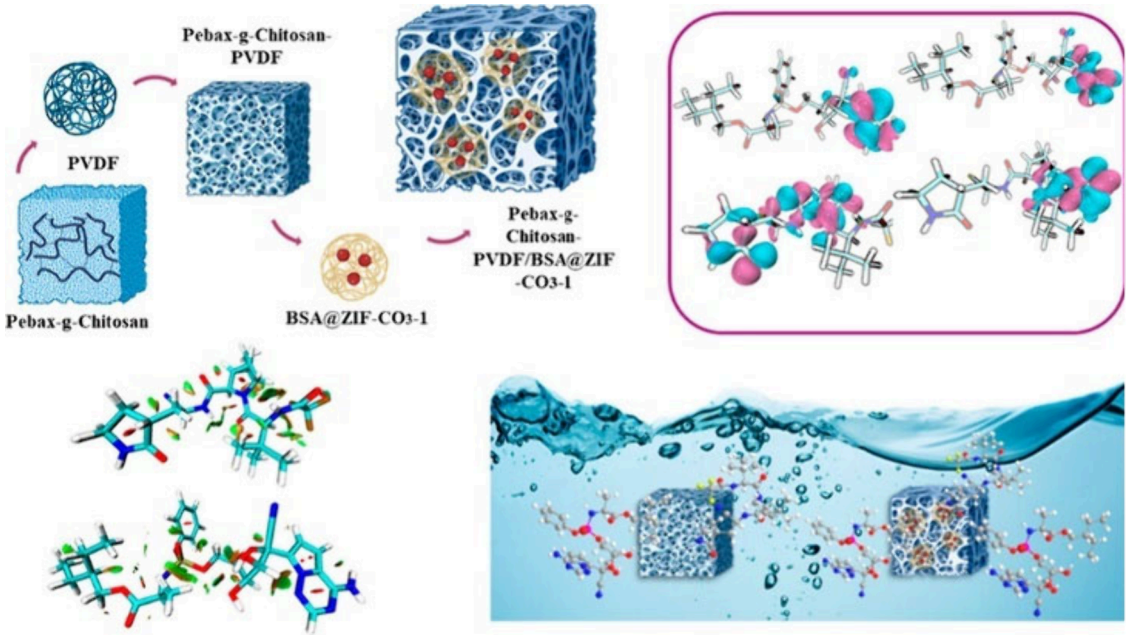

Figure 59. Schematic depicting the design of MMMS from Pebax-g-Chitosan integrated with PVDF and BAS@ZIF-CO3−1 to form composite membranes for water treatment and removal of organic pharmaceutical pollutants. Reproduced with permission from ref (210). Copyright 2023 American Chemical Society.

membrane adsorbers were then fabricated by incorporating these particles into porous PVDF hollow fiber membranes using wet spinning. When tested in dynamic adsorption experiments with pharmaceuticals in tap water (5 mg/L), the MMM adsorbers demonstrated high adsorption capacities. The DCF removal capacity was as high as 13.7 g/m^2 (relative to the membrane filter area), while SMX was adsorbed simultaneously with a capacity of 0.60 g/m^2. These results highlight the potential of MMM adsorbers for effective removal of pharmaceutical contaminants in water, offering a promising solution for enhancing water treatment processes.[208]

The preparation process for polyethyleneimine (PEI)@Mm-PDA is depicted in the accompanying figure (Figure 57). Membranes made from PES, PVDF, PA6, and MCE were immersed in a specific concentration of dopamine solution (10 mM Tris-HCl), 2 mg/mL (Figure 58). The membranes produced through this method are referred to as PEI@PES−PDA and PEI@PVDF−PDA. This study explored four types of membrane materials with varying functional groups and three surface modification techniques aimed at enhancing the functional groups of the membrane to assess the impact on the adsorption capacity of the modified membranes (MAs). Experimental findings indicate that the C−F bonds on the PVDF membrane may form hydrogen bonds with the amine groups on PEI, potentially enhancing the protein adsorption capacity of the MAs. The functional groups introduced by PDA deposition on the PVDF membrane, along with a uniform pore size distribution, likely contribute to improved protein adsorption performance. In contrast, functional groups generated through alkali and oxidation treatments had minimal effects. The preparation conditions for PEI@PVDF−PDA were also examined. The influence of membrane structure on the adsorption performance of MAs remains unclear and will be the subject of further investigation in future studies. This research offers new insights into how functional groups can enhance binding capacity, and PEI@PVDF−PDA demonstrates significant potential for applications in protein adsorption and desorption.[209]

https://doi.org/10.1021/acs.chemrev.4c00996
Chem. Rev. XXXX, XXX, XXX−XXX

The use of pharmaceuticals in COVID-19 treatments, such as remdesivir (REMD) and nirmatrelvir (NIRM), has resulted in the release of these drugs into aquatic and terrestrial environments. Researchers explored an *in silico* approach toward the use of mixed matrix membranes (MMMs) as adsorbents to remove REMD and NIRM from aqueous environments. The MMMs were composed of a Pebax 1657-*g*-chitosan-PVDF(PEX-*g*-CHS-PVDF) matrix combined with bovine serum albumin (BSA)@ZIF-CO3−1 (Figure 59). The incorporation of chitosan (CHS) improves the stability and uniformity of the MMM structure. Grafting CHS onto Pebax-1657 further enhances drug adsorption capacity by increasing surface area and hydrophilicity, which helps retain drugs in the membrane. Thin-film nanocomposites (TFNs) comprised of PVDF or PEX can further boost the performance of MMMs, offering high mechanical stability and thermal resistance. The incorporation of BSA@ZIF-CO3−1 into the PEX-*g*-CHS-PVDF matrix improved the physicochemical properties of the MMMs, enhancing their compatibility and interfacial adhesion by an increase of electrostatic interactions, van der Waals forces, and hydrogen bonding between the materials. The simulations indicated that adsorption is influenced by factors such as molecular size, shape, and the presence of functional groups on the drugs, with the MMMs demonstrating a higher affinity for REMD compared to NIRM, The pores of the ZIF filler acted as a scaffold for the polymer, increasing surface area and providing additional adsorption sites. Functional groups on the ZIF particles can interact with the drugs, further increasing the adsorption energy. MMMs composed of PEX-*g*-CHS-PVDF and BSA@ZIF-CO3−1 are potentially an effective approach for removing pharmaceutical pollutants such as REMD and NIRM from aqueous environments.[210]

Membrane processes are commonly used in drinking water treatment and medical applications to filter out viruses but backwashing alone does not completely remove viruses. In this study, supercritical CO_2 ($SCCO_2$) treatment is explored as a potential method for inactivating viruses on organic membranes without affecting their performance. The results indicate that $SCCO_2$ treatment, regardless of pressure (100−150 bar), contact time (20, 120, 660 min), or membrane material (such as PES or PVDF), does not affect the permeability or retention properties of the membranes. Transmission electron microscopy (TEM) revealed that the integrity of viruses was compromised after treatment. This suggests that $SCCO_2$ is a promising, robust method for virus inactivation on organic membranes. The study also found that the $SCCO_2$ treatment effectively inactivated the Tulane virus, as seen in scanning electron microscopy (SEM) images demonstrating no visible active virus. The study demonstrates the feasibility of $SCCO_2$ treatment for virus inactivation on organic membranes, but further research is needed. Future steps will include testing more complex virus samples, assessing the stability of the membrane in real-world conditions, and performing more detailed analyses (e.g., ATR-FTIR, FE-SEM) to understand the full impact of $SCCO_2$ on membrane integrity, surface properties, and sterilization potential.[211]

1.10. Photodynamic Therapy

Singlet oxygen ($^1O_2$) is a key active species in photodynamic therapy (PDT). While biocompatible dyes are known as effective photosensitizers for singlet oxygen generation, the ability of matrix materials such as organic solvents and metal oxide surfaces to generate singlet oxygen has not been extensively studied. PTFE, a biocompatible material, was investigated by researchers to examine its potential in singlet oxygen generation under UV and visible light irradiation. PTFE exhibits a broad photoluminescence (PL) spectrum, spanning from violet to red regions, with the concentration of molecular oxygen in the material influencing the formation of optical photoluminescence. PTFE is recognized for enhancing charge separation in common catalysts like TiO_2 due to the high electronegativity of its fluorine atoms, making it an ideal matrix for composite photosensitizers to synergistically improve ROS generation. Near-infrared (NIR) photoluminescence (PL) from PTFE samples excited by UV and visible LED radiation displayed a characteristic singlet oxygen phosphorescence peak at 1270.0 ± 1.5 nm. The results indicated that oxygen dissolved within the polymer was efficiently excited into the singlet state, with high efficiency comparable to or exceeding that of carbon tetrachloride. Cooling to −20 °C increased the concentration of singlet oxygen, indicating that temperature plays a role in ROS production. A small amount of singlet oxygen was detected in the air above the PTFE surface, suggesting some release of oxygen into the gas phase during irradiation. PTFE was identified as a notable singlet oxygen generator, indicating potential applications of PTFE-based materials in medical devices and implants for new photodynamic treatment designs.[212]

1.11. Protective Coatings and Surfaces

Researchers have successfully created a superhydrophobic microstructure on PTFE surfaces using femtosecond laser treatment. 0.3 mm thick PTFE sheets were subject to femtosecond laser ablation, leading to instantaneous melting and gas ejection that created solid microholes and nanoscale protrusions as the molten particles resolidified. The resulting contact angles for all treated surfaces exceeded 150°, surpassing the threshold for superhydrophobicity. Surfaces remain stable at temperatures up to 200 °C and retain their hydrophobic properties even after abrasion with sandpaper. Additionally, they maintain hydrophobicity after immersion in harsh chemicals such as 10 M sodium hydroxide, 98% concentrated sulfuric acid, 40% hydrofluoric acid, and aqua regia for 24 h. This laser ablation process results in a micro/nanoscale hierarchical structure characterized by micropores and a specific degree of re-entrant curvature. As a result, the treated samples exhibit superhydrophobicity, enabling them to repel various liquids including water, 10,000 ppm bovine serum albumin, cola, 10,000 ppm glucose, juice, and saline. The ultralow surface energy of PTFE combined with the laser-induced hierarchical rough microstructures and the partially re-entrant surface curvature, allows complex liquid droplets to maintain a stable Cassie state on the surface. This innovation has potential applications across various fields, including cell engineering, medical instruments, food packaging, microfluidics technology, and chemical engineering.[213]

In tribological applications surface contaminants are often transferred and pure PTFE has high wear rates. Additives such as graphite, bronze, or MoS_2 are often added and reduce wear by around 3 times. Bronze is known to increase mechanical properties of PTFE such as stiffness, hardness, and lowers wicking and expansion coefficients. Gamma or electron beam irradiation is further known to improve the polymer properties, and the effects of bronze-containing PTFE were examined

https://doi.org/10.1021/acs.chemrev.4c00996
Chem. Rev. XXXX, XXX, XXX−XXX

when irradiated with an electron beam of 10 MeV from 26 to 156 kGy. The material was examined to determine the effect on the thermal, spectrophotometric, mechanical, and tribological properties compared to virgin PTFE. A bronze content of 40% was found to decrease the degree of crystallinity by 2-fold and reduce melting heat by 60% under the same levels of radiation compared to pure PTFE. FTIR indicates photodegradation as the main contributing effect on the structural change, with the increase in degree of crystallinity correlating with a decrease in molecular weight, indicating easier rearrangement in the crystallization process due to increased chain mobility. Bronze shows an increase of mechanical properties, and the best results were attained at 104 kGy of radiation, as higher doses resulted in excessive material degradation. Composite irradiation further reduced the wear by 2.5 times in a dose proportional manner. The material demonstrates an increase in crystallinity by DSC and the use of bronze could potentially allow for energy dissipation over the additive particles, with the overall material properties improved compared to virgin PTFE. This may potentially extend the life cycle of PTFE is various applications, especially in high mechanical wear scenarios.[214]

The risk of infection is a factor to consider with any implanted or tissue-contacting medical device. In about 90% of cases of contamination bacteria can adapt to different environments and can colonize the surface of the device to form a resistant biofilm. Chitosan is a natural biological material with antimicrobial properties, is highly effective in surface coatings, and is low cost, biocompatible, and highly available. The deacetylation degree (DD) and molecular weight must reach an appropriate ratio in order to have a coating that is both stable and antimicrobial against representative *S. aureus, E. coli*, and *P. aeruginosa*. Four samples of chitosan were analyzed for MW and DD and then tested to determine the minimum inhibitory concentration. CHI80MW was found to have the most ideal properties for antibacterial applications (79.7% DD and 7.0×10^5 Da) and used to functionalize plasma-treated PTFE surfaces. Higher MW samples generally have better antibacterial properties, also seen in samples with higher DD. Chitosan also displays better antibacterial activity against Gram-positive bacteria. The chosen chitosan sample exhibits good antimicrobial behavior in both MIC and MBC. Poly(ethylene glycol) bis-(carboxymethyl) ether (PEG) or poly(ethylene-alt-maleic anhydride) (PA) were used as spacers to graft CHI80MW, with PTFE-Plasma-*co*-PA-*co*-CHI80MW having better antibacterial properties compared to PEG, with a bacterial reduction of 77−90% versus 25−30%.[215]

Touchscreen devices are prone to harboring pathogenic microorganisms which can spread to the human body through direct contact, posing a risk of infection. Researchers have developed an eco-friendly, transparent coating made of PTFE-coated zinc-doped silicon oxide (SZO/PTFE) as an effective antireflective and antibacterial film for smartphone panels. Thin films of SZO were sputter-coated onto glass substrates, resulting in a thickness of 30 nm, then further coated with a 15 nm layer of PTFE. The refractive indices of the SZO thin films ranged from 1.47 to 1.53, similar to that of bulk SiO_2 films and glass. The PTFE-coated films had a lower refractive index of 1.465, which increased with higher zinc content. PTFE-coated films exhibited a wetting angle of up to 105.2°, indicating hydrophobicity. The addition of an ultrathin PTFE layer on the SZO film enhances its hydrophobic properties without compromising its antibacterial activity. These films also demonstrate good mechanical durability and long-term stability, maintaining consistent transmittance and hydrophobicity. The antibacterial properties of these films were tested by incubating them with *E. coli* and *S. aureus* bacteria. Both SZO and SZO/PTFE films demonstrated a substantial reduction in bacterial growth, with 99.9995% and 99.9981% reductions, respectively. While physical tapping with bare fingers caused a slight decrease in transmittance, cleaning restored it to its original value.[216]

This study presents a step-by-step deposition strategy for creating slippery liquid-infused porous surfaces on various substrates and shapes. The process begins by depositing a PDA layer onto the substrate. The PDA layer also provides reactive sites that can interact with nucleophiles like amines, thiolates, and organosilanes. Next, (3-aminopropyl) triethoxysilane (APTES) is anchored onto the PDA layer, providing primary amine groups that act as both a passivation film for anticorrosion and a site for further reactions. Finally, fluorinated poly(hexafluorobutyl methacrylate-*co*-glycidyl methacrylate) (PFG) polymers are grafted onto the surface through nucleophilic addition, leading to a surface with both hydrophilic amino groups and hydrophobic fluorinated segments. This polar contrast drives spontaneous microphase separation on the surface, which allows for the infusion of lubricating perfluorocarbon oil, forming the SLIPS. The resulting SLIPS exhibits a combination of desirable properties, including antifouling, anticorrosion, anti-icing, and antiscaling capabilities. Additionally, the surface's oil-locking ability is highly stable, ensuring robust performance under challenging conditions such as blood flow, in vivo transplantation, mechanical wear, hydrodynamic shear stress, and even boiling or ultrasound exposure. These properties make SLIPS a promising solution for a wide range of applications, including biomedical devices, surgical equipment, medical implants, and industrial or marine facilities.[217]

This research introduces a novel polycationic membrane filtration system that continuously kills and releases bacteria, even after undergoing sterilization at 121 °C. The innovation lies in creating a self-cleaning membrane capable of sustaining its bacterial-removal effectiveness through multiple cycles, overcoming limitations caused by chemical cleaning and regeneration in traditional systems. The polycationic membrane was fabricated using the vapor-induced phase separation (VIPS) process, combining PVDF with a new copolymer, poly(butyl methacrylate-*co*-(trimethylamino)propyl methacrylamide chloride) (PVDF/PBTP). The study tests the impact of substituting methacrylamide for methacrylate in the copolymer to enhance the bacteria-killing and releasing functions. This process relies on electrostatic interactions, modulated by multivalent negatively charged ions to control the membrane's interaction with microorganisms. The PVDF/PBTP membrane showed excellent bacteria-killing efficiency (over 80%) even after high-pressure steam sterilization. After five cycles of bacterial filtration, the membrane maintained a bacteria-killing rate above 82% and a bacteria-releasing rate of 75%. These results demonstrate that the membrane can effectively remove harmful microorganisms in water, offering a promising solution for reducing bacterial contamination in domestic and industrial wastewater and minimizing environmental pollution.[218]

Fluorocarbon polymers (FPs) are highly valued for their nonadhesive qualities, low friction, and resistance to heat and chemicals, making them ideal for coatings on sliding parts in

https://doi.org/10.1021/acs.chemrev.4c00996
Chem. Rev. XXXX, XXX, XXX−XXX

Scheme 15. (A) Proposed Mechanism of Covalent Polymerization of Phenylamines and (B) Proposed Noncovalent Interactions between Monomers in Oxidative Polymerization of Phenylamines[a]

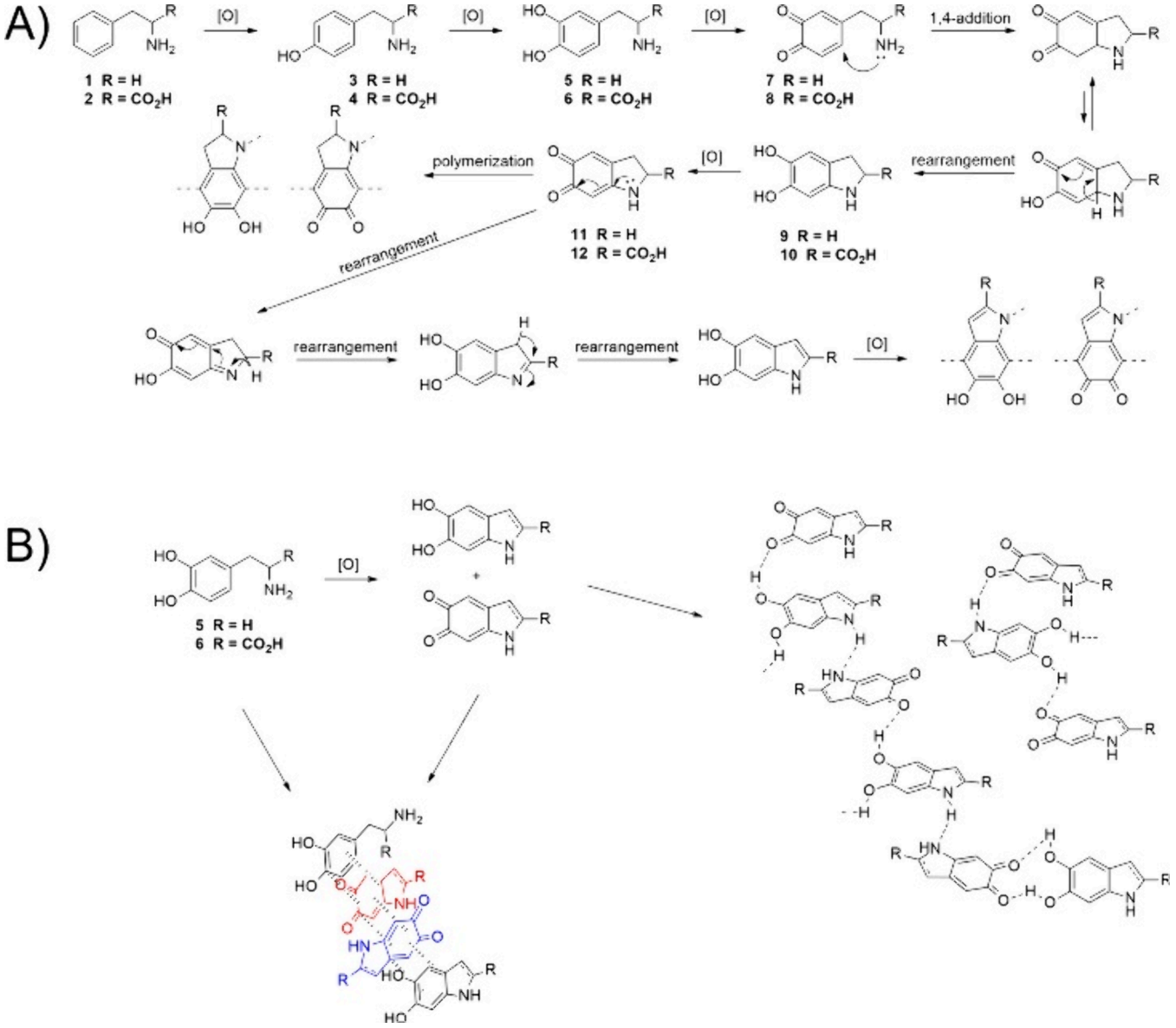

[a]Reproduced with permission from ref (226). Copyright 2022 American Chemical Society.

various industries, including automotive, medical, and semiconductor manufacturing. However, their nonadhesive nature limits their ability to bond with metals, restricting their application. Recent studies indicate that applying high-energy electron irradiation during the coating process can enhance the adhesion of fluorocarbon polymers to metal surfaces. In this study, the authors investigate the interaction between FEP and Al substrates during the coating process. Using advanced techniques like time-of-flight secondary ion mass spectrometry (TOF-SIMS), scanning transmission electron microscopy (STEM)-energy-dispersive X-ray spectroscopy (EDS), and X-ray photoelectron spectroscopy (XPS), they reveal how high-energy electron irradiation improves adhesion. The irradiation causes F atoms from the FEP layer to diffuse into the Al substrate, replacing oxygen atoms in the native Al_2O_3 layer with fluorine atoms. Additionally, it leads to the formation of C−O−Al bonds, which enhance the bonding between the FEP coating and the Al surface. The electron irradiation process modifies the nanostructure at the Al−FEP interface, significantly improving the adhesion between the two materials.[219]

The *in vitro* suppression of platelet adhesion on ePTFE through the surface grafting of poly(2-methacryloyloxyethyl phosphorylcholine) (PMPC) is a significant advancement in the field of biomaterials. However, concerns regarding the long-term hemocompatibility of such materials are valid, as maintaining a balance between coagulation and endothelialization is crucial for the functionality of blood-contacting devices. The strategy developed involved the treatment of ePTFE with argon plasma followed by grafting with 2-methacryloyloxyethyl phosphorylcholine (MPC) and MAA. The incorporation of integrin $\alpha 4\beta 1$-positive circulating blood cell-specific peptides, such as REDV and the original hemocompatible peptide-1 (HCP-1), enhances the surface's ability to capture circulating mononuclear cells while maintaining antiplatelet properties.

https://doi.org/10.1021/acs.chemrev.4c00996
Chem. Rev. XXXX, XXX, XXX−XXX

This dual functionality is essential for improving hemocompatibility and promoting endothelialization. The findings regarding the improved spreading and proliferation of human umbilical vein endothelial cells (HUVEC) on the modified surfaces further support the effectiveness of the poly(MPC-*co*-MAA) surface modifier. The use of an *in situ* porcine closed-circuit system for evaluating coagulation and endothelialization processes over 18 hours is a robust method to assess the performance of their biomaterial in a more physiologically relevant context.[220]

The exploration of hierarchical structures inspired by the lotus leaf for self-cleaning surfaces is innovative. The development of a biomimetic structure with PVDF microfibers coated with oleic acid and ZnO nanowires, achieving superhydrophobicity with a water contact angle greater than 150°, demonstrates significant potential for various applications. The self-cleaning properties, along with water resistance and permeability to air and water vapor, could indeed expand the utility of these materials in medical devices, surgical implants, and other fields. Overall, the research presents a comprehensive approach to enhancing the hemocompatibility of ePTFE while also exploring novel surface properties that could lead to broader applications in biomaterials.[221]

The physical and chemical property changes of two types of partially cross-linked PTFE (designated as XF1B) and fully cross-linked PTFE (designated as XF2) subjected to Co-60 γ-ray treatment were investigated. The results indicated that XF1B experienced a reduction in tensile breaking strength at an irradiation dose of 1 kGy, whereas the tensile breaking strength of XF2 decreases only at a significantly higher dose of 50 kGy. X-ray diffraction analysis revealed an increase in the intensity of the (004) peak for XF1B following irradiation, although this increase was not directly proportional to the irradiation doses. In contrast, no increase in peak intensity was observed for XF2, suggesting that irradiation-induced crystallization occurred in XF1B, while structural changes in XF2 were minimal. Raman spectroscopy further demonstrated an increase in spectral intensity for XF1B with higher irradiation doses, while XF2 exhibited no significant changes in spectral intensity. This suggests that XF1B may have been broken down into its constituent subunits. Overall, the cross-linked PTFEs studied did not exhibit significant differences in mechanical or chemical proper ties compared to non-cross-linked PTFE reported in previous studies. Consequently, fully cross-linked PTFE is anticipated to be a promising material for medical applications involving sterilization through irradiation.[222]

1.12. Sensors

Gu and colleagues developed a dual-network (DN) conductive hydrogel designed for flexible sensors, utilizing a combination of sodium alginate, poly(vinyl alcohol), *acacia mangium* tannin, and carbon nanotubes (SA-PBA/PVA/AMT/CNTs). This innovative material demonstrated remarkable properties, including an impressive stretchability of 717%, excellent biocompatibility, and a self-healing capability of 99.67%. Additionally, it exhibited strong antibacterial characteristics and significant sensitivity, with a gauge factor of 8.89 within a strain range of 250−525%. The presence of tannins, specifically catechol and pyrogallol structures, contributed to the effective adhesion of the hydrogel to a variety of substrates, including plastic, wood, glass, PTFE, nitrile gloves, and aluminum.[223]

In this study, abdominal mesh coating of titanium or the interweaving of PVDF with PP were not found to prevent adhesion to tissue. Hybrid meshes demonstrated proper integration and an increase in mRNA levels of collagen type 1 (Col 1) in the implant area compared to Surgipro or Preclude. The reticular design of the meshes, regardless of whether they were made from PP alone, PP combined with PVDF, or PP with titanium, significantly influenced adhesion outcomes due to the inability of mesothelial cells to form a continuous monolayer over the entire mesh surface, which would otherwise protect against injury to opposing surfaces.[224]

Research indicated that the use of PP and PVDF meshes does not necessarily lead to uniform outcomes. Co-staining observations were not limited to a specific polymer; both polypropylene and polyvinylidene fluoride fibers exhibited coexpression, albeit at varying rates. The ongoing variability in these cells, without a corresponding reduction in their functional differentiation into mature cell types, may contribute to inadequate healing at the mesh interfaces.[225]

These researchers present innovative polycatecholamine coatings derived from the oxidative polymerization of L-tyrosine, L-phenylalanine, and 2-phenylethylamine, inspired by mussel adhesive chemistry. The thickness, roughness, and stability of the polycatecholamine coatings were found to depend on the chemical structure of the oxidized phenylamine. Researchers optimized the reaction parameters and compared the properties of these coatings to those obtained from polydopamine (Scheme 15) and applied them to various materials used in implantable medical devices, such as polyurethane, PDMS, PTFE, and stainless steel. The coating process significantly increased the hydrophilicity of the surfaces, reducing the water contact angle by approximately 50% to 80% for PTFE and polyurethane, respectively. *In vitro* studies demonstrated excellent hemocompatibility of their coatings and a marked enhancement in the adhesion and proliferation of human umbilical vein endothelial cells. After 14 days of culture, the cell layer remained continuous and defect-free for both PTFE and polyurethane indicating that even less stable coatings made from phenylamines with carboxyl groups (PTYR, PFA) are effective for modifying materials used in tissue engineering. The rapid adhesion and proliferation of cells on these coatings likely prevent the polycatecholamines from being washed away from the coated surfaces. Overall, their findings suggest that the new polycatecholamine coatings hold significant promise for various biomedical applications, particularly in devices that encounter blood or tissue scaffolds, and they offer a cost-effective alternative to the commonly used polydopamine.[226]

Researchers have validated the hypothesis that PDA can be effectively utilized in systems designed to create polymer patterns that facilitate smooth muscle cell (SMC) adhesion and growth. The benefits of a 3D-printed microfluidic micropattern device, combined with the properties of PDA to enhance cell adhesion, can be leveraged for the patterned growth of SMCs on specific materials used in tissue engineering and regenerative medicine. The study focused on the development of PDA patterns on various materials, specifically PTFE, poly(L-lactic acid-*co*-D,L-lactic acid) (PLA), and poly(lactic acid-co-glycolic acid) (PLGA). The researchers covalently attached the Val-Ala-Pro-Gly (VAPG) peptide to these PDA patterns to enhance the adhesion of smooth muscle cells (SMCs). The results demonstrated that the PDA patterns facilitated selective adhesion of mouse

https://doi.org/10.1021/acs.chemrev.4c00996
Chem. Rev. XXXX, XXX, XXX−XXX

fibroblasts and human SMCs within just 30 min of *in vitro* cultivation. After a 7-day culture period, SMCs proliferated exclusively along the PDA patterns on PTFE, while on PLA and PLGA, cell growth occurred uniformly across the entire surface, indicating that these materials did not benefit from the patterning. However, further research is needed to assess the applicability of their system for the patterned growth of other cell types that naturally form aligned tissues, such as nerve cells.[227]

In this study, this research group developed an artificial catheter incorporating cinnamon essential oil, a known antibacterial agent, into polycaprolactone (PCL), a biocompatible polymer. This addition aims to prevent the accumulation of foreign substances and the formation of biosludge, which is a primary cause of ureteral stricture. Additionally, researchers coated the PCL layer with PVDF, a piezoelectric polymer, ensuring that the PVDF layer is in contact with the ureter muscle. When stimulated by bodily fluid flow or muscle movement, the piezoelectric properties of PVDF generate an electric current, which may help stimulate and treat malignant tumors in the ureter. The artificial conduit developed in this study is anticipated to be applicable not only to the ureter but also to blood vessels and various tissues throughout the body.[228]

The researchers focused on achieving hydrophilic functional PVDF polymer coatings using the one-step matrix-assisted pulsed evaporation (MAPLE) method for the first time. Researchers evaluated the necessity of postdeposition thermal treatment and analyzed the preliminary capacity of these coatings to support the survival of MC3T3-E1 preosteoblast cells. Given that osteoblasts prefer rough surfaces, researchers investigated MAPLE deposition parameters to create coatings with roughness ranging from tens to hundreds of nanometers while preserving the chemical properties of the original material. *In vitro* studies indicated that all surfaces supported the survival of viable osteoblasts with active metabolism, similar to the control sample, and showed no significant differences between thermally treated and untreated materials. This finding suggests that a secondary step for obtaining hydrophilic PVDF coatings is unnecessary. The physical and chemical characteristics of the films, along with the *in vitro* analyses, indicate that MAPLE is a suitable technique for fabricating PVDF thin films for future biomedical applications. Overall, these results suggest that the new PVDF coating materials hold promise as candidates for bone tissue engineering applications.[229]

One therapeutic approach is deep brain stimulation (DBS), which is an effective treatment for motor disorders in patients with Parkinson's disease (PD). This therapy involves implanting electrodes into the subthalamic nucleus (STN). However, there remains a need to optimize these electrodes. Plasma-synthesized polypyrrole doped with iodine (PPPy/I) has been identified as a biocompatible and anti-inflammatory biomaterial that promotes nervous system regeneration. The objective of this study was to develop and characterize a PPPy/I-coated electrode for implantation into the STN. For the design and fabrication of deep stimulation electrodes, researchers utilized a stainless steel microwire with a diameter of 76.2 μm, coated with a 63.5 μm thick layer of Fluon-Perfluoroalkoxy (PFA) insulation. In this article, researchers successfully developed PPPy/I coatings for intracranial electrodes aimed at enhancing the acquisition of electrical signals, particularly from the STN. Their findings demonstrated that, despite its primarily insulating nature, researchers were able to create a protective layer of adequate thickness that safeguarded the electrode while allowing electric current to pass through at its tip.[230]

The most popular version of mathematical modeling of the relaxation properties of textile elastomers used in implantology is given above in Table 7, along with the important parameters for a qualitative assessment of the material relaxation properties.[231]

Table 7. Relaxation Parameters of Textile Threads-Bases for Preparing Textile Elastomers Used in Implantology (Average Relation Time)[a]

Thread type	E_0, GPa	E_∞, GPa	$A_{n\varepsilon}$	$\bar{\tau}$, s
Polyacrylonitrile thread	7	1.3	2.7	540
Polyester thread	8	1.2	2.9	520
Polypropylene thread	7.5	1.4	3.1	490
Poly(vinylidene fluoride) thread	6.4	1.1	3	510
Nylon thread	9	1.3	3.4	590

[a]Copyright 2023, reproduced with permission from Springer.

Flexible pressure sensors are desirable due to their ability to be used in wearable electronics for healthcare monitoring, human-machine interfaces, and medical diagnostics. In these sensors external compressive force is converted into an electrical signal. Flexible capacitive pressure sensors (FCPS) are extremely sensitive, fast, and display low hysteresis and typically consist of 2 thin, flexible, parallel electrodes with a dielectric layer such as PVDF. Researchers created a device consisting of 2 PDMS-Au electrodes with surface convex microarrays synthesized by colloidal self-assembly separated by an ultrathin spin-coated PVDF dielectric layer. PVDF was sandwiched between 2 PDMS surface convex microarrays to make a flexible pressure sensor which was found to display ultrahigh sensitivities of 30.2 kPa^{-1} with a detection limit of 0.7 Pa, response time of 25 ms, and stability up to 100,000 cycles under 15 Pa pressure. Biological signals can be successfully monitored in humans and robot hand movement, with the sensor successfully detecting breathing, pulse, human voice, elbow-bending, leg-bending, and pressure distribution. A robot hand grabbing objects was also analyzed, with the electrical signals recorded correspond directly to the force applied, with the example of a sponge showing gradual increase of force during the gripping action due to the easy deformation of the surface and lightweight.[232]

Typical electrospinning of PVDF takes place at 10 cm from the collecting plate and requires hundreds of thousands of volts, resulting in a random spraying of fibers and a weakened piezoelectric effect. Near-field electrospinning uses lower voltage (600 V) and shortens the distance between the needle and collecting plate to 500 μm, producing good piezoelectric fibers (50−500 μm) with good order. A graphene nanoparticle-doped PVDF piezoelectric fiber sensor was fabricated using near-field electrospinning technology and applied voltage, drum speed range, electrode gap, and graphene doping ratios were examined. The materials increased in conductivity when doped with graphene from 19.6 $\mu S\ cm^{-1}$ (pure PVDF) to 115.8 $\mu S\ cm^{-1}$ (11 wt % graphene doping), with larger amounts of graphene correlating to greater conductivity. The material was found to deliver a maximum output voltage of 4.56 V at 5 wt % graphene doping, 11.54 times more than pure PVDF sensors. The sensor was also

https://doi.org/10.1021/acs.chemrev.4c00996
Chem. Rev. XXXX, XXX, XXX−XXX

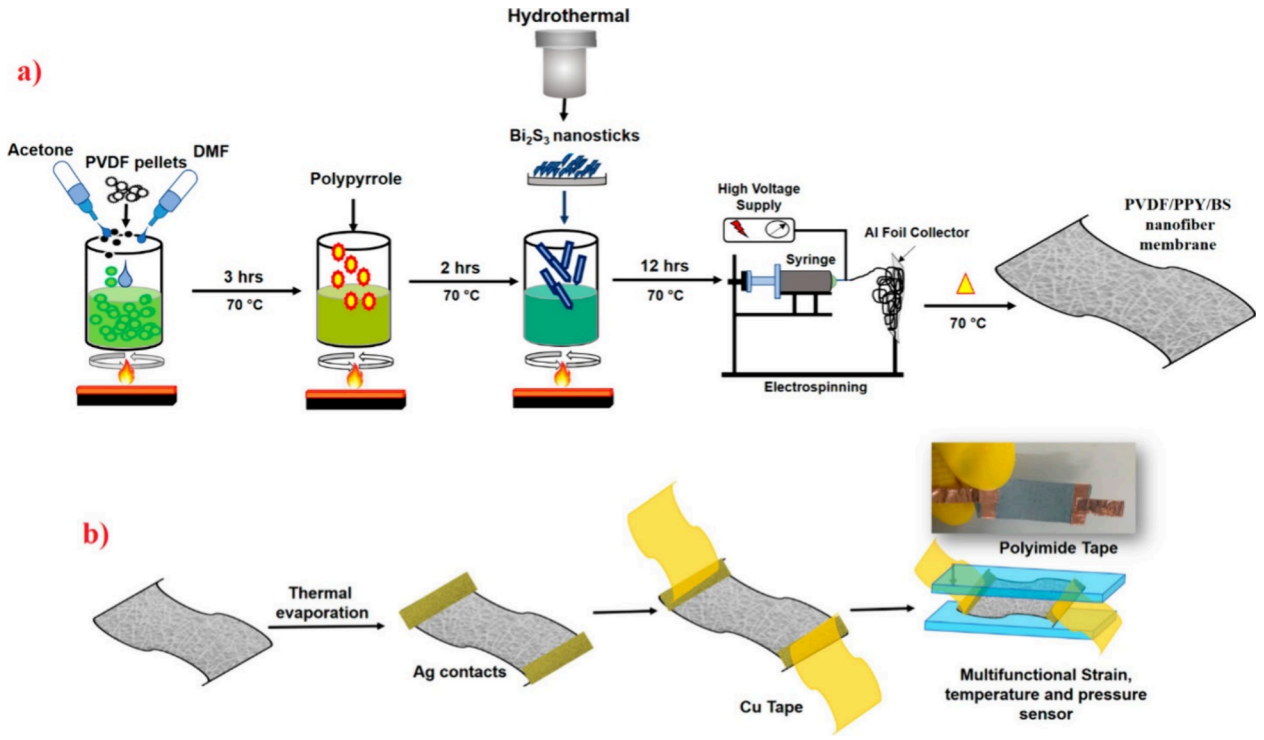

Figure 60. (a) Synthesis of Bi_2S_3-embeeded PVDF−PPy nanofiber composite through hydrothermal mixing and spin coating, and (b) fabrication of the sensor device. Reproduced with permission from ref (238). Copyright 2020 American Chemical Society.

found to show outputs for human activity such as saliva-swallowing, wrist extension/flexion (0.84 V), standing/sitting (1.6 V), speaking (0.2−0.4 V), and drinking water and eating food (0.5−1.0 V). This indicates the material can function as a wearable sensor for diagnostics and medical treatment with relatively low-cost starting materials and facile fabrication techniques.[233]

Researchers developed a facemask-based sensor system utilizing TENG technology, with the goal of developing a sensing platform that can collect a large amount of respiratory information through continuous tracking to determine early onset symptoms of COVID-19 and other respiratory diseases. The RS-TENG is constructed from a conductive cloth tape sandwiched between an FEP film and Al foil, covered in acrylic, and housed in a facemask. Upon breathing in, the FEP film and Al foil come close together, generating charge on the surface due to triboelectric effect, with exhalation allowing the films to separate and induce a potential difference between the Al and conductive cloth tape to generate electric current through breathing. The respiratory-sensing TENG (RS-TENG) has a maximal output voltage of 8 V and maximal output current of 0.8 μA. The material was connected to an apnea alarm system to demonstrate broader scope of application in respiratory monitoring. Weak breathing exhibits a potential of about 1 V, whereas normal breathing sits around 1.4 V. Moderate breathing gives an output of 1.6 V, and high-intensity breathing gives an output of 4 V. Mouth breathing increases the output voltage, with weak breathing giving 1.5 V, normal breathing around 4.5 V, moderate intensity around 6 V, and high intensity a maximum of 8 V. The device was further demonstrated to have a stable output for up to 20 min and produces no current for wind speed up to 0.945 m/s, indicating suitability for outside use.[234]

Power outages can present an extremely dangerous situation for those with disabilities and elderly patients, potentially resulting in death or injury. Self-powered wearable sensors that could transmit emergency requests via satellite would be extremely helpful to medical personnel and potentially reduce the risk of life-threatening scenarios. The researchers developed a single-electrode triboelectric nanogenerator (SETENG) operated by a graphene oxide-cuprite ion [GO-Cu(II)] laser-engraved electret coated on PTFE. The electret, a negative triboelectric material in contact with a conductive GO-Cu(II) electrode, can attain self-power if in contact with a positive triboelectric silk-Mg(II)−Ca(II) material. This SETENG is capable of a peak power density of 41 μW cm^{-2} and high current density of 1.52 μA cm^{-2} when under a load of 20 N. When integrated with a voltage multiplier circuit (VMC), the sensor can increase charge accumulation to capacitors, reaching 0.32 mC m^{-2} in a few minutes. The material demonstrates high sensitivity of 1.5 kPa^{-1} under 2.2 kPa of force, and has an overall detection limit of 1.9 Pa. Fast response times of 25.8 ms are possible, and the sensor exhibits durability up to 17,500 cycles. A pressure of 10 kPa induces a current of 5.5 μA kPa^{-1}, and the SETENG was able to harvest energy to power several LEDs. The material can be powered via finger pressure and send signals to a satellite, demonstrating capability as an emergency self-powered sensor. Using human finger skin as a positive triboelectric layer, letters were laser engraved into the device to create a "password" that if pressed would send requests to urgent care to a satellite.[235]

Particle detection is desirable in many fields, including agricultural processing, industrial processing, equipment monitoring, and medicine. A self-powered particle sensor based on a TENG device (PS-TENG) was found to be capable of differentiating and characterizing particles based on triboelectric outputs from interactions between the particles

https://doi.org/10.1021/acs.chemrev.4c00996
Chem. Rev. XXXX, XXX, XXX−XXX

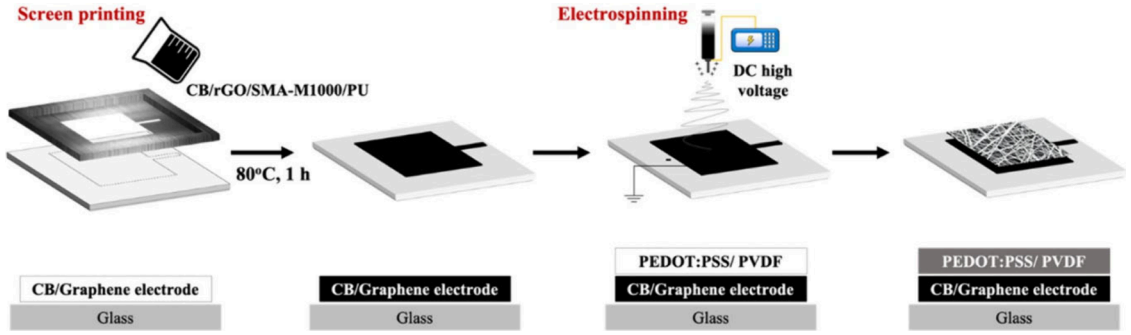

Figure 61. Fabrication of the composite sensor by screen printing and annealing the CB/graphene electrode, followed by electrospinning with PEDOT:PSS/PVDF. Reproduced with permission from ref (239). Copyright 2021 American Chemical Society.

and a PTFE surface. As particles such as carbon steel (CS) enter, the voltage increases slowly over time as the number of particles increase and charge builds up. Further, different diameter CS particles correspond to different voltages, with 0.5 mm particles giving 6.6 mV and 3 mm particles giving 155.1 mV, providing a method to monitor particle size. The charge-to-mass ratio increases as the particles get smaller in diameter, with Al particles of 3 mm diameter having a specific charge of 0.081 nC g^{-1} and 0.5 mm particles having a specific charge of 1.23 nC g^{-1}. Specific charges were found to be different for various materials of the same diameter such as Si_3N_4, SiC, ZrO_2, Al_2O_3, Nylon, and PEEK, allowing for identification of particle species. With a double-electrode PS-TENG the particle mass flow and average velocity can also be measured, resulting in sensors which can detect mass flow and do real time analysis. When coupled to an external rectifier circuit, the summative charge is found to be proportional to the mass of the particles for 3 mm and 2.5 mm diameter, allowing for real time detection of mass flow or energy storage.[236]

Enzyme-based biofuel cells (BFC) are a form of wearable power source with high power output, consisting of either wearable noninvasive devices powered by sweat, tears, and urine, or miniature needle arrays. In the case of needle-type enzyme BFC's, high ionic conductivity between the anode and cathode is required, as well as high performance of the needle itself. A needle-type biofuel cell (BFC) device that relies on glucose as an energy source was developed and tested in various fruit such as grapes, kiwi, and apples to analyze its performance. The biocathode is fabricated from hydrophobic single wall carbon nanotubes (SWCNT) and PTFE particles dropped on to carbon fibers and coated with hydrophilic CNTs and bilirubin oxidase to give a BOD/CNT/PTFE-CNT/fiber for O_2 diffusion and O_2 reduction from the air. The bioanode needle-type device was created from a carbon nanotube (CNT)/glucose oxidase/Os-based polymer/CNT composite nanofiber and found to produce a high current density of 10 mA cm^{-2} in 5 mM glucose. The energy harvesting capabilities were 55 μW, 44 μW, and 33 μW respectively, with the needle-type BFC being inserted into the fruit. The device itself has applications as a self-powered glucometer and was found to generate power from glucose in both heart tissue (16.3 μW at 0.29 V) and in the abdominal cavity (8.5 μW at 0.20 V). This material has applications in wearable, self-powered electronics that can be inserted into the body and survive based on surrounding glucose in tissue.[237]

Polypyrrole is a conductive polymer which has excellent electron transfer properties, low toxicity, and high biocompatibility. Bi_2S_3 is a n-type semiconductor with a bandgap of 1.3–1.7 eV with good carrier mobility, carrier concentration, and thermoelectric properties. Researchers developed a highly stretchable pressure sensor from electrospun 2D-Bi_2S_3-embedded piezoelectric PVDF/polypyrrole(PPy) and used to analyze arterial pulse and fast-response temperature sensing (Figure 60). The ultrasensitive material exhibits a pressure sensitivity of 1.51 kPa^{-1}, response time of 0.04 s, stability of over 5000 cycles, and a detection range of 1–55 kPa. The strain sensor was tested over the range of 3.1–61.5% and found to be stable over 5000 bending cycles, exhibited a robust gauge factor of 45.4, and a response time of 0.1 s. Testing the wearable sensor demonstrated facile detection of small hand gestures response to applied microstrains. Temperature sensing exhibits a detection range of 24–48 °C with a response time of 0.33 s and a temperature coefficient of resistance (TCR) value of −0.1117 $°C^{-1}$. The device demonstrates extreme scalability, as a clean room is not necessary for its fabrication.[238]

Electrocardiography (ECG) is a technique for diagnostics of heart conditions, electromyography (EMG) is a technique to diagnose signal transmission to muscles, and electroencephalography (EEG) is a technique for measuring weak brain signals from electrical activity on the scalp. These techniques typically utilize Ag/AgCl electrodes with a conductive gel to increase contact with the skin. Conductive gel deterioration over time causes interference with readings and makes this technique inappropriate for long-term monitoring. A nanofiber carbon electrode was developed with applications in fabrication of ECG and EMG smart wearable devices. A comb-shaped styrene-maleic anhydride and polyether-amine (SMA-M1000) copolymer facilitated the dispersion of carbon black (CB) and reduced graphene oxide (rGO) in the material, with the ratio of SMA-M100 providing tunable degree of dispersion, increased conductivity, and higher stretchability (Figure 61). The composite was mixed with polyurethane and cast on glass to form a carbon collector. PVDF was electrospun on top of the composite with PEDOT/PSS to prevent bead formation and increase both conductivity and hydrophobicity. The now fabricated electrode can be integrated into smart clothing, producing more stable and reliable readings under dynamic conditions than a standard Ag/AgCl wet electrode. The material displays high electrical conductivity with surface resistance of 2.5×10^1 ohms sq^{-1}, good mechanical durability (stable after 3000 uses), and hydrophobicity with a WCA of 146°. The electrode can monitor muscle movement and EMG signals, additionally displaying low resistance, high WCA, good electrical signal, and high durability, indicating good performance for long-term biosensing and wearable technology.[239]

https://doi.org/10.1021/acs.chemrev.4c00996
Chem. Rev. XXXX, XXX, XXX−XXX

Wearable sensors allow for noninvasive and comfortable monitoring, with fiber-shaped triboelectric nanogenerators (FS-TENGs) giving large degrees of freedom to the wearer, due to their high flexibility. Using a helical fiber strain sensor (HFSS), very small tensile strains can be monitored, and allowed for the development of a wearable, real-time respiratory monitoring system which allows for measurement of breathing parameters for disease prevention. HFSS devices change the contact between triboelectric layers of PTFE and nylon with slight stretching, causing an effective electrical signal and response to detection limits of <1%. Silver-plated nylon fibers and PTFE fibers are utilized as triboelectric materials, and the material was wound around a stretchable substrate fiber (Figure 62). The material is self-powered and

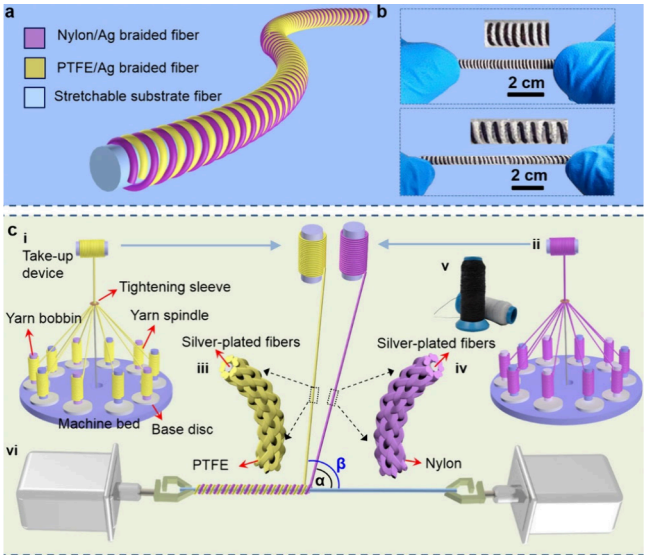

Figure 62. (a) Graphical representation of the FS-TENG incorporating Nylon and PTFE, (b) demonstration of the stretchability of the fibers, and (c) fabrication process to produce PTFE and nylon yarns and the composite FS-TENG. Reproduced with permission from ref (240). Copyright 2022 American Chemical Society.

can be used to monitor human respiration, developing a smart real-time sensor which contains a spirometer. The V_{oc} of the HFPSS in a human subject matched the results of a commercial electronic spirometer, allowing for a self-powered smart spirometer to be developed, quantifying airflow volume in an exhalation, and allowing for diagnosis of respiratory disorders based on airflow. Further, a self-powered intelligent alarm was developed, capable of triggering a mobile phone call in the event the patient stops breathing longer than 6 s.[240]

Dense semiconductor films and elastic rubbers lack air permeability, causing inconvenience and discomfort for long-term wearable sensors. Developing a sensitive, breathable, and wearable pressure sensor for patient monitoring is then required for medical monitoring in a long-term clinical setting. Textiles show inherent porosity and air permeability as well as excellent mechanical flexibility, making them an ideal platform for sensors. A sensor consisting of a PVDF/Ag nanowire nanofibrous membrane (NFM), an ethyl cellulose (EC) NFM, and two further layers of conductive fabrics (Figure 63) were fabricated. The electrospun NFMs display a hierarchically rough structure, with sensing and structure relating to electrospinning parameters. The device demonstrated wear-

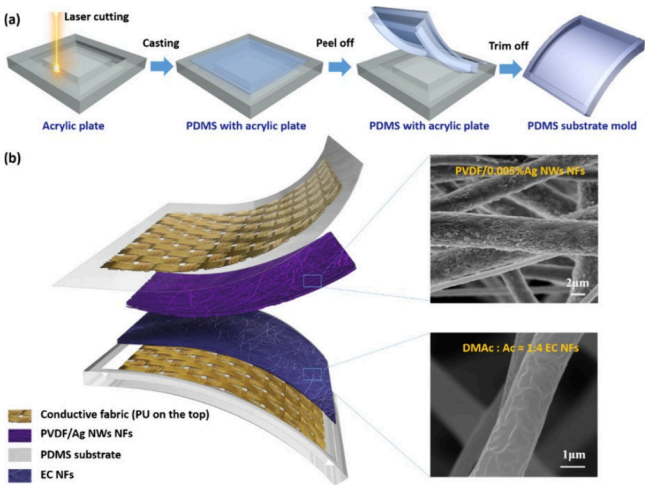

Figure 63. (a) Molding of PDMS by laser cutting of an acrylic plate and (b) fabrication of a flexible TENG-based sensor with conductive fabric, PVDF/Ag NWs NFs, PDMS, and EC NFs. Reproduced with permission from ref (241). Copyright 2019 American Chemical Society.

ability and high shape adaptability due to the rough structure on the nanofibers and further reaches a sensitivity of 1.67 V kPa^{-1} in the range of 0−3 kPa pressure, and 0.20 V kPa^{-1} in the range of 3−32 kPa pressure. After 7200 cycles the sensor still displayed excellent mechanical stability and was found to be conformable to various body parts for pulse-monitoring and motion sensing. The self-powered device can detect and quantify joint motion as well as capture pulse signals from the carotid artery. The sensor could determine joint angle based on voltage, as the angle of bending increased pressure on the sensor. Wearing the device on the carotid artery found excellent pulse estimation of a healthy subject (84 bpm), and the pulse wave was found to be able to determine radial artery augmentation index, indicating potential applications in cardiac disease evaluation. Furthermore, the device is air permeable, aiding in wearer comfort.[241]

A typical PVDF copolymer film has a longitudinal piezoelectric coefficient of −60 pm V^{-1}, much less than the longitudinal piezoelectric coefficient of inorganic materials such as Pb(Zr, Ti)O_3 (408 pm V^{-1}). Increasing the net polarization of a PVDF copolymer mixture through poling or inorganic additives increases the content of β-phase and therefore the piezoelectric effect. A group has overcome these issues by designing composite materials using a piezoelectric polymer matrix of PVDF-TrFE with 10 wt % niobium-doped Pb(Zr,Ti)O_3) filler nanoparticles (Figure 64). Trimethoxysilylpropyl methacrylate (TMSPM) functionalization of the NPs allowed for linkage between the filler and polymer matrix. High functional properties are seen due to the long-rang dipole−dipole interactions, increasing crystallinity of the material. The TMSPM linker also contributed to an increase in piezoelectric strain coefficient, good dispersion of filler particles, and increased electrical interaction between phases. This composite PENG exhibits an increased remnant polarization of 9.1 μC cm^{-2} at 100 Hz. The material exhibits a very high longitudinal piezoelectric coefficient of 101 pm V^{-1}, and a 200% greater output (9.8 V in mechanical bending) compared to typical PVDF-TrFE films and was demonstrated in a TENG device. The device successfully powered 10 red LED and displayed an

https://doi.org/10.1021/acs.chemrev.4c00996
Chem. Rev. XXXX, XXX, XXX−XXX

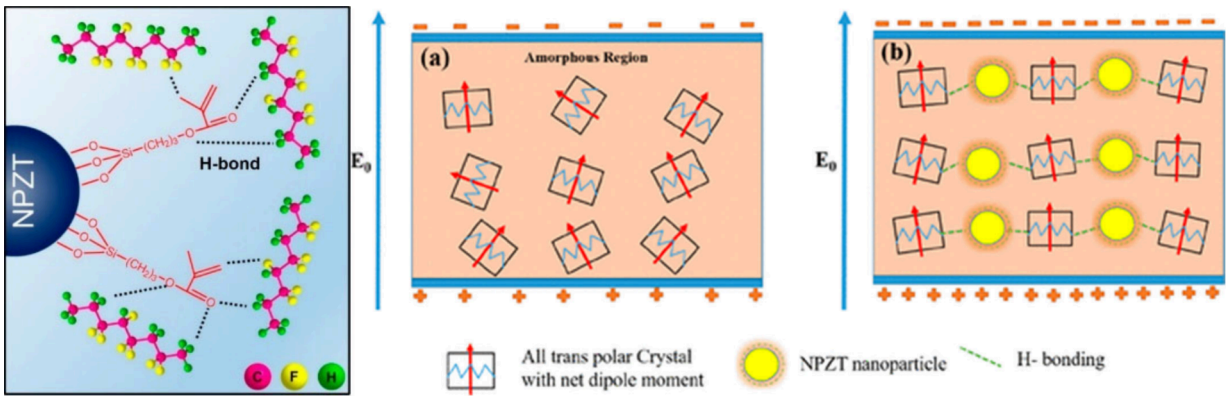

Figure 64. (a) Hydrogen bonding of methacrylate-functionalized NPZT with PVDF and (b) polarization of composite NPZT-PVDF networks through hydrogen bonding. Adapted with permission from ref (242). Copyright 2019 American Chemical Society.

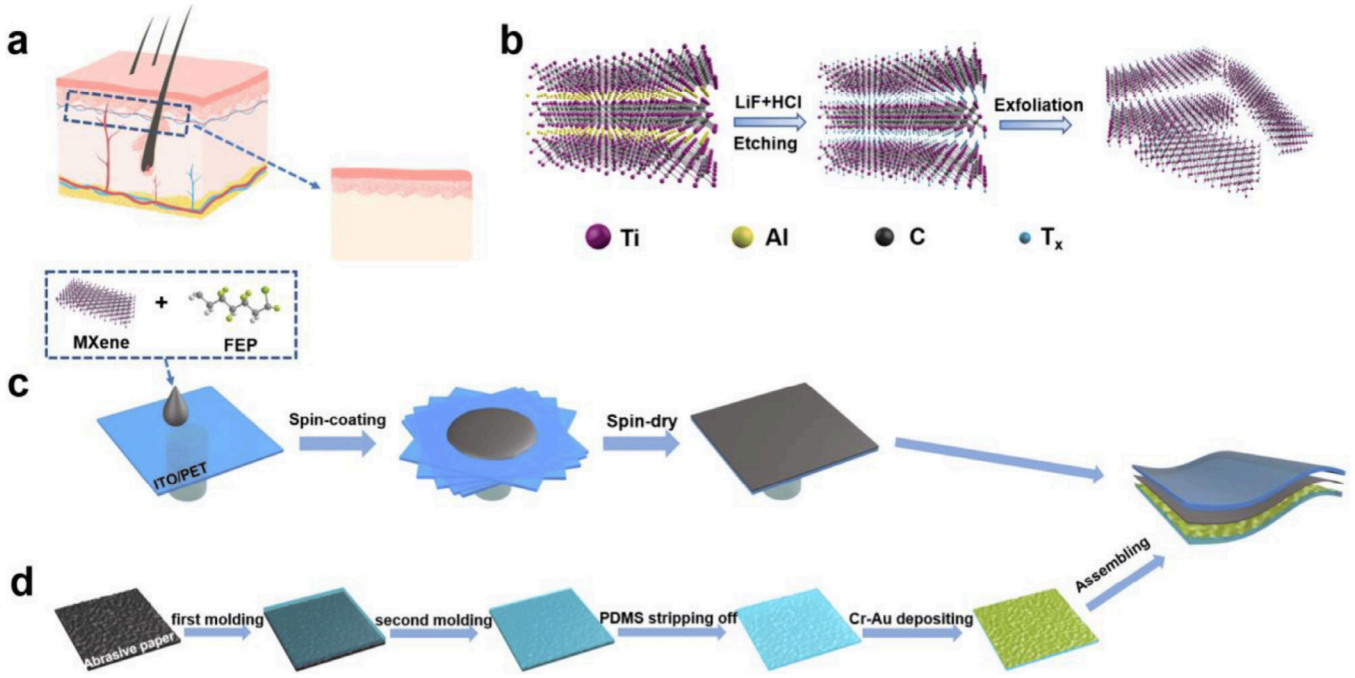

Figure 65. (a) Cross section of human skin and enlarged spinosum between the dermis and epidermis, (b) etching process to produce MXenes from Ti_3AlC_2, (c) pressure sensor MXene layer fabrication through spin coating of MXenes with FEP, followed by drying, and (d) molding of surface patterned PDMS, deposition of Cr−Au on PDMS, and fabrication of the device. Reproduced with permission from ref (243). Copyright 2021 MDPI.

average V_{oc} of 56 V, indicating good potential for applications in low powered medical devices.[242]

Electronic skins or E-skins are an attractive option for health monitoring and human-machine interfacing, giving real-time updates of physiological condition and motion sensing. Nanocomposites fabricated through the addition of fillers to the polymer matrix improve dielectric properties while retaining flexibility. MXenes, or 2D transition-metal carbide, nitride, or carbonitrides, have high electronic conductivity, large surface area, and high aspect ratios, are becoming attractive materials to make polymer nanocomposites. A research group has fabricated $Ti_3C_2T_x$-based capacitive pressure sensor with a ferroelectric polymer (P(VDF-TrFE-CFE)) nanocomposite as the dielectric layer on micro-patterned PDMS flexible electrodes micropatterned with Cr−Au constructed from abrasive paper (Figure 65). The device exhibits a low detection limit of 8.9 Pa, quick response times within 229 ms, high sensitivity with good linearity of 16.0 kPa^{-1}, and a high dielectric constant for the active layer, detecting a range of physiological signals including voice recognition, knuckle movement, and typing. The sensor can function as a keyboard and has a good correlation between pressure and keystroke logging. Airflow of different frequencies also exhibits good detection, indicating potential applications in weather forecasting. Attaching the device to the knuckle joint demonstrates different responses with increasing flexion angle, indicating applications in muscle assessments and neurological rehabilitation. The device also displays variable signals with voice monitoring, giving different patterns for words with different sounds and multiple syllables, indicating possibilities for human-machine interfacing.[243]

Cardiovascular disease can be predicted from pulse wave analysis of heart waveforms, giving real-time data on patients with pre-existing heart conditions. Normally, this uses bulky or

https://doi.org/10.1021/acs.chemrev.4c00996
Chem. Rev. XXXX, XXX, XXX−XXX

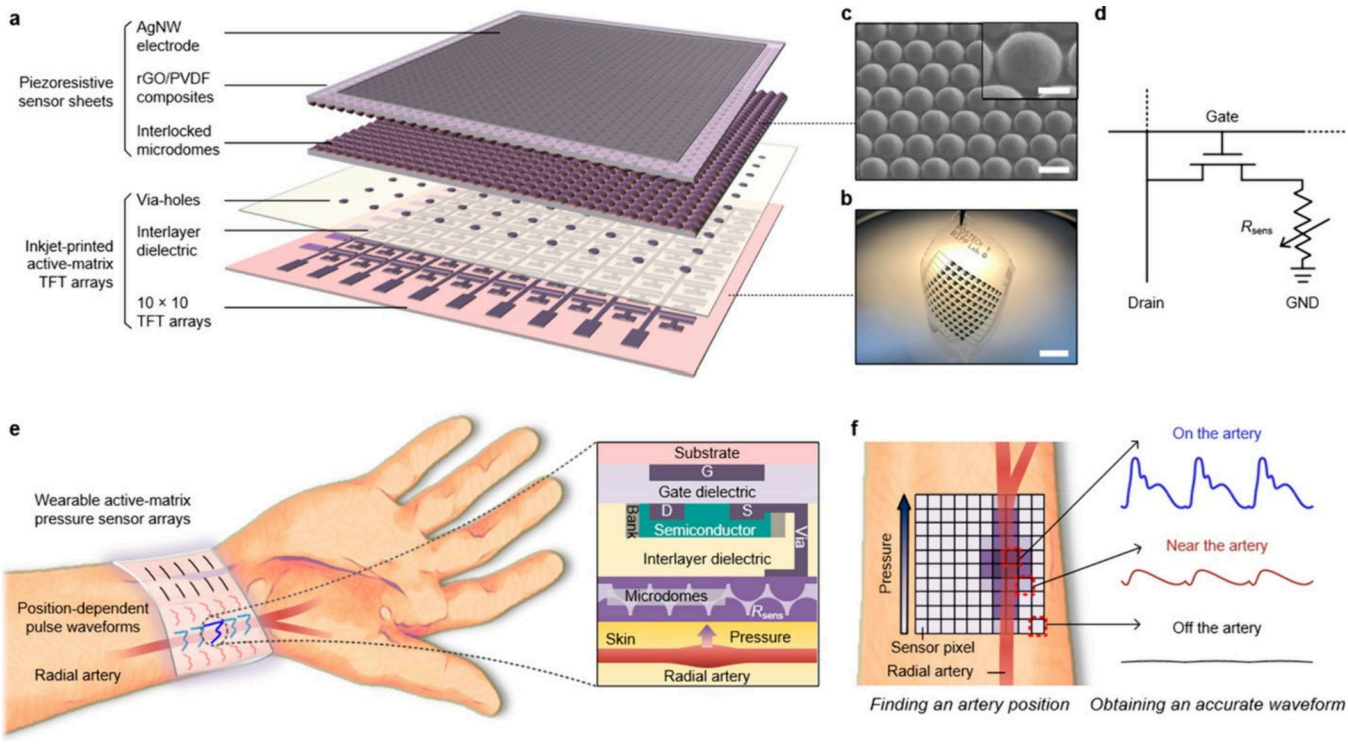

Figure 66. (a–d) Layers of piezoresistive sensor sheets and TFT arrays comprising the pulse sensor (e,f) placement of the sensor on the wrist determines artery position and pulse waveform by the TFT array. Reproduced with permission from ref (244). Copyright 2021 American Chemical Society.

rigid devices such as oscillometric or photoplethysmography devices, which make applications difficult in day-to-day life for a patient. Spatiotemporal pulse wave measurements offer an alternative, where a transistor-based sensor array can create a spatial pulse wave map which can derive arterial position from pixels very reliably. Researchers developed an active-matrix pressure sensor array to acquire accurate pulse waveforms using thin-film transistor (TFT) arrays from an inkjet printing process. The sensor is inkjet printed on ultrathin plastic foil for flexibility, and the sensor sheets comprised of rGO/PVDF composite films (Figure 66). Two microstructured films were sandwiched facing each other to facilitate an interlocked geometry and amplify pressure signals. Silver nanowire was spray coated overtop of the device as an electrode, forming 10 × 10 pixel devices. These TFTs are integrated with sensitive piezoresistive films to induce pressure sensitivity, and arterial pulse waves were successfully recorded in real-time and mapped over the radial artery to determine augmentation index, creating a position-free and wearable pulse wave monitoring device for simply pulse wave analysis. The device shows low power consumption of 10^1 nW and high-pressure sensitivity of 16.8 kPa^{-1}, making a 2D pulse pressure wave map on the wrist.[244]

A low Curie temperature (T_c) causes depolarization in poled ceramic piezoelectric sensors, however in flexible piezoelectric sensors small alterations of force cause larger polarization changes. This research group developed continuous piezoelectric films for human motion sensing based on $BaTi_{0.88}Sn_{0.12}O_3$ (BTS), which has a low T_c (close to human body temperature) and a high piezoelectric coefficient. Glass fiber fabric (GFF) composites with BTS were synthesized by impregnation of glass fibers in a solution of BTS, then annealed and spin coated with PVDF to create flexible composite films. The sensor performance is due to a low energy barrier of polarizing rotation near the T_c, inducing charge by material deformation, and as the temperature gets closer to the Curie temperature, spontaneous polarization is more likely to occur with external force. Further, the sensors are further quite robust, enduring up to 40 N of external force for 5000 cycles with little change. Various stimuli induce a response in this extremely sensitive sensor, ranging from falling water drops, finger joint motions, and turning of the head. Finger bending of 30°, 60°, and 90° produces a proportional V_{oc} of 4.4, 10.3, and 14.1 V respectively. The voltages are additionally proportional to speed of bending, giving different frequencies in the output signal, however there are limitations if the frequency is too small. Small drops of water (~500 mg) dropped from ~ 3 cm can generate an obvious voltage signal of around 1.6 V. Attaching the sensor to a balloon surface to mimic the abdomen shows detection of "breathing" by interval pressing at frequencies of ~ 0.8, ~ 1.6, and ~ 3.2 Hz, with voltage being proportional and ranging from ~ 4.6-~3.7 V. Attaching the sensor to the side of the head displays detectable motion at a frequency of 0.25–0.75 Hz turning to the left, giving a sensor output of 3 V, indicating applications in human motion monitoring.[245]

A composite piezoelectric nanogenerator (C-PNG) was synthesized from a MOF-reinforced PVDF composite nanofibrous mat. The [Cd(II)-μ-I_4] two-dimensional (2D) MOF incorporates 98% electroactive phases in the material with a high piezoelectric coefficient of 41 pC N^{-1}, mostly due to $-CH_2-/-CF_2-$ dipoles of PVDF. The MOF consists of CdI_2 and 1,5-diaminonapthalene (NAP) as an organic linker, and electrospun in a PVDF solution to create a C-PNG (Figure 67). Periodic pressure stimuli produced an open-circuit voltage of 22 V and a maximum power density of 24 $\mu W\ cm^{-2}$ with a 5

https://doi.org/10.1021/acs.chemrev.4c00996
Chem. Rev. XXXX, XXX, XXX–XXX

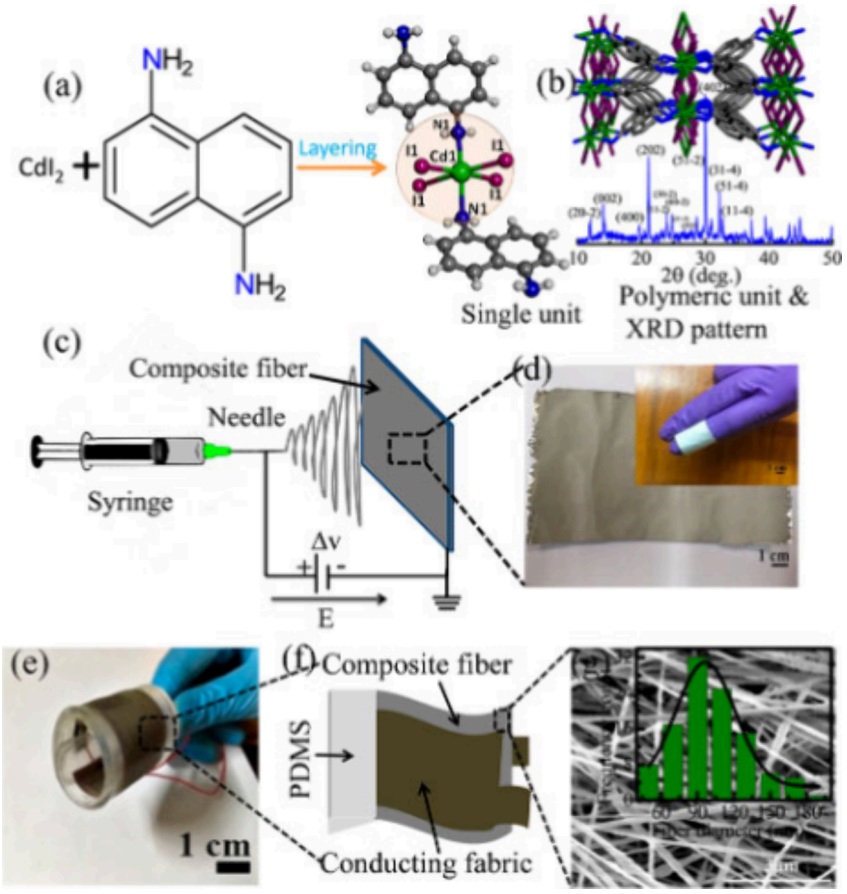

Figure 67. (a) Synthesis of the Cd 2D MOF, (b) polymeric structure and powder XRD pattern of the MOF, (c,d) electrospinning of the MOF with PVDF to fabricate the C-PNG, (e,f) demonstration of the material flexibility, and (g) FE-SEM of the nanofiber composite with a histogram showing the distribution of fiber diameter. Reproduced with permission from ref (246). Copyright 2021 American Chemical Society.

ms response time, making this a high-output material. Dynamic motion of human joints shows distinct patterns for movements such as squatting. Specific wave forms relating to the complex rolling and gliding of the knee changes the deformation site, with changes in the waveform becoming apparent throughout the movement. The material was able to monitor walking, jogging, and jumping, suggesting that the C-PNG can be implemented in shoes to analyze walking speed and gait. Attaching the device to the throat of a volunteer resulted in different waveforms for words such as "acoustic," "motion," and "naphthalene," indicating utility in speech therapy. Furthermore, the material displays effective conversion of acoustic vibration to electrical energy, with a power density of 6.25 μW and 0.95 V Pa^{-1} of acoustic sensitivity, in addition to an acoustoelectric output of 6 V under 110 dB of acoustic vibration. The material is efficient enough operate some consumer electronics such as blue LEDs from an instrumental chorus song at 110 dB, and the material can distinguish by voltage pattern between different instruments. Alphabetic characters additionally possess unique voltage patterns at 80 dB, indicating further applications in voice recognition and low-frequency noise detections.[246]

Traditional thermoelectric generators are based on solid-state semiconductors which have a limited performance due to their low Seebeck coefficients. Hydrogels have excellent physical properties and are soft, having a low elastic modulus of around 100 kPa. Human body temperature often presents an energy gradient of around 10 °C compared to the environment, giving potential applications in passive thermal energy harvesting. A flexible poly(vinyl alcohol) (PVA) gel electrolyte-based thermogalvanic generator was developed, relying on Fe^{3+}/Fe^{2+} as a redox pair that displays moderate thermoelectric performance and excellent flexibility (Figure 68). A PVDF diaphragm creates a thermal barrier, reducing the thermal conductivity and improving the Seebeck coefficient.

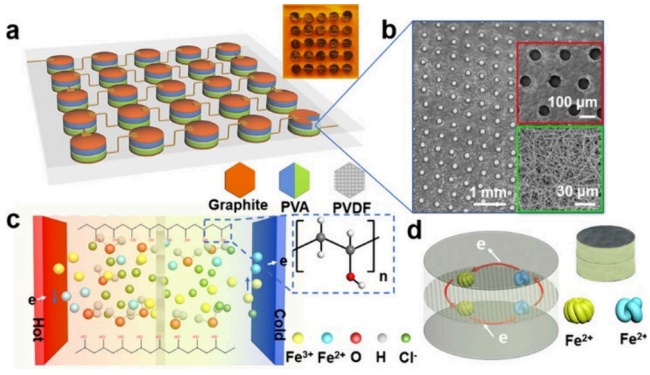

Figure 68. (a) Thermocells comprised of PVDF inserted between PVA gels and sandwiched in PI, (b) SEM image of the PVDF diaphragm, (c) diagram of the potential induced from thermal energy with various molecules present, and (d) diagram of the operation of a single thermal cell. Reproduced with permission from ref (247). Copyright 2021 American Chemical Society.

https://doi.org/10.1021/acs.chemrev.4c00996
Chem. Rev. XXXX, XXX, XXX−XXX

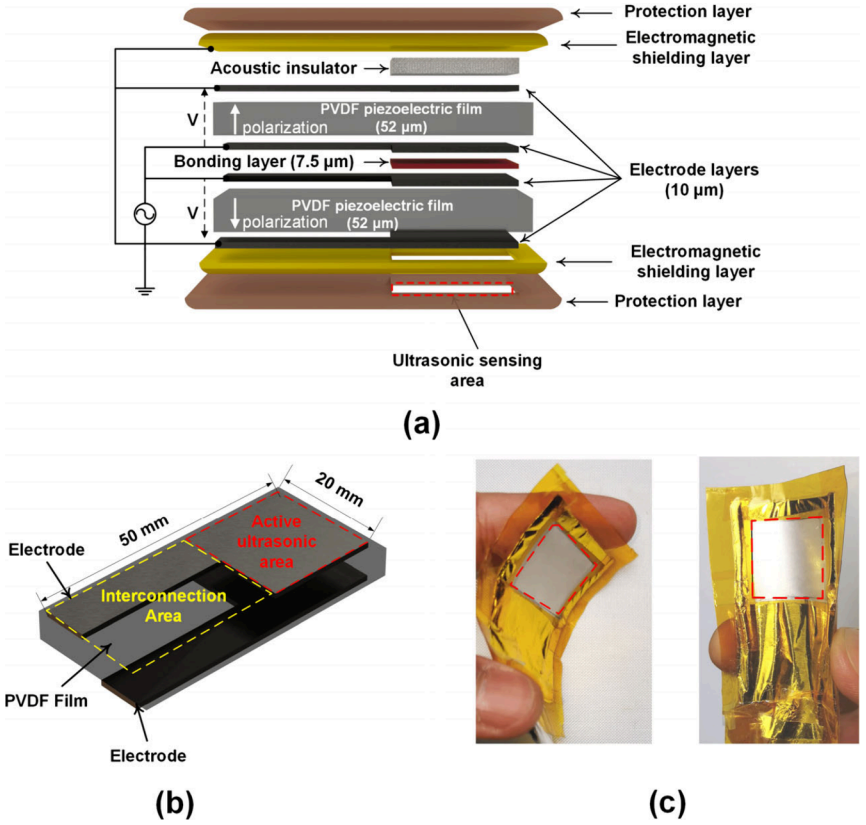

Figure 69. (a) Schematic of the wearable ultrasonic sensor (WUS) device, (b) a schematic of the PVDF film coupled with electrodes before packaging into the device, and (c) the completed WUS device. Reproduced with permission from ref (250). Copyright 2020 MDPI.

Temperature monitoring systems were affixed to the forehead of a patient, and the device self-powered through body heat. A 4 cm × 2 cm patch on the forehead, neck, and wrist results in a current of more than 60 μA, indicating good conversion capacity. The gel patch shows rapid current output, with 80% of the maximum value reached in 2 s when near the heat source proportional output to the heat source. The gel patch also presents possible cooling applications for feverish patients due to its high specific heat capacity.[247]

Wearable medical devices for respiratory monitoring are of great significance to an aging population or obese patients, who typically experience sleep quality issues due to respiratory issues. Obstructive sleep apnea syndrome (OSAS) is of high incidence in these populations and can cause death during sleeping. Researchers developed a multiarch-structure pressor sensor (MASP sensor) with a radius of 5 mm and curvature of 200 m^{-1} based on PVDF integrated into a flexible printed circuit (FPC) and found that the curvature of the sensor was a major factor in electrical output performance. The PVDF sensor was sandwiched between 2 layers of PDMS for structural integrity and to protect against sensor wear. Compared to a planar sensor, detection signal amplitude was increased by 141% and the device was found to have a high signal-to-noise ratio. The device was fabricated into a belt with the goal of respiratory monitoring. The sensor is easily wearable, does not require skin contact, and eliminates thermal interference by being away from human body heat. Movement, coughing, and speaking were found to be monitorable by the belt system as well as respiration during various activities such as sleeping, standing, and doing seated work. Various movements were found to have specific waveforms, provided the subject was calm and not in an emotionally heightened state which could interfere with the waveforms. The device can be used to develop pattern recognition for respiration, thus finding irregular patterns associated with disease.[248]

Thermoluminescence devices are important in scientific research and medicine due to their ability to absorb a dose of ionizing radiation and emit light when heated. The proportionality of the phosphor emission allows for radiation exposure to be quantified, thus allowing for devices to be fabricated for workers in fields which require ionizing radiation. Borates are often utilized as they have a tissue-equivalent absorption coefficient, high thermal stability, low cost, and low melting points. Copper-doped lithium tetraborate (LTB, Cu content 0.1%) was found to enhance the thermoluminescence properties of LTB. Mixing Cu-doped LTB with PTFE pellets in a 4:1 PTFE:LTB ratio allowed for the synthesis of crystals of 154 nm which are stronger than the base LTB phosphor, producing mechanically stable dosimeters. The resulting powder was pressed into pellets of 50 mg, 5 mm thickness, and 4 mm diameter and annealed with graphene to generate a reducing atmosphere to avoid defects from oxygen. Thermoluminescence properties were analyzed with X-ray radiation using a ^{60}Co source to attain a dose−response from 1 to 6 Gy at a rate of 17.70 μGy s^{-1}, exhibiting a linear dose-dependent fit. The minimum detectable dose for a 10 mg sample of the pellet was found to be 27 μGy, and fading studies demonstrate that 18.5% of the material fades in 1 day, and 81.1% in 40 days.[249]

Skeletal muscle analysis is of interest for the examination of the efficacy of physical training, rehabilitation, neuromuscular disease diagnostics, injury risk estimation, and prosthetic

https://doi.org/10.1021/acs.chemrev.4c00996
Chem. Rev. XXXX, XXX, XXX−XXX

device control. Ultrasound is promising for direct analysis, but most sensors are bulky and can affect the natural motion due to the size or attachment method. A wearable ultrasonic sensor (WUS) was developed based on a double layer of PVDF films, presenting a simple, low-cost, and potentially disposable device for measuring skeletal muscle contractile parameters. Two 52-μm thick PVDF films were bound together utilizing a low-viscosity epoxy resin and connected in parallel electrically and in series acoustically (Figure 69). Transmitter and receiver WUS devices were set on the opposite sides of the muscle and the time of travel between signals was measured (TOF). The piezoelectric polarization directions were set antiparallel to improve electromechanical performance. The material was used to monitor gastrocnemius (GC) muscle contractions of a human subject using electrical muscle stimulation (EMS) from 2 Hz up to 30 Hz. Thickness of contractile tissue was measured through time-of-flight in ultrasonic through-transmission mode, and the device demonstrated tissue thickness monitoring in both fused and unfused tetanic contractions. Contractile parameters such as maximum contraction thickness (T_h), contraction time (T_c), contraction velocity (V_c), sustain time (T_s), and half-relaxation (T_r) were all extracted from data on tissue thickness changes, and the tetanic progression level was assessed quantitatively using the fusion index (FI) parameter attained from the measurements.[250]

Organic−inorganic lead halide perovskites have many applications in electronic devices due to their excellent piezoelectric properties and flexible nature when combined with polymers such as PVDF and PDMS. Methylammonium tin iodide ($MASnI_3$) is known for having the highest piezoelectric effect of all organometal halide perovskites and is a promising lead-free alternative. Researchers developed an antisolvent-assisted collision technique (ACT) that can synthesize $MASnI_3$ perovskites under ambient conditions, giving a lead-free perovskite which display a high dielectric constant of 65 at 100 kHz, low-leakage current density of 7×10^{-7} A cm^{-2} at 50 kV cm^{-1}, high piezoelectric coefficient of 20.8 pm V^{-1}, and well-developed P-E hysteresis loops. The material is synthesized from an antisolvent-assisted collision technique (ACT), where the starting materials are slurried in an antisolvent at high stirring rate at ambient conditions. Thin films were fabricated by spray coating of the perovskite film on an Au/Ti coated polyimide (PI) substrate with a top electrode consisting of commercial ITO-coated PET subsequently spin coated with PDMS. Fabrication of composite PVDF-$MASnI_3$ devices with poling at 60 kV cm^{-1} increased the output voltage to $\sim$ 12.0 V and current density to $\sim$ 4.0 μA cm^{-2}, with a maximum power output of 21.6 μW cm^{-2}. The PENG can light a green LED without a storage device at 0.5 MPa at a frequency of 1 Hz and has demonstrable stability up to 90 days.[251]

Cardiac catheterization represents a portable technique for monitoring; however, it is extremely invasive and can cause tissue infections, making it nonfeasible for long-term monitoring. Most cardiovascular sensors based on pulse sensors cannot acquire multiple cardiovascular indicators, limiting the assessment of the cardiovascular system. A self-powered ultrasensitive pulse sensor (SUPS) utilizing TENG technology is fabricated for noninvasive cardiovascular monitoring. The SUPS was fabricated from a 100 μm FEP film etched with reactive ion etching (RIE) to create a nanowire array on the surface, and a polyamide (PA) nanofiber was electrospun on copper foil to act as the triboelectric layers. The short circuit current and open-circuit voltage of the device is 75 nA and 15 V, and the material has a high sensitivity of 10.29 nA kPa^{-1} from a low-pressure range of 0.3 to 1.5 kPa, indicating good suitability for pulse measurement. A 5 mg weight on the SUPS produces 0.7 nA, indicating a low detection limit, with a response time of 30 ms under periodic pressure. The material possesses high durability over 20,000 cycles at 3 kPa of pressure, with consistent 50 nA output. Unique waveform peaks are distinguishable in different arteries, and the SUPS is comparable to commercial ECG in accuracy, sitting within errors of the standard of the Association for the Advancement of Medical Instrumentation (AAMI). Indicators such as wave velocity, heart rate, and blood pressure can be monitored based on peak position differences, with blood pressure being successfully monitored using brachial-fingertip pulse transit time (PTT) comparable to a blood pressure cuff.[252]

Researchers reported a cost-effective and scalable method to produce a high-performance piezoresistive sensor incorporating a common polymeric substrate and conventional conductive components. An electrospun ionic liquid/multi-walled carbon nanotube/PVDF (IL/MWCNTs/PVDF) ternary composite was found to create a filamentous, porous conductive network with urchin-shaped beads filled with MWCNTs. This type of electrospinning increases the charge transfer channels through the MWCNTs and gives the material excellent compressibility. The resulting material is highly sensitive to pressure, with a piezoresistive sensor range from 0 Pa to 307 kPa, a maximum sensitivity of 0.075 kPa^{-1}, a low detection limit of 1.0 Pa, a fast response/recovery time of 120/80 ms, and high stability over 14,000 cyclic pressings. The ternary composite can analyze arterial pulse on a human wrist after mild exercise, displaying characteristic pulse waveforms and showing potential application in cardiovascular disease diagnosis. Attaching the composite to a facemask allowed the device to be used for respiratory analysis, monitoring a normal respiratory cycle of approximately 25 cycles/min. Human joint movement and stepping can be analyzed, swallowing and distinct sounds can be recognized, and the material can be used for keyboard recognition and array mapping of spatial pressure distribution.[253]

Most symptoms of cardiovascular disease sudden onset, giving no prior indication or symptoms. Long-term monitoring is the most conducive method of effective assessment, with flexible pressure sensors (FPS) being important for personal health monitoring. Unfortunately, these devices are difficult to fabricate conveniently or affordably. This research group utilized PTFE and Cu powder with a conductive double-sided adhesive to develop a triboelectric nanogenerator capable of high precision measurement of epidermal pulse. A conductive double-sided adhesive (CDA) was made from a conductive nonwoven substrate and conductive acrylic acid. The CDA was coated with copper powder and pressed into a film for adhesion, creating a natural graded microstructure on a 500 nm scale on the Cu powder layer, then coated with a PTFE film. The material achieved a sensitivity of 1.65 V kPA^{-1}, a response time of 17 ms, and stability up to 4500 cycles. The device gave results with good correlation to commercial devices, with a 0.9949 Pearson correlation coefficient compared to a high-precision laser vibrometer. The device could measure pulse waveforms on various parts of the body and monitor arterial pulse change in real time, with applications toward blood pressure analysis. The device

https://doi.org/10.1021/acs.chemrev.4c00996
Chem. Rev. XXXX, XXX, XXX−XXX

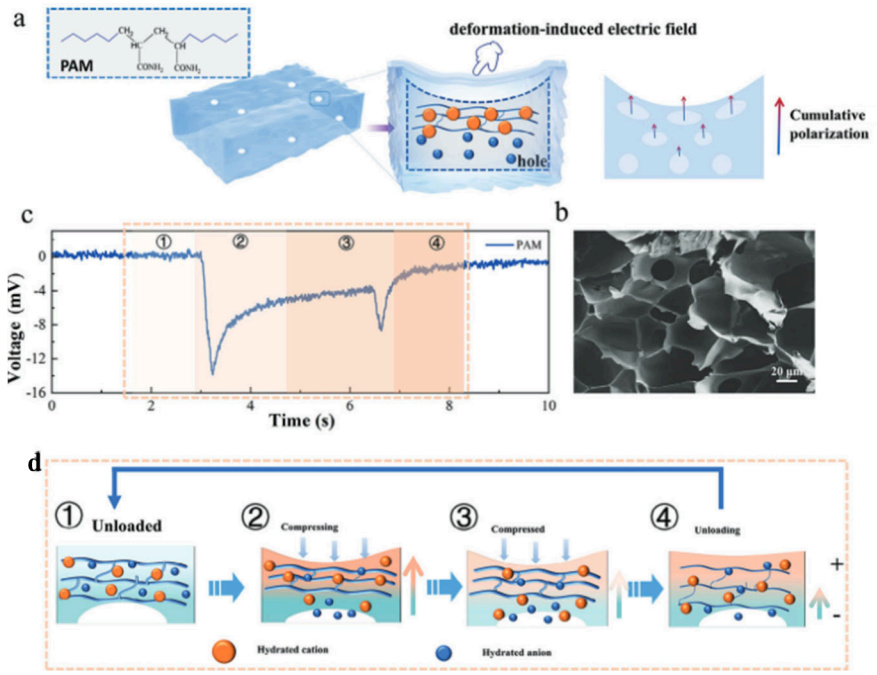

Figure 70. (a) Schematic of the PAM hydrogel and mechanism of deformation-induced electric field, (b) a SEM of the hydrogel, (c) a cycle of the piezoionic response of the hydrogel, and (d) a schematic of the piezoionic process for loading and unloading of the material. Reproduced with permission from ref (257). Copyright 2023 John Wiley & Sons Inc.

additionally can send information to a mobile phone for data processing via Bluetooth.[254]

Vibration-based sensors are extremely valuable, as they can be applied to the monitoring of machines, engines, structural health monitoring, environmental monitoring, and human-machine interactions. Vibration events range from a few kHz to over 100 kHz and consequently require broadband sensors to be practically applied. TENG-based vibrational sensors have been developed, but only work over a 0.1−10 kHz range, too low to be utilized in vibrational applications. Researchers developed a TENG-based self-powered broadband vibration sensor fabricated with a layer-powder-layer structure incorporating Ag micro powder and PTFE, optimally in a ratio of 1:10 by mass. A graphite-coated alumina ceramic sheet was fitted with an acrylic gasket, and the middle component filled with mixed PTFE and Ag micro powder, then a second graphite-coated alumina sheet was glued to the outside. The sensor vibrates under external stimuli and has a broad response range of 3−133 kHz. This offers distinct advantages over previously reported vibration sensors, with the 133 kHz frequency being 1−3 orders of magnitude higher than previously reported sensors. The material displays a good frequency resolution of 0.01 kHz, directional independence, small hysteresis, and displays real-time detection capabilities in burst vibration (breaking of pencil lead, falling steel balls), rail track fractures, automobile engine monitoring, and geological exploration. Applying force to an iron block with a hammer generates vibrational signals into various media such as soil, sand or stone. These waves exhibit differences in amplitude due to attenuation of the waves in the material, indicating it is possible to do geological surveys and analysis through vibrational analysis, with 0−1 kHz propagating faster in soil, 1−2 kHz is propagating faster in sand, and 2−3 kHz propagating faster in stone. As water content of the media increases, vibrational signal amplitude decreases, indicating potential applications in geological surveys.[255]

Flexible magnetoelectric (ME) composites are promising materials for converting ambient magnetic energy into usable power, making them a potential autonomous energy source for wearable devices. A ME-based harvesting system works by coupling a magnetostrictive material (like NiO) with a piezoelectric material. NiO−CNF (nickel oxide-carbon nanofiber) is a class of one-dimensional magnetic materials that possess favorable biocompatibility, making them suitable for biosensing and energy harvesting applications. When an applied magnetic field deforms the magnetostrictive material, it induces strain in the piezoelectric material and generates electrical potential due to the magneto-mechano-electric coupling effect. AlN (aluminum nitride) is a promising piezoelectric material due to its significant energy bandgap of 6.2 eV. Researchers prepared flexible ME composites based on PVDF-AlN (polyvinylidene fluoride-aluminum nitride) and NiO−CNF (nickel oxide - carbon nanofibers) and compared solution-casting and electrospinning as fabrication techniques. The ME coupling was confirmed by measuring the ferroelectric and magnetic properties of the composites. The ME coupling coefficient for the electrospun fibers was significantly higher at 10.6 V/cm-Oe compared to the solution-casting film-based composite at 1.3 V/cm-Oe, with measurements taken at a 1 kHz AC magnetic field under off-resonance conditions. A flexible magneto-mechano-electric (MME) generator was designed using the electrospun material. This generator harvested a sinusoidal wave, producing a peak-to-peak voltage of 9.02 V with an optimal DC power density of 97 μW m^{-2} when exposed to a weak AC magnetic field of 6 Oe at 50 Hz. The electrospun material also have potential for energy storage, successfully charging a 10 μF capacitor to an output voltage of 1.74 V in 400 s. In practical tests, the electrospun material demonstrated real-time harvesting capacity near

https://doi.org/10.1021/acs.chemrev.4c00996
Chem. Rev. XXXX, XXX, XXX−XXX

electronic devices, generating output voltages of 1.04 V near a hair dryer, 1.60 V near an electric kettle, and 3.40 V near a muffle furnace.[256]

Researchers have developed a porous, phase-blending hydrogel structure capable of generating electricity through piezoionic effects, which is particularly relevant in biorelevant applications such as tissue engineering, artificial skin, and medical treatments that require electrical regulation of physical activities. The hydrogel is based on poly(acrylamide) (PAM), and its gel skeleton is composed of amide groups and mobile ions (Na^+ and Cl^-) which generate electricity under mechanical stimulation (Figure 70). When deformed, the cations and anions migrate at different speeds, creating a nonhomogeneous charge distribution and generating a piezoionic potential. The material generates sufficient electricity to induce neural responses. Blending PAM with PVDF-HFP through solvent displacement reduces the pore size to 2−14 μm, converting the hydrogel to a p-type piezoionic material and improving piezoelectric efficacy. This enhancement preserves the high sensitivity of force-electricity generation, with voltages of up to 25 mV generated under low-frequency forces (1−5 Hz, 3 N), mimicking human touch. The hydrogel was tested in simulated bodily fluids (SBF) and through subcutaneous implantation in mice, where the piezoelectric voltages observed were consistent with those on the bench. The power density of the PVDF-HFP/PAM hydrogel ranges from 0.03 to 0.06 μW cm^{-3} across various loading conditions, higher than that of PVDF-HFP films due to the ionic currents in the hydrogel. In practical applications, the hydrogel was fixed onto the fingers of a robot palm, enabling it to differentiate between hot (∼100 °C) and ambient (∼25 °C) temperatures. Additionally, a 2 × 2 pixel sensing array was developed, where each pixel independently responded to mechanical stimuli.[257]

Traditional PCR-based NAATs require bulky, expensive equipment, limiting their use to medical laboratories. Researchers have developed a portable device for real-time monitoring of isothermal nucleic acid amplification tests (INAATs) using an electrochemical method, ideal for at-home SARS-CoV-2 testing. This device incorporates a disposable, plug-and-play pH-sensitive potentiometric sensor for label-free nucleic acid detection, known as electrochemical-INAAT (E-INAAT). The device consists of a single-chip microcomputer, a voltage amplifier, a thermostatic heating module, a Bluetooth module, and the system is powered by a lithium-ion battery. The sensor utilizes a Nafion-coated polyaniline-based working electrode, which exhibits a linear potentiometric pH response between pH 6.0 and 8.5 with a slope of −37.45 ± 1.96 mV/pH unit. The disposable sensor includes gold nanoparticles (GNP)-carbon working electrodes, a silver reference electrode, and a carbon counter electrode. The device operates by detecting pH changes during the Loop-mediated Isothermal Amplification (LAMP) reaction, which alters the pH by approximately 2.5 units in a nonbuffered solution. The sensor provides a linear, sub-Nernstian response to H^+ ions and is unaffected by common interfering ions (e.g., Cl^-, SO_4^{2-}, Na^+, K^+). Bluetooth integration allows for real-time smartphone monitoring, eliminating the risk of human error in result interpretation. When applied to SARS-CoV-2 nucleocapsid protein gene detection the E-INAAT demonstrated a sensitivity of 2 × 10^2 copies/test within 25 min, comparable to fluorescence and colorimetric assays. Unlike antigen tests which can yield false negatives due to virus concentration variability, nucleic acid amplification tests (NAATs) are more reliable for detecting the virus. Test results can be read via indicator LEDs, or a real-time curve displayed on a smartphone, making the device an efficient tool for ultrafast, portable COVID-19 testing.[258]

Polysomnography (PSG) is commonly used to assess sleep disturbances, but the discomfort of the electrodes and wires used in traditional PSG methods has led to interest in noninvasive technologies. Researchers have developed a triboelectric pressure sensor for monitoring physiological functions during sleep, which generates low-frequency mechanical vibrations that can be used to assess vital polysomnographic (PSG) parameters. The sensor is made from nonwoven TPU combined with either PVDF or aromatic hyperbranched polyester (P−Ar.HBP-2) as dielectric materials, both of which enable the device to be highly sensitive and self-powered. The sensor was created by stacking electrospun PVDF/P−Ar.HBP-2 nanofibers with TPU, with Ni−Cu coated conducting polyester electrodes and PET insulation. The sensor converts kinetic energy from physiological vibrations into electrical energy, producing output signals of 0.85 V for TPU/PVDF and 6.27 V for TPU/P−Ar.HBP-2. Respiratory monitoring was possible, giving a rate of 18 BPM (0.30 Hz) and heartbeat at 82.2 BPM (1.37 Hz), demonstrating potential for medical applications such as intelligent beds for activity monitoring in comatose patients, cardiovascular disease monitoring, and sleep apnea detection.[259]

Humidity detection on human skin has potential applications in health assessments, skin condition monitoring, and in human-machine interactions such as noncontact control of devices and virus prevention. Polyelectrolytes are typically humidity-sensitive, but often exhibit slow response times, large hysteresis, and high impedance in high humidity. MXenes offer fast response but low sensitivity and were combined with polyelectrolytes to enhance performance in this work. Researchers developed a flexible humidity sensor with high sensitivity and stability, ideal for applications in physiological activity monitoring, medical devices, and intelligent terminals. The sensor was fabricated using a composite of poly(diallyldimethylammonium chloride) (PDDA) and Ti_3C_2Tx, integrated onto 3D hollow fiber PVDF membranes through pressure filtration and immersion deposition. The resulting sensor exhibits significant impedance changes of 3 orders of magnitude between relative humidity (RH) levels of 10% and 90%, with linear sensing characteristics and low hysteresis (∼5% RH). The sensor can monitor respiration and detect subtle movements such as fingertip motions within 1 mm. The high performance is attributed to the large specific surface area and good conductivity of Ti_3C_2Tx, the sensitivity of PDDA, and the moisture transport channels in the PVDF membrane. The fabricated 3D hollow fiber membrane flexible humidity sensor (3D HFMFHS) showed a response and recovery time of 36 and 30 s, respectively. The low hysteresis and rapid response are attributed to the sensor's humidity sensing mechanism through hydrogen bonding on the sensor surface, indicating a weak and reversible interaction. The sensor was also capable of detecting respiration by generating response curves based on exhaled and inhaled gas, with peak intervals corresponding to respiration frequency during various activities. Additionally, a water droplet on an operator's finger generated a microhumid environment detectable by the sensor within a 1−6 mm range.[260]

https://doi.org/10.1021/acs.chemrev.4c00996
Chem. Rev. XXXX, XXX, XXX−XXX

Electrospinning of PVDF causes the alignment of dipoles in an electric field, leading to a transition from the α- to the β-phase. The incorporation of nanofillers, such as SiC, can increase the β-phase content up to a certain point. Inorganic salts such as $FeCl_3$ can further enhance the material by creating strong electric dipoles, with the combination of ceramic nanofillers and inorganic salt doping resulting in a synergistic effect and significantly boosting the piezoelectric output. Researchers developed composite nanofiber membranes based on PVDF and doped with SiC and $FeCl_3$. The PVDF/SiC/$FeCl_3$ composite nanofiber-based piezoelectric nanogenerator (PENG) demonstrated the best output performance, with a synergistic effect from SiC and $FeCl_3$ increasing the β-phase content and improving the piezoelectric properties. The combination of 1% SiC and 0.5% $FeCl_3$ doping resulted in a maximum current of 2.0 μA and an output voltage of 17.2 V, far exceeding the performance of pure PVDF nanofibers. The sensor demonstrated stable performance up to 5000 cycles and exhibited good moisture resistance at 80% humidity. Bending tests at 1 Hz for 200 cycles resulted in minimal performance change, indicating excellent stability. This material was applied in smart socks for gait monitoring, with potential applications in sports and medical monitoring. An array of 11 PENG units was integrated into self-powered socks for energy harvesting and pressure sensing during gait monitoring. These sensors displayed distinct patterns for walking, running, and jumping. The distribution of sensors across the feet could potentially detect gait issues, such as in-toeing or out-toeing.[261]

An intelligent insole based on flexible capacitive pressure sensors was developed for motion monitoring. The sensors are integrated into a portable microprocessor system that collects and processes data, which is then transmitted to a cloud platform via a Wi-Fi module and visualized through a WeChat mini-program. The insole's flexible substrate is made from PDMS, with nanoiron powder and PVDF as sensitizing materials. An external magnetic field is applied during the curing of PDMS to control the distribution of the iron nanoparticles, enhancing sensor sensitivity (Figure 71). The nanoiron powder particles are coated with PDMS and act as electric dipoles, aligning under the influence of the magnetic field and enhancing polarization during pressure or motion events, improving sensor performance. The insole has five pressure sensors located in key regions of the foot: the forefoot, arch, plantar, and lateral areas. These sensors are designed as sandwich structures with a PDMS dielectric layer. The system has a range of functionalities, including gait analysis, step counting, calorie expenditure calculation, and real-time movement monitoring. A fall detection mechanism is integrated into the program that sends an alert when a user falls and remains on the ground. The sensor data allows for detailed analysis of walking patterns, identifying issues like arch collapse during walking. The low power consumption and wireless capability make the smart insole an effective tool for medical monitoring, postural correction, and motion tracking.[262]

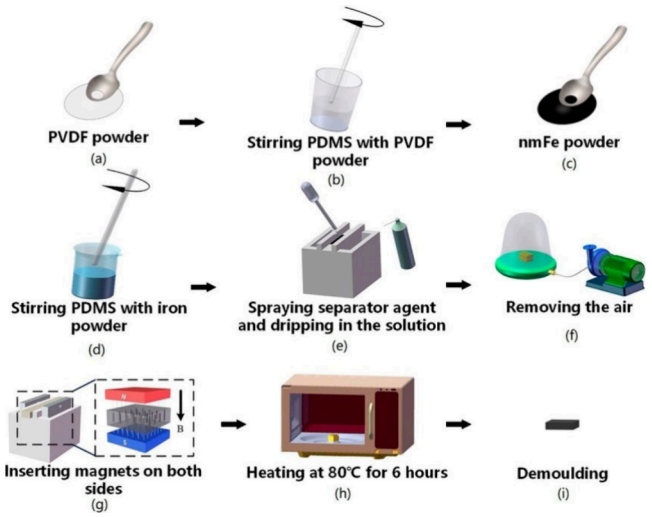

Figure 71. Schematic for the production of the insole sensor by mixing PDMS with PVDF powder and nmFe powder, then curing with an applied magnetic field to sensitize the pressure sensor to improve performance. Reproduced with permission from ref (262). Copyright 2024 AIP Publishing.

Researchers have developed a sensitive, conformal pressure sensor inspired by the kirigami structure, designed to address the issue of motion artifacts in wearable pulse sensors. Kirigami is a technique where polymer substrates are patterned with cuts to create stretchable devices. The deformations caused by these cuts govern material elasticity. While kirigami structures typically operate in the horizontal direction, researchers exploited vertical kirigami cuts to improve the device's stretchability, conformability, and ability to reduce motion artifacts. The new kirigami-inspired pressure (KIP) sensor is capable of measuring pulse waves on different artery sites under dynamic conditions, such as body movement, and provides an excellent sensitivity of 35.2 mV Pa^{-1} and stability for over 84,000 cycles. The KIP sensor was fabricated from PTFE and PET triboelectric layers, with indium tin oxide (ITO) electrodes (Figure 72). PTFE was patterned into a vertical kirigami structure and nanowires were added to improve surface roughness and increase triboelectrification, leading to higher sensitivity. The KIP sensor is lightweight, thin, transparent, and has enhanced elastic deformation capacity. The device operates over a wide frequency range of approximately 15 Hz. A wireless, cardiovascular monitoring system capable of real-time pulse analysis based on the KIP sensor was developed and the device transmitted to a mobile phone. The system demonstrate comparable accuracy as commercial medical devices, effectively eliminating motion artifacts without requiring additional hardware or complex computation, unlike traditional approaches relying on signal processing or AI. The kirigami structure significantly improves sensitivity by more than 4.9 times as the structured PTFE compresses more under pressure, resulting in higher deformation and a greater output voltage. It also successfully detects finger movements and pulse, allowing for simple heart rate calculation.[263]

Traditional analytical tools for blood conductivity are often bulky, making them unsuitable for point-of-care (POC) and remote monitoring applications. Blood electrical conductivity is primarily influenced by the concentration of electrolytes, such as sodium and chloride ions, which are essential to many physiological processes. As a result, blood conductivity serves as a valuable metric for assessing conditions like hematocrit (Hct), erythrocyte sedimentation rate (ESR), cardiac output, and even Alzheimer's disease. It can also indicate medical issues such as dehydration, electrolyte imbalances, and more complex disorders. Researchers have developed a portable, self-powered, millifluidic nanogenerator lab-on-a-chip device

https://doi.org/10.1021/acs.chemrev.4c00996
Chem. Rev. XXXX, XXX, XXX−XXX

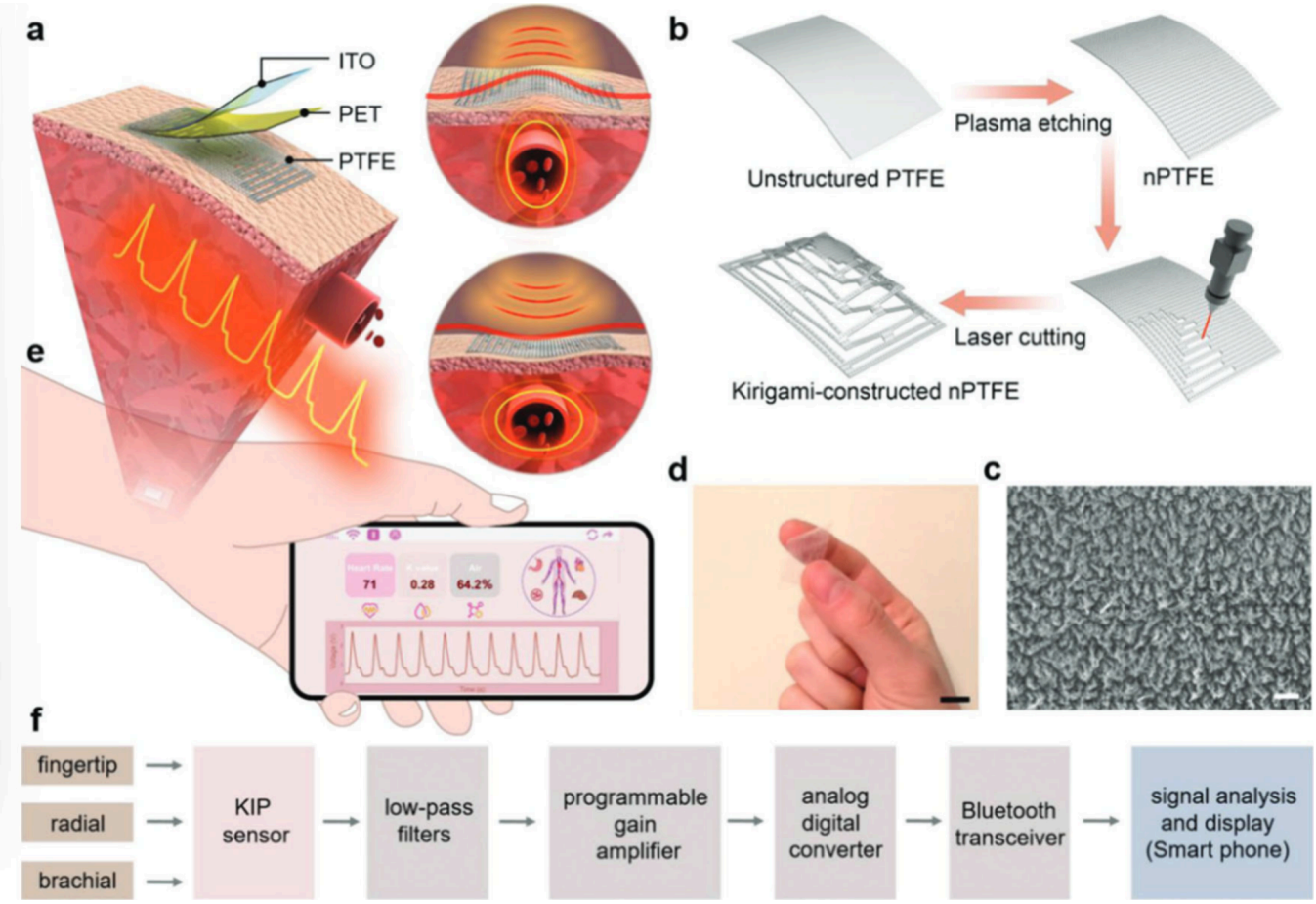

Figure 72. (a) Schematic of the wearable KIP sensor on an artery for pulse sensing, (b) schematic of the kirigami laser cutting process to make the kirigami-constructed nPTFE, (c) SEM image of the kirigami patterned sensor, (d) picture of the clear sensor, (e) pictorial representation of the device display being fed to a smart phone, and (f) flowchart describing the source of signal processed through low-pass filters, amplifiers, analog digital converters, a Bluetooth transceiver, and signal analysis/display through a smart phone. Reproduced with permission from ref (263). Copyright 2022 John Wiley & Sons Inc.

designed to measure blood conductivity at a low frequency of 1 Hz. The device consists of a sealed hollow chamber for the blood sample, a PTFE disc, copper electrodes, PMMA elements, a spring-loaded push trigger cap, and a cap shaft (Figure 73). Blood is acquired through a fingerstick lancing device, transferred into the chamber, and forms a conductive layer between two PMMA layers, enabling the TENG functionality. Blood acts as the conductive substance in the triboelectric nanogenerator (TENG) system and generates a voltage that is analyzed to determine its electrical conductivity. This self-powered device eliminates the need for embedded electronics or external electrodes, making it a simpler and more accessible tool for blood conductivity assessment. Artificial intelligence (AI) models are employed to analyze the voltage patterns and estimate blood conductivity with high accuracy. The device is portable, easy to use, disposable, and provides rapid blood conductivity measurements with only a few drops of blood, which are crucial for monitoring various health parameters. When compared to a commercial benchtop conductivity meter, the device shows promising accuracy in real-time blood conductivity measurements, making it a potential tool for efficient, on-site health assessments.[264]

Researchers developed a novel piezoelectric pressure sensor based on a composite thin film made of PVDF and ZrO_2 nanofillers to analyze finger tapping for medical applications and robotics. Nanocomposite films were fabricated by solution casting with varying ZrO_2 concentrations, and the films were sandwiched between aluminum electrodes which were then coated with flexible PET substrates. The incorporation of ZrO_2 nanofillers enhanced the piezoelectric properties of PVDF, with a 2 wt % ZrO_2 composite film demonstrating a 4-fold increase maximum output voltage compared to pure PVDF (210 mV at 0.88 kPA), and a sensitivity of 0.255 ± 0.083 kPa^{-1}. Under manual tapping the sensor recorded a maximum voltage of 115 mV, while impulsive pressure from a 38 g load resulted in 76 mV, a high pressure from a 108 g load produced 150 mV, and a low pressure from a 45 g load generated 90 mV. Efficiency measurements based on polarization-electric hysteresis loops exhibited 90% efficiency at an electric field of 5 kV/cm. The sensor exhibited a response time of approximately 1.5 ms and a recovery time of 1.8 ms, with good long-term durability and reusability, maintaining consistent performance after 8 months of periodic testing.[265]

Eye tracking analyzes visual behaviors, attentional processes, and decision-making based on gaze points and blinks, and is valuable in various fields such as medicine, commerce, and engineering. Researchers developed a transparent, flexible, and ultrapersistent electrostatic sensing interface for active eye tracking (AET) based on the electrostatic induction effect. The interface consists of a triple-layer structure consisting of a

https://doi.org/10.1021/acs.chemrev.4c00996
Chem. Rev. XXXX, XXX, XXX−XXX

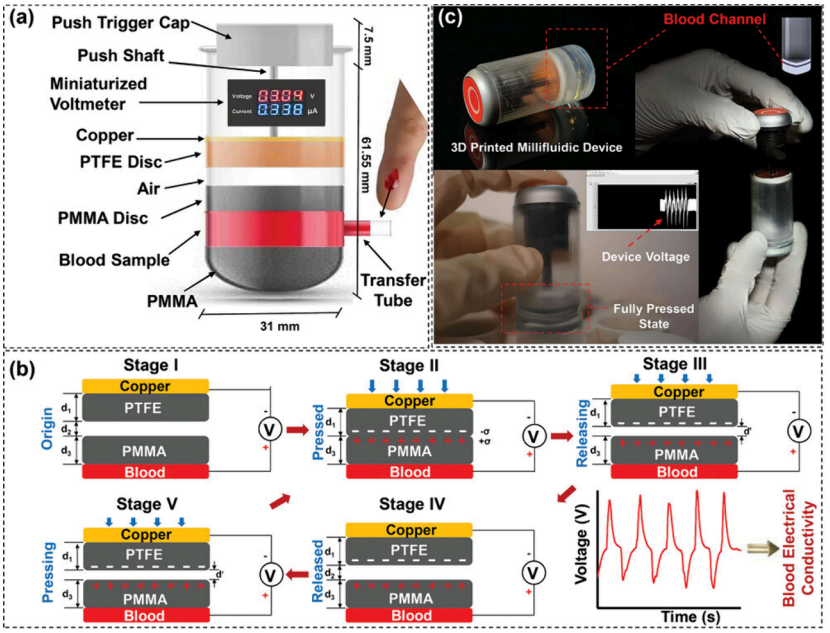

Figure 73. (a) Schematic of the hollow blood-based milifluidic device for blood conductivity measurements comprised of PTFE and copper as triboelectric layers, (b) design for the operation of the milifluidic device with the introduction of blood, and (c) the completely fabricated device and signal output from a sample. Reproduced with permission from ref (264). Copyright 2024 John Wiley & Sons Inc.

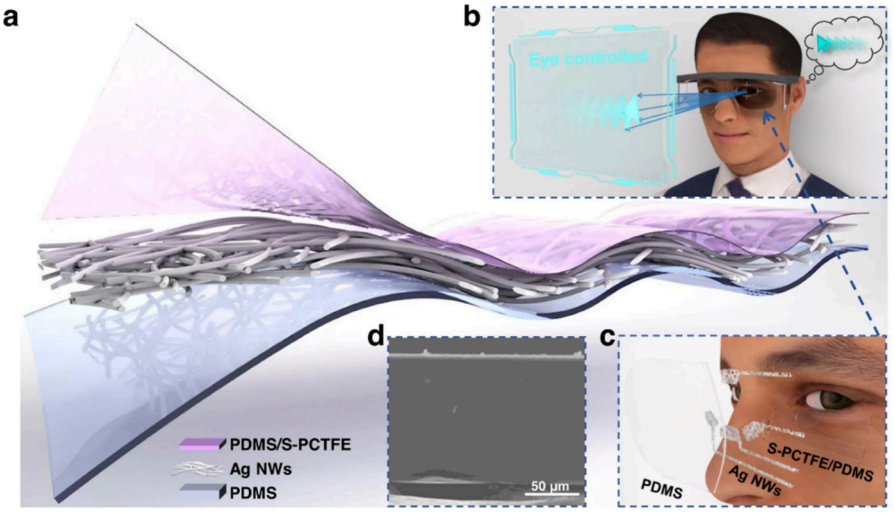

Figure 74. (a) Pictorial representation of the Ag NWs sandwiched between PDMS and PDMS/S-PCTFE as a AET system, (b,c) graphical representation of the glasses-based sensor for eye tracking and applications in monitoring eye movement relative to a screen, (d) SEM of the fabricated composite. Adapted with permission from ref (266). Copyright 2023 Nature Portfolio.,.

dielectric bilayer and a rough-surface silver nanowire (Ag NW) electrode layer, which significantly enhances the inherent capacitance and interfacial trapping density, leading to unprecedented charge storage capacity. The device is constructed from a 20 μm thick stretchable bilayer made by grafting PCTFE onto plasma-treated PDMS, with etched Ag NWs applied as electrodes (Figure 74). The electrostatic charge density of the interface reached 1671.10 μC m^{-2}, with a charge-keeping rate of 96.91% after 1000 noncontact operation cycles, allowing for noncontact eye tracking with an angular resolution of 5°. The AET system utilizes deep learning for decoding eye movements and gaze to analyze commercial preferences. The system demonstrates potential for eye-controlled computer interaction, particularly for hands-free technology, medical monitoring, and applications for ALS patients.[266]

Detecting disease and managing prognoses in infants and young children who cannot communicate their symptoms is a challenge for physicians. Continuous monitoring is a promising approach; however, children and infants are not typically compliant with uncomfortable monitoring devices. Further, pressure sensors have significant difficulties posed by infants' lighter weight and different body structure. Researchers developed a noninvasive, sheet-type PVDF pressure-sensitive sensor to monitor vital signs in sleeping infants and young children under 6 years old (Figure 75). The sensor device is made from a PVDF film as the pressure-sensitive layer and polyethylene naphthalate (PEN) films with printed silver electrodes and is less than 1 mm thick. The sensor detects

https://doi.org/10.1021/acs.chemrev.4c00996
Chem. Rev. XXXX, XXX, XXX−XXX

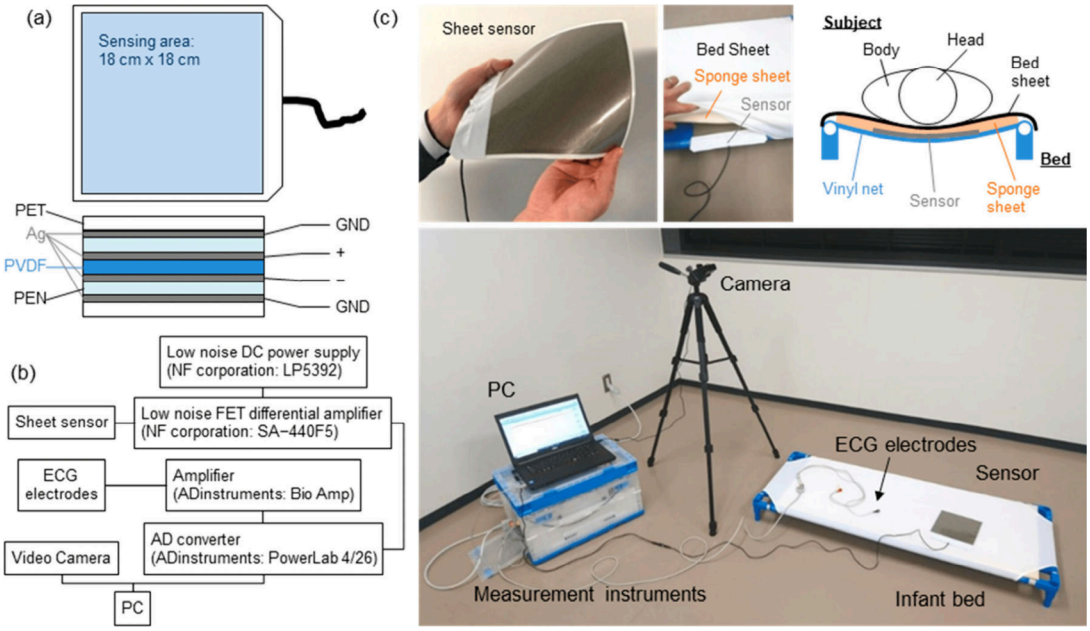

Figure 75. (a) Schematic for the fabrication of the sheet-type sensor, (b) processing system for the measurement system to attain a meaningful pulse signal, and (c) pictures of the sheet sensor and measurement setup for sleep monitoring of infants and young children. Reproduced with permission from ref (267). Copyright 2023 MDPI.

ballistocardiograms (BCG) and phonocardiograms (PCG) during sleep, with the peak-to-peak interval (PPI) from these signals indicating strong correlations with the R-to-R interval (RRI) from ECG, allowing for accurate monitoring of heart rate and other vital signs. The PVDF pressure sensor, integrated under a mattress, captures biological signals such as heartbeat and respiration through vibrations from the body. These signals are processed to separate the heart-related BCG (which reflects blood pumping into the aorta) from the higher-frequency PCG (which corresponds to heart sounds). To improve signal quality, a differential amplifier circuit was used to enhance the signal-to-noise ratio (S/N), allowing weak heartbeat waveforms to be detected in infants. The system uses specific filtering techniques to isolate BCG and PCG signals based on their distinct frequency bands. The system was validated by simultaneous ECG and sensor measurements, with results indicating that the PPI from the sensor correlates well with the RRI from the ECG. In addition, the system can monitor changes in respiration and heart rate during awakening, observing an increase in both after jerking motions in preparation for waking. This noninvasive, long-term monitoring system, enhanced by AI analysis, holds promise for infant care and can be used for elderly and young children who struggle with traditional wearable devices.[267]

Electrochromic devices (ECDs) are known for their low cost and energy efficiency, as they only require power when altering the color of the display, which makes them suitable for applications such as energy-saving windows. Researchers developed an integrated piezo-electrochromic tactile sensing display (PETSD) that combines a PVDF matrix as a pressure sensor and a polyaniline organic electrochromic device (OECD) as the display module. The device is constructed by sandwiching PVDF cast films between silver electrodes, with the upper electrode attached to a PDMS layer. Polyaniline is deposited on ITO arrays on a PET film. The PANI-ITO-PET and ITO-PDMS films serve as the upper and lower electrode plates respectively and are assembled into the PETSD system with adhesive tape and liquid electrolyte. Conductive polymers provide high discoloration efficiency and fast response times, and the system offers reliable real-time tracking of movement, such as fingertip or pen tip motion, with fast color-changing capabilitiesWhen pressure is applied by a pen, the device shows clear patterns and color differences, turning dark blue under 200 kPa of pressure and returning to light yellow once the pen is removed. Color change times are as low as 1.4 s, with a bleaching time of 1.98 s and a color contrast of 62.2% due to the memory effect of polyaniline. The PETSD system demonstrates excellent durability, retaining 94.9% of its color contrast after 1600 continuous cycles. The device operates with low power consumption, only consuming power when changing colors, making it ideal for energy-efficient applications.[268]

A hydrophobic CNT/TPU nanocomposite fibrous mat was developed using a layer-by-layer self-assembly method to create a stretchable and flexible strain sensor. The CNTs serve as the conductive layer, while polyhedral oligomeric silsequioxane (POSS) and 1*H*,1*H*,2*H*,2*H*-perfluorooctyltrimethoxysilane (FAS) form a hydrophobic layer. The fibrous mat was electrospun from TPU, then dip-coated with PDA, sonicated in a CNT suspension, followed by sonication with POSS, and then dip-coated with FAS to create the hydrophobic layer (Figure 76). The resulting CNT/F-TPU nanocomposite mat displays a water contact angle (WCA) of 159°, indicating strong hydrophobic properties, with a WCA above 145° after a wash test. Despite mechanical abrasion or twisting, the material retains its superhydrophobic characteristics. Mechanical testing reveals no hysteresis after 100 cycles at 100% strain, indicating strong self-healing ability. This nanocomposite exhibits excellent hydrophobicity and mechanical stability, with a tensile strain of 550%. The sensor exhibits excellent sensitivity, with gauge factors (GFs) of 1.6 at 0−60% strain and 2.86 at 60−100% strain, a short response time of 110 ms, and stability over 5000 testing cycles. The sensor's hydrophobic surface ensures reliable operation in diverse

https://doi.org/10.1021/acs.chemrev.4c00996
Chem. Rev. XXXX, XXX, XXX−XXX

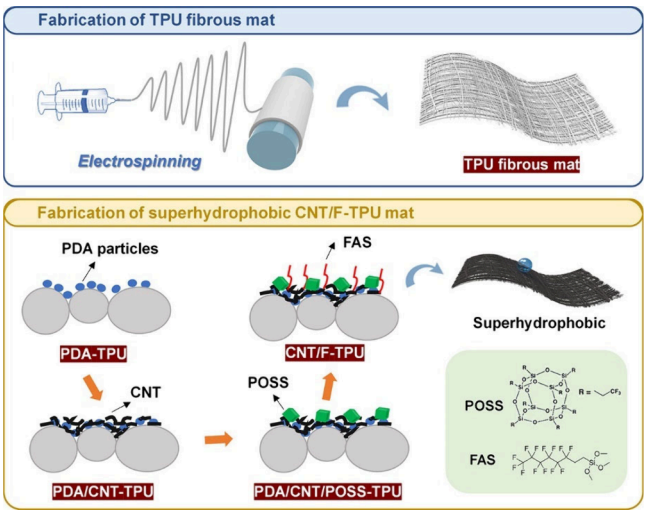

Figure 76. Fabrication process for the TPU fibrous mat by electrospinning (top) and the superhydrophobic CNT/F-TPU mat fabricated through treatment with PDA to allow adherence of CNTs, then treatment with POSS and FAS as hydrophobic layers. Reproduced with permission from ref (269). Copyright 2023 American Chemical Society.

environments, even in the presence of moisture, acids, or alkalis. The CNT/F-TPU strain sensor was tested on various body parts such as fingers, wrists, elbows, and knees. The material exhibited stable and periodic sensing signals during joint bending, with regular response curves for small deformations (0−30°). The device also effectively tracked signal patterns correlating to facial expressions like smiling, blinking, swallowing, and voice recognition.[269]

Researchers developed a series of stretchable, self-powered tactile and motion sensors for healthcare monitoring and AI applications, based on single-electrode-mode TENG. These sensors are composed of ultraelastic polyacrylamide (PAAm)/PVP/$CaCl_2$ conductive hydrogels and surface-modified silicon rubber thin films. The PAAm/PVP/$CaCl_2$ (PAC) hydrogel is created by adding acrylamide (AAm), PVP, cyclodextrin, and $CaCl_2$ with a cross-linking agent, then templated and annealed to form the hydrogel (Figure 77). PVDF nanofibers were electrospun, homogenized, and dip-coated onto a patterned silicon wafer to create either single-side or double-side thin films with microstructures. The films are then coated with silicone rubber and encapsulated in Ecoflex, with copper tape used as electrodes. These sensors demonstrated excellent sensitivity of 20.1 V N^{-1} (8.03 V kPa^{-1}) and can detect forces ranging from 0.1 to 30 N at low frequencies. The sensors can monitor human motion, such as movements of the knee, finger, wrist, neck, and voice recognition. The PAC hydrogel exhibits excellent mechanical properties, with 1241% elongation and a tensile strength at break of 141.5 kPa, while the single-side PVDF nanofiber thin film displaying an even higher elongation of 1372% and tensile strength at break of 230.5 kPa. The material maintains electrical stability over 2000 cycles at 0−100% strain at 2 Hz. The double-sided sensor produces significant voltage outputs when applied to various joints such as the neck, wrist, and knee, even from small joint movements like finger bending. Additionally, the sensor can capture dynamic voltage outputs from vocal cord vibrations, identifying specific sounds, such as the letters "S," "Z," and "U," based on their waveform patterns.[270]

1.13. Sutures (Ligaments, Dental, and Tendons)

Pelvic organ prolapse (POP) is the decent of a structure in the small pelvis from its usual location. Defects of the uterosacral ligaments (USL) cause laxity of the anterior vaginal wall, thus prolapse and potential urinary incontinence. Repair of the ligaments by cervicosacropexy (CESA) and vaginosacropexy (VASA) leads to restoration of urinary continence in 64% of cases and 69% in the case of urgency incontinence. In these procedures the USL is replaced by PVDF tape, typically through laparoscopic suturing. The biomechanical properties

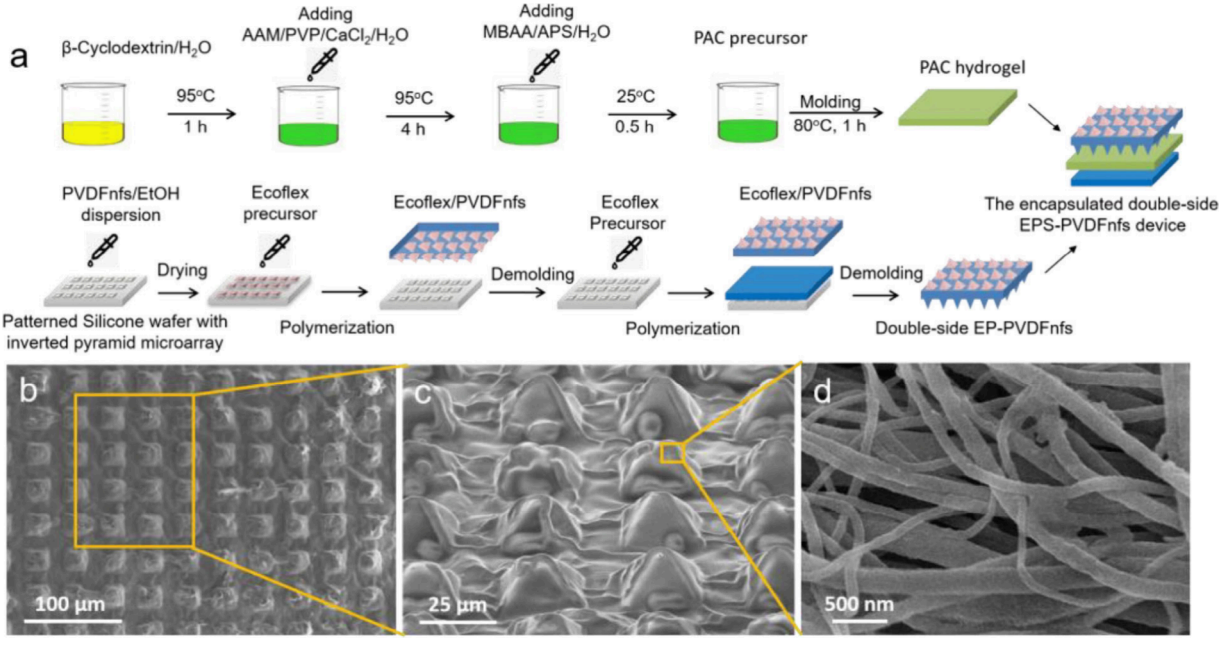

Figure 77. (a) Fabrication of EPS-PVDFnfs to make microstructured PVDF films and (b−d) SEM images of showing wrinkled micropyramid units and PVDF nanofibers of the films. Reproduced with permission from ref (270). Copyright 2023 MDPI.

https://doi.org/10.1021/acs.chemrev.4c00996
Chem. Rev. XXXX, XXX, XXX−XXX

Table 8. Suture Materials and Their Composition Used in the Study[a]

Suture Material	Composition	Degradation	Manufacturer
Silk	Natural braided	Nonabsorbable	Mersilk, Ethicon, J&J Pvt. Ltd., Mumbai, India.
Polyglactin 910	Synthetic braided	Absorbable	Vicryl, Ethicon, J&J Pvt. Ltd., Mumbai, India.
Polypropylene	Synthetic monofilament	Nonabsorbable	Prolene, Ethicon, J&J Pvt. Ltd., Germany.
Polytetrafluoroethylene	Synthetic monofilament	Nonabsorbable	Dental-A, Golnit Ltd., Kiev, Ukraine.

[a]Copyright 2022, reprinted with permission from MDPI.

of fixation tape and fixation methods were analyzed in porcine cadaver sacral spins to examine displacement at failure, maximum load, and stiffness of the fixation technique. The gold standard method consists of PVDF tape and PVDF sutures. PVDF sutures were compared to titanium tacks, a more expensive but faster method of tape affixation. Two single sutures lead to a max load of 65 ± 12 N, 3 titanium tacks in a triangle gave a maximum load of 38 ± 12 N, and 3 titanium tacks in a row gave 25 ± 10 N. While tacks are faster to install, 2 single sutures remain significantly stronger than a triangular arrangement of tacks, verifying the effectiveness of the gold-standard method. However, if tacks are used surgically, data on porcine cadavers suggests that they should be oriented in a triangle for maximum efficacy. All techniques are assumed to be more effective in live humans due to wound healing and eventual ingrowth of the mesh.[271]

Sutures in an oral environment require additional properties to ensure smooth healing, and suture selection is paramount. Most of these materials are polymers, and can be absorbable or nonabsorbable, with absorbable sutures degraded by hydrolysis or proteolytic enzymes (Table 8). Toothpastes and mouthwashes further induce another variable in suture integrity. The researchers studied 288 suture samples in 4 types of mouthwash (Avohex, Aloedent, Paradontax, and Betadine) on the mechanical properties of Vicryl (polyglactin 910), PTFE, Prolene (polypropylene), and Mersilk suture materials, with tensile load, tensile strength, and percent elongation was evaluated at 3, 7, 10, and 14 days of exposure to the types of mouthwash. Suture material was kept in artificial saliva, then exposed to the media for 2 min 2 times per day and returned to the saliva. Tensile load and strength were maintained for all materials except for Mersilk across the solutions. After 14 days of inoculation, all specimens have the highest tensile load values in Paradontax and lowest in Betadine, a value repeated in the tensile strength experiments. The percent elongation tests demonstrate difference in percent elongation depending on the media, with PTFE having a significant difference in Aloedent and Betadine, Vicryl in Betadine, and Prolene and Mersilk exhibiting differences in Aloedent and Paradontax. The faster degradation of Mersilk could be due to its natural origin, where proteolytic enzymes may be more inclined to decompose the suture. Further, it is not a polymer and is mainly composed of 70% protein fiber and 30% gum. However, Mersilk retains approximately 90% of its strength until day 7 of treatment, so it can be determined to be useful up to 7 days. However, the type of mouthwash is important and Parodontax should be used in applications with Mersilk sutures. If prolonged immobilization is required, PTFE should be used over Vicryl or Prolene, with Aloedent or Parodontax as a mouthwash. This study demonstrates that there is no standard rule in suture use across clinical settings, leaving the choice up to the type of surgery and surgeon's preference.[272]

PVDF is proposed as an alternative suture material to replace polypropylene (PP) for tendon repairs due to its superior biocompatibility and mechanical properties. Ideal tenorrhaphy should ensure ease of placement, secure knots, smooth tendon apposition, minimal gap at the repair site, and sufficient strength for postoperative activity. Barbed knotless sutures (Figure 78) offer advantages by reducing cross-sectional area and distributing stress evenly, facilitating healing. The FDA has approved barbed sutures made from nylon, polydioxanone (PDA), and polypropylene, but PVDF remains unexplored for human tendon repair. The higher tensile strength of PVDF (related to its 59% crystallinity compared to 43% for PP) and superior creep resistance contribute to its potential as a preferred suture material, especially as PVDF sutures lose only 7.5% of tensile strength after 9 years in hydrolytic conditions compared to 46.6% for PP. This study compared size 2−0 PVDF and PP bidirectional barbed sutures in patellar tendon repairs using 60 porcine samples. The ultimate tensile force was significantly higher for PVDF sutures (22.4 ± 2.1 N) compared to PP (14.0 ± 1.7 N), showing a 60% improvement. Additionally, the maximum pullout force for PVDF was 35% greater (70.8 ± 7.8 N) than that of PP (52.4 ± 5.8 N), translating to an increase of 8.4 N in ultimate tensile strength and 18.4 N in tendon suture pullout strength. Both sutures demonstrated similar force requirements to create a 2 mm gap, indicating repair failure, with PVDF requiring 29.2 ± 5.0 N and PP requiring 25.6 ± 3.1 N. Notably, both barbed sutures exceeded the force thresholds for nonbarbed sutures of the same size, suggesting enhanced anchoring performance with barbed sutures.[273]

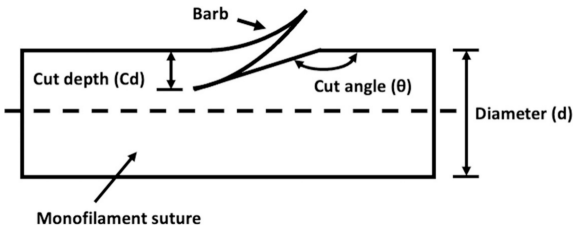

Figure 78. Schematic representation of a monofilament suture with cut barbs to improve anchoring performance. Reproduced with permission from ref (273). Copyright 2022 John Wiley & Sons, Inc.

1.14. Tissue and Bone Engineering

Ionic polymer−metal composites (IPMCs) are flexible, lightweight, and quiet electro-active polymers (EAPs) seeing use in dynamic sensors, artificial muscles, micro robotic actuators, and medical applications. IPMCs display large bending displacement for low voltage input and often display biocompatibility. Subjecting an IPMC to an electrical potential causes water molecules to migrate toward the cathode, causing bending deflection. Typically, low blocking forces prevent IPMCs from industrial applications, though research has been moving toward higher blocking forces with low input voltage. IPMCs usually use platinum, gold, palladium, or silver as

https://doi.org/10.1021/acs.chemrev.4c00996
Chem. Rev. XXXX, XXX, XXX−XXX

electrodes, making these devices expensive. Multilayered IPMC actuators show larger actuation force at the same thickness of a single layer IPMC when stimulated. Researchers used electroless plating to fabricate an Ag-IPMC by pretreating a Nafion-117 membrane with NaOH, sorbing silver nitrate to the surface, and reduction with glucose to fabricate the IPMC device. An IPMC was designed using the Taguchi orthogonal array method to design an Ag-IPMC actuator to produce a maximal bending response, exhibiting an increase of 30% response in the optimized conditions compared to a normal single-layer IPMC actuator. These IPMCs have potential applications in small scale robotics.[274]

In this study, a high specific surface area was achieved by directionally roughening the Nafion surface. Pd/Pt composite electrodes were then deposited on the Nafion matrix using isopropanol-assisted electroless plating, improving the electromechanical properties of the IPMC. The resulting IPMC demonstrated impressive actuation performance, including a tip displacement of 36.5 mm, a large blocking force of 2.4 MPa, and high power density (3966 J/m^3). These actuators can lift objects up to 20 times their own weight, displaying excellent load capacity. Additionally, the actuators mimicked biomimetic behaviors, such as petal opening/closing and wing flapping of bees at a high frequency (21 Hz). Compared to traditional IPMCs with pure Pt electrodes, the roughened Nafion surface and the Pd buffer layer enhanced electrolyte transport and provided a highly capacitive interface with the Pt layer, leading to better performance. The Pd/Pt composite electrodes significantly improved the IPMC's actuation, making them suitable for applications in medical devices and biomimetic robots. This study highlights the potential of high-performance IPMC actuators for diverse applications, particularly in the field of soft robotics and biomimetic systems.[275]

Traditional bone defect treatments face challenges like limited autologous bone supply, immune rejection of allogeneic grafts, and high medical costs. Bone tissue engineering offers a promising alternative, with electroactive scaffolds being commonly used for bone repair. However, single-function electroactive scaffolds are often insufficient, and multifunctional ones can be complex and expensive to create. To address these challenges, this study introduces a novel approach using carbon-based materials for bone tissue engineering. The team developed a hydroxyapatite/carbon nanofiber (HAp/CNF) scaffold by electrospinning hydroxyapatite (HAp)-doped PVDF and then carbonizing the fibers. Biochemical tests on human adipose-derived stem cells (h-ADSCs) cultured on the HAp/CNF scaffold showed that the material promoted osteogenic differentiation in the absence of external osteogenic factors. The study found that the electroactive carbon nanofibers promoted osteogenesis, and the HAp/CNF scaffold induced more osteogenic differentiation compared to carbon nanofibers alone. This is due to the combined effect of the scaffold's electrical activity and the release of calcium ions (Ca^{2+}) from HAp. Overall, this research presents a simple, cost-effective, and efficient method to create carbon-based scaffolds, offering a new strategy for bone tissue engineering.[276]

This body of work by Suzuki et al. investigates the chemical changes in PTFE under bending stress using hard X-ray photoelectron spectroscopy (HAXPES) and soft X-ray absorption spectroscopy (TFY-XAS). The results indicate that bending stress leads to the breaking of C−F bonds in the side chains of PTFE, with the appearance of C−C bonds in the main chain on the surface. The breaking of C−F bonds was more pronounced under tensile stress caused by bending, with the bond scission increasing as the tensile strain due to bending increased. However, C−F bonds were not significantly affected by uniaxial tensile stress. The findings suggest that the bending stress, which applies force toward the center of curvature, causes the breaking of C−F bonds, unlike uniaxial tensile stress. This bond scission primarily occurs near the surface of PTFE, as indicated by the deeper detection depths, indicating little change. These results offer new insights into the behavior of PTFE under bending stress, which is relevant for applications in nanofluidics and medical engineering. Additionally, the study suggests that the breaking of C−F bonds could enable the creation of carbon-rich structures, potentially advancing the fabrication of two-dimensional materials like graphene.[277]

Wang et al. investigate a novel electroactive artificial nerve conduit made from PVDF PLCL (poly(L-lactic acid-*co*-ε-caprolactone)), and PEDOT, which combines piezoelectric and electrically conductive properties. The conduit demonstrated excellent electrical activity, strong suture resistance, and antitwisting capabilities. The electroactive conduit effectively promoted sciatic nerve regeneration in rats in both *in vitro* and *in vivo* studies, improving both nerve conduction and motor function. The study also explored the underlying mechanisms and found that the electroactive material regulates the immune microenvironment. It activates the PI3K/AKT-Nrf2 signaling pathway (involving Phosphoinositide 3-kinase/Protein Kinase B-Nuclear factor erythroid 2-related factor 2), which encourages macrophages to adopt an M2 (anti-inflammatory) phenotype. This, in turn, helps recruit Schwann cells (which support nerve regeneration) and promotes myelin formation, aiding nerve repair. Blocking these immune signaling pathways reduced the conduit's effectiveness, highlighting the critical role of immune modulation in peripheral nerve regeneration.[278]

This research introduces a novel approach for creating 3D in vitro tissue barrier models, which better replicate physiological conditions than traditional 2D models. These models simulate complex cell−cell and cell−extracellular matrix (ECM) interactions and are vital for mimicking the body's natural environments. However, creating perfusable luminal structures that maintain high cellular density and are supplied with nutrients and oxygen over extended periods has been a significant challenge. The technique described in this study uses a molding-based method to create high-density, perfusable tissue constructs. It employs a PTFE-coated stainless steel wire as a template for creating perfusable channels in PDMS wells. A bioink mixture of cells and collagen is added, and the cells self-assemble around the wire, forming a dense cellular layer. After removing the wire, a hollow, perfusable construct remains, which can be connected to an inlet and outlet for fluid perfusion. This method is scalable, allowing for varying dimensions and multicellular configurations. The human umbilical vein endothelial cells that migrate to the surface after assembly form functional barriers with adherent junctions. Permeability tests and fluorescence imaging show that these constructs replicate the in vivo endothelial barrier permeability more accurately than existing 3D models, exhibiting the lowest permeability seen in literature. Unlike traditional methods that often result in uneven endothelial cell seeding and poor barrier formation, this technique offers a straightforward and effective way to build complex, perfusable

https://doi.org/10.1021/acs.chemrev.4c00996
Chem. Rev. XXXX, XXX, XXX−XXX

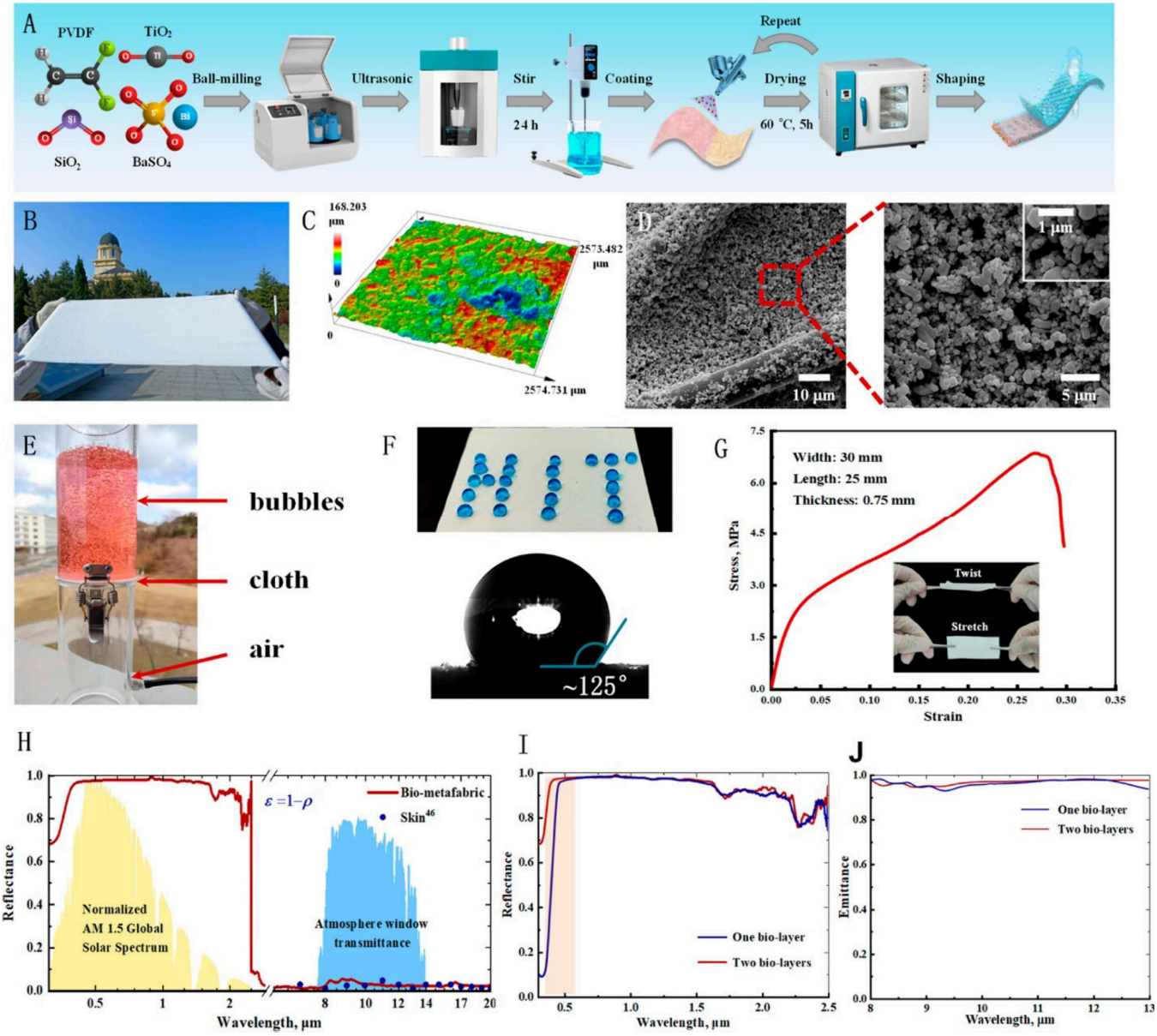

Figure 79. Preparation and characterization of the bioskin-inspired PDRC metafabric. (A) Fabrication process of the bio-PDRC metafabric. (B) Image of the fabricated roll of bio-PDRC metafabric. (C) Image of the bio-PDRC metafabric surface in the 3D scanning mode of an optical microscope. (D) SEM image of the slab-type microporous medium in bio-PDRC metafabric. (E) Measurement of the breathability and waterproofness of the bio-PDRC metafabric. (F) Demonstration of self-cleaning properties of the bio-PDRC metafabric. The upper image is the hydrophobicity pattern (HIT), and the lower image is the contact angle test image. (G) Mechanical strength tests of the fiber strength versus elongation. (H) Measured spectral reflectance of the metafabric (0.3−20 μm) in the normalized ASTM G173 global solar spectrum and "atmospheric transmission window" spectrum and measured spectral reflectance of human skin in the "atmospheric transmission window" spectrum. (I) Measured spectral reflectance of the one- and two-biolayer metafabric in the normalized ASTM G173 global solar spectrum. (J) Measured spectral emittance of the one- and two-biolayer metafabric. Reproduced with permission from ref (282). Copyright 2023 American Chemical Society.

3D tissue constructs. These constructs are ideal for applications in tissue engineering, drug screening, and disease modeling.[279]

This study aims to conduct a systematic review and network meta-analysis to evaluate the effects of various membranes on vertical bone regeneration and clinical complications associated with guided bone regeneration (GBR) and guided tissue regeneration (GTR). Researchers compared the following membranes: high-density polytetrafluoroethylene (d-PTFE), ePTFE, cross-linked collagen membrane (CCM), noncrosslinked collagen membrane (CM), titanium mesh (TM), titanium mesh combined with noncrosslinked collagen (TM + CM), titanium mesh combined with cross-linked collagen (TM + CCM), titanium-reinforced d-PTFE, titanium-reinforced e-PTFE, PLA, PEG, and polylactic acid 910 (PLA910). Utilizing the PICOS framework to establish inclusion criteria, researchers gathered articles from PubMed, Web of Science, and other databases. Researchers assessed the risk of bias and the quality of evidence according to the Cochrane Evaluation Manual and GRADE guidelines. Ultimately, 27 articles were included, with 19 of these contributing to a network meta-analysis focused on vertical

https://doi.org/10.1021/acs.chemrev.4c00996
Chem. Rev. XXXX, XXX, XXX−XXX

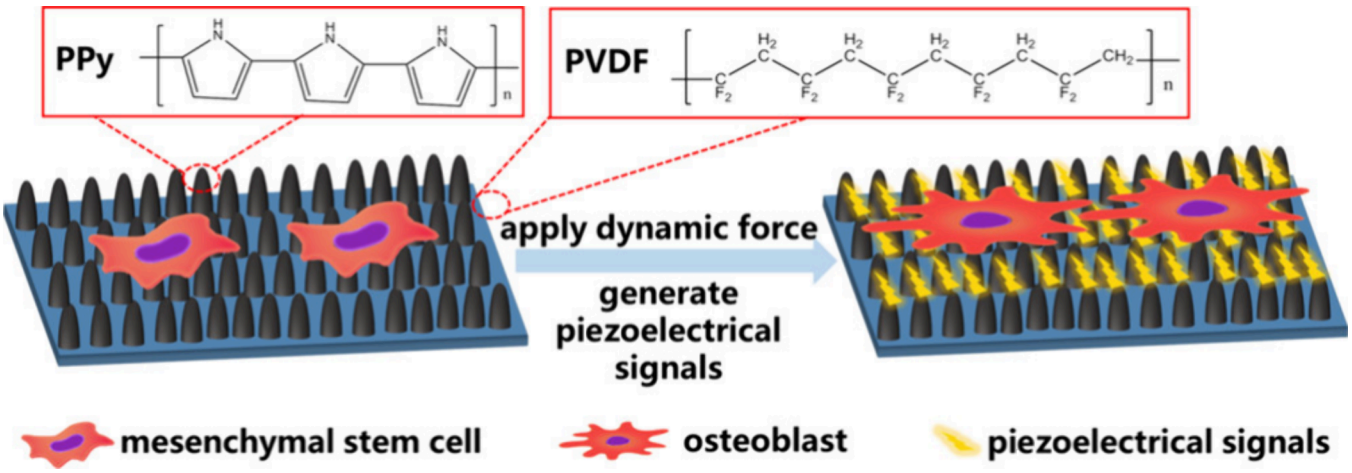

Figure 80. Fabrication and design of a PPy-PVDF composite which stimulates oxteoblasts and mesenchymal stem cells to increase osteogenesis and BMSC adhesion for bone regeneration. Reproduced with permission from ref (283). Copyright 2019 American Chemical Society.

bone increment as the primary outcome measure. The network meta-analysis features network diagrams, paired-comparison forest plots, funnel plots, surface under the cumulative ranking curve (SUCRA) plots, and sensitivity analysis plots. The SUCRA analysis indicated that titanium-reinforced d-PTFE produced the most significant vertical bone increment. Additionally, researchers examined complications across 19 studies and identified soft tissue injury and membrane exposure as the most prevalent issues.[280]

The combination of hydrogels and solid materials offers enhanced functionality for applications such as tissue engineering scaffolds and soft machines. However, the weak adhesion between hydrogels and solids limits their effectiveness. This study presents a versatile approach to creating mechanically robust solid-hydrogel hybrid materials by employing surface-embedded radicals generated through plasma immersion ion implantation (PIII) on polymer surfaces. The findings demonstrate that these reactive radicals serve a dual purpose: they initiate surface-initiated, spontaneous polymerization of hydrogels and facilitate the binding of hydrogels to the surfaces. Acrylamide and silk hydrogels are synthesized and covalently bonded through spontaneous reactions with the radicals on PIII-activated polymer surfaces, without the need for cross-linking agents or initiators. The quantity of hydrogel formed increases with longer incubation times, higher monomer concentrations, and elevated temperatures. Stability tests reveal that 95% of the hydrogel remains intact even after four months in PBS solution. T-peel tests indicate that failure occurs at the interface between the tape and hydrogel, with the interfacial adhesion strength of the hydrogel-PIII-treated PTFE exceeding 300 N m^{-1}. Cell assays indicate no adhesion to the synthesized hydrogels; however, hydrogels synthesized with fibronectin promote cell adhesion and spreading. These results indicate that polymers functionalized with surface-embedded radicals provide excellent solid platforms for creating robust solid-hydrogel hybrid structures suitable for biomedical applications.[281]

Passive daytime radiative cooling (PDRC) is an innovative zero-energy cooling technology aimed at reducing global fossil fuel consumption, and it has garnered significant interest. However, a major challenge for PDRC lies in overcoming the trade-off between achieving exceptional dual-band optical properties (for both solar and atmospheric windows) and meeting various functional requirements for practical applications. To address this, researchers introduced a photon slab-porous effect that enhances sunlight backward scattering, drawing inspiration from the structure of human skin (epidermis and dermis), which has documented medical infrared emittance and multifunctional capabilities. Researchers developed an effective design strategy for dual-band optical properties in PDRC. Using a straightforward and scalable dip-dyeing process, researchers created a bioskin-inspired PDRC metafabric that demonstrated outstanding dual-band optical characteristics, achieving solar reflectance and atmospheric window emittance rates of 97%. Field tests revealed that the bio-PDRC metafabric could lower temperatures by as much as 12.6 °C during the day. Additionally, a person wearing a hat made from this material experienced a temperature reduction of 16.6 °C compared to someone wearing a standard hat. The bio-PDRC metafabric also excelled in breathability, waterproofing, flexibility, strength, and durability, effectively meeting the diverse needs for personal thermal management, ventilation, and automotive covers (Figure 79).[282]

1.15. Wound Care and Dressings

There has been increased interest in utilizing electrical stimulation to influence stem cell differentiation and tissue regeneration. Micro- and nanotopographies have shown the ability to mechanically regulate bone mesenchymal stem cell (BMSC) differentiation, while electrical stimulation is involved in modulating cell behavior and fate. Dynamic electrical stimulation is particularly important for bone growth and regeneration, leveraging the inherent piezoelectricity of bone that generates potential under dynamic stress. A dynamic piezoelectric stimulation effect is generated in a composite of PVDF and PPy, creating effective and continuous dynamic piezoelectric signals for cells. The PVDF membrane is fabricated via solvent evaporation, followed by electrochemical polymerization of PPy. The integration of PPy nanocones with dynamic piezoelectric stimulation allows for modulation of cell behavior, paving the way for further exploration of cellular responses to dynamic electrical stimulation (Figure 80). This PPy-PVDF nanocomposite enhances the adhesion, spreading, and osteogenic differentiation of BMSCs. Under dynamic loading of 5 N at a frequency of 0.5 Hz, the mean short circuit current values measured were 100 pA for PVDF, 120 pA for PPy-PVDF IFS, and 150 pA for PPy-PVDF NS (Nanocone

https://doi.org/10.1021/acs.chemrev.4c00996
Chem. Rev. XXXX, XXX, XXX−XXX

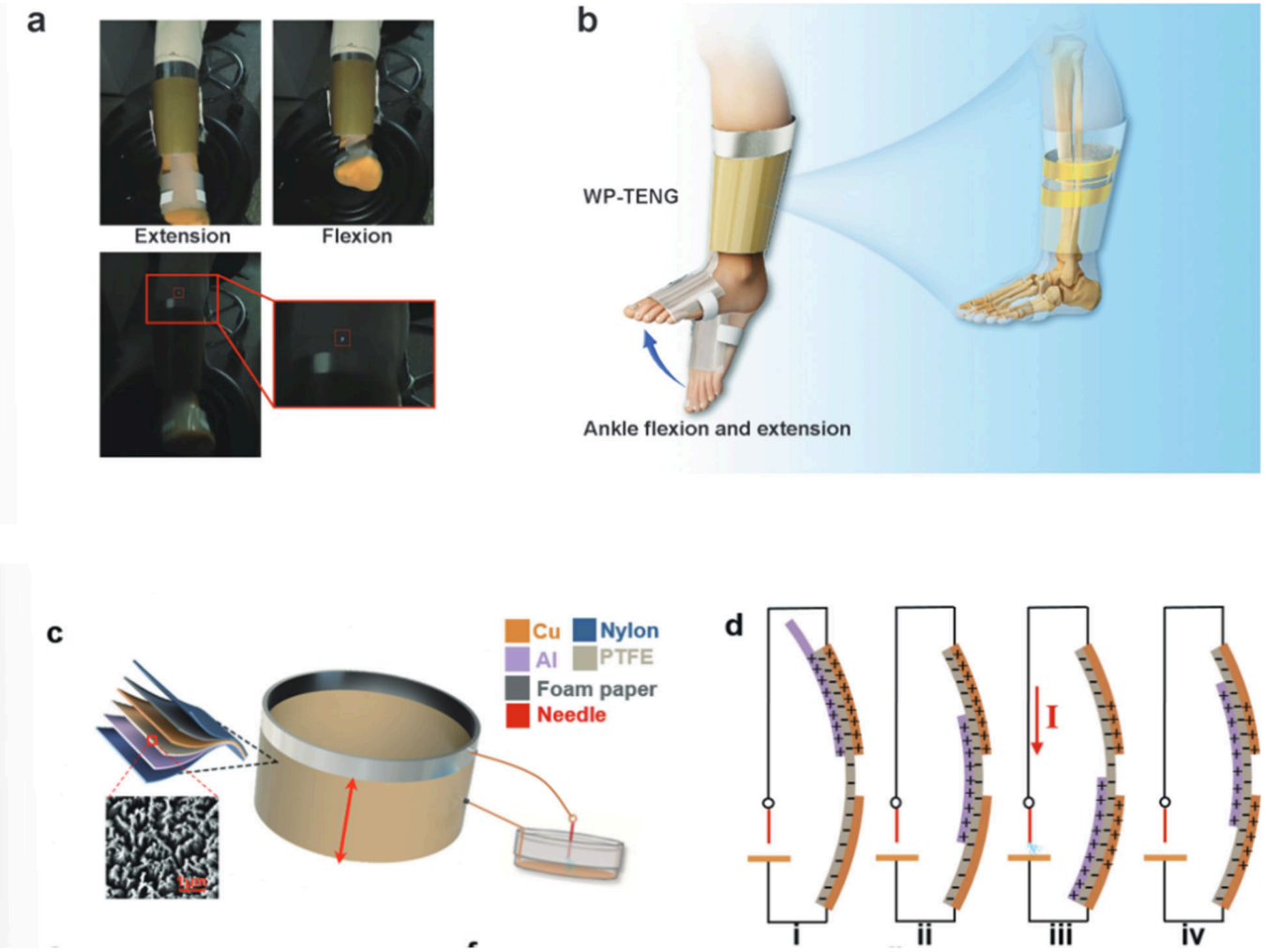

Figure 81. (a,b) Demonstration of the WP-TENG device for monitoring and stimulation of BSMCs in ankle rehabilitation, (c) schematic representation of the WP-TENG device, and (d) mechanism of voltage generation through material deformation. Reproduced with permission from ref (284). Copyright 2022 John Wiley & Sons Inc.

Surface). The PPy-PVDF NS demonstrates effective dynamic piezoelectric stimulation, promoting BMSC adhesion and differentiation toward osteogenesis. This indicates that the combination of piezoelectric stimulation and nanotopography can facilitate material exchange between the cell membrane and the extracellular matrix.[283]

Efficient bone defect repair is particularly challenging in aged individuals due to the decreased osteogenic differentiation and angiogenic ability of BMSCs. Aged stem cells also generate an inflammatory degenerative niche that slows healing. Mechanical and electrical stimulation, however, can enhance both osteogenesis and angiogenesis, promoting bone regeneration and retraining inflammatory reactions. The mechanosensitization of the Piezo1 ion channel protein plays a key role in the rejuvenation of aged BMSCs, enhancing their osteogenic potential and angiogenic capacity, while also increasing the tube formation capacity of (HUVEC) to support bone repair and regeneration. Researchers identified the signal transduction mechanisms involved, particularly the activation of Piezo1 and the regulation of intracellular calcium (Ca^{2+}). A wearable pulsed triboelectric nanogenerator (WP-TENG) was developed to stimulate bone repair in elderly patients. The WP-TENG device was fabricated with Cu foil electrodes, and PTFE and Al foil as triboelectric layers (Figure 81). Triboelectric stimulation activated the mechanosensitive ion channel Piezo1, rejuvenating aged BMSCs, enhancing osteogenic differentiation, and promoting HUVEC tube formation. This stimulation improved calcium nodulus formation, alkaline phosphatase (ALP) activity, and HUVEC tubule formation, demonstrating that triboelectric stimulation can enhance the biological function of aged cells. The stimulation upregulated the expression and activation of Piezo1, promoted intracellular Ca^{2+} concentration, and regulated the expression of the transcription factor HIF-1α, leading to the upregulation of osteogenesis-related genes and increased secretion of angiogenic factors. *In vivo* tests using a rat cranial defect model confirmed that BMSCs activated by WP-TENG could promote bone defect repair, with the process being dependent on the activation of Piezo1. This study highlights the potential of triboelectric stimulation as a novel approach to bone repair and regenerative medicine for aging populations.[284]

Hydrophilic cationic antibacterial hemostatic materials are limited in applications due to the contradictory relationship between antibacterial properties and biocompatibility. Researchers used bactericidal quaternary ammonium salts and hydrophobic fluoropolymers to develop a multifunctional temperature-triggered antibacterial hemostatic material which

https://doi.org/10.1021/acs.chemrev.4c00996
Chem. Rev. XXXX, XXX, XXX−XXX

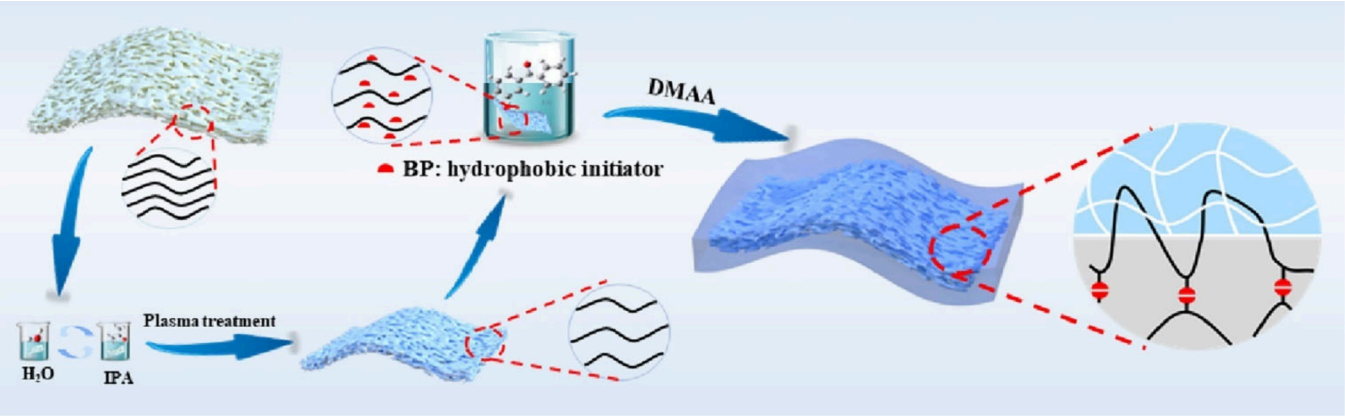

Figure 82. Schematic for the preparation of the PVDF/PDMAA$_n$ hydrogel from plasma treatment, followed by UV curing to form the hydrogel patch with a PVDF core. Reproduced with permission from ref (288). Copyright 2023 American Chemical Society.

kills bacteria at room temperature and switches to bacterial repulsion at physiological temperature. The poly(N,N-dimethylaminoethylmethacrylate)-b-poly(1*H*,1*H*,2*H*,2*H*-heptadecafluorodecyl acrylate) (PDMA-b-PFOEMA) block copolymers are self-assembled and quaternized to create an aggregate coating. Bacterial attachment and proliferation are inhibited at room temperature, and at physiological temperature the fluorinated block migrates to the material surface to promote biocompatibility and antiadhesion properties. The fluorinated block further displays rapid coagulation, lowered blood loss, minor secondary bleeding, and lowered bacterial infiltration. Quaternized PDMA$_7$-b-PFOEMA$_{20}$ aggregates relieve the contradiction of antibacterial and biocompatible materials and possess antiadhesion and antibacterial properties against *S. aureus* at room temperature with good hemocompatibility (<5% hemolysis). At physiological temperature the material switches to an antiadhesion hemostatic surface with no cytotoxicity, with quaternary ammonium salts being buried and XPS analysis indicating mainly fluorinated groups are present on the material surface. The material displays rapid clotting with no blood loss and unforced detachment, leading to minimized secondary bleeding. Tail incision studies in rodents display fast coagulation, small blood spread, no blood penetration, and easy removal from the wound site.[285]

A nanofibrous wound dressing for burn wounds was developed through a multihierarchical assembly process combining electro-microencapsulation, electro-interpenetration, and electrodeposition. The dressing's core consists of n-hexadecane encapsulated by a PVDF shell, fabricated using coaxial electro-spinning to create a phase-transition thermal management system. The n-hexadecane has a phase transition temperature of 16−18 °C and absorbs heat upon melting to provide a cooling effect, while the PVDF shell prevents leakage of the material. The interpenetration step involved electrospinning PVA and the PVDF@n-hexadecane core−shell material via heterologous coelectrospinning, which regulated the moisture absorption and retention properties by adjusting the area density and continuity of the hydrophilic and hydrophobic phases. The final step involved electro-spraying and electrodepositing PCL nanocapsules containing dual-component antibacterial agents onto the interpenetrated membrane. These antibacterial agents including Hein-Schiff base, N-halamine, and quaternary ammonium salt groups (HSNQAS), are effective against typical pathogens such as *E. coli* and *S. aureus*. The wound dressing demonstrates excellent performance in moisture absorption for exudate removal, moisture retention for tissue regeneration, and provides a cooling effect, making it suitable for second-degree burn healing. The dressing effectively manages the exudation phase and the infection phase, removing exudate to help prevent bacterial growth. The PVDF outer shell enhances the stability and durability of the n-hexadecane during phase transition, while the in situ electrodeposition of PCL/chitosan@HSNQAS nanocapsules ensures firm adhesion and maximized exposure of antibacterial components. These components do not leach, minimizing the impact on healthy cells. *In vivo* tests using white rat models showed that the dressing accelerated healing in level 2 burn wounds. After 3 days, the wound area had decreased by 400%, and near-complete healing was observed after 12 days.[286]

Electrical stimulation has been demonstrated to reduce edema, improve cell proliferation and migration during wound healing and is typically delivered in clinical settings using implanted electrodes. The requirement for multiple patient visits may result in noncompliance, and research has been conducted toward self-powered devices for at-home use. Researchers have developed self-powered silver nanoparticle-containing electro-active hydrogel particles as an advanced wound dressing and are particularly beneficial for complex wounds with irregular contours and deep cavities. The hydrogel microparticles are based on carboxymethylcellulose and cross-linked sodium carboxymethylcellulose, with *in situ* synthesized AgNPs that provide antibacterial and electrical properties. When hydrated, these microparticles swell to form a bulk hydrogel with a maximum swelling ratio of approximately 400% within 16 h. The electrical stimulation is self-generated via a piezoelectric PVDF membrane, eliminating the need for an external power source and enhancing patient compliance. When integrated with a PVDF membrane, the Ag-gel generates an open-circuit voltage of 4.6 V and a short-circuit current of 2 μA under external pressure (15 kPa). The hydrogel exhibits strong antibacterial activity against *E. coli* and *S. aureus*, with a clear zone of inhibition and a sustained release of AgNPs over time. In rodent wound healing studies, the Ag-gel with PVDF displayed the most effective healing, with 89% wound closure by day 14, compared to 65% for the control, 69.5% for PVDF alone, and 72% for the Ag-gel without PVDF. This advanced dressing is user-friendly, effective in promoting wound closure, and particularly suitable for deep, complex wounds, offering

https://doi.org/10.1021/acs.chemrev.4c00996
Chem. Rev. XXXX, XXX, XXX−XXX

both antimicrobial effects and continuous electrical stimulation to accelerate healing.[287]

Researchers developed a bioactive wound healing patch for the functional recovery of scald wounds, integrating both electrically and chemically active components. The patch is designed for use with daily 10 min massages during recovery and is made of a piezoelectric PVDF-HFP film and a self-adhesive poly(N,N-dimethylacrylamide) (PDMAA) hydrogel layer. The PVDF film is created via aqueous phase inversion or ammonia−water phase conversion methods, followed by plasma treatment to enhance hydrophilicity. The resulting PVDF/PDMAA composite film is then UV-cured with benzophenone (BP) to form the final patch with a hydrogel shell and PVDF core (Figure 82). The hydrogel enables reversible adhesion to skin wounds, and the patch achieves frequency-dependent electrical and chemical dose delivery through mechanical stimuli, creating electrical-chemical cross-talk. Unlike traditional TENG and PENG devices, which primarily focus on electrical signaling, this bioactive patch incorporates both electrical and chemical responses, closely resembling biological tissue in nature. The piezoelectric PVDF component generates electricity, while the hydrogel molecules respond in a frequency-specific manner to modulate voltage output, affecting the molecular delivery speed of bioactive agents in the hydrogel layer. Mechanical stimuli at 1 Hz produce the highest response, with a current amplitude of 2×10^{-7} A and an open-circuit voltage of 6 V. The piezoelectric performance of the device is frequency-dependent, with effective frequencies ranging from 0.5 to 64 Hz. The patch demonstrates high biocompatibility, with cell viability rates exceeding 95%. In an animal study, scalded mice with grade I and shallow grade II scald wounds were treated with the hydrogel patch loaded with recombinant human epidermal growth factor (rhEGF) and massaged daily at 56 Hz. Significant healing was observed after 18 days and the patch was found to promote effective recovery, inducing collagen deposition, hair follicle regeneration, and blood vessel and gland formation, while untreated wounds remained visible, indicating efficacy of the dressing for scald wounds.[288]

Researchers developed an artificial intelligence-enabled wearable sensor, FLEX-AI, to monitor chronic hard-to-heal wounds, aiming to improve clinical efficiency and minimize infection risks. This smart sensor integrates a deep artificial neural network (ANN) for real-time chronic wound monitoring, using short-range communication to connect with an MXene-attached, radio frequency-tuned, wound dressing-integrated SMART-WD bandage. The system is trained with on-contact pH-responsive voltage output and demonstrated 94.6% accuracy in recognizing healing stages. The wound dressing is comprised of poly(vinyl acrylic) gel@PANI/Cu_2O nanoparticles, which generates a pH-responsive current during healing. It operates with a chip-free tag, using capacitive MXene/PTFE electret and adhesive materials to match the resonance frequency of the wearable antenna. The wound dressing exhibits an exponential increase in current as higher activation voltage is applied, allowing monitoring of healing stages including fast-curing, slow-curing, and noncuring phases. Testing the device on skin conditions like psoriasis, urticaria, and dermatitis, the system effectively monitored wound healing for pH levels between 6 and 9 during corticosteroid treatments. As the wound becomes more acidic, hydrogen ion translocation triggers a transition from Cu(I) to Cu(II) in the dressing, allowing the deep ANN algorithm to predict wound reorganization. This contactless healthcare system provides real-time wound management and has potential for remote monitoring and therapeutic evaluation, particularly when drug treatments are ineffective.[289]

1.16. Conclusions

Fluoropolymers display many favorable properties for medical applications due to their superior hemocompatibility, chemical and biological stability, and antithrombogenic properties. Current medicinal applications of fluoropolymers are directed toward antibiofouling surfaces for implants and wound care applications, triboelectric and piezoelectric nanogenerators for energy harvesting in medical devices, TENG- and PENG-based sensors for noninvasive medical monitoring, suture and mesh prosthesis materials, air filtration devices including medical masks, and membranes for both water treatment and gas exchange. Fluoropolymers have been demonstrated to be clearly superior in many cases compared to conventional hydrocarbon polymers (especially in suture and mesh materials), however, to our knowledge, researchers concentrate on only a small number of fluoropolymers in medicine. Much of the work done in the last 5 years has been concentrated on PTFE, ePTFE, and PVDF (with P(VDF-TrFE) as a subcategory of PVDF). Derivatization of conventional monomers with fluorinated components has been attempted with success, however this represents a small portion of the current state-of-the-art. Typically, PVDF is utilized in PENG applications for sensors and wearable devices, with further applications in suture materials and some implants, while PTFE and ePTFE tend to see applications in antibiofouling surfaces, membranes, suture materials, and TENG devices.

PVDF and PTFE derivatives have proved to have a broad range of applications in medicine, however the limitation of the scope of materials raises the question of whether alternative fluoropolymers could provide more wide-reaching medicinal applications. Heavily fluorinated materials are difficult to synthesize, potentially making production cost-prohibitive and providing a possible reason for the narrow range of materials used in current research. Much research has utilized an engineering approach toward medical device design, mainly focusing on processing of existing materials toward composite devices. This presents a stark gap in the literature, and more research is required to have a comprehensive understanding of how alternative fluoropolymers interact with the human body. Moving forward, an approach toward integrating the concept of basic research toward novel medicinal applications of fluoropolymers would aid in developing new materials and provide greater understanding of material design for clinical applications.

While fluorinated materials are currently under scrutiny due to fear over PFAS and potential PFAS materials, the unique properties of partially and perfluorinated molecules make them essential in the medical field. Future research may look at block copolymers, particularly those of PVDF due to its lower fluorine content and piezoelectric effect. PVDF block copolymers and star polymers can also be utilized to take advantage of the self-assembly effect of fluorous materials, with the goal of creating cross-linked piezoelectric materials for applications in sensing and pacemakers. Materials incorporating biobased blocks for biocompatible composites would contribute positively toward lowering fluorine content of medical devices. End-to-end recycling and material degradation studies of such medical devices are also missing, with just

https://doi.org/10.1021/acs.chemrev.4c00996
Chem. Rev. XXXX, XXX, XXX−XXX

a handful of studies examining the effects of implants over time on surrounding tissue. Finally, polymers and networks based on variant feedstocks such as fluorinated epoxides (such as hexafluoropropylene epoxide), oxetanes (such as tetrafluorooxetane), hexafluoroacetone hydrate,[290] trifluorovinyl ethers,[291] PFPAEs, and fluorinated amides/polyamides appear to be vastly underutilized in medical applications. Basic research with these polymers in medicinal applications will allow researchers to gain a greater understanding of new polymers that can be used as base materials or cross-linking agents to modulate material properties that currently do not appear to be explored. Synthesis of new fluorinated and fluorine-containing monomers will expand the pool of materials utilized and hopefully represent a new era of medicinal fluoropolymer chemistry and new applications.

AUTHOR INFORMATION

Corresponding Authors

Chadron M. Friesen − *Neufeld Science Centre, Department of Chemistry, Trinity Western University, Langley, British Columbia V2Y 1Y1, Canada;* orcid.org/0000-0001-9955-5695; Email: chad.friesen@twu.ca

Jason Pulfer − *Department of Chemistry, Simon Fraser University, Burnaby, British Columbia V5A 1S6, Canada;* Email: jmp23@sfu.ca

Complete contact information is available at: https://pubs.acs.org/10.1021/acs.chemrev.4c00996

Author Contributions

The data acquisition, summarizing, writing, and editing of this work was performed equally by Chadron M. Friesen and Jason Pulfer.

Notes

The authors declare no competing financial interest.

Biographies

Chadron M. Friesen was born in Säffle, Sweden but grew up in a rural town in southwest Kansas, USA. He received a B.S. and a B.S.E from John Brown University in Arkansas in 1995 and then soon after, pursued a Ph.D. from The University of Alabama in fluorine and analytical chemistry underneath the direction of Dr. Joseph S. Thrasher. In 1998, he was employed at E.I. du Pont de Nemours and Co., Inc. in New Jersey, USA under the supervision of Dr. Jon L. Howell to conduct research into new lubricant additives for high-temperature stability and anticorrosion for aerospace applications. In 2000, he accepted a position as Assistant Professor of Chemistry at Trinity Western University in British Columbia, Canada. He was promoted to Associate Professor in 2005, Full Professor in 2010, and Department Chair from 2021-to the present. He has also been a visiting scientist at DuPont in 2001 and 2006-2007 and at the Ecole Nationale Supérieure de Chimie de Montpellier, France in 2013-2014. From 2020-2023, he received a U.S. Air Force Research Lab (AFRL) *Summer Faculty Fellowship* from the Air Force Office of Scientific Research to continue work in materials applicable to aerospace. His current interests range from exploring new synthetic designs and methodologies to create novel fluorinated polymers for relevant industrial applications of today or to add specified and localized amounts of fluorine to pharmaceuticals. Critical to these pursuits is the isolation and structural determination of these new materials and products. He is also a member of the Division of Fluorine Chemistry of the American Chemical Society since 1996, served as Vice-Chair/Secretary (2009-2021), Chair (2013), Past-Chair (2014), and Fellow of the American Chemical Society (2024) for this division.

Jason Pulfer was born in White Rock, British Columbia, Canada. He received a B.Sc in chemistry from Trinity Western University in 2020. Currently he is in pursuit of his Ph.D. in a cosupervisory arrangement between Trinity Western University and Simon Fraser University in fluorine chemistry and polymer chemistry under the supervision of Dr. Chadron M. Friesen and Dr. Tim Storr. His current research interests range from synthetic methods towards novel fluoropolymer materials, composite material design, and the synthesis and characterization of exotic organometallic species.

ACKNOWLEDGMENTS

The authors would like to thank the National Sciences and Engineering Research Council of Canada for funding the work (Grant No. RGPIN-2022-05143), and Thomas Karpiuk for providing the TOC graphic.

ABBREVIATIONS

AA, acrylic acid; ABP, acryloyloxy benzophenone; ABTS, azino-bis(3-ethylbenzothiazoline-6-sulfonic acid; AC, activated carbon; AD, aortic dissection; AET, active eye tracking; AF, amorphous fluoropolymers; AFB, acid-fast bacilli; AFM, atomic force microscopy; AGET, activator generated by electron transfer; AI, artificial intelligence; AKT, serine/threonine protein kinase; ALFS, all optical flow sensor; ALG, alginate; ANN, artificial neural network; API, active pharmaceutical ingredients; APTAP, AgNY/PVDF@TiO_2/Ag/PVDF; APTES, 3-(aminopropyl) triethoxysilane; ATPS, all-textile piezoelectric sensor; ATR, attenuated transfer reflectance; ATRP, atom-transfer radical polymerization; BAB, triblock copolymer; BCI, blood clotting index; BDMI, 1-butyl-2,3-dimethylimidazolium hexafluorophosphate; BFC, biofuel cells; BFE, bacterial filtration efficiency; BIC, blocked isocyanate; BMIM, butyl-3-methylimidazolium; BMSC, bone mesenchymal stem cells; BOD, bilirubin oxidase; BPM, beats per minute; BS, bismuth sulfide; BSA, bovine serum albumin; BTO, barium titanate; CAD, charged aerosol detection; CADR, clean air delivery rate; CBZ, carbamazepine; CCM, curcumin; CDA, cellulose diacetate; CESA, cervicosacropexy; CF, carbon fiber; CFE, chlorofluoroethylene; CFU, colony count units; CHS, CS, and CTS, chitosan; CIP, ciprofloxacin; CKD, chronic kidney disease; CL, epsilon-Caprolactone; CLD; CM, cell membrane; CNF, cellulose nanofibril; CNT, carbon nanotube; CNTX, multiwalled carbon nanotubes; COVID, coronavirus disease; CPB, cardiopulmonary bypass; CPEI, concentration of polyethyleneimine; CPNC, conducting polymer nanocomposite; CRC, chemical rubber company; CT, computed tomography; CTEM, charge-laden triaxial electrospinning membrane; CTFE, chlorotrifluoroethylene; CV, crystal violet; DAPI, 4′,6-diamidino-2-phenylindole; DBS, deep brain stimulation; DCF, diclofenac; DCS, 3-(3−4,dihydroxyphenyl) propionic acid modified chitosan cross-linker; DD, degree of deacetylation; DDS, dichloro(dimethyl)-silane; DEEA, N,N-diethylaminoethyl acrylamide; DFU, diabetic foot ulcers; DI, deionized; DLP, digital light processing; DMAEMA, 2-(dimethylamino)ethyl methacrylate; DMNOBA, N,N-dimethyl-N-(2-nitrobenzyl)-ethaneamine acrylamide; DNA, DNA; DOX, doxorubicin hydrochloride; DSC, differential scanning calorimetry; DSF, disulfiram; DSSM, direct sputum smear microscopy; EBD, electron beam deposition; EC, ethyl cellulose; ECG, echocardiogram;

https://doi.org/10.1021/acs.chemrev.4c00996
Chem. Rev. XXXX, XXX, XXX−XXX

ECM, extracellular matrix; ECMO, extracorporeal membrane oxygenators; EDC, 1-ethyl-3-(3-dimethylaminopropyl) carbodiimide hydrochloride; EEG, electroencephalography; EGCG, epigallocatechin 3-gallate; EGD, electrogenerative dressing; EH, energy harvester; EIS, electrochemical impedance spectroscopy; EISA, evaporation-induced self-assembly; EL, electroluminescent; EMG, electromyography; EMS, electrical muscle stimulation; EPR, electron pair resonance; EPS, extracellular polymeric substances; ePTFE, expanded polytetrafluoroethylene; ERK, extracellular signal-regulated kinase; EVAR, endovascular aortic repair; EW, electron-withdrawing; FAHFiP, 1,1,1,3,3,3-hexafluoropropan-2-yl 2-fluoroacrylate; FAS, 1H,1H,2H,2H-perfluorooctyltrimethoxysilane; FDA, food and drug administration; FE, filtration efficiency; FEP, fluoroethylene propylene; FET, field-effect transistor; FI-NES, fabricate an implantable neural electrical stimulation; FiR NV, fluoropolymer-modified rabies nanovaccine; FMA, fluorinated methacrylate; FOMA, 1H,1H,2H,2H-perfluorooctyl methacrylate; FPA, fibrinopeptide A; FPBA, formylphenylboronic acid; FPC, flexible printed circuit; FSPEU, fluorinated silicon-containing polyurethane; FTIR, Fourier-transformed infrared; FW, free water; GA, glycolic acid; GBR, guided bone regeneration; GF, glass fiber; GFF, glass fiber fabric; GMA, glycidyl methacrylate; GNP, graphene suspension of nanoplatelets; GPC, gel-permeation chromatography; GPL, general purpose lubricant; GPU, gas permeation unit; GRADE, grading of recommendations assessment, development and evaluation; GTR, guided tissue regeneration; HA, hyaluronic acid; HAMA, methacrylated hyaluronic acid; HAXPES, hard X-ray photoelectron spectroscopy; HCP, hemocompatible peptide; HDPE, high-density polyethylene; HEMA, 2-hydroxyethyl methacrylate; HENM, electrospinning nanofiber membrane; HFBA, hexafluoro butyl methacrylate; HFIP, hexafluoro isopropanol; HFMFHS, hollow fiber membrane flexible humidity sensor; HFP, hexafluoropropylene; HFPSS, hexafluoropropylene sulfonated styrene; HIF, hypoxia-inducible factor; HMUiO, hexamethyl ureido imino oxide; HPFM, hybrid perfluorinated electret nanofibrous membrane; HPLC, high-pressure liquid chromatography; HPMA, N-(2-hydroxypropyl) methacrylamide; HTCC, 2-hydroxypropyltrimethylammonium chloride chitosan; H-UEH, biocompatible ultrasonic energy harvester; HUVEC, human umbilical vein endothelial cells; IAV, influenza A virus; ICP, induced coupled-plasma; ID, intradermal; IDCSA, innovation and development center of sustainable agriculture; IEPY, piezoelectric polymer yarn with an internal electrode structure; IFS, irregular film surface; IL, ionic liquid; INAAT, isothermal nucleic acid amplification test; IPMC, Ionic polymer−metal composite; IPST, intraperitoneal colostoma mesh prosthesis; iRABV, inactivated rabies virus; ISC, short-circuit currents; ISO, international organization for standardization; iTENG, implanted triboelectric nanogenerator; ITO, tin-doped indium oxide; IW, intermediate water; IWFS, intelligent wearable filtration system; KF, Freundlich constants; KIP, kirigami-inspired pressure; KPS, potassium persulfate; LA, lactic acid; LAMP, loop-mediated Isothermal Amplification; LBL, layer-by-layer; LC-MS, liquid chromatography−mass spectrometry; LCST, lower critical solution temperature; LDA, lysine-dopamine; LEP, liquid entry pressure; LOD, limit of detection; LSA, left subclavian artery; LTB, lithium tetraborate; L-VIP, UV cured 1,3,5,7-tetravinyl-2,4,6,8-tetramethylcyclotetrasiloxane (V4D4) and 1H,1H,2H,2H-perfluorooctyl methacrylate (PFOMA) in fused with Perfluoropolyether (PFPE, Krytox GPL 101); MAA, methacrylic acid; MAPK, mitogen-activated protein kinase; MAPLE, matrix-assisted pulsed evaporation; MASP, multiarch-structure pressure; MB, methylene blue; MBA, N,N′-methylenebisacrylamide; MBC, minimum bactericidal concentration; MCE, Microporous Chitosan Extract; MCF, Michigan Cancer Foundation; MF, microfiltration; MHV, murine hepatitis virus; MIC, minimum inhibitory concentration; MJ, megajoule; MMG, mechanomyography; MMM, mixed matrix membrane; MOF, metal−organic framework; MPC, 2-methacryloyloxyethyl phosphorylcholine; MPEI, molecular weight of polyethyleneimine; MPPS, most penetrating particle size; MRI, magnetic resonance imaging; MRSA, methicillin-resistant *Staphylococcus aureus*; MS, mass-spectrometry; MTG, Membrane Technology Group; MTP, metoprolol; MTT, 3-(4,5-dimethylthiazol-2-yl)-2,5-diphenyltetrazolium bromide; MW, molecular weight; MWCNT, multiwalled carbon nanotube; MXENE, $M_{n+1}X_nT_y$, where M = early transition metal, X = carbon or nitrogen and T= terminating groups such as halides or chalcogens; NAVI, nonanticoagulated venous implant; NFM, nanofiber membrane; NFW, Nonfreezing water; NGC, nerve guide conduit; NHS, N-hydroxysulfosuccinimide; NIR, near-infrared; NIRM, nirmatrelvir; NMR, nuclear magnetic resonance; NO, nitric oxide; NP, nanoparticles; NPWT, negative-pressure wound therapy; Nrf2, Nuclear factor erythroid 2-related factor 2; NS, nanocone surface; NTS, neural tactile sensor; OCT, octenidine dihydrochloride; OSAS, obstructive sleep apnea syndrome; PA, poly(ethylene-alt-maleic anhydride); PA6, polyamide 6; PAAN, polyacrylonitrile-acrylamide-styrene sulfate; PAC, polyacrylamide/polyvinyl pyrrolidone/calcium chloride; PAH, polyallylamine hydrochloride; PAN, polyacrylonitrile; PANI, Polyaniline; PBTP, poly(butyl methacrylate-co-(trimethylamino)propyl methacrylamide chloride); PC, polycarbonate; PCB, paclitaxel coated balloon; pCD, poly(2-carboxyethyl acrylate-co-2-(dimethylamino)ethyl acrylate); PCG, phonocardiograms; PCL, polycaprolactone; PCR, polymerase chain reaction; PCTFE, poly-(chlorotrifluoroethylene); PCZ, polycarbazole; PD, Parkinson's disease; PDA, polydopamine; PDDA, poly-(diallyldimethylammonium chloride); PDFEA, poly[N-(2,2-difluoroethyl)acrylamide]; PDFHMA, poly-(dodecafluoroheptyl methacrylate); PDHI, poly(5,6-dihydroxyindole); PDMAEMA, poly(2-(dimethylamino)ethyl methacrylate); PDMS, poly(dimethyl siloxane); PDO, P-Dioxanone; PDRC, passive daytime radiative cooling; PEDOT, poly(3,4-ethylenedioxythiophene); PEEK, polyetheretherketone; PEG, poly(ethylene glycol); PEGMA, poly(ethylene glycol) methyl ether methacrylate); PEGSH, sebacic acid-terminated PEG modified with p-hydroxybenzaldehyde; PEI, polyethyleneimine; PENG, piezoelectric nanogenerator; PEO, poly(ethylene oxide); PEP, postexposure prophylaxis; PES, polyethersulfone; PET, polyethylene terephthalate; PETG, glycol-modified poly-(ethylene terephthalate); PETSD, piezo-electrochromic tactile sensing display; PEU, polyurethane; PEX, polyether block amide; PFA, perfluoroalkyl; PFAS, perfluoroalkyl substances; PFDA, 1H,1H,2H,2H-perfluorododecyl acrylate; PFDTS, perfluorodecyltrichlorosilane; PFMC, partially fluorinated with meltblown cloth; PFND, 1H,1H,9H,9H-perfluoro-1,9-nonanediol; PFOA, perfluoro octanoic acid; PFOEMA, poly(1H,1H,2H,2H-heptadecafluorodecyl acrylate); PFPAE, perfluoropolyalkylether; PGA, polyglycolic acid; PGMA, poly-(glycidyl methacrylate); PHB, polyhydroxybutyrate; PHEMA, poly(2-hydroxyethyl methacrylate); PHMB, poly-

https://doi.org/10.1021/acs.chemrev.4c00996
Chem. Rev. XXXX, XXX, XXX−XXX

(hexamethylene biguanide) hydrochloride; PI, pressure injury; PI3K, Phosphoinositide 3-kinase; PIBO,) poly(isobutylene oxide); PICOS, (population, interventions, comparators and outcomes); PLA, polylactic acid; PLCL, poly(L-lactic acid-co-ε-caprolactone); PLGA, poly(lactic acid-co-glycolic acid); PM, particulate matter; PMAA, poly(methacrylic acid); PMBU, poly(2-methacryloyloxyethyl phosphorylcholine-co-methacryloyloxyethyl butylurethane); PMMA, polymethylmethacrylate; PMP, polymethylpentene; PMPC, poly(2-methacryloyloxyethyl phosphorylcholine); PNI, peripheral nerve injury; PNIPAM, poly(N-isopyopyl) acrylamide; POP, pelvic organ prolapse; POSS, polyhedral oligomeric silsequioxane; PP, polypropylene; PPFC, plasma-polymer-fluorocarbon; PPFPA, poly-(pentafluorophenyl acrylate); PPI, peak-to-peak interval; PRINT, particle replication in nonwetting templates; PSA, poly(styrene-acrylic acid); PSG, polysomnography; PTFE, poly(tetrafluoroethylene); PTFS, poly(3,3,3-trifluoropropyl-methylsiloxane); PTX, paclitaxel; PTYR, poly(L-tyrosine); PU, polyurethane; PUA, polyurethane acrylate; pV4D4, poly(1,3,5,7-tetramethyl-1,3,5,7-tetravinyl cyclotetrasiloxane); PVA, poly(vinyl alcohol); PVB, polyvinyl butyral; PVC, poly(vinylchloride); PVDF, poly(vinylidene fluoride); PVP, polyvinylpyrrolidone; PVPA, poly(vinylphosphonic acid); PWBM, permeable waterproof based membranes; QF, quality factor; QPDMAEMA, quaternary poly(2-(dimethylamino)-ethyl methacrylate); QSC, charge storage capacity; RAFT, reversible addition−fragmentation chain transfer; RB, rhodamine B; RCM, red cell membrane; REMD, remdesivir; RF, riboflavin; RGO, reduced graphene oxide; RH, relative humidity; ROS, reactive oxygen species; RRI, R-to-R interval; SA, sodium alginate; SARS, severe acute respiratory syndrome; SC, supercritical; SEI, solid-electrolyte interphase; SEM, scanning electron microscopy; SEMG, surface electromyography; SEPS, self-powered endocardial pressure sensor; SERS, surface-enhanced Raman scattering; SETENG, single-electrode triboelectric nanogenerator; SF, sodium fluorescein; SFV, sandwich filtration vessel; SFV-CSSM, sandwich filtration vessel-concentrated sputum/specimen smear microscopy; SHP, superhydrophobic; SLIPS, slippery liquid-infused porous surfaces; SMA, styrene-maleic anhydride; SMC, smooth muscle cell; SMX, sulfamethoxazole; SN, self-powered nanogenerator; SPCA, styrene, polymerized with citric acid; SPE, solid-state polymer electrolytes; SPI, soybean protein isolate; STN, subthalamic nucleus; SUCRA, surface under the cumulative ranking curve; SUD, single-use disposable mask; SUPS, self-powered ultrasensitive pulse sensor; SWCNT, single wall carbon nanotube; SZO, zinc-doped silicon oxide; TB, tuberculosis; TBO, toluidine blue O; TC, thermocompression; TCR, temperature coefficient of resistance; TENG, triboelectric nanogenerator; TFEMA, 2,2,2,-trifluoroethyl methacrylate; TFN, Thin-film nanocomposites; TFT, thin-film transistor; TGA, thermogravimetric analysis; THP, tohoku hospital pediatrics; TI, thermal insulating; TIEL, triboelectrification-induced electroluminescence; TM, titanium mesh; TMC, trimethylene carbonate; TMSPM, trimethoxysilylpropyl methacrylate; TOB, tobramycin; TOF, time-of-flight; TPFS, (trichloro(1H,1H,2H,2H-perfluorooctyl)silane; TPU, thermoplastic polyurethane; TrFE, trifluoroethylene; UCT, ultrasound computed tomography; UF, ultrafiltration; UHMWPE, ultrahigh molecular weight poly(ethylene); US, United States; USL, uterosacral ligaments; UV LED, ultraviolet light-emitting diode; VAPG, Val-Ala-Pro-Gly; VIPS, vapor-induced phase separation; VMC, voltage multiplier circuit; VNA, virus-neutralizing antibody; VOC, open-circuit voltage; WAR, waterborne acrylic resins; WFE, water-based fluoropolymer emulsions; WP-TENG, wearable pulsed triboelectric nanogenerator; WSN, Washington state; WUS, wearable ultrasonic sensor; WVTR, water vapor transmission rate; XPS, X-ray Photoelectron Spectroscopy; ZIF, zeolitic imidazolate frameworks; ZPFSA, zinc-doped poly(vinylidene fluoride-co-hexafluoropropylene) sulfonated acrylamide.

REFERENCES

(1) Améduri, B. Fluoropolymers as Unique and Irreplaceable Materials: Challenges and Future Trends in These Specific Per or Poly-Fluoroalkyl Substances. *Molecules.* **2023**, *28* (22), 7564.

(2) Ameduri, B. Fluoropolymers: A Special Class of per- and Polyfluoroalkyl Substances (PFASs) Essential for Our Daily Life. *J. Fluor Chem.* **2023**, *267*, 110117.

(3) Roina, Y.; Auber, F.; Hocquet, D.; Herlem, G. EPTFE Functionalization for Medical Applications. *Mater. Today Chem.* **2021**, *20*, 100412.

(4) Roina, Y.; Auber, F.; Hocquet, D.; Herlem, G. EPTFE-Based Biomedical Devices: An Overview of Surgical Efficiency. *J. Biomed. Mater. Res. B Appl. Biomater.* **2022**, *110* (2), 302−320.

(5) Puts, G. J.; Crouse, P.; Ameduri, B. M. Polytetrafluoroethylene: Synthesis and Characterization of the Original Extreme Polymer. *Chem. Rev.* **2019**, *119* (3), 1763−1805.

(6) Koguchi, R.; Jankova, K.; Tanaka, M. Fluorine-Containing Bio-Inert Polymers: Roles of Intermediate Water. *Acta Biomater.* **2022**, *138*, 34−56.

(7) Wu, Y.; Ma, Y.; Zheng, H.; Ramakrishna, S. Piezoelectric Materials for Flexible and Wearable Electronics: A Review. *Mater. Des.* **2021**, *211*, 110164.

(8) Alam, S. N.; Ghosh, A.; Shrivastava, P.; Shukla, U.; Garg, K.; Edara, A. C.; Sahoo, N. An Introduction to Triboelectric Nanogenerators. *Nano-Struct. Nano-Obj.* **2023**, *34*, 100980.

(9) Sukumaran, S.; Chatbouri, S.; Rouxel, D.; Tisserand, E.; Thiebaud, F.; Ben Zineb, T. Recent Advances in Flexible PVDF Based Piezoelectric Polymer Devices for Energy Harvesting Applications. *J. Intell. Mater. Syst. Struct.* **2021**, *32* (7), 746−780.

(10) Cui, J.; Du, L.; Meng, Z.; Gao, J.; Tan, A.; Jin, X.; Zhu, X. Ingenious Structure Engineering to Enhance Piezoelectricity in Poly(Vinylidene Fluoride) for Biomedical Applications. *Biomacromolecules.* **2024**, *25* (9), 5541−5591.

(11) Kujawa, J.; Boncel, S.; Al-Gharabli, S.; Koter, S.; Kaczmarek-Kedziera, A.; Korczeniewski, E.; Terzyk, A. P. Current and Future Applications of PVDF-Carbon Nanomaterials in Energy and Sensing. *Chem. Eng. J.* **2024**, *492*, 151856.

(12) Smith, A. A.; Li, R.; Xu, L.; Tse, Z. T. H. A Narrative Review of In-Textile Sensors in Human Health Applications. *Adv. Mater. Technol.* **2024**, *9* (16), 2302141.

(13) Krafft, M. P.; Riess, J. G. Therapeutic Oxygen Delivery by Perfluorocarbon-Based Colloids. *Adv. Colloid Interface Sci.* **2021**, *294*, 102407.

(14) Ameduri, B. From Vinylidene Fluoride (VDF) to the Applications of VDF-Containing Polymers and Copolymers: Recent Developments and Future Trends. *Chem. Rev.* **2009**, *109* (12), 6632−6686.

(15) Lv, J.; Cheng, Y. Fluoropolymers in Biomedical Applications: State-of-the-Art and Future Perspectives. *Chem. Soc. Rev.* **2021**, *50* (9), 5435−5467.

(16) Chipara, A. C.; Brunetto, G.; Ozden, S.; Haspel, H.; Kumbhakar, P.; Kukovecz, Á.; Kónya, Z.; Vajtai, R.; Chipara, M.; Galvao, D. S.; Tiwary, C. S.; Ajayan, P. M. Nature Inspired Solid-Liquid Phase Amphibious Adhesive. *Soft Matter.* **2020**, *16* (25), 5854−5860.

(17) Song, F.; Kong, Y.; Shao, C.; Cheng, Y.; Lu, J.; Tao, Y.; Du, J.; Wang, H. Chitosan-Based Multifunctional Flexible Hemostatic Bio-Hydrogel. *Acta Biomater.* **2021**, *136*, 170−183.

https://doi.org/10.1021/acs.chemrev.4c00996
Chem. Rev. XXXX, XXX, XXX−XXX

(18) Zhao, S.; Zhang, D.; Jiang, Y.; Gao, C.; Liu, L.; Liu, Y. A Silicone Coating Containing Natural Borneol Fluorinated Side Chains with Excellent Static Antifouling Properties. *Eur. Polym. J.* **2023**, *193*, 112064.
(19) Zhao, X.; Hao, H.; Pang, H.; Jiang, M.; Duan, Y. Design and Fabrication of Superamphiphobic Coating Based on Raspberry-like F-SiO2@PSA Hybrid Nanocomposite Particles. *Mater. Chem. Phys.* **2023**, *309*, 128369.
(20) Koguchi, R.; Jankova, K.; Tanaka, Y.; Yamamoto, A.; Murakami, D.; Yang, Q.; Ameduri, B.; Tanaka, M. Altering the Bio-Inert Properties of Surfaces by Fluorinated Copolymers of MPEGMA. *Biomat. Adv.* **2023**, *153*, 213573.
(21) Han, X.; Boix, G.; Balcerzak, M.; Moriones, O. H.; Cano-Sarabia, M.; Cortés, P.; Bastús, N.; Puntes, V.; Llagostera, M.; Imaz, I.; Maspoch, D. Antibacterial Films Based on MOF Composites That Release Iodine Passively or Upon Triggering by Near-Infrared Light. *Adv. Funct. Mater.* **2022**, *32* (19), 2112902.
(22) Kim, H.; Song, Y.; Park, S.; Kim, Y.; Mun, H.; Kim, J.; Kim, S.; Lee, K. G.; Im, S. G. Synthesis of a Stretchable Polyampholyte Hydrophilic Film with Compositional Gradient for Long-Term Stable, Substrate-Independent Fouling-Resistant Coating. *Adv. Funct. Mater.* **2022**, *32* (26), 2113253.
(23) Kim, T. Y.; An, S.; Kim, Y.; Han, S. Y.; Lee, J.; Park, K.; Kim, S.; Park, J.; Kim, S. A.; Chung, J. J.; Cho, S.-W.; Seo, J. Lubricant-Infused Polymeric Interfaces: A Stretchable and Anti-Fouling Surface for Implantable Biomaterials. *Adv. Funct. Mater.* **2024**, *34* (14), 2312740.
(24) Yang, L.; Li, L.; Li, H.; Wang, T.; Ren, X.; Cheng, Y.; Li, Y.; Huang, Q. Layer-by-Layer Assembled Smart Antibacterial Coatings via Mussel-Inspired Polymerization and Dynamic Covalent Chemistry. *Adv. Healthc. Mater.* **2022**, *11* (12), 2200112.
(25) Chien, C.-H.; Chen, T.-L.; Wu, X.-Y.; Chen, Y.-C.; Lee, P.-Y.; Lin, L.-Y.; Wang, W.-L.; Hsueh, H.-Y. Bilayer Lubricant-Infused Particulate Films as Slippery Protective Coatings with Durable Anticorrosion and Antifouling Performance. *Adv. Mater. Interfaces.* **2022**, *9* (11), 2102144.
(26) Afonso, E.; Bayat, F.; Ladouceur, L.; Khan, S.; Martínez-Gómez, A.; Weitz, J. I.; Hosseinidoust, Z.; Tiemblo, P.; García, N.; Didar, T. F. Highly Stable Hierarchically Structured All-Polymeric Lubricant-Infused Films Prevent Thrombosis and Repel Multidrug-Resistant Pathogens. *ACS. Appl. Mater. Interfaces.* **2022**, *14* (48), 53535−53545.
(27) Hukum, K. O.; Caliskan, T. D.; Caykara, T.; Demirel, G. Toward Water and Oil Repellent Coating: Synthesis of Fluorinated Methacrylate-Glycidyl Methacrylate Copolymers. *ACS Omega.* **2024**, *9* (32), 34650−34660.
(28) Khlyustova, A.; Kirsch, M.; Yang, R. Amphiphilic Copolymer Thin Films with Short Fluoroalkyl Side Chains for Antibiofilm Properties at the Solid-Liquid-Air Interface. *ACS Sustain. Chem. Eng.* **2022**, *10* (48), 15699−15713.
(29) Liu, S.; Xu, L.; Yu, J.; Si, Y.; Ding, B. Amphiphobic, Thermostable, and Stretchable PTFE Nanofibrous Membranes with Breathable and Chemical-Resistant Performances for Protective Applications. *ACS Appl. Polym. Mater.* **2023**, *5* (2), 1464−1473.
(30) Abd-Elshafy, D. N.; Abdallah, H.; Nadeem, R.; Shalaby, M. S.; Shaban, A. M.; Bahgat, M. M. Production of Disinfective Coating Layer to Facial Masks Supplemented with Camellia Sinensis Extract. *Curr. Microbiol.* **2024**, *81* (7), 198.
(31) Vaz, J. M.; Taketa, T. B.; Hernandez-Montelongo, J.; Fiúza, L. M. C. G.; Rodrigues, C.; Beppu, M. M.; Vieira, R. S. Antibacterial Noncytotoxic Chitosan Coatings on Polytetrafluoroethylene Films by Plasma Grafting for Medical Device Applications. *J. Coat. Technol. Res.* **2022**, *19* (3), 829−838.
(32) Guo, Y.; Liu, Y.; Wang, D.; Li, Z.; Zhang, T.; Ding, K.; Wang, X.; Li, Q. Preparation and Performance of an Antibacterial Fiber Mat with High Breathability and Moisture Permeability Based on Electrospinning. *Fiber. Polym.* **2024**, *25* (6), 2093−2106.
(33) Xia, F.; Li, K.; Yang, J.; Chen, J.; Liu, X.; Gong, M.; Gu, J. DNase-Mimetics Based on Bimetallic Hierarchically Macroporous MOFs for the Efficient Inhibition of Bacterial Biofilm. *Sci. China. Mater.* **2024**, *67* (1), 343−354.
(34) Sinha, S. D.; Choudhuri, M.; Basu, T.; Gupta, D.; Datta, A. Decisive Role of Polymer-Bovine Serum Albumin Interactions in Biofilm Substrates on "Philicity" and Extracellular Polymeric Substances Composition. *Langmuir.* **2022**, *38* (6), 1966−1976.
(35) Ren, J.; Wang, X.; Bao, T.; Shen, X.; Yin, D.; Liang, Q.; Sun, S.; Xiao, C.; Deng, C. Piezoelectric Dual Network Dressing with Adaptive Electrical Stimulation for Diabetic Infected Wound Repair via Antibacterial, Antioxidant, Anti-Inflammation, and Angiogenesis. *Chem. Eng. J.* **2024**, *491*, 151801.
(36) Wu, H.; Zhi, C.; Chen, Y.; Zhou, X.; Wang, C.; Lam, R. H. W.; Qin, T.; Fu, G.; Xiong, Z.; Huang, K.; Lin, J.-H.; Shi, S.; Hu, J. Skin-like Breathable Wound Dressings with Antimicrobial and Hemostatic Properties. *Giant.* **2024**, *19*, 100300.
(37) Kim, Y.-I.; Kim, M.-W.; An, S.; Yarin, A. L.; Yoon, S. S. Reusable Filters Augmented with Heating Microfibers for Antibacterial and Antiviral Sterilization. *ACS Appl. Mater. Interfaces.* **2021**, *13* (1), 857−867.
(38) Li, S.; Guo, Z.; Zhang, H.; Li, X.; Li, W.; Liu, P.; Ren, Y.; Li, X. ABC Triblock Copolymers Antibacterial Materials Consisting of Fluoropolymer and Polyethylene Glycol Antifouling Block and Quaternary Ammonium Salt Sterilization Block. *ACS Appl. Bio. Mater.* **2021**, *4* (4), 3166−3177.
(39) Li, W.; Zhang, Y.; Ding, J.; Zhang, S.; Hu, T.; Li, S.; An, X.; Ren, Y.; Fu, Q.; Jiang, X.; Li, X. Temperature-Triggered Fluorocopolymer Aggregate Coating Switching from Antibacterial to Antifouling and Superhydrophobic Hemostasis. *Colloids. Surf. B Biointerfaces.* **2022**, *215*, 112496.
(40) Nguyen, N.; Lin, Z.-H.; Barman, S. R.; Korupalli, C.; Cheng, J.-Y.; Song, N.-X.; Chang, Y.; Mi, F.-L.; Song, H.-L.; Sung, H.-W.; Lin, Y.-J. Engineering an Integrated Electroactive Dressing to Accelerate Wound Healing and Monitor Noninvasively Progress of Healing. *Nano Energy.* **2022**, *99*, 107393.
(41) Sharma, A.; Panwar, V.; Mondal, B.; Prasher, D.; Bera, M. K.; Thomas, J.; Kumar, A.; Kamboj, N.; Mandal, D.; Ghosh, D. Electrical Stimulation Induced by a Piezo-Driven Triboelectric Nanogenerator and Electroactive Hydrogel Composite, Accelerate Wound Repair. *Nano Energy.* **2022**, *99*, 107419.
(42) Chen, B.; Lei, K.; Zhu, D.; Yang, C.; Sun, C.; Xiao, W.; Zheng, Z.; Wang, X. A Topological Stitching Strategy for Biocompatible Wet Adhesion Using Mussel-Inspired Polyurethane. *Adv. Mater. Interfaces.* **2021**, *8* (18), 2100657.
(43) Luo, R.; Liang, Y.; Yang, J.; Feng, H.; Chen, Y.; Jiang, X.; Zhang, Z.; Liu, J.; Bai, Y.; Xue, J.; Chao, S.; Xi, Y.; Liu, X.; Wang, E.; Luo, D.; Li, Z.; Zhang, J. Reshaping the Endogenous Electric Field to Boost Wound Repair via Electrogenerative Dressing. *Adv. Mater.* **2023**, *35* (16), 2208395.
(44) Ma, C.; Pang, H.; Liu, H.; Yan, Q.; Li, J.; Zhang, S. A Tough, Adhesive, Self-Healable, and Antibacterial Plant-Inspired Hydrogel Based on Pyrogallol-Borax Dynamic Cross-Linking. *J. Mater. Chem. B* **2021**, *9* (20), 4230−4240.
(45) Li, Y.; Fu, R.; Guan, Y.; Zhang, Z.; Yang, F.; Xiao, C.; Wang, Z.; Yu, P.; Hu, L.; Zhou, Z.; Ning, C. Piezoelectric Hydrogel for Prophylaxis and Early Treatment of Pressure Injuries/Pressure Ulcers. *ACS Biomater. Sci. Eng.* **2022**, *8* (7), 3078−3086.
(46) Maggay, I. V.; Venault, A.; Fang, C.-Y.; Yang, C.-C.; Hsu, C.-H.; Chou, C.-Y.; Ishihara, K.; Chang, Y. Zwitterionized Nanofibrous Poly(Vinylidene Fluoride) Membranes for Improving the Healing of Diabetic Wounds. *ACS Biomater. Sci. Eng.* **2021**, *7* (2), 562−576.
(47) Hillig, N.; Hamedy, A.; Koethe, M. Listeria Monocytogenes Detection on Food Contact Surfaces: Suitability of Different Swab Materials. *J. Consum. Prot. Food S.* **2023**, *18* (4), 443−450.
(48) Xie, C.; Yan, J.; Cao, S.; Liu, R.; Sun, B.; Xie, Y.; Qu, K.; Zhang, W.; Weng, Z.; Wang, Z. Bi-Layered Disulfiram-Loaded Fiber Membranes with Antibacterial Properties for Wound Dressing. *Appl. Biochem. Biotechnol.* **2022**, *194* (3), 1359−1372.
(49) Yuan, R.; Yang, N.; Fan, S.; Huang, Y.; You, D.; Wang, J.; Zhang, Q.; Chu, C.; Chen, Z.; Liu, L.; Ge, L. Biomechanical Motion-

https://doi.org/10.1021/acs.chemrev.4c00996
Chem. Rev. XXXX, XXX, XXX−XXX

Activated Endogenous Wound Healing through LBL Self-Powered Nanocomposite Repairer with PH-Responsive Anti-Inflammatory Effect. *Small.* **2021**, *17* (50), 2103997.
(50) Wang, A.; Shao, M.; Yang, F.; Shao, C.; Chen, C. Preparation and Properties of Antibacterial PVDF Composite Thin Films. *Eur. Polym. J.* **2021**, *160*, 110803.
(51) Yang, Y.; Ma, Y.; Wang, J.; You, L.; Zhang, R.; Meng, Q.; Zhong, S.; He, W.; Cui, X. Chitosan-Based Mussel-Inspired Hydrogel for Rapid Self-Healing and High Adhesion of Tissue Adhesion and Wound Dressings. *Carbohydr. Polym.* **2023**, *316*, 121083.
(52) Zhang, S.; Zhang, Q.; Lin, Q.; Yang, T.; Jiang, G.; Chen, F.; Ma, P. Large-Scale Manufacturing of Soluble Hemostatic Spacer Dressing with Excellent Mechanical and Comfortable Properties. *Mater. Des.* **2023**, *229*, 111896.
(53) An, X.; Li, W.; Zhang, Y.; Ding, J.; Zhang, S.; Hu, T.; Li, S.; Ren, Y.; Liu, P.; Li, X. Antibacterial and Superhydrophobic Hemostatic Properties of Fluorinated Random Copolymer Composite Nanocoatings. *Prog. Org. Coat.* **2022**, *168*, 106869.
(54) Venault, A.; Lin, K.-H.; Tang, S.-H.; Dizon, G. V.; Hsu, C.-H.; Maggay, I. V. B.; Chang, Y. Zwitterionic Electrospun PVDF Fibrous Membranes with a Well-Controlled Hydration for Diabetic Wound Recovery. *J. Membr. Sci.* **2020**, *598*, 117648.
(55) Shi, S.; Wu, H.; Zhi, C.; Yang, J.; Si, Y.; Ming, Y.; Fei, B.; Hu, J. A Skin-like Nanostructured Membrane for Advanced Wound Dressing. *Compos. B Eng.* **2023**, *250*, 110438.
(56) Abednejad, A.; Ghaee, A.; Morais, E. S.; Sharma, M.; Neves, B. M.; Freire, M. G.; Nourmohammadi, J.; Mehrizi, A. A. Polyvinylidene Fluoride-Hyaluronic Acid Wound Dressing Comprised of Ionic Liquids for Controlled Drug Delivery and Dual Therapeutic Behavior. *Acta Biomater.* **2019**, *100*, 142−157.
(57) Amini, F.; Semnani, D.; Karbasi, S.; Banitaba, S. N. A Novel Bilayer Drug-Loaded Wound Dressing of PVDF and PHB/Chitosan Nanofibers Applicable for Post-Surgical Ulcers. *Int. J. Polym. Mater. Polym. Biomater.* **2019**, *68* (13), 772−777.
(58) Ansarizadeh, M.; Haddadi, S. A.; Amini, M.; Hasany, M.; Ramazani SaadatAbadi, A. Sustained Release of CIP from TiO2-PVDF/Starch Nanocomposite Mats with Potential Application in Wound Dressing. *J. Appl. Polym. Sci.* **2020**, *137* (30), 48916.
(59) Liang, J.; Zeng, H.; Qiao, L.; Jiang, H.; Ye, Q.; Wang, Z.; Liu, B.; Fan, Z. 3D Printed Piezoelectric Wound Dressing with Dual Piezoelectric Response Models for Scar-Prevention Wound Healing. *ACS Appl. Mater. Interfaces.* **2022**, *14* (27), 30507−30522.
(60) Zheng, W. J.; Chen, Q.; Zou, W.; Fu, Z.; Li, Y.; Liu, Z.; Yan, J.; Yang, H.; Yang, F. Waterproof and Breathable Wound Dressing Composited By Expanded Polytetrafluoroethylene Backing and Hydrogel. *Macromol. Biosci.* **2022**, *22* (8), 2200131.
(61) Song, M.; Zhao, Q.; Wang, X.; Shi, C.; Hu, X.; Li, J. A Hydrophilic/Hydrophobic Janus Membrane Used as Wound Dressings with Enhanced Antibacterial Properties. *Fiber. Polym.* **2022**, *23* (9), 2511−2516.
(62) Dzhimak, S. S.; Malyshko, V. V.; Goryachko, A. I.; Sokolov, M. E.; Moiseev, A. V.; Basov, A. A. Adsorption of Silver Nanoparticles on Mono- and Polyfilament Fibers. *Nanotechnol. Russ.* **2019**, *14* (1), 48−54.
(63) Gómez-Gil, V.; Rodríguez, M.; García-Moreno Nisa, F.; Pérez-Köhler, B.; Pascual, G. Evaluation of Synthetic Reticular Hybrid Meshes Designed for Intraperitoneal Abdominal Wall Repair: Preclinical and in Vitro Behavior. *PLoS One.* **2019**, *14* (2), e0213005.
(64) Eickhoff, R. M.; Bolle, T.; Kossel, K.; Heise, D.; Kroh, A.; Lambertz, A.; Blaeser, A.; Gries, T.; Jockenhoevel, S.; Neumann, U. P.; Klink, C. D. Improved Biocompatibility of Profiled Sutures through Lower Macrophages Adhesion. *J. Biomed. Mater. Res. B Appl. Biomater.* **2019**, *107* (6), 1772−1778.
(65) Maeda, S.; Funatsu, T.; Kondoh, H.; Shibukawa, T.; Yokota, T.; Kainuma, S.; Toda, K.; Sawa, Y.; Taniguchi, K. Intermediate-Term Outcomes of Our Original Multiple-Knot Technique Using EPTFE Sutures for Anterior Mitral Leaflet Prolapse. *Surg. Today.* **2019**, *49* (4), 350−356.
(66) Jiao, L.; Xu, Q.; Tong, J.; Liu, S.; Hu, Y.; Guo, Q.; Wu, H.; Li, W.; Zhao, Q.; Chen, R. Facile Preparation of Pliable Super-amphiphobic Papers with High and Durable Liquid Repellency for Anti-Corrosion and Open Surface Microfluidics. *Appl. Surf. Sci.* **2022**, *606*, 154845.
(67) Rao, Z.-K.; Wang, T.-Q.; Li, Y.; Zhu, H.-Y.; Liu, Y.; Hao, J.-Y. Body Temperature Polymerization and in Situ Drug Encapsulation in Supercritical Carbon Dioxide. *Polym. Chem.* **2020**, *11* (42), 6821−6831.
(68) Zhang, S.; Yu, P.; Zhang, Y.; Ma, Z.; Teng, K.; Hu, X.; Lu, L.; Zhang, Y.; Zhao, Y.; An, Q. Remarkably Boosted Molecular Delivery Triggered by Combined Thermal and Flexoelectrical Field Dual Stimuli. *ChemistrySelect.* **2020**, *5* (22), 6715−6722.
(69) Liu, Z.; Nie, J.; Miao, B.; Li, J.; Cui, Y.; Wang, S.; Zhang, X.; Zhao, G.; Deng, Y.; Wu, Y.; Li, Z.; Li, L.; Wang, Z. L. Self-Powered Intracellular Drug Delivery by a Biomechanical Energy-Driven Triboelectric Nanogenerator. *Adv. Mater.* **2019**, *31* (12), 1807795.
(70) Sachan, R.; Sachan, A.; Lu, J.; Erdmann, D.; Zhang, J. Y.; Narayan, R. J. 3D Printing of Polytetrafluoroethylene Hollow Needles for Medical Applications. *JOM.* **2021**, *73* (12), 3798−3803.
(71) Tzafriri, A. R.; Muraj, B.; Garcia-Polite, F.; Salazar-Martín, A. G.; Markham, P.; Zani, B.; Spognardi, A.; Albaghdadi, M.; Alston, S.; Edelman, E. R. Balloon-Based Drug Coating Delivery to the Artery Wall Is Dictated by Coating Micro-Morphology and Angioplasty Pressure Gradients. *Biomaterials.* **2020**, *260*, 120337.
(72) Deng, J.; Wang, Z.; Zhou, Z.; Yu, W.; Li, X.; Song, Z.; Han, H.; Zhao, L. Transdermal Delivery of Fluoropolymer-Modified Microneedle Vaccines against Rabies Elicits Potent Humoral Immunity. *Chem. Eng. J.* **2023**, *474*, 145496.
(73) Fernandes, M. M.; Martins, P.; Correia, D. M.; Carvalho, E. O.; Gama, F. M.; Vazquez, M.; Bran, C.; Lanceros-Mendez, S. Magnetoelectric Polymer-Based Nanocomposites with Magnetically Controlled Antimicrobial Activity. *ACS Appl. Bio. Mater.* **2021**, *4* (1), 559−570.
(74) Lin, S.; Huang, X.; Guo, R.; Chen, S.; Lan, J.; Theato, P. UV-Triggered CO2-Responsive Behavior of Nanofibers and Their Controlled Drug Release Properties. *J. Polym. Sci. A Polym. Chem.* **2019**, *57* (14), 1580−1586.
(75) Mehta, P. P. Dry Powder Inhalers: Upcoming Platform Technologies for Formulation Development. *Ther. Delivery* **2019**, *10* (9), 551−554.
(76) Shikata, K.; Koshiba, Y.; Horike, S.; Ishida, K. P(VDF/TrFE) Thin-Film Piezoelectric Actuators Sealed Parylene C for Medical Micropumps. *Physica. Status. Solidi. A* **2023**, *220* (24), 2300250.
(77) Li, J.; Yan, Y.; Fang, Q.; Chen, Y.; Jing, Q.; Lee, H. K.; Wang, L.-N. Highly Flexible and Controllable Hierarchical MOF Membrane for Efficient Drug Release. *Sci. China. Mater.* **2024**, *67* (5), 1509−1520.
(78) Chen, S.; Wang, T.; Song, W.; Tang, Z.; Cao, Z.; Chen, H.; Lian, Y.; Hu, X.; Zheng, W.; Lian, H. A Novel Particulate Matter Sampling and Cell Exposure Strategy Based on Agar Membrane for Cytotoxicity Study. *Chemosphere.* **2022**, *300*, 134473.
(79) Fu, Q.; Liu, Y.; Liu, T.; Mo, J.; Zhang, W.; Zhang, S.; Luo, B.; Wang, J.; Qin, Y.; Wang, S.; Nie, S. Air-Permeable Cellulosic Triboelectric Materials for Self-Powered Healthcare Products. *Nano Energy.* **2022**, *102*, 107739.
(80) Yun, H.; Seo, J. H.; Yang, J. Development of Particle Filters for Portable Air Purifiers by Combining Melt-Blown and Polytetrafluoroethylene to Improve Durability and Performance. *Indoor Air.* **2024**, *2024* (1), 5055615.
(81) Kang, L.; Huang, S.; Qin, X.; Gao, X.; Li, Y.; Zhang, X. Ag Nanoparticles-Decorated PVDF Nanofiber/Net Membranes with Enhanced Filtration and Antibacterial Efficiency for Personal Protective Equipment. *ACS Appl. Nano. Mater.* **2024**, *7* (8), 9252−9261.
(82) Kang, L.; Ma, C.; Wang, J.; Gao, X.; An, G. PTFE/PVA-PVDF Conjugated Electrospun Nanofiber Membrane with Triboelectric Effect Used in Face Mask. *Fiber. Polym.* **2023**, *24* (6), 1975−1982.

https://doi.org/10.1021/acs.chemrev.4c00996
Chem. Rev. XXXX, XXX, XXX−XXX

(83) Su, C.; Zhang, L.; Zhang, Y.; Huang, X.; Ye, Y.; Xia, Y.; Gong, Z.; Qin, X.; Liu, Y.; Guo, S. P(VDF-TrFE)/BaTiO3 Nanofibrous Membrane with Enhanced Piezoelectricity for High PM0.3 Filtration and Reusable Face Masks. *ACS Appl. Mater. Interfaces.* **2023**, *15* (4), 5845−5855.
(84) Sun, X.; Yuan, J.; Zhu, Q.; Sun, Y.; Chen, H.; Liao, S.; Yan, J.; Cai, J.; Wei, Y.; Luo, L. Wood Fiber-Based Triboelectric Material with High Filtration Efficiency and Antibacterial Properties and Its Respiratory Monitoring in Mask. *ACS Omega.* **2024**, *9* (31), 33643−33651.
(85) Tang, L.; Wang, D.; Sun, S.; Cheng, Q.; Zhang, L.; Xia, W.; Zheng, J.; Cui, J.; Wang, Y.; Zhou, H. Fiber-in-Tube Electrifiable Structure for Virus Filtration Self-Generated Static Electricity by Vibration/Sound. *ACS Appl. Mater. Interfaces.* **2024**, *16* (19), 25160−25168.
(86) Luo, C.; Shao, Y.; Yu, H.; Ma, H.; Zhang, Y.; Gu, L.; Yin, B.; Yang, M. Preparation and Application of High Performance PVDF/PS Electrospinning Film-Based Triboelectric Nanogenerator. *Chem. Phys. Lett.* **2023**, *813*, 140276.
(87) Li, Y.; Cao, L.; Yin, X.; Si, Y.; Yu, J.; Ding, B. Ultrafine, Self-Crimp, and Electret Nano-Wool for Low-Resistance and High-Efficiency Protective Filter Media against PM0.3. *J. Colloid Interface Sci.* **2020**, *578*, 565−573.
(88) Singh, S.; Shauloff, N.; Sharma, C. P.; Shimoni, R.; Arnusch, C. J.; Jelinek, R. Carbon Dot-Polymer Nanoporous Membrane for Recyclable Sunlight-Sterilized Facemasks. *J. Colloid Interface Sci.* **2021**, *592*, 342−348.
(89) Thomberg, T.; Ramah, P.; Lust, A.; Nerut, J.; Koppel, M.; Romann, T.; Palm, R.; Månsson, M.; March, N. M. F.; Junninen, H.; Külaviir, M.; Paiste, P.; Kirsimäe, K.; Punapart, M.; Viru, L.; Merits, A.; Lust, E. Preparation of Nanofibrous Materials Activated with Metal Clusters for Active and Long-Lasting Air Filters. *Sep. Purif. Technol.* **2022**, *288*, 120697.
(90) He, R.; Li, J.; Chen, M.; Zhang, S.; Cheng, Y.; Ning, X.; Wang, N. Tailoring Moisture Electroactive Ag/Zn@cotton Coupled with Electrospun PVDF/PS Nanofibers for Antimicrobial Face Masks. *J. Hazard. Mater.* **2022**, *428*, 128239.
(91) Van Goethem, C.; Op de Beeck, D.; Ilyas, A.; Thijs, M.; Koeckelberghs, G.; Aerts, P. E. M.; Vankelecom, I. F. J. Ultra-Thin and Highly Porous PVDF-Filters Prepared via Phase Inversion for Potential Medical (COVID-19) and Industrial Use. *J. Membr. Sci.* **2021**, *639*, 119710.
(92) Al-Attabi, R.; She, F.; Zhao, S.; Dumée, L. F.; Schütz, J. A.; Xing, W.; Zhong, Z.; Kong, L. Durable and Comfortable Electrospun Nanofiber Membranes for Face Mask Applications. *Sep. Purif. Technol.* **2023**, *322*, 124370.
(93) Wu, J.; Rao, Y.; Lin, B.; Zhou, H.; Zhou, Q.; Xu, C.; Feng, S.; Zhong, Z.; Xing, W. Design of PTFE/PP Multilayer Composite Membrane as Mask Filter Layer with Steady Filtration Efficiency and High Dust Holding Capacity. *Sep. Purif. Technol.* **2023**, *326*, 124782.
(94) Tan, N. P. B.; Paclijan, S. S.; Ali, H. N. M.; Hallazgo, C. M. J. S.; Lopez, C. J. F.; Ebora, Y. C. Solution Blow Spinning (SBS) Nanofibers for Composite Air Filter Masks. *ACS Appl. Nano Mater.* **2019**, *2* (4), 2475−2483.
(95) Wang, S.; Liu, Y.; Xu, M.; Hu, F.; Yu, Q.; Wang, L. Polymersomes as Virus-Surrogate Particles for Evaluating the Performance of Air Filter Materials. *Giant.* **2022**, *10*, 100104.
(96) Ray, S. S.; Soni, R.; Huyen, D. T. T.; Ravi, S.; Myung, S.; Lee, C. Y.; Kwon, Y.-N. Chemical Engineering of Electrospun Nanofibrous-Based Three-Layered Nonwoven Polymeric Protective Mask for Enhanced Performance. *J. Appl. Polym. Sci.* **2023**, *140* (10), e53584.
(97) Kim, H.; Lee, S.; Shin, Y. R.; Choi, Y.-N.; Yoon, J.; Ryu, M.; Lee, J. W.; Lee, H. Durable Superhydrophobic Poly(Vinylidene Fluoride) (PVDF)-Based Nanofibrous Membranes for Reusable Air Filters. *ACS Appl. Polym. Mater.* **2022**, *4* (1), 338−347.
(98) Shen, H.; Zhou, Z.; Wang, H.; Chen, J.; Zhang, M.; Han, M.; Shen, Y.; Shuai, D. Photosensitized Electrospun Nanofibrous Filters for Capturing and Killing Airborne Coronaviruses under Visible Light Irradiation. *Environ. Sci. Technol.* **2022**, *56* (7), 4295−4304.
(99) Kang, D. H.; Kim, N. K.; Kang, H. W. Electrostatic Charge Retention in PVDF Nanofiber-Nylon Mesh Multilayer Structure for Effective Fine Particulate Matter Filtration for Face Masks. *Polymers.* **2021**, *13* (19), 3235.
(100) Toptas, A.; Calisir, M. D.; Gungor, M.; Kilic, A. Enhancing Filtration Performance of Submicron Particle Filter Media through Bimodal Structural Design. *Polym. Eng. Sci.* **2024**, *64* (2), 901−912.
(101) Liu, H.; Li, D.; Shen, Y.; Deng, B. Preparation and Characterization of PTFE/PI Nanofiber Composite Assembled Sponges. *Fiber. Polym.* **2021**, *22* (3), 664−675.
(102) Kang, L.; Ma, C.; Wang, J.; Gao, X.; An, G. PTFE/PVA-PVDF Conjugated Electrospun Nanofiber Membrane with Triboelectric Effect Used in Face Mask. *Fiber. Polym.* **2023**, *24* (6), 1975−1982.
(103) Lin, S.; Wang, S.; Yang, W.; Chen, S.; Xu, Z.; Mo, X.; Zhou, H.; Duan, J.; Hu, B.; Huang, L. Trap-Induced Dense Monocharged Perfluorinated Electret Nanofibers for Recyclable Multifunctional Healthcare Mask. *ACS Nano* **2021**, *15* (3), 5486−5494.
(104) Kim, M.; Lee, G.; Jang, S.; Yu, D. I.; Kim, S. M. Reusable and Transparent Impaction-Based Filter with Micro Apertured Multiscale Polymeric Stencil for Particulate Matter Capture. *Macromol. Mater. Eng.* **2024**, *309* (2), 2300285.
(105) Shen, H.; Zhou, Z.; Wang, H.; Zhang, M.; Han, M.; Durkin, D. P.; Shuai, D.; Shen, Y. Development of Electrospun Nanofibrous Filters for Controlling Coronavirus Aerosols. *Environ. Sci. Technol. Lett.* **2021**, *8* (7), 545−550.
(106) Mills, R.; Vogler, R. J.; Bernard, M.; Concolino, J.; Hersh, L. B.; Wei, Y.; Hastings, J. T.; Dziubla, T.; Baldridge, K. C.; Bhattacharyya, D. Aerosol Capture and Coronavirus Spike Protein Deactivation by Enzyme Functionalized Antiviral Membranes. *Commun. Mater.* **2022**, *3* (1), 34.
(107) Nongnual, T.; Kaewpirom, S.; Damnong, N.; Srimongkol, S.; Benjalersyarnon, T. A Simple and Precise Estimation of Water Sliding Angle by Monitoring Image Brightness: A Case Study of the Fluid Repellency of Commercial Face Masks. *ACS Omega.* **2022**, *7* (15), 13178−13188.
(108) Nageh, H.; Emam, M. H.; Ali, F.; Abdel Fattah, N. F.; Taha, M.; Amin, R.; Kamoun, E. A.; Loutfy, S. A.; Kasry, A. Zinc Oxide Nanoparticle-Loaded Electrospun Polyvinylidene Fluoride Nanofibers as a Potential Face Protector against Respiratory Viral Infections. *ACS Omega.* **2022**, *7* (17), 14887−14896.
(109) Ullah, S.; Ullah, A.; Lee, J.; Jeong, Y.; Hashmi, M.; Zhu, C.; Joo, K. Il; Cha, H. J.; Kim, I. S. Reusability Comparison of Melt-Blown vs Nanofiber Face Mask Filters for Use in the Coronavirus Pandemic. *ACS Appl. Nano. Mater.* **2020**, *3* (7), 7231−7241.
(110) Mariello, M.; Qualtieri, A.; Mele, G.; De Vittorio, M. Metal-Free Multilayer Hybrid PENG Based on Soft Electrospun/-Sprayed Membranes with Cardanol Additive for Harvesting Energy from Surgical Face Masks. *ACS Appl. Mater. Interfaces.* **2021**, *13* (17), 20606−20621.
(111) Leung, W. W.-F.; Sun, Q. Charged PVDF Multilayer Nanofiber Filter in Filtering Simulated Airborne Novel Coronavirus (COVID-19) Using Ambient Nano-Aerosols. *Sep. Purif. Technol.* **2020**, *245*, 116887.
(112) Muensterman, D. J.; Cahuas, L.; Titaley, I. A.; Schmokel, C.; De la Cruz, F. B.; Barlaz, M. A.; Carignan, C. C.; Peaslee, G. F.; Field, J. A. Per- and Polyfluoroalkyl Substances (PFAS) in Facemasks: Potential Source of Human Exposure to PFAS with Implications for Disposal to Landfills. *Environ. Sci. Technol. Lett.* **2022**, *9* (4), 320−326.
(113) K C, P. B.; Maharjan, A.; Acharya, M.; Lee, D.; Kusma, S.; Gautam, R.; Kwon, J.-T.; Kim, C.; Kim, K.; Kim, H.; Heo, Y. Polytetrafluorethylene Microplastic Particles Mediated Oxidative Stress, Inflammation, and Intracellular Signaling Pathway Alteration in Human Derived Cell Lines. *Sci. Total Environ.* **2023**, *897*, 165295.
(114) Hao, X.; Nie, L.; Zhu, X.; Zeng, G.; Liu, C.; Teng, Z.; Liu, H.; Yue, Y.; Yu, X.; Wang, T. High-Resolution X-Ray Image from

https://doi.org/10.1021/acs.chemrev.4c00996
Chem. Rev. XXXX, XXX, XXX−XXX

Copper-Based Perovskite Hybrid Polymer. *ACS Appl. Mater. Interfaces.* **2024**, *16* (22), 29210−29216.
(115) Zeqiri, B.; Baker, C.; Pounder, A.; Sarno, D.; Rajagopal, S. Large-Area Pyroelectric-Based Differential Detector for Medical Ultrasound Computed Tomography. *IEEE Sens. J.* **2023**, *23* (16), 18276−18291.
(116) Sepesy, M.; Fugate, B.; Duval, C. E. Amine-Functionalized Membrane Adsorbers to Purify Copper from Acidic Solutions. *ACS Appl. Polym. Mater.* **2022**, *4* (5), 3034−3044.
(117) Saidzhonov, B. M.; Yorov, K. E.; Yuan, P.; Nematulloev, S.; Karluk, A. A.; Ahmad, T.; Mohammed, O. F.; Bakr, O. M.; Bayindir, M. Multimaterial Fibers with Nanoemitters Enable Conformal X-Ray Imaging with 3D Printed and Woven Scintillators. *ACS Mater. Lett.* **2024**, *6* (5), 1779−1789.
(118) Mil'man, I. I.; S, A. I.; A, R. M.; T, A. N.; B, N. E.; A, E. N.; P, M. A. Polytetrafluorethylene in High-Dose EPR Dosimetry for Monitoring Radiation Technologies. *Russ. J. Nondestruct. Test.* **2019**, *55*, 868−874.
(119) Hu, Y.; Han, C.; Huo, X.; Cao, X.; Chen, Y.; Cao, Z.; Xu, Y.; Tao, L.; Wu, Z. Flexible Sensor for Real-Time Monitoring of Motion Artifacts in Magnetic Resonance Imaging. *ACS Sens.* **2024**, *9* (5), 2614−2621.
(120) Kolouchova, K.; Groborz, O.; Slouf, M.; Herynek, V.; Parmentier, L.; Babuka, D.; Cernochova, Z.; Koucky, F.; Sedlacek, O.; Hruby, M.; Hoogenboom, R.; Van Vlierberghe, S. Thermoresponsive Triblock Copolymers as Widely Applicable 19F Magnetic Resonance Imaging Tracers. *Chem. Mater.* **2022**, *34* (24), 10902−10916.
(121) Kolouchova, K.; Cernochova, Z.; Groborz, O.; Herynek, V.; Koucky, F.; Jaksa, R.; Benes, J.; Slouf, M.; Hruby, M. Multiresponsive Fluorinated Polymers as a Theranostic Platform Using 19F MRI. *Eur. Polym. J.* **2022**, *175*, 111381.
(122) Kolouchova, K.; Groborz, O.; Cernochova, Z.; Skarkova, A.; Brabek, J.; Rosel, D.; Svec, P.; Starcuk, Z.; Slouf, M.; Hruby, M. Thermo- and ROS-Responsive Self-Assembled Polymer Nanoparticle Tracers for 19F MRI Theranostics. *Biomacromolecules.* **2021**, *22* (6), 2325−2337.
(123) Chen, Y.; Tillman, B.; Go, C.; Cho, S. K.; Clark, W. W.; Hur, T. B.; Ding, Y.; Chun, Y. A Novel Customizable Stent Graft That Contains a Stretchable EPTFE with a Laser-Welded Nitinol Stent. *J. Biomed. Mater. Res. B Appl. Biomater.* **2019**, *107* (4), 911−923.
(124) Chon, M. K.; Shin, D. H.; Jung, S. J.; Park, H. J.; Kim, J. H. A Percutaneous Catheter Solution as a Spacer for Regurgitant Heart Valve Disease. *Coatings.* **2021**, *11* (8), 926.
(125) Li, Y.; Yuan, L.; Ming, H.; Li, X.; Tang, L.; Zhang, J.; Wang, R.; Wang, G.; Jiang, Y.; Li, Z.; Luo, F.; Li, J.; Tan, H.; Fu, Q. Enhanced Hydrolytic Resistance of Fluorinated Silicon-Containing Polyether Urethanes. *Biomacromolecules.* **2020**, *21* (4), 1460−1470.
(126) Dong, L.; Closson, A. B.; Oglesby, M.; Escobedo, D.; Han, X.; Nie, Y.; Huang, S.; Feldman, M. D.; Chen, Z.; Zhang, J. X. J. In Vivo Cardiac Power Generation Enabled by an Integrated Helical Piezoelectric Pacemaker Lead. *Nano Energy.* **2019**, *66*, 104085.
(127) Kim, S. H.; Kim, J. W.; Jang, Y. J. Radiologic Findings of Complicated Alloplastic Implants in the Nasal Dorsum. *Clin. Exp. Otorhinolaryngol.* **2021**, *14* (3), 321−327.
(128) Khalifehzadeh, R.; Ratner, B. D. Trifluoromethyl-Functionalized Poly(Lactic Acid): A Fluoropolyester Designed for Blood Contact Applications. *Biomater. Sci.* **2019**, *7* (9), 3764−3778.
(129) Koguchi, R.; Jankova, K.; Hayasaka, Y.; Kobayashi, D.; Amino, Y.; Miyajima, T.; Kobayashi, S.; Murakami, D.; Yamamoto, K.; Tanaka, M. Understanding the Effect of Hydration on the Bio-Inert Properties of 2-Hydroxyethyl Methacrylate Copolymers with Small Amounts of Amino- or/and Fluorine-Containing Monomers. *ACS Biomater. Sci. Eng.* **2020**, *6* (5), 2855−2866.
(130) Liu, Z.; Ma, Y.; Ouyang, H.; Shi, B.; Li, N.; Jiang, D.; Xie, F.; Qu, D.; Zou, Y.; Huang, Y.; Li, H.; Zhao, C.; Tan, P.; Yu, M.; Fan, Y.; Zhang, H.; Wang, Z. L.; Li, Z. Transcatheter Self-Powered Ultrasensitive Endocardial Pressure Sensor. *Adv. Funct. Mater.* **2019**, *29* (3), 1807560.
(131) Wang, G.; Gao, C.; Xiao, B.; Zhang, J.; Jiang, X.; Wang, Q.; Guo, J.; Zhang, D.; Liu, J.; Xie, Y.; Shu, C.; Ding, J. Research and Clinical Translation of Trilayer Stent-Graft of Expanded Polytetrafluoroethylene for Interventional Treatment of Aortic Dissection. *Regen. Biomater.* **2022**, *9*, rbac049.
(132) Marlena, J.; Tan, J. K. S.; Lin, Z.; Li, D. X.; Zhao, B.; Leo, H. L.; Kim, S.; Yap, C. H. Monolithic Polymeric Porous Superhydrophobic Material with Pneumatic Plastron Stabilization for Functionally Durable Drag Reduction in Blood-Contacting Biomedical Applications. *NPG Asia Mater.* **2021**, *13* (1), 58.
(133) Shi, H.; Wang, J.; Vorvolakos, K.; White, K.; Duraiswamy, N. Pre-Clinical Evaluation of Surface Coating Performance in Guidewire Surrogates: Potential Implications for Coated Interventional Surgical Devices. *J. Biomater. Appl.* **2020**, *34* (7), 928−941.
(134) Wang, B.; Yang, P.; Ding, Y.; Qi, H.; Gao, Q.; Zhang, C. Improvement of the Biocompatibility and Potential Stability of Chronically Implanted Electrodes Incorporating Coating Cell Membranes. *ACS Appl. Mater. Interfaces.* **2019**, *11* (9), 8807−8817.
(135) Gómez-Gil, V.; Rodríguez, M.; García-Moreno Nisa, F.; Pérez-Köhler, B.; Pascual, G. Evaluation of Synthetic Reticular Hybrid Meshes Designed for Intraperitoneal Abdominal Wall Repair: Preclinical and in Vitro Behavior. *PLoS One.* **2019**, *14* (2), e0213005.
(136) Qu, X.; Cheng, S.; Liu, Y.; Hu, Y.; Shan, Y.; Luo, R.; Weng, S.; Li, H.; Niu, H.; Gu, M.; Fan, Y.; Shi, B.; Liu, Z.; Hua, W.; Li, Z.; Wang, Z. L. Bias-Free Cardiac Monitoring Capsule. *Adv. Mater.* **2024**, *36* (33), 2402457.
(137) Abdollahi, S.; Stephens, E. D.; Uy, M. A.; Fatehi Hassanabad, A.; Fedak, P. W. M.; Badv, M. Super-Repellent and Flexible Lubricant-Infused Bacterial Nanocellulose Membranes with Superior Antithrombotic, Antibacterial, and Fatigue Resistance Properties. *ACS Appl. Mater. Interfaces.* **2023**, *15* (22), 26417−26430.
(138) Wan, X.; Chen, P.; Xu, Z.; Mo, X.; Jin, H.; Yang, W.; Wang, S.; Duan, J.; Hu, B.; Luo, Z.; Huang, L.; Zhou, J. Hybrid-Piezoelectret Based Highly Efficient Ultrasonic Energy Harvester for Implantable Electronics. *Adv. Funct. Mater.* **2022**, *32* (24), 2200589.
(139) Ai, Y.; Gu, Z.-X.; Wang, P.; Tang, Y.-Y.; Chen, X.-G.; Lv, H.-P.; Li, P.-F.; Jiang, Q.; Xiong, R.-G.; Zhang, J.-J.; Zhang, H.-Y. Biodegradable Ferroelectric Molecular Plastic Crystal HOCH2(CF2)-7CH2OH Structurally Inspired by Polyvinylidene Fluoride. *Adv. Mater.* **2024**, *36* (35), 2405981.
(140) Nzulumike, A. N. O.; Thormann, E. Fibrin Adsorption on Cardiovascular Biomaterials and Medical Devices. *ACS Appl. Bio. Mater.* **2023**, *6* (7), 2667−2676.
(141) Shui, Z.; Chen, Y.; Zhao, W.; Chen, X. Flexible Aluminum-Air Battery Based on Ionic Liquid-Gel Polymer Electrolyte. *Langmuir.* **2022**, *38* (35), 10791−10798.
(142) Zhang, S.; Liang, X.; Gadd, G. M.; Zhao, Q. Advanced Titanium Dioxide-Polytetrafluorethylene (TiO2-PTFE) Nanocomposite Coatings on Stainless Steel Surfaces with Antibacterial and Anti-Corrosion Properties. *Appl. Surf. Sci.* **2019**, *490*, 231−241.
(143) Petersmann, S.; Spoerk, M.; Van De Steene, W.; Üçal, M.; Wiener, J.; Pinter, G.; Arbeiter, F. Mechanical Properties of Polymeric Implant Materials Produced by Extrusion-Based Additive Manufacturing. *J. Mech. Behav. Biomed. Mater.* **2020**, *104*, 103611.
(144) Wang, H.; Klosterhalfen, B.; Müllen, A.; Otto, T.; Dievernich, A.; Jockenhövel, S. Degradation Resistance of PVDF Mesh in Vivo in Comparison to PP Mesh. *J. Mech. Behav. Biomed. Mater.* **2021**, *119*, 104490.
(145) Eickhoff, R.; Heise, D.; Kroh, A.; Helmedag, M.; Klinge, U.; Neumann, U. P.; Klink, C. D.; Lambertz, A. Improved Tissue Integration of a New Elastic Intraperitoneal Stoma Mesh Prosthesis. *J. Biomed. Mater. Res. B Appl. Biomater.* **2020**, *108* (5), 2250−2257.
(146) Li, Z.; Giarto, J.; Zhang, J.; Kulkarni, N.; Mahalingam, E.; Klipstine, W.; Turng, L.-S. Anti-Thrombotic Poly(AAm-Co-NaAMPS)-Xanthan Hydrogel-Expanded Polytetrafluoroethylene (EPTFE) Vascular Grafts with Enhanced Endothelialization and Hemocompatibility Properties. *Biomater. Adv.* **2023**, *154*, 213625.
(147) Tan, J. K. S.; Chen, E. S. A.; Dong, Y.; Fang, H.; Koh, C. Y.; Kini, R. M.; Kim, S.; Leo, H. L.; Yap, C. H. Antithrombotic and Flow

https://doi.org/10.1021/acs.chemrev.4c00996
Chem. Rev. XXXX, XXX, XXX−XXX

Drag-Reducing Material for Blood-Contacting Medical Devices. *Adv. Mater. Interfaces.* **2023**, *10* (10), 2202270.
(148) Pourbafrani, M.; Azimi, S.; Yaghoobi Nia, N.; Zendehdel, M.; Abolhasani, M. M. The Effect of Electrospinning Parameters on Piezoelectric PVDF-TrFE Nanofibers: Experimental and Simulation Study. *Energies.* **2023**, *16* (1), 37.
(149) Nai, G. A.; Medina, D. A. L.; Martelli, C. A. T.; de Oliveira, M. S. C.; Portelinha, M. J. S.; Henriques, B. C.; Caldeira, I. D.; Almeida, M. de C.; Eller, L. K. W.; Neto, F. V. de O.; Marques, M. E. A. Does Washing Medical Devices before and after Use Decrease Bacterial Contamination?: An In Vitro Study. *Medicine.* **2021**, *100* (13), e25285.
(150) Park, A.; Song, Y.; Yi, E.; Duy Nguyen, B. T.; Han, D.; Sohn, E.; Park, Y.; Jung, J.; Lee, Y. M.; Cho, Y. H.; Kim, J. F. Blood Oxygenation Using Fluoropolymer-Based Artificial Lung Membranes. *ACS Biomater. Sci. Eng.* **2020**, *6* (11), 6424−6434.
(151) Han, D. J.; Heo, H. J.; Park, I. J.; Kang, H. S.; Lee, S. G.; Lee, S.-B.; Lee, J.-C.; Sohn, E.-H. Fluorinated Methacrylate-Grafted P(VDF-CTFE) and Albumin Layers for Reducing Fibrinogen Adsorption. *ACS Appl. Polym. Mater.* **2020**, *2* (2), 178−188.
(152) Jin, F.; Li, T.; Yuan, T.; Du, L.; Lai, C.; Wu, Q.; Zhao, Y.; Sun, F.; Gu, L.; Wang, T.; Feng, Z.-Q. Physiologically Self-Regulated, Fully Implantable, Battery-Free System for Peripheral Nerve Restoration. *Adv. Mater.* **2021**, *33* (48), 2104175.
(153) Egorov, I. M.; Kiselev, S. V.; Makarov, A. G.; Klimova, N. S. Physical Analysis of the Creep of Polypropylene and Polyvinylidene Fluoride Threads for Medical Purposes. *Fibre Chemistry.* **2021**, *53* (2), 127−131.
(154) Kang, T.-W.; Kim, S. H.; Kim, M.; Cho, E.; Lee, S.-J. Highly Flexible, Hydrophobic, and Large Area Plasma-Polymer-Fluorocarbon/Cu/SiNx Transparent Thin Film Heater and Thermotherapy Pad Application. *Plasma Process. Polym.* **2020**, *17* (4), 1900188.
(155) Cheng, B.; Inoue, Y.; Ishihara, K. Surface Functionalization of Polytetrafluoroethylene Substrate with Hybrid Processes Comprising Plasma Treatment and Chemical Reactions. *Colloids Surf. B Biointerfaces.* **2019**, *173*, 77−84.
(156) Patel, M.; Jamiolkowski, M. A.; Vejendla, A.; Bentley, V.; Malinauskas, R. A.; Lu, Q. Effect of Temperature on Thrombogenicity Testing of Biomaterials in an In Vitro Dynamic Flow Loop System. *ASAIO Journal.* **2023**, *69* (6), 576.
(157) Wang, G.; Feng, Y.; Gao, C.; Zhang, X.; Wang, Q.; Zhang, J.; Zhang, H.; Wu, Y.; Li, X.; Wang, L.; Fu, Y.; Yu, X.; Zhang, D.; Liu, J.; Ding, J. Biaxial Stretching of Polytetrafluoroethylene in Industrial Scale to Fabricate Medical EPTFE Membrane with Node-Fibril Microstructure. *Regen. Biomater.* **2023**, *10*, rbad056.
(158) Sengupta, A.; Das, S.; Dasgupta, S.; Sengupta, P.; Datta, P. Flexible Nanogenerator from Electrospun PVDF-Polycarbazole Nanofiber Membranes for Human Motion Energy-Harvesting Device Applications. *ACS Biomater. Sci. Eng.* **2021**, *7* (4), 1673−1685.
(159) Tang, X.-Y.; Liu, Z.; Liu, W.-Y.; Pu, X.-Q.; Liu, L.-Y.; Chen, S.-K.; Xie, R.; Ju, X.-J.; Wang, W.; Chu, L.-Y. Moisture-Responsive Actuators Based on Hyaluronic Acid with Biocompatibility and Fast Response as Smart Breather Valves. *ACS Appl. Polym. Mater.* **2023**, *5* (1), 815−827.
(160) Kalasin, S.; Sangnuang, P.; Khownarumit, P.; Tang, I. M.; Surareungchai, W. Salivary Creatinine Detection Using a Cu(I)/Cu(II) Catalyst Layer of a Supercapacitive Hybrid Sensor: A Wireless IoT Device To Monitor Kidney Diseases for Remote Medical Mobility. *ACS Biomater. Sci. Eng.* **2020**, *6* (10), 5895−5910.
(161) Pavliuk, G.; Pavlov, D.; Mitsai, E.; Vitrik, O.; Mironenko, A.; Zakharenko, A.; Kulinich, S. A.; Juodkazis, S.; Bratskaya, S.; Zhizhchenko, A.; Kuchmizhak, A. Ultrasensitive SERS-Based Plasmonic Sensor with Analyte Enrichment System Produced by Direct Laser Writing. *Nanomaterials.* **2020**, *10* (1), 49.
(162) Pham Ba, V. A.; Cho, D.; Hong, S. Nafion-Radical Hybrid Films on Carbon Nanotube Transistors for Monitoring Antipsychotic Drug Effects on Stimulated Dopamine Release. *ACS Appl. Mater. Interfaces.* **2019**, *11* (10), 9716−9723.
(163) Li, G.-Y.; Li, J.; Li, Z.-J.; Zhang, Y.-P.; Zhang, X.; Wang, Z.-J.; Han, W.-P.; Sun, B.; Long, Y.-Z.; Zhang, H.-D. Hierarchical PVDF-HFP/ZnO Composite Nanofiber-Based Highly Sensitive Piezoelectric Sensor for Wireless Workout Monitoring. *Adv. Compos. Hybrid Mater.* **2022**, *5* (2), 766−775.
(164) Alotaibi, A. Flexible 3D Force Sensor Based on Polymer Nanocomposite for Soft Robotics and Medical Applications. *Sensors.* **2024**, *24* (6), 1859.
(165) Park, K.; Kim, S.; Jo, Y.; Park, J.; Kim, I.; Hwang, S.; Lee, Y.; Kim, S. Y.; Seo, J. Lubricant Skin on Diverse Biomaterials with Complex Shapes via Polydopamine-Mediated Surface Functionalization for Biomedical Applications. *Bioact. Mater.* **2023**, *25*, 555−568.
(166) Paul, D. C.; Ngeow, Y. F.; Yap, S. F.; Dony, J. F.; Avoi, R.; Mohammad, R.; Ng, H. F. Concentrated Specimen Smear Microscopy Utilising a Polymer Membrane Sandwich Filtration Vessel for the Detection of Acid-Fast Bacilli in Health Facilities in Sabah, East Malaysia. *Tuberculosis.* **2022**, *133*, 102183.
(167) Su, L.; Xiong, Q.; Zhu, Y.; Zi, Y. A Liquid-Solid Contact Electrification Based All-Optical Liquid Flow Sensor for Microfluidic Analysis in Biomedical Applications. *Adv. Funct. Mater.* **2022**, *32* (45), 2207096.
(168) Huang, A.; Zhu, Y.; Peng, S.; Tan, B.; Peng, X. Improved Energy Harvesting Ability of Single-Layer Binary Fiber Nanocomposite Membrane for Multifunctional Wearable Hybrid Piezoelectric and Triboelectric Nanogenerator and Self-Powered Sensors. *ACS Nano* **2024**, *18* (1), 691−702.
(169) Lin, Y.; Long, Z.; Liang, S.; Zhong, T.; Xing, L. A Wearable Exhaling-Oxygen-Sensing Mask Based on Piezoelectric/Gas-Sensing Coupling Effect for Real-Time Monitoring and Uploading Lung Disease Information. *J. Phys. D Appl. Phys.* **2022**, *55* (22), 224001.
(170) Jiao, H.; Lin, X.; Xiong, Y.; Han, J.; Liu, Y.; Yang, J.; Wu, S.; Jiang, T.; Wang, Z. L.; Sun, Q. Thermal Insulating Textile Based Triboelectric Nanogenerator for Outdoor Wearable Sensing and Interaction. *Nano Energy.* **2024**, *120*, 109134.
(171) Chun, S.; Son, W.; Kim, H.; Lim, S. K.; Pang, C.; Choi, C. Self-Powered Pressure- and Vibration-Sensitive Tactile Sensors for Learning Technique-Based Neural Finger Skin. *Nano Lett.* **2019**, *19* (5), 3305−3312.
(172) Shiroud Heidari, B.; Dodda, J. M.; El-Khordagui, L. K.; Focarete, M. L.; Maroti, P.; Toth, L.; Pacilio, S.; El-Habashy, S. E.; Boateng, J.; Catanzano, O.; Sahai, N.; Mou, L.; Zheng, M. Emerging Materials and Technologies for Advancing Bioresorbable Surgical Meshes. *Acta Biomater.* **2024**, *184*, 1−21.
(173) Gong, X.; Ji, Y.; Liu, X.; Yu, J.; Zhang, S.; Ding, B. Biomimetic and Durably Superhydrophobic Nanofibrous Membranes for High-Performance Waterproof and Breathable Textiles. *Adv. Funct. Mater.* **2024**, *34* (26), 2316030.
(174) Ryu, C. H.; Cho, J. Y.; Jeong, S. Y.; Eom, W.; Shin, H.; Hwang, W.; Jhun, J. P.; Hong, S. Do; Kim, T.; Jeong, I. W.; Sung, T. H. Wearable Piezoelectric Yarns with Inner Electrodes for Energy Harvesting and Signal Sensing. *Adv. Mater. Technol.* **2022**, *7* (6), 2101138.
(175) Li, X.-P.; Wu, M.-M.; Peng, H.-K.; Zhang, X.-F.; Wang, Y. T.; Li, T.-T.; Lou, C.-W.; Lin, J.-H. Hierarchically Structured Polyvinylidene Fluoride Core-Shell Composite Yarn Based on Electrospinning Coating Method to Improve Piezoelectricity. *Polym. Adv. Technol.* **2022**, *33* (5), 1457−1467.
(176) Wan, X.; Shen, Y.; Luo, T.; Xu, M.; Cong, H.; Chen, C.; Jiang, G.; He, H. All-Textile Piezoelectric Nanogenerator Based on 3D Knitted Fabric Electrode for Wearable Applications. *ACS Sens.* **2024**, *9* (6), 2989−2998.
(177) Lv, M.; Wang, L.; Liu, J.; Kong, F.; Ling, A.; Wang, T.; Wang, Q. Surface Energy, Hardness, and Tribological Properties of Carbon-Fiber/Polytetrafluoroethylene Composites Modified by Proton Irradiation. *Tribol. Int.* **2019**, *132*, 237−243.
(178) Shao, G.; Su, C.; Shi, C.; Xu, Z.; Ye, M.; Chen, N.; Yu, R.; Liu, X. Y. Highly Flexible and High Energy Density Fiber Supercapacitors Based upon Spiral Silk Composite Membranes Encapsulation. *Electrochim. Acta* **2022**, *404*, 139611.

https://doi.org/10.1021/acs.chemrev.4c00996
Chem. Rev. XXXX, XXX, XXX−XXX

(179) Wu, Y.; Ma, Y.; Zheng, H.; Ramakrishna, S. Piezoelectric Materials for Flexible and Wearable Electronics: A Review. *Mater. Des.* **2021**, *211*, 110164.
(180) Chen, Y.; Tong, W.; Wang, X.; Zhang, P.; Wang, S.; Zhang, Y. MXene Effectively Enhances the Electron-Withdrawing (EW) Ability and Dielectric Properties of PVDF-TrFE Nanofibers for Triboelectric Nanogenerators. *Colloids Surf. A Physicochem. Eng. Asp.* **2023**, *664*, 131172.
(181) Zhou, W.; Gong, X.; Li, Y.; Si, Y.; Zhang, S.; Yu, J.; Ding, B. Environmentally Friendly Waterborne Polyurethane Nanofibrous Membranes by Emulsion Electrospinning for Waterproof and Breathable Textiles. *Chem. Eng. J.* **2022**, *427*, 130925.
(182) Ng, J. L.; Putra, V. D. L.; Knothe Tate, M. L. In Vitro Biocompatibility and Biomechanics Study of Novel, Microscopy Aided Designed and ManufacturEd (MADAME) Materials Emulating Natural Tissue Weaves and Their Intrinsic Gradients. *J. Mech. Behav. Biomed. Mater.* **2020**, *103*, 103536.
(183) Qin, S.; Wang, Z.; Ren, Y.; Yu, Y.; Xiao, Y.; Chen, J.; Zhang, J.; Zhang, S.; Sun, C.; Xiao, J.; Zhang, L.; Hu, W.; Yang, H. A Meltblown Cloth Reinforced Partially Fluorinated Solid Polymer Electrolyte for Ultrastable Lithium Metal Batteries. *Nano Energy.* **2024**, *119*, 109075.
(184) Mahanty, B.; Maity, K.; Sarkar, S.; Mandal, D. Human Skin Interactive Self-Powered Piezoelectric e-Skin Based on PVDF/MWCNT Electrospun Nanofibers for Non-Invasive Health Care Monitoring. *Mater. Today Proc.* **2020**, *21*, 1964−1968.
(185) Salvadores Fernandez, C.; Jaufuraully, S.; Bagchi, B.; Chen, W.; Datta, P.; Gupta, P.; David, A. L.; Siassakos, D.; Desjardins, A.; Tiwari, M. K. A Triboelectric Nanocomposite for Sterile Sensing, Energy Harvesting, and Haptic Diagnostics in Interventional Procedures from Surgical Gloves. *Adv. Healthc. Mater.* **2023**, *12* (17), 2202673.
(186) Fountain, J. N.; Hawker, M. J.; Hartle, L.; Wu, J.; Montanari, V.; Sahoo, J. K.; Davis, L. M.; Kaplan, D. L.; Kumar, K. Towards Non-Stick Silk: Tuning the Hydrophobicity of Silk Fibroin Protein. *ChemBioChem.* **2022**, *23* (22), e202200429.
(187) Yu, K.; Yao, Y.; Zhang, K.; Sheng, J.; Liao, H.; Zhai, Y.; Wang, X.; Li, Z.; Yan, Z. Multifunctional Poly(Vinylidene Fluoride)/Polyurethane/Titanium Dioxide Nanofibrous Membranes with Enhanced Ultraviolet-Proof, Resistant to Blood Penetration, and Waterproof Performance. *New J. Chem.* **2023**, *47* (23), 11188−11195.
(188) Galante, A. J.; Haghanifar, S.; Romanowski, E. G.; Shanks, R. M. Q.; Leu, P. W. Superhemophobic and Antivirofouling Coating for Mechanically Durable and Wash-Stable Medical Textiles. *ACS Appl. Mater. Interfaces.* **2020**, *12* (19), 22120−22128.
(189) Kondratov, A. P.; Lozitskaya, A. V.; Volinsky, A. A. Production and Properties of Electrically Conductive Polymer Composites Reinforced with Cotton Threads. *J. Appl. Polym. Sci.* **2024**, *141* (21), No. e55410.
(190) Jin, H.; Nayeem, M. O. G.; Lee, S.; Matsuhisa, N.; Inoue, D.; Yokota, T.; Hashizume, D.; Someya, T. Highly Durable Nanofiber-Reinforced Elastic Conductors for Skin-Tight Electronic Textiles. *ACS Nano* **2019**, *13* (7), 7905−7912.
(191) Avdeeva, E.; Petkevich, A.; Mikhalko, A.; Shumskaya, A.; Sychik, S.; Dudchik, N.; Anisovich, M.; Yarmolenko, M.; Halinouski, N.; Rogachev, A.; Agabekov, V. Modification of Nonwoven Polymer Materials for Increasing of Their Filtration and Antibacterial Properties. *Polym. Eng. Sci.* **2023**, *63* (11), 3831−3842.
(192) Kang, S.; Hou, S.; Chen, X.; Yu, D.-G.; Wang, L.; Li, X.; Williams, G. R. Energy-Saving Electrospinning with a Concentric Teflon-Core Rod Spinneret to Create Medicated Nanofibers. *Polymers.* **2020**, *12* (10), 2421.
(193) Ibtehaj, K.; Jumali, M. H. Hj.; Al-Bati, S.; Ooi, P. C.; Al-Asbahi, B. A.; Ahmed, A. A. A. Effect of β-Chain Alignment Degree on the Performance of Piezoelectric Nanogenerator Based on Poly-(Vinylidene Fluoride) Nanofiber. *Macromol. Res.* **2022**, *30* (3), 172−182.
(194) Shi, S.; Si, Y.; Li, Z.; Meng, S.; Zhang, S.; Wu, H.; Zhi, C.; Io, W.-F.; Ming, Y.; Wang, D.; Fei, B.; Huang, H.; Hao, J.; Hu, J. An Intelligent Wearable Filtration System for Health Management. *ACS Nano* **2023**, *17* (7), 7035−7046.
(195) Chen, Q.; Wang, A.; Yang, D.; Wei, X.; Zhang, L.; Wu, Z.; Wang, L.; Qin, Y. Largely Improving the Output Performance of Stretchable Triboelectric Nanogenerators via Thermo-Compressive Technology. *Small.* **2024**, *20* (12), 2307070.
(196) Liao, Y.; Fatehi, P.; Liao, B. Surface Properties of Membrane Materials and Their Role in Cell Adhesion and Biofilm Formation of Microalgae. *Biofouling.* **2023**, *39* (8), 879−895.
(197) Zhang, H.; Cao, Y.; Zhen, Q.; Hu, J.-J.; Cui, J.-Q.; Qian, X.-M. Facile Preparation of PET/PA6 Bicomponent Microfilament Fabrics with Tunable Porosity for Comfortable Medical Protective Clothing. *ACS Appl. Bio. Mater.* **2022**, *5* (7), 3509−3518.
(198) Zhou, W.; Yu, X.; Li, Y.; Jiao, W.; Si, Y.; Yu, J.; Ding, B. Green-Solvent-Processed Fibrous Membranes with Water/Oil/Dust-Resistant and Breathable Performances for Protective Textiles. *ACS Appl. Mater. Interfaces.* **2021**, *13* (1), 2081−2090.
(199) Liagkouridis, I.; Awad, R.; Schellenberger, S.; Plassmann, M. M.; Cousins, I. T.; Benskin, J. P. Combined Use of Total Fluorine and Oxidative Fingerprinting for Quantitative Determination of Side-Chain Fluorinated Polymers in Textiles. *Environ. Sci. Technol. Lett.* **2022**, *9* (1), 30−36.
(200) Gariya, N.; Kumar, P.; Prasad, B.; Singh, T. Soft Pneumatic Actuator with an Embedded Flexible Polymeric Piezoelectric Membrane for Sensing Bending Deformation. *Mater. Today Commun.* **2023**, *35*, 105910.
(201) Khan, A.; Rashid, M.; Grabher, G.; Hossain, G. Autonomous Triboelectric Smart Textile Sensor for Vital Sign Monitoring. *ACS Appl. Mater. Interfaces.* **2024**, *16* (24), 31807−31816.
(202) Liu, C.; Wang, W.; Li, Y.; Cui, F.; Xie, C.; Zhu, L.; Shan, B. PMWCNT/PVDF Ultrafiltration Membranes with Enhanced Anti-fouling Properties Intensified by Electric Field for Efficient Blood Purification. *J. Membr. Sci.* **2019**, *576*, 48−58.
(203) Wang, Q.; Zhu, L.; Ismail, N.; Zhou, Q.; He, T.; Zhou, Y.; Wang, Z.; Cui, Z.; Tavajohi, N. Annealing of Grain-like Poly (Vinylidene Fluoride-Trifluoroethylene) Membranes with a Single-Crystalline Electroactive Phase and High Anti-Fouling Activity. *J. Membr. Sci.* **2022**, *644*, 120089.
(204) Yi, E.; Kang, H. S.; Lim, S. M.; Heo, H. J.; Han, D.; Kim, J. F.; Park, A.; Choi, D. H.; Park, Y.-I.; Park, H.; Cho, Y. H.; Sohn, E.-H. Superamphiphobic Blood-Repellent Surface Modification of Porous Fluoropolymer Membranes for Blood Oxygenation Applications. *J. Membr. Sci.* **2022**, *648*, 120363.
(205) Zhang, M.; Wang, X.; Xue, Y.; Li, J.; Wang, J.; Fang, C.; Zhu, L. Robust and Scalable In Vitro Surface Mineralization of Inert Polymers with a Rationally Designed Molecular Bridge. *ACS Appl. Mater. Interfaces.* **2023**, *15* (6), 8730−8741.
(206) Zhang, K.; Ma, F.; Wu, Y. Membrane Adsorbers with Ultrahigh Metal-Organic Framework Loading for High Flux Selective Separations to Isomer. *Sep. Purif. Technol.* **2023**, *323*, 124462.
(207) Ren, J.; Zhang, Y.; Wang, C. Understanding Adsorption Behavior of Polysorbate-20 to Sterile Filters in Therapeutic Proteins Final Filtration Process. *Biotechnol. Prog.* **2024**, *40* (2), No. e3401.
(208) Uebele, S.; Goetz, T.; Ulbricht, M.; Schiestel, T. Mixed-Matrix Membrane Adsorbers for the Simultaneous Removal of Different Pharmaceutical Micropollutants from Water. *ACS Appl. Polym. Mater.* **2022**, *4* (3), 1705−1716.
(209) Zhang, L.; Yang, J.; Yan, Y.; Zhang, W. Effect of Functional Groups on Protein Adsorption Performance of Membrane Adsorbers. *Separations.* **2023**, *10* (3), 211.
(210) Salahshoori, I.; Montazeri, N.; Yazdanbakhsh, A.; Golriz, M.; Farhadniya, R.; Khonakdar, H. A. Insights into the Adsorption Properties of Mixed Matrix Membranes (Pebax 1657-g-Chitosan-PVDF-Bovine Serum Albumin@ZIF-CO3−1) for the Antiviral COVID-19 Treatment Drugs Remdesivir and Nirmatrelvir: An In Silico Study. *ACS Appl. Mater. Interfaces.* **2023**, *15* (26), 31185−31205.

https://doi.org/10.1021/acs.chemrev.4c00996
Chem. Rev. XXXX, XXX, XXX−XXX

(211) Martino, M.; Taligrot, H.; Cordier, C.; Moulin, P. Supercritical Fluid Treatment of Organic Membranes. *J. Membr. Sci.* **2022**, *661*, 120892.
(212) Kiselev, V. M.; Kislyakov, I. M.; Bagrov, I. V.; Starodubtsev, A. M.; Gogoleva, N. G.; Wang, J. Singlet Oxygen Generation under Optical Excitation of Polytetrafluoroethylene. *React. Funct. Polym.* **2023**, *193*, 105755.
(213) Xi, M.; Yong, J.; Chen, F.; Yang, Q.; Hou, X. A Femtosecond Laser-Induced Superhygrophobic Surface: Beyond Superhydrophobicity and Repelling Various Complex Liquids. *RSC Adv.* **2019**, *9* (12), 6650−6657.
(214) Barylski, A.; Aniołek, K.; Swinarew, A. S.; Kaptacz, S.; Gabor, J.; Waśkiewicz, Z.; Stanula, A. Novel Organic Material Induced by Electron Beam Irradiation for Medical Application. *Polymers.* **2020**, *12* (2), 306.
(215) Vaz, J. M.; Taketa, T. B.; Hernandez-Montelongo, J.; Fiúza, L. M. C. G.; Rodrigues, C.; Beppu, M. M.; Vieira, R. S. Antibacterial Noncytotoxic Chitosan Coatings on Polytetrafluoroethylene Films by Plasma Grafting for Medical Device Applications. *J. Coat. Technol. Res.* **2022**, *19* (3), 829−838.
(216) Ippili, S.; Kim, B.; Jella, V.; Jung, J.-S.; Vuong, V.-H.; Yoon, S.-G. Antireflective, Transparent, Water-Resistant, and Antibacterial Zn-Doped Silicon Oxide Thin Films for Touchscreen-Based Display Applications. *ACS Sustain. Chem. Eng.* **2022**, *10* (6), 2136−2147.
(217) Li, S.; Zhao, F.; Bai, Y.; Ye, Z.; Feng, Z.; Liu, X.; Gao, S.; Pang, X.; Sun, M.; Zhang, J.; Dong, A.; Wang, W.; Huang, P. Slippery Liquid-Infused Microphase Separation Surface Enables Highly Robust Anti-Fouling, Anti-Corrosion, Anti-Icing and Anti-Scaling Coating on Diverse Substrates. *Chem. Eng. J.* **2022**, *431*, 133945.
(218) Chiu, C.-Y.; Yen, T.-J.; Chang, Y. Intelligent Sterilizable Self-Cleaning Membranes Triggered by Sustainable Counterion-Induced Bacteria Killing/Releasing Procedure. *Chem. Eng. J.* **2022**, *440*, 135798.
(219) Kubo, Y.; Sonohara, Y.; Uemura, S.; Saito, Y. High-Energy Electron-Irradiated Fluorinated Ethylene Polypropylene Copolymer Coatings on Al Substrates for Enhanced Metal Adhesion and Protection. *ACS Appl. Nano. Mater.* **2022**, *5* (5), 6757−6769.
(220) Liu, Y.; Munisso, M. C.; Mahara, A.; Kambe, Y.; Yamaoka, T. Anti-Platelet Adhesion and in Situ Capture of Circulating Endothelial Progenitor Cells on EPTFE Surface Modified with Poly(2-Methacryloyloxyethyl Phosphorylcholine) (PMPC) and Hemocompatible Peptide 1 (HCP-1). *Colloids Surf. B Biointerfaces.* **2020**, *193*, 111113.
(221) Chen, R.; Wan, Y.; Wu, W.; Yang, C.; He, J.-H.; Cheng, J.; Jetter, R.; Ko, F. K.; Chen, Y. A Lotus Effect-Inspired Flexible and Breathable Membrane with Hierarchical Electrospinning Micro/Nanofibers and ZnO Nanowires. *Mater. Des.* **2019**, *162*, 246−248.
(222) Saito, H.; Furuta, M.; Matsugaki, A.; Nakano, T.; Oishi, M.; Okazaki, M. Radiation-Resistant Properties of Cross-Linking PTFE for Medical Use. *Polym. Bull.* **2019**, *76* (12), 6111−6122.
(223) Fan, X.; Zhao, L.; Ling, Q.; Liu, J.; Gu, H. Mussel-Induced Nano-Silver Antibacterial, Self-Healing, Self-Adhesive, Anti-Freezing, and Moisturizing Dual-Network Organohydrogel Based on SA-PBA/PVA/CNTs as Flexible Wearable Strain Sensors. *Polymer.* **2022**, *256*, 125270.
(224) Gómez-Gil, V.; Rodríguez, M.; García-Moreno Nisa, F.; Pérez-Köhler, B.; Pascual, G. Evaluation of Synthetic Reticular Hybrid Meshes Designed for Intraperitoneal Abdominal Wall Repair: Preclinical and in Vitro Behavior. *PLoS One.* **2019**, *14* (2), e0213005.
(225) Klinge, U.; Dievernich, A.; Tolba, R.; Klosterhalfen, B.; Davies, L. CD68+ Macrophages as Crucial Components of the Foreign Body Reaction Demonstrate an Unconventional Pattern of Functional Markers Quantified by Analysis with Double Fluorescence Staining. *J. Biomed. Mater. Res. B Appl. Biomater.* **2020**, *108* (8), 3134−3146.
(226) Kopeć, K.; Ryżko, A.; Major, R.; Plutecka, H.; Więcek, J.; Pikus, G.; Trzciński, J. W.; Kalinowska, A.; Ciach, T. Polymerization of L-Tyrosine, l-Phenylalanine, and 2-Phenylethylamine as a Versatile Method of Surface Modification for Implantable Medical Devices. *ACS Omega.* **2022**, *7* (43), 39234−39249.
(227) Kopeć, K.; Podgórski, R.; Ciach, T.; Wojasiński, M. System for Patterning Polydopamine and VAPG Peptide on Polytetrafluoroethylene and Biodegradable Polyesters for Patterned Growth of Smooth Muscle Cells In Vitro. *ACS Omega.* **2023**, *8* (24), 22055−22066.
(228) Lee, J. C.; In, S. H.; Lee, J. H.; Park, C. H.; Kim, C. S. Electrospun Polycaprolactone/Polyvinylidene Fluoride Composite Nanofibers for Fabricating Artificial Conduits for Ureteral Stricture Treatment. *ACS Appl. Nano Mater.* **2023**, *6* (24), 22757−22766.
(229) Dumitrescu, L. N.; Neacsu, P.; Necula, M. G.; Bonciu, A.; Marascu, V.; Cimpean, A.; Moldovan, A.; Rotaru, A.; Dinca, V.; Dinescu, M. Induced Hydrophilicity and In Vitro Preliminary Osteoblast Response of Polyvinylidene Fluoride (PVDF) Coatings Obtained via MAPLE Deposition and Subsequent Thermal Treatment. *Molecules.* **2020**, *25* (3), 582.
(230) Ruiz-Diaz, D.; Manjarrez-Marmolejo, J.; Diaz-Ruiz, A.; Ríos, C.; Olayo, M. G.; Olayo, R.; Cruz, G. J.; Salgado-Ceballos, H.; Mendez-Aramenta, M.; Morales-Corona, J. Development and Characterization of Electrodes Coated with Plasma-Synthesized Polypyrrole Doped with Iodine, Implanted in the Rat Brain Subthalamic Nucleus. *Polymers.* **2024**, *16* (6), 823.
(231) Egorov, I. M.; Kozlov, A. A. Mathematical Modeling of Relaxation Properties of Textile Elastomers Used in Implantology. *Fibre Chem.* **2023**, *55* (2), 85−87.
(232) Xiong, Y.; Shen, Y.; Tian, L.; Hu, Y.; Zhu, P.; Sun, R.; Wong, C.-P. A Flexible, Ultra-Highly Sensitive and Stable Capacitive Pressure Sensor with Convex Microarrays for Motion and Health Monitoring. *Nano Energy.* **2020**, *70*, 104436.
(233) Lee, M. C.; Lin, G. Y.; Hoe, Z. Y.; Pan, C. T. Development of Piezoelectric Silk Sensors Doped with Graphene for Biosensing by Near-Field Electrospinning. *Sensors.* **2022**, *22* (23), 9131.
(234) Lu, Q.; Chen, H.; Zeng, Y.; Xue, J.; Cao, X.; Wang, N.; Wang, Z. Intelligent Facemask Based on Triboelectric Nanogenerator for Respiratory Monitoring. *Nano Energy.* **2022**, *91*, 106612.
(235) Kalasin, S.; Sangnuang, P.; Surareungchai, W. Wearable Triboelectric Sensors with Self-Powered Energy: Multifunctional Laser-Engraved Electrets to Activate Satellite Communication for Life-Emergency Alert in Pandemics. *ACS Appl. Electron. Mater.* **2021**, *3* (12), 5383−5392.
(236) Wang, L.; Li, J.; Tao, J.; Hu, M.; Dai, Z. Sensitive Self-Powered Particles Detection Based on Cumulative Triboelectric Charging. *Nano Energy.* **2021**, *89*, 106393.
(237) Yin, S.; Liu, X.; Kobayashi, Y.; Nishina, Y.; Nakagawa, R.; Yanai, R.; Kimura, K.; Miyake, T. A Needle-Type Biofuel Cell Using Enzyme/Mediator/Carbon Nanotube Composite Fibers for Wearable Electronics. *Biosens. Bioelectron.* **2020**, *165*, 112287.
(238) Veeralingam, S.; Badhulika, S. Bi2S3/PVDF/Ppy-Based Freestanding, Wearable, Transient Nanomembrane for Ultrasensitive Pressure, Strain, and Temperature Sensing. *ACS Appl. Bio. Mater.* **2021**, *4* (1), 14−23.
(239) Huang, C.-Y.; Chiu, C.-W. Facile Fabrication of a Stretchable and Flexible Nanofiber Carbon Film-Sensing Electrode by Electrospinning and Its Application in Smart Clothing for ECG and EMG Monitoring. *ACS Appl. Electron. Mater.* **2021**, *3* (2), 676−686.
(240) Ning, C.; Cheng, R.; Jiang, Y.; Sheng, F.; Yi, J.; Shen, S.; Zhang, Y.; Peng, X.; Dong, K.; Wang, Z. L. Helical Fiber Strain Sensors Based on Triboelectric Nanogenerators for Self-Powered Human Respiratory Monitoring. *ACS Nano* **2022**, *16* (2), 2811−2821.
(241) Lou, M.; Abdalla, I.; Zhu, M.; Yu, J.; Li, Z.; Ding, B. Hierarchically Rough Structured and Self-Powered Pressure Sensor Textile for Motion Sensing and Pulse Monitoring. *ACS Appl. Mater. Interfaces.* **2020**, *12* (1), 1597−1605.
(242) Gupta, S.; Bhunia, R.; Fatma, B.; Maurya, D.; Singh, D.; Prateek; Gupta, R.; Priya, S.; Gupta, R. K.; Garg, A. Multifunctional and Flexible Polymeric Nanocomposite Films with Improved

https://doi.org/10.1021/acs.chemrev.4c00996
Chem. Rev. XXXX, XXX, XXX−XXX

Ferroelectric and Piezoelectric Properties for Energy Generation Devices. *ACS Appl. Energy Mater.* **2019**, *2* (9), 6364−6374.
(243) Shen, X. Q.; Li, M. D.; Ma, J. P.; Shen, Q. D. Skin-Inspired Pressure Sensor with MXene/P(VDF-TrFE-CFE) as Active Layer for Wearable Electronics. *Nanomaterials.* **2021**, *11* (3), 716.
(244) Baek, S.; Lee, Y.; Baek, J.; Kwon, J.; Kim, S.; Lee, S.; Strunk, K.-P.; Stehlin, S.; Melzer, C.; Park, S.-M.; Ko, H.; Jung, S. Spatiotemporal Measurement of Arterial Pulse Waves Enabled by Wearable Active-Matrix Pressure Sensor Arrays. *ACS Nano* **2022**, *16* (1), 368−377.
(245) Yu, D.; Zheng, Z.; Liu, J.; Xiao, H.; Huangfu, G.; Guo, Y. Superflexible and Lead-Free Piezoelectric Nanogenerator as a Highly Sensitive Self-Powered Sensor for Human Motion Monitoring. *Nanomicro Lett.* **2021**, *13* (1), 117.
(246) Roy, K.; Jana, S.; Mallick, Z.; Ghosh, S. K.; Dutta, B.; Sarkar, S.; Sinha, C.; Mandal, D. Two-Dimensional MOF Modulated Fiber Nanogenerator for Effective Acoustoelectric Conversion and Human Motion Detection. *Langmuir.* **2021**, *37* (23), 7107−7117.
(247) Bai, C.; Wang, Z.; Yang, S.; Cui, X.; Li, X.; Yin, Y.; Zhang, M.; Wang, T.; Sang, S.; Zhang, W.; Zhang, H. Wearable Electronics Based on the Gel Thermogalvanic Electrolyte for Self-Powered Human Health Monitoring. *ACS Appl. Mater. Interfaces* **2021**, *13* (31), 37316−37322.
(248) Xin, Y.; Liu, T.; Xu, Y.; Zhu, J.; Lin, T.; Zhou, X. Development of Respiratory Monitoring and Actions Recognition Based on a Pressure Sensor with Multi-Arch Structures. *Sens. Actuators A Phys.* **2019**, *296*, 357−366.
(249) Thiyagarajan, S.; Vallejo, M. A.; Cerón, P.; Gomez-Solis, C.; Wiechers, C.; Montes, E.; Navarro, R.; Sosa, M. A. Thermoluminescence of Cu-Doped Li2B4O7+PTFE Annealed by Graphene Exposed to X-Rays and Gamma Radiation. *J. Mol. Eng. Mater.* **2020**, *08* (03n04), 2050005.
(250) Almohimeed, I.; Ono, Y. Ultrasound Measurement of Skeletal Muscle Contractile Parameters Using Flexible and Wearable Single-Element Ultrasonic Sensor. *Sensors.* **2020**, *20* (13), 3616.
(251) Ippili, S.; Jella, V.; Eom, J.-H.; Kim, J.; Hong, S.; Choi, J.-S.; Tran, V.-D.; Van Hieu, N.; Kim, Y.-J.; Kim, H.-J.; Yoon, S.-G. An Eco-Friendly Flexible Piezoelectric Energy Harvester That Delivers High Output Performance Is Based on Lead-Free MASnI3 Films and MASnI3-PVDF Composite Films. *Nano Energy.* **2019**, *57*, 911−923.
(252) Xu, L.; Zhang, Z.; Gao, F.; Zhao, X.; Xun, X.; Kang, Z.; Liao, Q.; Zhang, Y. Self-Powered Ultrasensitive Pulse Sensors for Noninvasive Multi-Indicators Cardiovascular Monitoring. *Nano Energy.* **2021**, *81*, 105614.
(253) Zhang, D.; Zhang, R.; Sun, J.; Zhang, J.; Zhao, Q.; He, H.; Huang, H.; Yang, L.; Xu, Y. Flexible Piezoresistive Sensor Constructing from ILs/MWCNTs/PVDF Ternary Composite for High Sensitivity and Wide Detection Range. *Sens. Actuators A Phys.* **2024**, *367*, 115037.
(254) Wang, X.; Feng, Z.; Xia, Y.; Zhang, G.; Wang, L.; Chen, L.; Wu, Y.; Yang, J.; Wang, Z. L. Flexible Pressure Sensor for High-Precision Measurement of Epidermal Arterial Pulse. *Nano Energy.* **2022**, *102*, 107710.
(255) Lin, Z.; Sun, C.; Liu, W.; Fan, E.; Zhang, G.; Tan, X.; Shen, Z.; Qiu, J.; Yang, J. A Self-Powered and High-Frequency Vibration Sensor with Layer-Powder-Layer Structure for Structural Health Monitoring. *Nano Energy.* **2021**, *90*, 106366.
(256) Ram, N.; Kaarthik, J.; Singh, S.; Palneedi, H.; Prasad, P. D.; Venkateswarlu, A. Boosting Energy Harvesting of Fully Flexible Magnetoelectric Composites of PVDF-AlN and NiO-Decorated Carbon Nanofibers. *Ceram. Int.* **2024**, *50* (10), 17465−17474.
(257) Lu, X.; Chen, Y.; Zhang, Y.; Cheng, J.; Teng, K.; Chen, Y.; Shi, J.; Wang, D.; Wang, L.; You, S.; Feng, Z.; An, Q. Piezoionic High Performance Hydrogel Generator and Active Protein Absorber via Microscopic Porosity and Phase Blending. *Adv. Mater.* **2024**, *36* (2), 2307875.
(258) Li, Q.; Li, Y.; Gao, Q.; Jiang, C.; Tian, Q.; Ma, C.; Shi, C. Real-Time Monitoring of Isothermal Nucleic Acid Amplification on a Smartphone by Using a Portable Electrochemical Device for Home-Testing of SARS-CoV-2. *Anal. Chim. Acta* **2022**, *1229*, 340343.
(259) Gunasekhar, R.; Anand Prabu, A. Polyvinylidene Fluoride/Aromatic Hyperbranched Polyester 2nd Generation Based Triboelectric Sensor for Polysomnographic and Health Monitoring Applications. *Sens. Actuators A Phys.* **2023**, *355*, 114311.
(260) Zhao, H.; Chen, H.; Yang, M.; Li, Y. Facile Fabrication of Poly (Diallyldimethyl Ammonium Chloride)/Ti3C2Tx/Poly (Vinylidene Fluoride) 3D Hollow Fiber Membrane Flexible Humidity Sensor and Its Application in the Monitoring of Health-Related Physiological Activity. *Sens. Actuators B Chem.* **2023**, *374*, 132773.
(261) Gong, Z.; Qin, J.; Liu, D.; Lv, S.; Du, Y.; Zhang, T.; Ke, Q. Flexible PVDF/SiC/FeCl3 Nanofiber Membrane Generators with Synergistically Enhanced Piezoelectricity. *Nano Energy.* **2024**, *122*, 109290.
(262) Qian, X.; Tian, B.; Zhang, J.; Fan, Z.; Ren, Y.; Pan, Y.; Guo, C.; Wang, C.; Kong, L.; Yu, H.; Huang, J. An Intelligent Insole Based on Wide-Range Flexible Pressure Sensor. *AIP Adv.* **2024**, *14* (3), 035128.
(263) Meng, K.; Xiao, X.; Liu, Z.; Shen, S.; Tat, T.; Wang, Z.; Lu, C.; Ding, W.; He, X.; Yang, J.; Chen, J. Kirigami-Inspired Pressure Sensors for Wearable Dynamic Cardiovascular Monitoring. *Adv. Mater.* **2022**, *34* (36), 2202478.
(264) Luo, J.; Lu, W.; Jang, D.; Zhang, Q.; Meng, W.; Wells, A.; Alavi, A. H. Millifluidic Nanogenerator Lab-on-a-Chip Device for Blood Electrical Conductivity Monitoring at Low Frequency. *Adv. Mater.* **2024**, *36* (32), 2403568.
(265) Siddiqui, A.; Das, S.; Bhattacharjee, M. Nanofillers Embedded Flexible Piezoelectric Polymer Sensor Pad for Robotic and Human Finger Tap Analysis. *Sens. Actuators A Phys.* **2024**, *375*, 115503.
(266) Shi, Y.; Yang, P.; Lei, R.; Liu, Z.; Dong, X.; Tao, X.; Chu, X.; Wang, Z. L.; Chen, X. Eye Tracking and Eye Expression Decoding Based on Transparent, Flexible and Ultra-Persistent Electrostatic Interface. *Nat. Commun.* **2023**, *14* (1), 3315.
(267) Kumaki, D.; Motoshima, Y.; Higuchi, F.; Sato, K.; Sekine, T.; Tokito, S. Unobstructive Heartbeat Monitoring of Sleeping Infants and Young Children Using Sheet-Type PVDF Sensors. *Sensors.* **2023**, *23* (22), 9252.
(268) Bi, S.; Jin, W.; Han, X.; Cao, X.; He, Z.; Asare-Yeboah, K.; Jiang, C. Ultra-Fast-Responsivity with Sharp Contrast Integrated Flexible Piezo Electrochromic Based Tactile Sensing Display. *Nano Energy.* **2022**, *102*, 107629.
(269) Meng, Y.; Cheng, J.; Zhou, C. Superhydrophobic and Stretchable Carbon Nanotube/Thermoplastic Urethane-Based Strain Sensor for Human Motion Detection. *ACS Appl. Nano Mater.* **2023**, *6* (7), 5871−5878.
(270) Cao, Z.; Xu, X.; He, C.; Peng, Z. Electrospun Nanofibers Hybrid Wrinkled Micropyramidal Architectures for Elastic Self-Powered Tactile and Motion Sensors. *Nanomaterials.* **2023**, *13* (7), 1181.
(271) Jansen, A. K.; Ludwig, S.; Malter, W.; Sauerwald, A.; Hachenberg, J.; Pahmeyer, C.; Wegmann, K.; Rudroff, C.; Karapanos, L.; Radosa, J.; Trageser, N.; Eichler, C. Tacks vs. Sutures: A Biomechanical Analysis of Sacral Bony Fixation Methods for Laparoscopic Apical Fixations in the Porcine Model. *Arch. Gynecol. Obstet.* **2022**, *305* (3), 631−639.
(272) Abullais, S. S.; Alosman, S. S.; Alqahtani, S. M.; Khan, A. A.; Nahid, R.; Basheer, S. A.; Jameel, A. S. Effect of Common Mouthwashes on Mechanical Properties of Suture Materials Used in Dental Surgeries: A Laboratory Experiment. *Polymers.* **2022**, *14* (12), 2439.
(273) Huang, Y.; Cadet, E. R.; King, M. W.; Cole, J. H. Comparison of the Mechanical Properties and Anchoring Performance of Polyvinylidene Fluoride and Polypropylene Barbed Sutures for Tendon Repair. *J. Biomed. Mater. Res. B Appl. Biomater.* **2022**, *110* (10), 2258−2265.
(274) Biswal, D. K.; Moharana, B. R.; Mohapatra, T. P. Bending Response Optimization of an Ionic Polymer-Metal Composite

https://doi.org/10.1021/acs.chemrev.4c00996
Chem. Rev. XXXX, XXX, XXX−XXX

Actuator Using Orthogonal Array Method. *Mater. Today Proc.* **2022**, *49*, 1550−1555.
(275) Liang, Y.; Zhang, H.; Lin, Z.; Ma, S.; Ren, L.; Ren, L. High Specific Surface Area Pd/Pt Electrode-Based Ionic Polymer-Metal Composite for High-Performance Biomimetic Actuation. *ACS Sustain. Chem. Eng.* **2022**, *10* (8), 2645−2652.
(276) Sun, B.; Sun, Y.; Han, S.; Zhang, R.; Wang, X.; Meng, C.; Ji, T.; Sun, C.; Ren, N.; Ge, S.; Liu, H.; Yu, Y.; Wang, J. Electroactive Hydroxyapatite/Carbon Nanofiber Scaffolds for Osteogenic Differentiation of Human Adipose-Derived Stem Cells. *Int. J. Mol. Sci.* **2023**, *24* (1), 530.
(277) Fujitani, K.; Utsumi, Y.; Yamaguchi, A.; Sumida, H.; Suzuki, S. Preferential Side Chain Scission of Polytetrafluoroethylene by Bending Stress. *Appl. Surf. Sci.* **2023**, *637*, 157891.
(278) Wang, Q.; Wei, Y.; Yin, X.; Zhan, G.; Cao, X.; Gao, H. Engineered PVDF/PLCL/PEDOT Dual Electroactive Nerve Conduit to Mediate Peripheral Nerve Regeneration by Modulating the Immune Microenvironment. *Adv. Funct. Mater.* **2024**, *34* (28), 2400217.
(279) Jalali, S.; Selvaganapathy, P. R. A Self-Assembly and Cellular Migration Based Fabrication of High-Density 3D Tubular Constructs of Barrier Forming Membranes. *Lab Chip.* **2024**, *24* (9), 2468−2484.
(280) Zhang, M.; Zhou, Z.; Yun, J.; Liu, R.; Li, J.; Chen, Y.; Cai, H.; Jiang, H. B.; Lee, E. S.; Han, J.; Sun, Y. Effect of Different Membranes on Vertical Bone Regeneration: A Systematic Review and Network Meta-Analysis. *Biomed. Res. Int.* **2022**, *2022* (1), DOI: 10.1155/2022/7742687.
(281) Walia, R.; Akhavan, B.; Kosobrodova, E.; Kondyurin, A.; Oveissi, F.; Naficy, S.; Yeo, G. C.; Hawker, M.; Kaplan, D. L.; Dehghani, F.; Bilek, M. M. Hydrogel-Solid Hybrid Materials for Biomedical Applications Enabled by Surface-Embedded Radicals. *Adv. Funct. Mater.* **2020**, *30* (38), 2004599.
(282) Zhang, X.; Cheng, Z.; Yang, D.; Dong, Y.; Shi, X.; Liang, H.; Wang, F.; Han, H.; Meng, W.; Shuai, Y.; Yan, Y. Scalable Bio-Skin-Inspired Radiative Cooling Metafabric for Breaking Trade-Off between Optical Properties and Application Requirements. *ACS Photonics.* **2023**, *10* (5), 1624−1632.
(283) Zhou, Z.; Yu, P.; Zhou, L.; Tu, L.; Fan, L.; Zhang, F.; Dai, C.; Liu, Y.; Ning, C.; Du, J.; Tan, G. Polypyrrole Nanocones and Dynamic Piezoelectric Stimulation-Induced Stem Cell Osteogenic Differentiation. *ACS Biomater. Sci. Eng.* **2019**, *5* (9), 4386−4392.
(284) Wang, B.; Li, G.; Zhu, Q.; Liu, W.; Ke, W.; Hua, W.; Zhou, Y.; Zeng, X.; Sun, X.; Wen, Z.; Yang, C.; Pan, Y. Bone Repairment via Mechanosensation of Piezo1 Using Wearable Pulsed Triboelectric Nanogenerator. *Small.* **2022**, *18* (30), 2201056.
(285) Li, W.; Zhang, Y.; Ding, J.; Zhang, S.; Hu, T.; Li, S.; An, X.; Ren, Y.; Fu, Q.; Jiang, X.; Li, X. Temperature-Triggered Fluorocopolymer Aggregate Coating Switching from Antibacterial to Antifouling and Superhydrophobic Hemostasis. *Colloids Surf. B Biointerfaces.* **2022**, *215*, 112496.
(286) Li, X.; Zhou, W.; Chen, H.; Zhang, Z.; Jiang, M.; Liu, P.; Zhang, S. Multi-Hierarchical Assemble Nano-Fibrous Dressing for Burn Wound Ultra-Fast Healing with Dynamical Exudate Regulation, Thermal Management, and Non-Leaching Sterilisation. *Polymer.* **2024**, *308*, 127393.
(287) Panwar, V.; Mondal, B.; Sharma, A.; Murugesan, P.; Arora, M.; Saini, D.; Mandal, D.; Ghosh, D. A Self-Powered, Anti-Bacterial, Moist-Wound Dressing Made with Electroactive Free-Flowing Hydrogel Particles, Encourage Faster Wound Closure. *Chem. Eng. J.* **2024**, *494*, 153063.
(288) Chen, Y.; An, Q.; Hu, X.; Zhao, R.; Teng, K.; Zhang, Y.; Zhao, Y. Effective Scald Wound Functional Recovery Patch Achieved by Molecularly Intertwined Electrical and Chemical Message in Self-Adhesive Assemblies. *ACS Appl. Mater. Interfaces.* **2023**, *15* (32), 38346−38356.
(289) Kalasin, S.; Sangnuang, P.; Surareungchai, W. Intelligent Wearable Sensors Interconnected with Advanced Wound Dressing Bandages for Contactless Chronic Skin Monitoring: Artificial Intelligence for Predicting Tissue Regeneration. *Anal. Chem.* **2022**, *94* (18), 6842−6852.
(290) Muñoz, G.; Chamberlain, K. M.; Solovyev, M. E.; Smith, D. W.; Pittman, C. U. Electrophilic Routes to 6F Polymers and Attempted Synthesis of Semi-Fluorinated Group IVB Metallocene Polymers. *J. Inorg. Organomet. Polym. Mater.* **2024**, *34* (7), 2834−2854.
(291) Park, J.; Kucukkal, T. G.; Oh, J.-M.; Stuart, S. J.; Creager, S. E.; Muñoz, G.; Smith, D. W., Jr. One-Pot Single-Step Copolymerization of Aromatic Trifluorovinyl Ethers toward Perfluorocyclobutyl (PFCB) Segmented Copolymers. *Polym. Chem.* **2024**, *15* (39), 3977−3982.

https://doi.org/10.1021/acs.chemrev.4c00996
Chem. Rev. XXXX, XXX, XXX−XXX